# The Role of YAP and Cell of Origin during the Progression of Pancreatic Neoplastic Lesions to Invasive Ductal Adenocarcinoma




Asmita Thapa
St Cross College
University of Oxford

Thesis submitted to the University of Oxford in partial fulfilment of the requirements for the degree of Doctor of Philosophy.

Michaelmas Term 2019

**Supervisor**

Prof. Eric O'Neill (University of Oxford)




The work presented in this thesis was performed at the Department of Oncology, Old Road Campus Research Building (ORCRB), University of Oxford. This study was funded by Pancreatic Cancer UK funded Prize Studentship.

## Declaration

I confirm that the work presented in this thesis is my own unless indicated. Whenever I have presented collaborated work and received technical help, I confirm that this has been credited in the thesis.

**Dedicated to my amazing family,**

**to whom I owe everything**

# Abstract


The role of YAP and Cell of Origin during the Progression of Pancreatic Neoplastic Lesions to Invasive Ductal Adenocarcinoma

A thesis submitted to the University of Oxford
for the degree of Doctor of Philosophy

Asmita Thapa, St Cross College, Michaelmas Term 2019

Pancreatic ductal adenocarcinoma (PDAC) is considered one of the most fatal cancer types with a very low survival rate. The development of dysplasia in normal ductal epithelium is the initiating step of the disease, which then undergoes multiple grades of pancreatic intraepithelial neoplasia (PanIN) lesions before developing into invasive adenocarcinoma. *KRAS* mutations occur during early stages of malignant transformation and act as a critical event in both initiating and maintaining PDAC development. Alongside, an oncogene, YAP, is emerging to play a role in the facilitation of neoplastic precursor lesions to invasive cancer in *KRAS* mutated pancreas. Canonically, YAP's activation is negatively regulated by the tumour suppressive Hippo pathway by inhibiting the protein's nuclear localisation. In order to elucidate the mechanism by which YAP promotes early progression of PanIN lesions, I explored the association of YAP with the components of KRAS-mediated MAPK signalling pathway. Firstly, I show an association between YAP and phosphorylated ERK1/2 both in pancreatic cancer cells and low-grade PanIN lesions of *Kras*-mutated mice. In these PanIN lesions, I demonstrate the nuclear expression of YAP to be heterogeneous and associate this with PanIN lesions' origin from different cell types. I show ductal-derived precursor lesions in *Kras* mutated mice and PDAC in human samples to positively correlate with high nuclear expression of YAP. To further understand this role of YAP in ductal-derived PDAC, I establish YAP depleted 3D pancreatic organoid system isolated from ductal cells of *Kras* mutated mouse pancreas. From this study, I present the potential role of YAP as a useful marker to identify ductal-derived PanIN lesions and PDAC.

# Acknowledgements

I would first like to thank my supervisor, Prof. Eric O'Neill. Your constant support, guidance and motivation to stay postive over the last four years has been extremely valuable. The scientist I am today is all because of your faith and confidence in me. It really helped to boost my self-confidence and taught me how to lead projects. Thank you for providing a thriving work environment that allowed me to nourish my skills as a scientist under your supervision. I would also like to say massive thank you to my funding body, Pancreatic Cancer UK, without whom this DPhil project would not have been possible. To get a constant support from them has been very motivating and inspiring.

I owe a debt of gratitude to everyone who have been so helpful in this project and throughout my DPhil. I appreciate all the expert knowledge I was able to receive from Prof. Robert Goldin about histopathology. Thank you for always being so accommodating with your time to meet for discussions, despite your busy schedule. I would also like to say a huge thank you to Dr Paul Miller for his extreme generosity in providing all the samples and H&E stainings.

I would like to express deepest appreciation to Frances, who has simply been incredible with extreme amount of help and guidance, and always finding solutions to any problem. I would also like thank Michael for all his help with the bioinformatics and IHC and Simone for helping me with the orthotopic injection experiment. My deepest appreciation goes to Maria (T) for holding my hand when I first started in the lab with lots of fears and doubts and leading me. A big thank you to Daniela for all her support, care and advice besides being always so joyful and a very great friend. Words fall short to express my gratitude to Luana, Maria (Ch) and Sophie for their incredible friendships and for bringing rays of happiness over the past years. The words of encouragement, extreme support, motivation to write my thesis besides all the laughter and craziness made this journey so much fun.

I would also like to thank Fiona for encouraging my critical thinking and improving my scientific knowledge and Dan for always being such a great listener along with words of wisdom whenever needed. I also want to say a huge thank you to past members: Leanne, Delia and Dafni, for all your encouragement and support. I am glad to have shared my time in Oxford with you, and Aline, Jelte and Viviana for making lab life lively and entertaining.

I would also like to extend my thank you to Florian for making Oxford life more fun and encouraging me to attend events outside life, I was able to collect many cherishing memories.

To my Oxford family – Luana, Sergio, Nico – thank you for being so wonderful. Having such great housemates meant I always laughed and felt happier, even in moments of stress and despair. I feel incredibly lucky to have a second family in the UK.

I also want to offer my special thanks to Sibyl for being an amazing "writing partner in crime" and Saloni and Muna for always being there to cheer me up.

I am also incredibly grateful to have my friends outside of Oxford. To Alina, Saru and Sushma – thank you for always being there for me whenever needed. You girls keep me grounded and sane amongst your insanity. To Ganga and Sabhyata, thank you so much for years of invaluable friendship.

Last but not the least I owe my deepest gratitude to my family who are simply the driving force of my existence. To my amazing siblings, Anu, Anisha and Sudesh, you are the prime reason of my happiness. Thank you for always bringing joy into my life. And my cousins aka "Idiots" – Abishek, Ajay, Ankur, Prexya and Prakriti – thank you for always entertaining and providing immense fun. To my incredible grandparents, your unconditional love, care and blessings are the most precious gift I could ever get. Finally, to my most amazing parents who have been the biggest pillars of my life. To my dad, Baba, thank you for teaching me to dream and have aspirations. If I hadn't learned that from you, I wouldn't even have the courage to think about doing a PhD. To my mother, Mummy, your sacrifices and hard work to make my life comfortable are immeasurable. You have provided so much of love, care support, all of which I could never repay you. You both are the reason that everything I am today and I may become tomorrow.

Thank you all!

# Table of Contents

Chapter 1

Introduction..... 1

1.1 Cancer Biology..... 1

1.2 Cancer in Pancreas..... 2

1.2.1 Biology of Pancreas (anatomy, physiology and development)..... 2

1.2.2 Types of pancreatic cancer..... 4

1.2.3 Epidemiology and Etiology..... 6

1.2.4 PDAC diagnosis..... 7

1.2.5 PDAC treatment..... 8

1.2.6 Pancreatic lesions..... 12

1.3 Molecular biology of pancreatic cancer..... 16

1.3.1 *KRAS* mutations..... 16

1.3.2 Other genetic mutations in PDAC..... 21

1.3.3 Introduction to Hippo pathway and its importance in cancer..... 22

1.4 Models to study PDAC development..... 31

1.4.1 Genetically engineered mouse models (GEMMs) in PDAC..... 31

1.4.2 3D organoids..... 34

1.5 Cell-type origin of PanIN lesions and PDAC..... 36

1.6 Aims of the project..... 40

Chapter 2 Materials and Methods..... 42

2.1 Materials..... 42

2.1.1 Mouse strains…… 42

2.1.2 Patient Materials……42

2.1.3 General Laboratory Reagents……43

2.1.4 Genotyping primers and probes…… 44

2.1.5 Antibodies used……44

2.1.6 Cell lines and cell culture reagents used……46

2.1.7 RNAi interference and Lenti-viral shRNA vectors for knockdown……48

2.2 Methods…… 48

2.2.1 Generation of a mouse model harbouring A133S SNP within the *Rassf1* gene…… 48

2.2.2 Genotyping……49

2.2.3 Immunohistochemical Staining (IHC)……51

2.2.4 Haematoxylin and Eosin Staining (H&E)…… 52

2.2.5 Alcian blue Staining (AB)…… 53

2.2.6 Cell Culture……54

2.2.7 Organoid Isolation……55

2.2.8 Organoid passaging and culture……57

2.2.9 Transient knockdown using RNAi interference……57

2.2.10 Stable knockdown using lentiviral shRNA vectors……59

2.2.11 Protein extraction from cell lines and organoids……61

2.2.12 Western blotting…… 62

2.2.13 Immunofluorescent staining of organoids…… 63

2.2.14 Orthotopic Injection of organoids into mouse pancreas……64

2.2.15 MRI Scanning…… 65

2.2.16 Image and statistical analyses……. 66

Chapter 3 Role of YAP in KRAS-mediated progression of PDAC (Results I)……..68

3.1 Introduction…… 68

3.1.1 Role of YAP and TAZ in PDAC……..68

3.1.2 Crosstalk between different components of Hippo and MAPK pathway… 69

3.2 Aims……70

3.3 Results…… 71

3.3.1 Transient YAP knockdown alters activation of ERK in pancreatic cancer cell lines……71

3.3.2 Stable YAP knockdown alters pERK and TAZ levels in pancreatic cancer cell lines……74

3.3.3 Role of upstream regulator of Hippo pathway, NF2, in the regulation of MAPK pathway in PDAC…… 80

3.3.4 Histological characterisation of normal exocrine structure and precursor lesions (PanINs) in the KC mouse model used in our study……83

3.3.5 YAP expression in *Kras* mutated PanIN lesions……85

3.3.6 pERK levels in *Kras* mutated PanIN lesions……89

3.3.7 YAP's activity in relation to pERK in *Kras* mutated PanIN lesions……91

3.4 Discussion……93

Chapter 4 Aggressive phenotype in PDAC in relation to cell of origin (Results II) …….97

4.1. Introduction…… 97

4.2 Aims……99

4.3 Results……100

4.3.1. Establishment of Alcian Blue as a method for determining the origin of precursor lesions……100

4.3.2. Optimisation to quantify Alcian Blue staining in pancreatic tissues from a cohort of PDAC patients……103

4.3.3. Survival curve analysis in PDAC patient cohort with Alcian blue staining….107

4.3.4. Quantification of corresponding precursor lesions stained with Alcian Blue and nuclear YAP staining in KC mice……109

4.3.5. Quantification of corresponding PDAC regions with Alcian Blue and nuclear YAP staining in patient cohorts……114

4.4 Discussion……117

Chapter 5 Generation of a genetically engineered mouse model, 3D organoids and an orthotopic model to study PDAC tumourigenesis (Results II)……121

5.1 Introduction……121

5.1.1 Role of RASS1A in PDAC progression……121

5.1.2 The application of 3D organoids and orthotopic model for the study of PDAC development……123

5.2 Aims……125

5.3 Results……126

5.3.1 Investigation of RASSF1A in the progression of PanIN lesions using GEMMs……126

5.3.2 Establishment of 3D pancreatic organoids……132

5.3.3 Orthotopic injection of organoids into the mouse pancreas……133

5.3.4 Histological assessment of orthotopic model of pancreatic tissue……140
5.3.5 GFP staining in the pancreatic tissue from the orthotopic model and KC-YFP+ve mouse ……143
5.3.6 Stable YAP knockdown in KC organoids……148
5.4 Discussion……150

Chapter 6 Final Discussion……155
6.1 Background Summary……155
6.2 Final Discussion of Chapter 3 ……157
6.2.1 Mechanisms by which YAP contribute to drive PDAC progression……157
6.2.2 Future research……160
6.3 Final Discussion of Chapter 4……163
6.3.1 The association of nuclear YAP expression with cell of origin of precursor lesions and PDAC……163
6.3.2 Future research……164
6.4 Final Discussion for Chapter 5……166
6.4.1 3D organoids as a model to understand YAP's role in PDAC from different cell of origin……166
6.4.2 Future research……168
6.4.3 The generation of GEMMs to study upstream regulator of the Hippo pathway in PDAC……169
6.5 Final Conclusion……170
Appendix A Appendix……173
Appendix B Copyright Licences……179

Bibliography……..181

# List of Figures

Figure 1.1: Anatomy of Pancreas. 4

Figure 1.2: Histology of pancreatic ductal adenocarcinoma (PDAC). 6

Figure 1.3: Schematic diagram representing progression model of pancreatic carcinogenesis. 14

Figure 1.4: Molecular alterations during the histological progression of precursor lesions into pancreatic ductal adenocarcinoma. 19

Figure 1.5: Simplified overview of the core components of Hippo pathway in (A) Drosophila and (B) Mammals. 24

Figure 1.6: Hippo pathway effectors, YAP and TAZ share 45% sequence homology. 28

Figure 1.7: Schematic diagram representing conditional *LSL-KRAS*$^{G12D}$ allele to generate KC mice. 33

Figure 1.8: Schematic diagram demonstrating the process of ductal isolation from mouse pancreas to their growth in culture as organoids. 36

Figure 3.1: Transient transfection of YAP for 24 h depletes MAPK/pERK signalling. 73

Figure 3.2: Transient transfection of YAP for 48 h enhances ERK activation. 74

Figure 3.3: Stable knockdown of YAP in mouse PDAC cell lines increases pERK levels. 76

Figure 3.4: Stable knockdown of YAP in human PDAC cell lines increases pERK levels. 76

Figure 3.5: Time-dependent stimulation of shYAP transduced KPC cells with serum. 78

Figure 3.6: Stable knockdown of YAP in mouse PDAC cell lines increases TAZ levels. 79

Figure 3.7: Stable knockdown of YAP in human PDAC cell lines increases TAZ levels. 80

Figure 3.8: Transient transfection of NF2 enhances pERK levels but has no effect in YAP activation. 82

Figure 3.9: Histological assessment of pancreatic tissue from *Kras$^{LSL.G12D/+}$; Pdx-Cre* (KC) mouse displays a spectrum of PanIN lesions. 85

Figure 3.10: Immunohistochemical analysis of YAP in PanIN lesions of KC mouse pancreata display heterogeneity. 88

Figure 3.11: Immunohistochemical analysis reveals strong levels of pERK in PanIN lesions of KC mouse pancreata. 90

Figure 3.12: Expression of YAP positively correlates with pERK levels in the nuclei of corresponding PanIN lesions of KC mouse pancreata. 92

Figure 4.1: Alcian Blue as a method to determine cell of origin in murine pancreatic precursor lesions. 102

Figure 4.2: Quantification of Alcian Blue Staining in human PDAC samples. 104

Figure 4.3: Quantification of Alcian Blue Staining in human PDAC using automated digital analysis. 105

Figure 4.4: Quantification of Alcian blue staining in human PDAC using visual assessment. 107

Figure 4.5: Five-year relative survival in PDAC patients based on the staining of Alcian Blue. 109

Figure 4.6: Comparative analysis between Alcian Blue and YAP staining in the ductal region and precursor lesions of KC mice. 110

Figure 4.7: Establishment of the quantification method for the correlation between Alcian Blue and YAP staining in the precursor lesions of KC mice. 112

Figure 4.8: Lower expression of nuclear YAP in a PanIN-like precursor lesion of KC mice. 113

Figure 4.9: Comparative analysis between Alcian Blue and YAP in the PDAC region of human cohort. 116

Figure 5.1: Association between RASSF1A and phosphorylated YAP in the apical membrane of PanIN lesions of KC mouse pancreata. 127

Figure 5.2: Generation of genetically engineered *Rassf1* SNP mice with *Kras* mutation in pancreas. 129

Figure 5.3: Heterozygous RASSF1A SNP in mice with *Kras* mutated pancreas revealed no distinct phenotype. 131

Figure 5.4: Expression of YAP in 3D organoids from mouse pancreas. 133

Figure 5.5: Orthotopic injection of pancreatic organoids into mouse pancreas orthotopically. 136

Figure 5.6: *In vivo* MRI images of mice abdomen analysed each week after orthotopically injected with pancreatic organoids. 137

Figure 5.7: *In vivo* MRI images of mice abdomen orthotopically injected with pancreatic organoids analysed before the harvesting of pancreas. 139

Figure 5.8: Ductal structures in pancreas with orthotopically injected organoids resembled normal ductal epithelium. 142

Figure 5.9: YFP expression in the pancreas of KC-YFP+ve mouse. 145

Figure 5.10: Investigation for YFP expression in mice injected with organoids isolated from KC-YFP+ve mouse. 147

Figure 5.11: Depletion of YAP expression in organoids isolated from KC mouse pancreas. 149

Figure 6.1: Proposed mechanism by which YAP activation leads to increased MAPK signalling in PDAC. 162

Figure 6.2. Working model illustrating role of YAP in the progression of neoplastic lesions to PDAC in relation to cell of origin based on the data in this thesis. 172

Figure 7.1: Generation of the rs2073498 SNP Mouse. 173

Figure 7.2: Genotyping for *Kras* mutation and *Rassf1* SNP allele. 173

Figure 7.3: Active YAP in normal ducts with increasing age of mice genetically modified to recapitulate early stages of PDAC. 174

Figure 7.4: Repeat of visually quantified Alcian blue staining in a human PDAC sample. 174

Figure 7.5: Determination of cut-off point to stratify PDAC patients into high and low Alcian blue. 175

Figure 7.6: A precursor lesion in KC mice demonstrated positive correlation between the staining of Alcian blue and nuclear YAP. 175

Figure 7.7: Nuclear expression of YAP associates with aggressive PDAC phenotype. 176

Figure 7.8: Establishment of pancreatic organoids. 176

Figure 7.9: Proliferation of ductal pancreatic organoids in culture. 177

Figure 7.10: Orthotopic injection of pancreatic cancer cells into mouse pancreas. 177

Figure 7.11: Histological analysis of pancreas from the orthotopic model for site of injection. 178

Figure 7.12: Alcian blue staining in the PanIN lesions of KC pancreas as a reference for Alcian blue positivity. 178

# List of Tables

Table 2.1: List of chemical reagents. 43

Table 2.2: Primers and probes used for genotyping for the study. 44

Table 2.3: Primary and Secondary antibodies for IHC. 44

Table 2.4: Primary and Secondary antibodies for Western Blot and IF. 45

Table 2.5: List of the cell lines used in this study. 46

Table 2.6: List of the cell culture reagents and supplements. 46

Table 2.7: List of reagents and supplements for Mouse Complete Feeding Media to culture organoids. 47

Table 2.8: siRNAs and shRNAs used for the study. 48

# Abbreviations

| | |
|---|---|
| 5FU | 5-Fluorouracil (5FU) |
| A | Adenosine |
| AB | Alcian Blue |
| $AB^-$ | Alcian Blue Negative |
| $AB^+$ | Alcian Blue Positive |
| ABL | Abelson Murine Leukemia Viral Oncogene Homolog |
| ACC | Acinar Cell Carcinoma |
| ADM | Acinar-To-Ductal Metaplasia |
| ADP | Adenosine Diphosphate |
| AF6 | Afadin |
| AGR2 | Anterior Gradient Protein 2 |
| Ala | Alanine, Also A |
| AMPK | 5' AMP-Activated Protein Kinase |
| AREG | Amphiregulin |
| ARID1A | AT-Rich Interaction Domain 1A |
| ATM | Ataxia Telangiectasia Mutated |
| AXL | AXL Receptor Tyrosine Kinase |
| BAX | Bcl-2-Associated X |
| BRCA2 | BRCA2, DNA Repair Associated |
| BRG1 | Brahma-Related Gene-1 |
| BSA | Bovine Serum Albumin |
| C-ABL | Mammalian Abelson Murine Leukemia Viral Oncogene Homolog 1 |
| C-Myc | MYC Proto-Oncogene, BHLH Transcription Factor |
| CA | Carbohydrate Antigen |
| CCND1 | Cyclin D1 |
| CDK6 | Cyclin Dependent Kinase 6 |
| CDKN2A | Cyclin Dependent Kinase Inhibitor 2A |
| CEA | Carcinoembryonic Antigen |
| CK19 | Cytokeratin-19 |
| $CO_2^-$ | Carboxylate |

| | |
|---|---|
| CPA1 | Carboxypeptidase A1 |
| CPG | Dinucleotide Consisting Of Cytosine Followed By Guanine |
| CRK | CT10 Regulator Of Kinase |
| CT | Computerised Tomography |
| CTGF | Connective Tissue Growth Factor |
| CTLA-4 | Cytotoxic T-Lymphocyte Associated Antigen 4 |
| CTRL | Control |
| $Cu^{+}$ | Cuprous Ion |
| DAB | 3,3'-Diaminobenzidine |
| DAPI | 4',6-Diamidino-2-Phenylindole |
| DCLK1 | Doublecortin-Like Kinase 1 |
| DMEM | Dulbecco's Modified Eagle Media |
| DMSO | Dimethyl Sulfoxide |
| DNA | Deoxyribonucleic Acid |
| DPC4 | Deleted In Pancreatic Carcinoma 4 |
| DPX | Di-N-Butyl Phthalate |
| ECL | Enhanced Chemiluminescence |
| EDTA | Ethylenediaminetetraacetic Acid |
| EGFR | Epidermal Growth Factor Receptor |
| Ela | Elastase |
| EMT | Epithelial-To-Mesenchymal Transition |
| ERK | Extracellular Signal-Regulated Kinase |
| ES | Embryonic Stem |
| EUS | Endoscopic Ultrasonography |
| FAMMM | Familial Atypical Mole And Multiple Melanoma |
| FBS | Fetal Bovine Serum |
| FBW7 | F-Box And WD Repeat Domain-Containing 7 |
| FDG-PET | $^{18}$F-Fluorodeoxyglucose- Positron Emission Tomography |
| FERM | 4.1 Protein, Ezrin, Radixin And Moesin |
| FFPE | Formalin Fixed Paraffin Embedded |
| FOLFIRINOX | Oxaliplatin, Irinotecan, Fluorouracil And Leucovorin |
| G | Guanosine |

| | |
|---|---|
| GAP | Gtpase Activating Protein |
| GAPDH | Glyceraldehyde-3-Phosphate Dehydrogenase |
| GDP | Guanosine Diphosphate |
| GEF | Guanine-Exchange Factor |
| GEMM | Genetically Engineered Mouse Model |
| GPR87 | G Protein-Coupled Receptor 87 |
| GRB2 | Growth Factor Receptor-Bound-2 Protein |
| GSK-3 | Glycogen Synthase Kinase-3 |
| GTP | Guanosine Triphosphate |
| h | Hour |
| H&E | Haematoxylin And Eosin |
| $H_2O$ | Water |
| HBEGF | Heparin Binding EGF Like Growth Factor |
| HDR | Homology Directed Repair |
| Hnf1a | Hepatocyte Nuclear Factor 1-Alpha |
| Hpo | Hippo |
| HRAS | Harvey Rat Sarcoma |
| HRP | Horseradish Peroxidase |
| HSP90 | Heat Shock Protein 90 |
| IF | Immunofluorescence |
| IHC | Immunohistochemistry |
| IPMN | Intraductal Papillary Mucinous Neoplasm |
| ITGA2 | Integrin Alpha 2 |
| IVC | Individually Ventilated Cage |
| Kb | Kilobase |
| KC | *LSL-Kras$^{g12d/+}$; Pdx-1-Cre* |
| KC-YFP+Ve | *Kras$^{g12d+/-}$; Pdx-Cre; Rosa YFP* |
| KCR1-Het | *Kras$^{g12d+/-}$; Pdx-Cre*; *RASSF1$^{SNP+/-}$* |
| KCR1-Hom | *Kras$^{g12d+/-}$; Pdx-Cre; RASSF1$^{SNP/SNP}$* |
| KDa | Kilodalton |
| KPC | *LSL-Kras$^{g12d/+}$;LSL-Trp53$^{R172H/+}$;Pdx-1-Cre* |
| KRAS | Kirsten Rat Sarcoma |

| | |
|---|---|
| LATS1/2 | Large Tumour Suppressor 1/2, Warts In Drosophila |
| LAPC | Locally Advanced Pancreatic Cancer |
| LGR5 | Leucine-Rich Repeat-Containing G-Protein Coupled Receptor 5 |
| LUC | Luciferase |
| MAPK | Mitogen-Activated Protein Kinase |
| MARK1 | MAP/Microtubule Affinity-Regulating Kinase 1 |
| Mats | Mob-As-Tumour Suppressor |
| MCN | Mucinous Cystic Neoplasm |
| MDM2 | Murine Double Minute 2 |
| MEK | Mitogen Activated Protein Kinase |
| MEN1 | Multiple Endocrine Neoplasia Type I |
| $MgCl_2$ | Magnesium Chloride |
| $MgSO_4$ | Magnesium Sulfate |
| Min | Minute |
| mg | Milligram |
| ml | Millilitre |
| mm | Millimetre |
| MLH1 | Mutl Homolog 1 |
| mM | Millimolar |
| MRI | Magnetic Resonance Imaging |
| mRNA | Messenger RNA |
| ms | Millisecond |
| MSH2/6 | Muts Homolog 2/6 |
| MST1/2 | Mammalian Sterile 20-Like Protein (Also Called KRS), Hpo In Drosophila |
| Muc | Mucin |
| NaCl | Sodium Chloride |
| $NaHCO_3$ | Sodium Bicarbonate |
| $NaN_3$ | Sodium Azide |
| NaOH | Sodium Hydroxide |
| NCK | Non-Catalytic Region Of Tyrosine Kinase |
| NF1 | Neurofibromatosis 1 |
| NF2 | Neurofibromatosis Type 2 |

| | |
|---|---|
| NOTCH2 | Neurogenic Locus Notch Homolog Protein 2 |
| NP-40 | Nonidet P-40 |
| NRAS | Neuroblastoma Rat Sarcoma |
| Nu/Nu | Nude/Nude |
| $P2Y_2R$ | P2Y Purinoceptor 2 |
| PanIN | Pancreatic Intraepithelial Neoplasia |
| PARP-1 | Poly (ADP-Ribose) Polymerases |
| PAS | Periodic Acid-Schiff |
| PBS | Phosphate-Buffered Saline |
| PBST | PBS With 0.01% Tween-20 |
| PD-1 | Programmed Death 1 |
| PD-L1 | Programmed Death Ligand 1 |
| PDAC | Pancreatic Ductal Adenocarcinoma |
| PDGFR | Platelet-Derived Growth Factor Receptor |
| PDX1 | Pancreatic And Duodenal Homeobox 1 |
| Pen-Strept | Penicillin/Streptomycin |
| PFA | Paraformaldehyde |
| PI3K | Phosphatidylinositol 3-Kinase |
| PIG3 | P53-Inducible Gene 3 |
| PIPES | 1,4-Piperazinediethanesulfonic Acid |
| PKA | Protein Kinase A |
| PLC | Phospholipase C |
| PMS2 | PMS1 Homolog 2, Mismatch Repair System Component |
| PNET | Pancreatic Neuroendocrine Tumour |
| POLO | Pancreas Cancer Olaparib Ongoing |
| PRF | Phenol Red Free |
| PRSS1 | Serine Protease 1 |
| PTF1 | Pancreas Transcription Factor 1 |
| PVDF | Polyvinylidene Fluoride |
| RAF | Raf-1 Proto-Oncogene, Serine/Threonine Kinase |
| RAL-GDS | Ral Guanine Nucleotide Dissociation Stimulator (Ral-GDS) |
| RAS | Ras Proto-Oncogene |

| | |
|---|---|
| RASSF1 | Ras Association Domain Family 1 |
| RIN1 | Ras And Rab Interactor 1 |
| RIPA | Radioimmunoprecipitation Assay Buffer |
| RNA | Ribonucleic Acid |
| RNA-Seq | RNA Sequencing |
| Rs2073498 | RASSF1 A133S |
| Rs2073498 | RASSF1 C.397G>T |
| RT | Room Temperature |
| S.E.M | Standard Error Of The Mean |
| SAV | Salvador |
| SDS | Sodium Dodecyl Sulphate |
| Sec | Second |
| Ser | Serine, Also S |
| SERP1 | Stress Associated Endoplasmic Reticulum Protein 1 |
| SH3 | Src Homology Domain 3 |
| SiRNA | Small Interfering RNA Molecule |
| SNP | Single Nucleotide Polymorphism |
| $SO_3^-$ | Suphanate |
| SOS | Son Of Sevenless |
| SPINK1 | Serine Peptidase Inhibitor Kazal Type 1 |
| ssODN | Single Stranded Oligonucleotide |
| STK11 | Serine/Threonine Kinase 11 |
| STRAD | STE20-Related Adaptor |
| TAZ | Transcriptional Co-Activator With PDZ-Binding Motif |
| TEAD | TEA Domain Family, Scalloped In Drosophila |
| Tff1 | Trefoil Factor 1 |
| TGF | Transforming Growth Factor |
| TIAM | T Cell Lymphoma Invasion And Metastasis |
| TP53 | Tumour Suppressor 53 |
| TR | Repetition Time |
| Tris-HCl | Tris (Hydroxymethyl) Aminomethane-Hydrochloride |
| TSC | Tuberous Sclerosis Complex |

| | |
|---|---|
| TSC1/2 | Tuberous Sclerosis ½ |
| VHL | Von Hippel-Lindau Disease |
| WB | Western Blot |
| Wnt | Wingless Related Integration Site |
| WT | Wild-Type |
| WTS | Warts |
| WWTR1 | WW Domain Containing Transcription Regulator 1 |
| YAP | Yes-Associated Protein |
| Yki | Yorkie |
| µg | Microgram |
| µl | Microlitre |
| µm | Micrometre |

# Chapter 1 Introduction

## 1.1 Cancer Biology

Cancer is a complex disease, with accumulation of a number of mutations in specific genes. The augmentation of these genetic alterations occurs in a multi-step process that transform normal cells to highly malignant derivatives. Together, the malignancy in the tumour cells emanate as the selective growth advantage of the normal cells allow them to outgrow surrounding cells and form microscopic clones with uncontrolled cell proliferating ability (Vogelstein et al., 2013). The steps of progression into invasive cancer is intermediated by lesions that represent pre-malignant state. Unlike normal cells that have anti-cancer defence mechanisms, cancerous cells acquire a number of genetic changes and display physiological changes that evade these mechanisms and allow them to maintain their aggressive form. Collectively, the cancer cells in different tumour types share some common functional capabilities that sustain their malignant growth. These acquired capabilities were defined by Hanahan and Weinberg in 2000 as hallmarks of cancer and summed as: growth signal autonomy, insensitivity to antigrowth signals, evasion of apoptosis, unlimited replication, sustained angiogenesis, tissue invasion and metastasis (Hanahan and Weinberg, 2000). Similarly, the complexity of tumours arises as the malignant growth of genetically altered tumour cells involves interaction with different cells types within the tumour microenvironment including immune inflammatory cells, cancer-associated fibroblasts, endothelial cells and cancer stem cells. In view of this, a decade later of first describing hallmarks of cancer, Hanahan and Weinberg proposed evasion of immune surveillance of cancer cells as an emerging hallmark. Alongside, reprogramming of energy metabolism, that fuel cell growth and division to substantiate

uncontrolled cell proliferation, was also added as another emerging hallmark of cancer (Hanahan and Weinberg, 2011). Despite the acquisition of the biological capabilities, directly or indirectly through a number of mutations, high genome maintenance ensure that mutations are rare events. Hence, the instability and variability in the genome was defined as a characteristic that enable the premalignant cells to acquire the physiological abilities and evolve into cancerous form. Besides, inflammation has also been described as another enabling characteristic in strengthening hallmark capabilities of the pre-malignant cells (Hanahan and Weinberg, 2011). In most tumour types, mutations of specific genes promote the tumourigenic process and provide selective advantage to the cancer cells. Typically, a tumour consists of two to eight mutations of these "driver" genes. These driver genes, in general, fall into cell signalling pathways that facilitate three core cellular processes: cell fate, cell survival and genome maintenance. Furthermore, in most cancers, the process of tumourigenesis is highly subjected to genetic heterogeneity and occur in four forms: intratumoural, intermetastatic, intrametastatic and interpatient heterogeneity. Understanding these different kinds of tumour heterogeneity is highly advantageous to make informed and effective treatment decisions (Vogelstein et al., 2013).

This thesis will focus on the cellular and molecular processes involved in the multi-step tumorigenesis of pancreatic ductal adenocarcinoma.

## 1.2 Cancer in Pancreas

### 1.2.1 Biology of Pancreas (anatomy, physiology and development)

The pancreas is a pear-shaped compound gland, which weighs around 70-150 g and measures 15-25 cm in length in the adult human, and is divided structurally as head, body

and tail. The word “pancreas” is derived from the Greek term in which “pan” means “all” and “creas” means “flesh” (Slack, 1995) . It is located in the upper abdomen —the head of the pancreas is encompassed by the duodenum whereas the tail is extended close to the spleen. Physiologically, the pancreas is divided into exocrine and endocrine portions (Figure 1.1). The endocrine region is composed of the Islets of Langerhans which are involved in the secretion of hormones including insulin, amylin, glucagon, somatostatin and pancreatic polypeptide into the bloodstream. The blood flow carrying the hormones enters the exocrine tissue surrounding the Islet of Langerhans and ultimately infiltrates the general circulation. On the other hand, 85% of the total mass of pancreas is comprised by the exocrine region, which consists of an acinus and a ductule system. The acini – Latin term for “berry in a cluster” – is either spherical or tubular in shape. The cells of the acinus are responsible for synthesising, storing and secreting enzymes involved in the digestion of several components. These include carbohydrates such as amylase, fat such as lipase, phospholipase and cholesterol esterase, and protein such as trypsin, chymotrypsin, elastase and carboxypolypeptidase. The secreted digestive enzymes from the acini, along with water and bicarbonate ions, flow through the ductule system in a tree-like series to the duodenum. This occurs as the ductule system lengthens from the acinar lumen into interlobular ducts and ultimately drains into the main pancreatic ductal system. The epithelium in intralobular ducts and small interlobular ducts are cuboidal in shape, whereas large interlobular ducts are lined by columnar epithelial cells (Encyclopaedia Britannica, 2019; Pandol, 2010). Developmentally, the presence of a specific domain containing multipotent progenitors – coexpressed by Pancreas transcription factor 1 (Ptf1), Pancreatic and duodenal homeobox 1 (Pdx1), c-Myc and Carboxypeptidase A1 (Cpa1) – at the tip of

the branching pancreatic tree lead to the formation of exocrine and endocrine cells in the pancreas (Zhou et al., 2007).

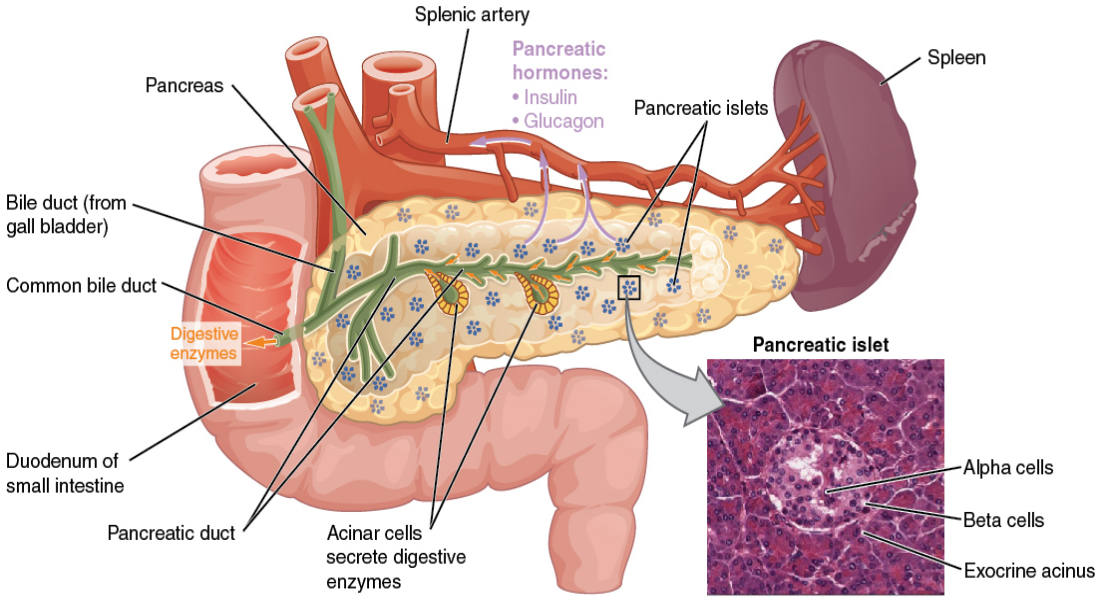


**Figure 1.1: Anatomy of Pancreas.** The Pancreas is divided into two regions, endocrine and exocrine. The endocrine portion consists of Islet of Langerhans which is comprised of alpha and beta cells. These cells are responsible in the production of hormones which get secreted into the bloodstream and passed through the exocrine portion before entering the general circulation. In the exocrine portion, digestive enzymes secreted by the acini pass through the ductule system before entering the duodenum. Figure taken from Anatomy and Physiology (Biga et al., 2018) and is an open access under the Creative Commons Attribution License.

## 1.2.2 Types of pancreatic cancer

Two distinct regions in pancreas – endocrine and exocrine – give rise to cancers with differing molecular, clinical and pathological features. Pancreatic neuroendocrine tumours (PNETs) arise from the Islet of Langerhans in the endocrine regions of pancreas. PNETs represent a rare group of neoplasms and generally develop sporadically. However, there are also some rare hereditary syndromes associated with PNETs including Multiple Endocrine Neoplasia type I (MEN1), von Hippel-Lindau disease (VHL), Neurofibromatosis 1 (NF1) and tuberous sclerosis complex (TSC) (Delle Fave et al., 2017). Although PNETs are the second most common pancreatic neoplasm (Scarpa et al., 2017), they account for less than 5% of all pancreatic cancers (Mullan et al., 2001).

More than 90% of pancreatic cancer is comprised by pancreatic ductal adenocarcinoma (PDAC) that arise from the exocrine pancreatic compartment. Hence, it is very common to interchangeably use the term “PDAC” with “pancreatic cancer” due to its dominance in the incidence rate amongst all pancreatic cancer types. PDAC is a highly aggressive disease, (Bardeesy and DePinho, 2002), with a very low 5-year survival rate of around 3% for patients at distant stage of the disease (American Cancer Society, 2020) . It is estimated to become the second main cause of cancer-related deaths by 2030 in the United States and Germany (Quante et al., 2016; Rahib et al., 2014). Several histological features define ductal adenocarcinoma in the pancreas including haphazard arrangement of glands within desmoplastic stroma, nuclear pleomorphism, incomplete glandular lumina, luminal necrosis, perineural invasion and lymphovascular invasion (Kamisawa et al., 2016) (Figure 1.2). Moreover, PDAC can be divided, based on their degree of differentiation, into three grades – well differentiated, moderately differentiated and poorly differentiated. This differentiation is mainly based on the prevalence of glandular formation (Garcia et al., 2013). Clincially, PDAC has more unfavourable prognosis in comparison to PNETs which are more indolent in nature (Fesinmeyer et al., 2005; Halfdanarson et al., 2008).

Additionally, the less common type of pancreatic cancer is acinar cell carcinoma (about 1%). As suggested by the name, this malignant form of neoplasm resemble acinar cell morphology and produce pancreatic exocrine enzymes. The etiology of the disease, however, is not well-understood (Chaudhary, 2015; Xing-mao et al., 2018).

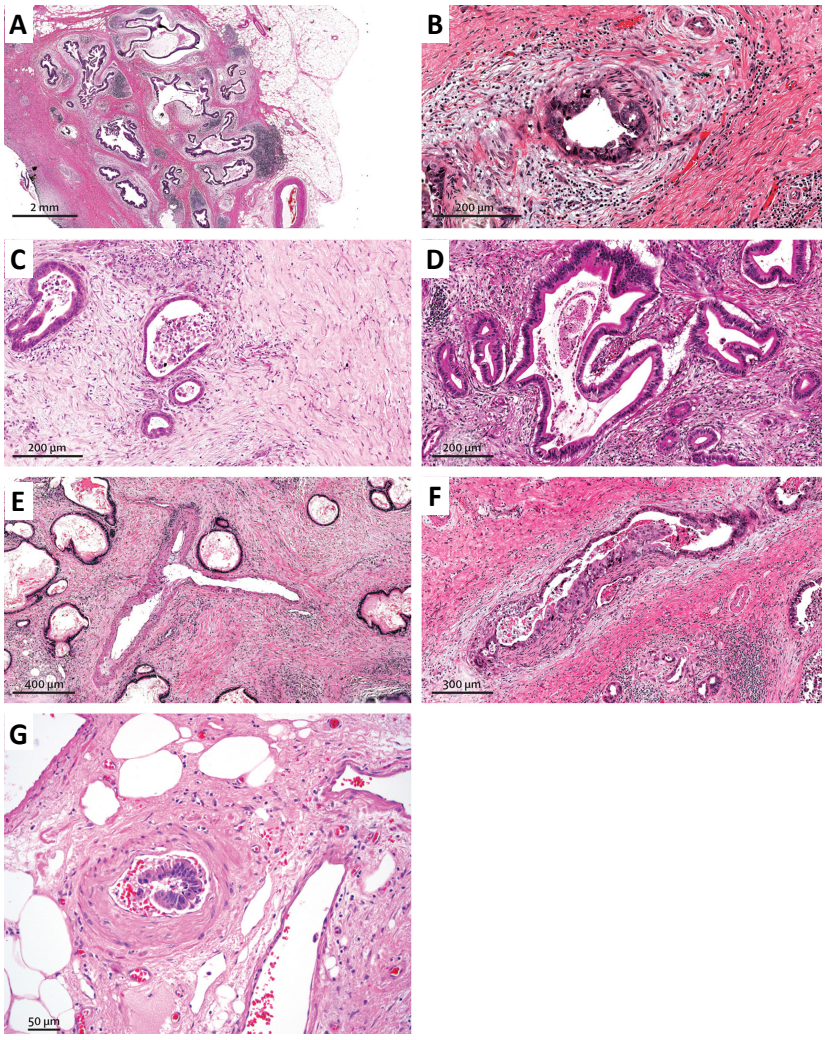


**Figure 1.2: Histology of pancreatic ductal adenocarcinoma (PDAC).** The histological characterisation of PDAC is defined by distinct features. These include (A) haphazard arrangement of glands, (B) nuclear pleomorphism, (C) incomplete glandular lumina, (D) luminal necrosis, (E) glands adjacent to muscular vessel, (F) perineural invasion and (G) lymphovascular invasion. Reprinted from (Kamisawa et al., 2016) with the permission from Elsevier, license number 4746071375060

## 1.2.3 Epidemiology and Etiology

Pancreatic cancer has been associated with several risk factors. These include: personal history of cigarette smoking (Iodice et al., 2008), ABO blood group alleles (Wolpin et al., 2010), chronic pancreatitis (Raimondi et al., 2010), obesity (Rawla et al., 2019), diabetes mellitus (Everhart and Wright, 1995), infectious disease such as Helicobacter pylori infection (Trikudanathan et al., 2011) and periodontal disease (Maisonneuve et al., 2017; Yadav and Lowenfels, 2013). Pancreatic cancer, in general, is associated with increasing

age, mostly prevalent in patients between 60-80 years of age. The incidence rate of the disease is 50% higher in men when compared to women (Kamisawa et al., 2016). Besides, approximately 10% of pancreatic cancer has a familial basis and carry germline mutations. These mutations are also generally associated with several other conditions such as: *PRSS1* and *SPINK1* mutation in hereditary pancreatitis (Lowenfels et al., 1997; Rebours et al., 2008), *CDKN2A* in familial atypical mole and multiple melanoma (FAMMM) (Lynch et al., 2008), DNA mismatch repair genes such as *MLH1, MSH2, MSH6* or *PMS2* in hereditary non-polyposis colorectal cancer (Lynch Syndrome) (Kastrinos et al., 2009), *STK11 (LKB1)* in Peutz-Jeghers syndrome (Korsse et al., 2013), and *BRCA2* in familial breast and ovarian cancer (Mocci et al., 2013). Taken together, the risk factors mentioned above share some common etiological pathways in pancreatic cancer including insulin resistance (Manami and Shoichiro, 2012), inflammation, DNA repair, immune response and pancreatic developmental genes as susceptibility factors for pancreatic cancer (Li et al., 2012).

## 1.2.4 PDAC diagnosis

Despite the identification of several risk factors, the survival rate of PDAC patients is very low — this is mostly attributed to the lack of early diagnosis. PDAC patients usually present as asymptomatic, with the disease being detectable only after they have advanced to later stage of development. Several techniques are currently utilised for the diagnosis of PDAC. Amongst these, the use of combined serum tumour markers is very common. PDAC express different molecular markers including carbohydrate antigen (CA)19-9, carcinoembryonic antigen (CEA), mucins such as MUC1, MUC4, MUC5AC and MUC16 (CA125) and cytokeratins such as CK7, CK19 and CK18 (Haeberle and Esposito, 2019). CA19-9, which is upregulated in the course of pancreatic cancer development, is most routinely used in the

diagnosis of PDAC. It has been demonstrated to provide reliable prognosis and predict overall survival and response to chemotherapy in symptomatic pancreatic cancer patients (Ballehaninna and Chamberlain, 2011). Moreover, the possible role of CA19-9 in early diagnosis of pancreatic cancer has been shown previously. During the study, they demonstrated significant upregulation of CA19-9 in pancreatic cancer patients up to 2 years before diagnosis (O'Brien et al., 2015). Recently, the mechanism of CA19-9 in the augmentation of aggressive phenotype of pancreatic cancer was shown using mouse model (Engle et al., 2019). Additionally, several imaging techniques have been employed for the diagnosis of pancreatic cancer including computerised tomography (CT), $^{18}$F-fluorodeoxyglucose- positron emission tomography (FDG-PET), endoscopic ultrasonography (EUS) and magnetic resonance imaging (MRI). The diagnostic accuracy of these methods has been reported in several studies (Kim et al., 2013; Park et al., 2009; Tummala et al., 2011; Yamaguchi et al., 2012).

## 1.2.5 PDAC treatment

Despite improved therapeutic interventions, surgical tumour resection still remains as the only curative option. The eligibility for this curative resection, however, is very low and mostly limited to only 10-20% of PDAC patients. Even among these patients with potentially resectable tumour, only around 20% patients achieve the 5-year survival period with macroscopic clearance. Most of the PDAC patients present with metastatic disease and account for 50-60% of cases. This occurs as PDAC is usually diagnosed at the late stage of tumourigenesis. The treatment regimen for these PDAC patients at the advanced disease stage commonly include palliative chemotherapy as the first-line therapy (Abbassi and Algul, 2019). This has mostly been conducted by using a single-agent drug,

gemcitabine, since being introduced in 1997 (Burris et al., 1997) . The use of gemcitabine, which is a nucleoside analogue, has so far provided minimal benefit to the overall survival of PDAC patients (Kim and Gallick, 2008). For better survival of locally advanced and metastatic PDAC patients, the use of gemcitabine-based combination therapy has been studied. Several agents have been used in addition to gemcitabine including erlotinib, capecitabine, platinum agents, 5-fluorouracil (5FU) and irinotecan (Sultana et al., 2008). Remarkably, two phase III clinical trials using first-line treatment regimens, FOLFIRINOX (oxaliplatin, irinotecan, fluorouracil (FU) and leucovorin) (Conroy et al., 2011) and nanoparticle albumin bound-paclitaxel plus gemcitabine (Von Hoff et al., 2013) displayed more favourable outcome for overall survival in patients with metastatic pancreatic cancer in comparison to gemcitabine alone.

Similarly, neoadjuvant therapy has been suggested for locally advanced, non-metastatic PDAC. A systematic review and meta-analysis of data from randomised control trials suggested that one-third of PDAC patients with initially unresectable tumours were qualified to undergo tumour resection following neoadjuvant chemo- and/or radiotherapy. Additionally, the survival rate for these patients was comparable to PDAC patients who were initially staged for resectable tumours (Gillen et al., 2010).

Radiation therapy has been utilised as local treatment in pancreatic cancer patients as neoadjuvant, adjuvant or definitive treatment. Chemoradiotherapy given preoperatively to patients with resectable or borderline resectable pancreatic cancer displayed improved resection rate in comparison to patients who underwent immediate surgery in a multicentre phase III clinical trial, PREOPANC-1 (Versteijne et al., 2020). The overall benefit in the patients' survival from the results of this study, however, appeared to be non-significant. Similarly, for locally, advanced pancreatic cancer (LAPC) patients, the role of

conventional, fractionated radiotherapy has been utilised without much benefit. In regard to this, a randomised phase III clinical trial, LAP07, was conducted to investigate the benefits of chemoradiotherapy – that included 54 Gy radiation dose and capecitabine as the chemotherapy drug – in LAPC patients in comparison to chemotherapy alone (gemcitabine with/without erlotinib). The results demonstrated no significant difference in the overall survival of LAPC patients who received chemoradiation treatment. Of note, prior to this consolidation chemoradiation, the patients in the LAP07 trial had undergone four months of induction chemotherapy (gemcitabine with/without erlotinib) and demonstrated progression-free survival (Hammel et al., 2016). Currently, a randomised phase II clinical trial, SCALOP-2, is being conducted in LAPC patients to examine the advantage of different chemoradiation schedules including standard- and high-dose radiotherapy with or without the addition of radiosensitiser, Nelfinavir, following induction combination chemotherapy of gemcitabine and nab-paclitaxel (Strauss et al. 2019). Furthermore, for patients with advanced or metastatic pancreatic cancer, previous studies demonstrated palliative radiotherapy to be effective with better pain relief in the majority of patients receiving the treatment (Ebrahimi et al., 2017; Wolny-Rokicka et al., 2016).

Other treatment strategies that could potentially be applied to guide personalised treatment decisions in PDAC patients at the advanced stage include genomic profiling (Chantrill et al., 2015). Similarly, targeting specific genetic aberrations or altered signalling pathways would also be greatly advantageous. In this context, a phase III trial, POLO (Pancreas Cancer Olaparib Ongoing) evaluated the efficacy of the PARP inhibitor, Olaparib. The study demonstrated that the administration of Olaparib, which allows DNA damage accumulation and death of tumour cell, displayed prolonged survival in metastatic PDAC patients with *BRCA1/2* mutations (Golan et al., 2019). Similarly, other therapeutic

approaches that hold promising results in future include therapies that target highly mutated *RAS* oncogene, desmoplastic stroma, hypoxia and pancreatic cancer metabolism (Kamisawa et al., 2016; Lanfredini et al., 2019). Additionally, immunotherapy provides yet another interesting avenue in the treatment of pancreatic cancer. The blockade of immune checkpoint including cytotoxic T-lymphocyte associated antigen 4 (CTLA-4) and programmed death 1/programmed death ligand 1 (PD-1/PD-L1) have been evaluated in clinical trial studies. These findings have, thus far, failed to show any positive clinical response(Shen et al., 2019; Torphy et al., 2018). Besides, vaccine therapy using mutated RAS peptide to induce T cell immunity has been shown by a previous study as a more viable option (Weden et al., 2011).

The tumour microenvironment of PDAC consists of intense stromal desmoplastic reaction and are composed of various components including pancreatic stellate cell, extracellular matrix proteins, fibroblasts and immune cells (Neesse et al., 2015). This tumour desmoplasia, in turn, has been speculated to act as a physical barrier in effective delivery of chemotherapy drugs to the tumour cells (Liu et al., 2017; Uzunparmak and Sahin, 2019). Accordingly, investigations to target and deplete the tumour stroma have been carried out. The data generated as a result of these studies have been, however, rather contradictory. A Phase II clinical study using a Hedgehog antagonist, Vismodegib, – to reduce stroma – plus gemcitabine displayed no favourable survival benefits in PDAC patients (Catenacci et al., 2015). Paradoxically, a number of studies using murine knockout model of Sonic Hedgehog (SHH) – which promotes desmoplastic stromal response in pancreatic cancer (Bailey et al., 2008) – showcased augmentation of tumour progression, reduced survival and increased vascular density (Lee et al., 2014; Rhim et al., 2014). Overall, further investigation is required to fully understand the complex biology of the tumour

microenvironment. This would, in turn, enable utilisation of the desmoplastic surrounding as a viable target for pancreatic cancer treatment (Torphy et al., 2018).

## 1.2.6 Pancreatic lesions

The progression of PDAC is commonly initiated through the incidence of precursor lesions. These precursor lesions were first suggested as early as 1953 by Sommers and colleagues where they reported high prevalence of hyperplastic ductal structures in pancreatic cancer patient samples. These histologically distinct, papillary proliferative lesions were present mostly in pancreas with ductal adenocarcinoma (Cubilla and Fitzgerald, 1976; Sommers et al., 1954). This was subsequently confirmed by histological analysis which suggested that ductal hyperplasia goes through progressive stages of non-papillary to papillary and atypical hyperplasia before forming invasive adenocarcinoma (Kozuka et al., 1979). Furukawa et al. further justified the classification of PDAC tumourigenesis – based on the stepwise progression of ductal epithelial atypia to hyperplasia – through morphometry and multivariate analysis (Furukawa et al., 1994). Strong support for ductal hyperplasia advancing into adenocarcinoma was provided by several case studies of pancreatic cancer patients. In these, patients with histologically identified papillary ductal atypia ultimately formed infiltrating ductal pancreatic adenocarcinoma (Brat et al., 1998; Brockie et al., 1998). Based on these observations, a more relevant nomenclature was given to the ductal hyperplastic structure and was termed as Pancreatic Intraepithelial Neoplasia (PanIN) lesion (Brat et al., 1998; Klimstra and Longnecker, 1994). By definition, PanIN lesions are microscopic (usually <5 mm in diameter), non-invasive epithelial neoplasia which are either flat or papillary in structure (Kawada et al., 2013).

PanIN lesions have been well-described at their histological, pathological and molecular

levels (Figure 1.3). Accordingly, based on the degree of cytological and architectural changes, these lesions were graded into different stages as PanIN-1A, PanIN-1B, PanIN-2 and PanIN-3. This classification system that defined the progression model for the PanIN lesion (Hruban et al., 2004; Kern et al., 2001) was developed at an international meeting sponsored by the U.S. National Cancer Institute in 1999. According to the definition, cuboidal cells in normal ductal epithelia transit into tall, columnar cells in PanIN-1A lesions with no atypia and basally located nuclei. PanIN-1B lesions are almost identical to PanIN-1A except for papillary or basally pseudostratified architecture. Mucinous PanIN-2 lesions are mostly known to be papillary and contain nuclear abnormalities including loss of polarity, nuclear crowding, enlargement of the nuclei and pseudostratification. PanIN-3 lesions are also papillary or micropapillary and display “budding off” of the epithelium into the lumen. Severe atypia is usually observed in PanIN-3 along with the presence of dystrophic goblet cells. However, unlike PDAC, PanIN-3 lesions lack invasion of the basement membrane (Hruban et al., 2004).

Although this full spectrum of PanIN lesions was informative, the relevance of PanIN-1 and PanIN-2 lesions presented little clinical significance. In order to match the clinical needs based on histological assessment of precursor lesions, the three-tier classification system was revised at an international meeting organised by Ralph H. Hruban and David S. Kilmstra in 2014. Precursor lesions were re-classified into two-tier system in which PanIN-1 and PanIN-2 were termed together as low-grade and PanIN-3 as high-grade PanIN lesions (Basturk et al., 2015).

While PanIN lesions are the most well-known precursor lesions of PDAC, other common precursor lesions comprise of cystic lesions such as: Intraductal Papillary Mucinous Neoplasm (IPMN) and Mucinous Cystic Neoplasms (MCN) (Distler et al., 2014). Briefly,

IPMNs arise from the main pancreatic duct or branch ducts and, similar to PanINs, are non-invasive, mucin-producing epithelial neoplasms. However, unlike PanINs they are grossly visible, mostly papillary in structure and rarely flat (Basturk et al., 2015). MCNs, in contrast, do not communicate with the pancreatic duct system and are presented as thick-walled, multiloculated, cystic neoplasm that are sheathed with columnar mucinous epithelium (Ricard Masia et al., 2011). Similar to PanIN lesions, both IPMNs and MCNs have recently been classified into two stages of low-grade and high-grade dysplasia (Basturk et al., 2015; Distler et al., 2014). Unlike non-cystic PanIN lesions which are usually only detectable from the microscopic assessment of pancreatic resection of biopsy specimens, the cystic lesions, IPMNs and MCNs, are commonly diagnosed through radiological examinations (Ren et al., 2019).

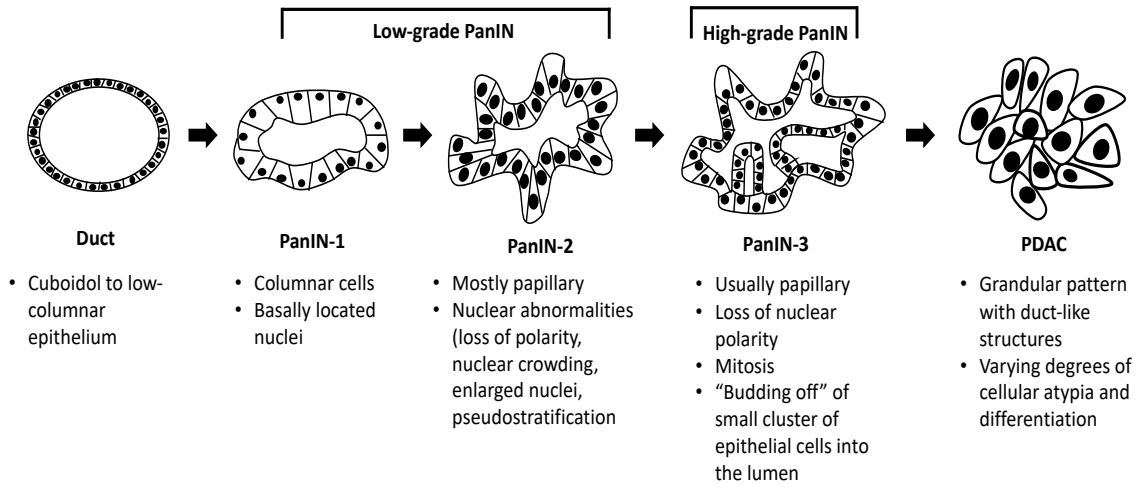


**Figure 1.3 : Schematic diagram representing progression model of pancreatic carcinogenesis.** A multi-step progression of tumourigenesis in pancreas, including a series of PanIN lesions representing specific architectural and cytological features. More recently, the classification model of PanIN lesions were revised from three-tier to two tier system. PanIN-1 and PanIN-2 were grouped together as low-grade PanIN lesions while PanIN-3 as high-grade lesions.

***Formation of PanIN lesions through acinar cell plasticity***

There are increasing number of evidences suggesting PanIN lesions formation to be preceded by the process of acinar cells transforming to acquire ductal phenotype. This is attributed to the high plasticity of acinar cells in adult pancreas, that enables the cells to transform their differentiation commitment and transdifferentiate to an embryonic progenitor phenotype expressing ductal markers. This process of transformation is termed as acinar-to-ductal metaplasia (ADM) (Storz, 2017) and can be induced by a number of factors including hyperactivated KRAS induced metabolic stress and enhanced epidermal growth factor receptor (EGFR)/mitogen-activated protein kinase (MAPK) signalling (Liou et al., 2016), inflammatory response including cytokines secreted by macrophage (Liou et al., 2013) and deregulation of epithelial cellular polarity (Hezel et al., 2008).

***Incidence and progression of PanIN lesions***

Peters et al. defined the time between PanIN onset to PDAC progression as “dwell time” (Peters et al., 2018). The importance of this dwell time was highlighted in early detection of PanIN lesions and PDAC treatment. Observational data presenting the sequential progression of PanIN lesions to PDAC is unattainable. This arises as there is a difficulty in directly detecting PanIN lesions which are observable only through pathology. Based on a simulation model of the natural history of PDAC in hypothetical populations, PanIN lesions were shown to increase slowly by age such that by age 80 almost 74% of both men and women would attain at least one PanIN-1 lesion. Of note, this simulation model fitted the data from the National Cancer Institute's Surveillance, Epidemiology, and End Results program and published literature on PanIN prevalence by age (Peters et al., 2018). The probability of PDAC formation in an individual, however, is highly dependent on the incidence of PanIN-3 lesions in the pancreas. It is attributed to the ability of PanIN-3 lesions

to invade beyond the basement membrane of pancreatic ductal epithelium (Kawada et al., 2013). As expected from their model, Peters et al. reported that the dwell time between PanIN-3 to PDAC was rapid – around 11.8 years– whereas that between PanIN-1 to PDAC was around 34.5 years (Peters et al., 2018). This stretched time period of PanIN-1 lesion progression to PDAC was also reiterated by Makahon-Moore et al. in 2008. In this study, high-grade PanIN-3 lesions were shown to act independently as a single neoplasm which invade the pancreatic ductal system. In turn, genetic and spatial changes is acquired over the course of progression of PanIN-3 lesions to PDAC. Similarly, the homology of genetic alterations with PDAC was stronger in high-grade PanIN-3 lesions when compared to the low-grade PanIN (PanIN-1 and PanIN-2) lesions (Makohon-Moore et al., 2018).

## 1.3 Molecular biology of pancreatic cancer

### 1.3.1 *KRAS* mutations

***Introduction to KRAS***

Major molecular events alter as low-grade PanIN lesions progress towards high-grade and eventually form PDAC. These irregularities in the PanIN lesions are observed at the genomic, transcriptomic and proteomic levels (Feldmann et al., 2007). In the context of genetic signatures, each stage of pancreatic lesion is associated with specific genetic mutations (Figure 1.4). Amongst these, activating mutations of *KRAS* occur as one of the most frequent events in PDAC tumourigenesis. Aberrant KRAS signalling due to the mutation in *KRAS* occurs very early on during PanIN-1 (low-grade) lesions, indicating a critical role of the mutated oncogene in PDAC initiation. Moreover, *KRAS* mutation also drives the progression of PDAC as it is present throughout various stages of PanIN lesions

along with the tumour (Waters and Der, 2018). KRAS was first discovered in 1967 due to its transforming activity in Kirsten rat sarcoma retrovirus (Kirsten and Mayer, 1967). Prior to this, the transforming activity of Harvey rat sarcoma retroviruses led to the discovery of HRAS (Harvey, 1964), another member of the RAS superfamily. Few years later, an additional member of the family, NRAS, was discovered in sarcoma, leukaemia and neuroblastoma cell lines (Hall et al., 1983). All three RAS isoforms induced oncogenic phenotype and led to tumour formation in human and mouse genome (DeFeo et al., 1981; Der et al., 1982; Parada et al., 1982; Vousden and Marshall, 1984). The *KRAS* gene, unlike the other two isoforms, gives rise to two splice variants, KRAS4A and KRAS4B due to alternative splicing (Capon et al., 1983; Tsai et al., 2015).

Despite the differences, all three isoforms of RAS share the same biochemical activity. RAS proteins (~21 KDa) shuttle between a GTP-bound active form, regulated by guanine-exchange factor (GEF), and a GDP-bound inactive form, regulated by GTPase activating protein (GAP). A number of growth factors and mitogens relay signals from the external environment to the plasma membrane where RAS proteins are primarily localised. Canonically, the stimulation of receptor tyrosine kinases, including platelet-derived growth factor receptor (PDGFR) and epidermal growth factor receptor (EGFR), enables the recruitment of the GEF protein, Son of Sevenless (SOS) to the plasma membrane, in close proximity to RAS. This recruitment takes place through the adaptor protein, Growth Factor Receptor-Bound-2 protein (GRB2). SOS, in turn, replaces GDP in RAS with GTP, leading to the protein activation (Bowtell et al., 1992; Egan et al., 1993; Gale et al., 1993; Li et al., 1993). In normal wild-type conditions, the termination of this RAS activation is ensured by a GAP protein which mediates GTP hydrolysis and converts the RAS proteins back into inactive state. The maintenance of homeostasis in normal tissue through the alternation

between GEF and GAP is aberrated during RAS oncogenic mutation. RAS proteins lose the ability to interact with GAPs. This attenuates GTP hydrolysis and, instead, accentuates GEF mediated RAS activation, enabling the RAS proteins to remain in constitutively active state (Ellis and Clark, 2000; Karnoub and Weinberg, 2008). RAF1 is a bona fide downstream effector of RAS. Downstream of active RAS, RAF1 subsequently transduces activation signals to mitogen activated protein kinase kinase (MEK) and ultimately extracellular signal-related kinase (ERK) 1/2 through phosphorylation (Moodie et al., 1993; Vojtek et al., 1993). Activated ERK 1/2 can, in turn, translocate into the nucleus and regulate a myriad of biological processes including cell cycle, apoptosis, proliferation, differentiation and migration (Eblen, 2018). Moreover, RAS is also associated with several other downstream effectors including Ral guanine nucleotide dissociation stimulator (Ral-GDS), phosphatidylinositol 3-kinase (PI3K), AF6, p120GAP, RASSF/NORE1, TIAM, RIN1, PLCε and PLCζ. Hence, KRAS/MAPK signalling has been shown to influence pro-tumourigenic effects in a number of cancer development and progression (Lanfredini et al., 2019; Rajalingam et al., 2007).

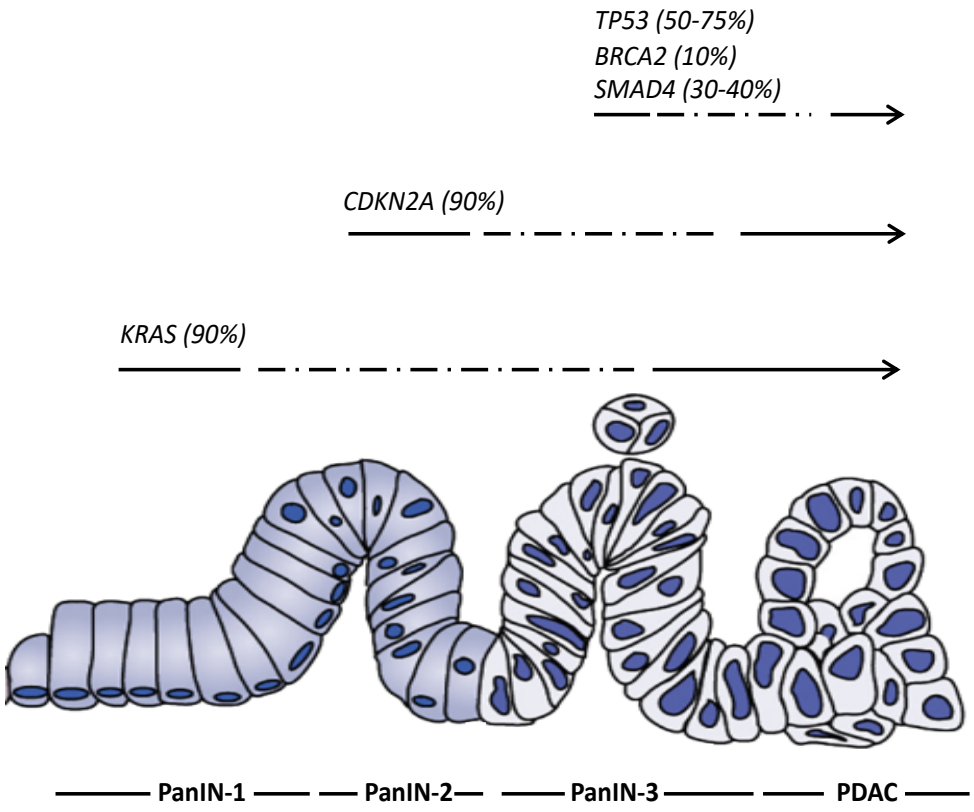


**Figure 1.4: Molecular alterations during the histological progression of precursor lesions into pancreatic ductal adenocarcinoma.** Each stage of PanIN lesions accumulate genetic and epigenetic changes during tumourigenesis that enable rapid progression and maintenance of PDAC. *KRAS* mutation occurs as an early event and is maintained throughout the multiple stages. 90% of PDAC cases harbour *KRAS* mutations by the time they transform into invasive adenocarcinoma. This is followed by inactivation of *CDKN2A* which occurs during the PanIN-2 lesion stage and is prevalent in 90% of pancreatic cancers. Inactivation of *TP53* and *SMAD4* occur as late event in 50-75% and 30-40% of pancreatic cancers respectively. Germline mutation of *BRCA2,* which takes place during the high-grade PanIN3 lesions, is observed in 10% of PDAC cases. Figure adapted from (Ferreira et al., 2017) and is an open access under the Creative Commons Attribution License.

### *KRAS mutation in PDAC*

Mutations of *RAS* occur through single base substitution at codons 12, 13 and 61 (G12, G13 and Q61) – each with the potential of converting into six amino acids. While each isoform displays differential mutation depending on cancer types, *KRAS* mutations are present, comparatively, at the highest frequency in cancer – 82% of which occur at G12 (Lanfredini et al., 2019; Prior et al., 2012). *KRAS* mutations occur in the majority of PDAC tumourigenesis; the early events of acinar-to-ductal metaplasia (ADM) and low-grade PanIN lesions presented *KRAS* mutations in up to 63% and 74% of cases respectively (Shi

et al., 2009), while in PDAC it arises up to 90% (Biankin et al., 2012; Kanda et al., 2012). In particular, the most frequent *KRAS* mutations in PDAC included the transversion of nucleotide guanine (G) to adenine (A) and thymine (T) at the second base, resulting in Glycine-to-Aspartate (G12D) and Glycine-to-Valine (G12V) mutations (Ying et al., 2016). Interestingly, this variation in KRAS codon mutation – that lead to differential amino acid replacement – determine variation in prognostic value in the clinic. In particular, G12D mutation in PDAC patients are presented with lower overall survival (Lanfredini et al., 2019). Similarly, whole-exome sequencing of PDAC presented mutations at Q61 of *KRAS* to associate with favourable clinical outcome (Witkiewicz et al., 2015). Similarly, the allelic imbalance due to increase in *Kras* G12D gene dosage, in a mouse model with conditional *Kras* mutations in pancreas, was associated with shorter overall survival, early progression and metastasis in PDAC (Mueller et al., 2018).

The mutational status of *KRAS*, however, is yet to predict therapeutic response in PDAC patients (Bournet et al., 2016). Additionally, direct targeting of KRAS for drug treatment is difficult. This primarily is due to the biochemical function and structural properties of the protein. Activating mutations favour the KRAS protein to remain in a GTP-bound active state. The affinity for KRAS binding with GTP is high – usually in the picomolar range. This, as a result, prevents binding of any competitive inhibitors. Structurally, the KRAS catalytic domain lacks any deep hydrophobic pockets. This makes the protein incompatible for targeting by high-affinity small binding molecules (Cox et al., 2014). While the National Cancer Institute has also enlisted targeting of KRAS as one of the crucial components in PDAC research, treatment strategies developed so far have proven ineffective. Hence, current efforts to target tumours with *KRAS* mutations, are focussed more on alternative

approaches including disruption of downstream signalling components and immunotherapy-based approach (Lanfredini et al., 2019).

### 1.3.2 Other genetic mutations in PDAC

Besides activating mutations of *KRAS*, additional genetic events are associated with the later stages of development of PanIN lesions. These genetic alterations include inactivation of tumour suppressor genes, *CDKN2A, SMAD4 and TP53*. The genetic change in the *CDKN2A* gene (chromosome 9p21), encoding for the cell-cycle checkpoint protein $p16^{INK4A}$ that inhibits cyclin dependent kinases CDK4 and CDK6, eliminates the inhibition of G1-S cell-cycle arrest (Feldmann et al., 2007; Serrano et al., 1993). Alongside, the inactivated *CDKN2A* also abrogates G1 and G2 cell cycle arrest as the gene encodes for another distinct protein, $p19^{ARF}$. $p19^{ARF}$, that arises from alternative reading frame of the *CDKN2A* gene, regulates cell cycle arrest by inhibiting MDM2 and as a result stabilising and augmenting the function of p53 transcription factor (Ivanchuk et al., 2001; Ouelle et al., 1995). *CDKN2A* inactivation presents in 90% of pancreatic cancers and occur due to several factors including intragenic mutation, homozygous deletion and hypermethylation of CpG islands of the gene (Schutte et al., 1997; Ueki et al., 2000). Similarly, inactivation of *TP53*, mainly due to intragenic deletion (Redston et al., 1994), occurs in the high grade PanIN-3 lesions and is prevalent in 50-75% pancreatic cancers. The consequent loss of p53 function (Jimenez et al., 1999) allows cells to bypass DNA damage checkpoints and apoptosis during PDAC tumourigenesis. Another late genetic event in PDAC progression is the loss of SMAD4, also known as Deleted in Pancreatic Carcinoma 4 (DPC4). Inactivation of *DPC4* also occur in PanIN-3 lesions and is present in 30-40% of pancreatic cancer. Consequently, the loss of SMAD4 disturbs the TGF-β signalling cascade, leading to increased cell proliferation (Feldmann et al., 2007). PDAC is most commonly identified as a sporadic disease. A few

percentages of PDAC cases (around 10%), however, have been associated with familial syndrome with germline mutations in a number of genes including *BRCA1*, *BRCA2*, *ATM*, *STK11*, *PRSS1, SPINK1* and DNA mismatch repair genes (Blair et al., 2018) (as described previously).

Despite the high prevalence of *KRAS* mutation during PDAC development, there is a small subset of tumours that lacks complete dependency on the protein's function. Muzumdar et al. demonstrated, through Crispr/Cas9-mediated knockout of KRAS expression in PDAC cells, the reliance of KRAS-deficient cells on other signalling pathways including phosphoinositide 3-kinase (PI3K)-dependent mitogen-activated protein kinase (MAPK) signalling for survival and proliferation (Muzumdar et al., 2017). Prior to this, an oncogene, YAP, had been identified to contribute in the progression of mutated *KRAS*-deficient PDAC using both *in vitro* and *in vivo* models (Kapoor et al., 2014; Shao et al., 2014). This will be discussed in more detail in the next section of this chapter.

### 1.3.3 Introduction to Hippo pathway and its importance in cancer

***Hippo pathway in Drosophila***

The Hippo pathway is an evolutionary conserved pathway, known primarily for its role in the control of organ size by orchestrating opposing functions of both cell proliferation and apoptosis. The pathway was first reported in *Drosophila* after the discovery of four protein components that formed the core kinase cascade of the pathway. Several groups reported the discovery of the Ste20-like protein kinase Hippo (Hpo) in 2003, which forms the upstream basis of the signalling hub (Harvey et al., 2003; Jia et al., 2003; Pantalacci et al., 2003; Udan et al., 2003; Wu et al., 2003). The Hpo protein transduces signal by partnering with the scaffold, WW domain containing protein called Salvador (Sav) (Tapon et al., 2002).

The Sav protein is bound to the NDR family kinase protein Warts (Wts) (Justice et al., 1995; Xu et al., 1995). This leads to Hpo-mediated phosphorylation of the Wts protein (Tapon et al., 2002). Additionally, Mob-as-tumour suppressor (Mats) was later reported by Lai et al. in 2005 to form complex with Wts and promote its kinase activity. Loss-of-function mutation in any of these components lead to tissue overgrowth (Lai et al., 2005). Subsequently, yeast two-hybrid screen for Wts-binding proteins revealed Yorkie (Yki) as the prime downstream target of Hpo-Sav-Mats-Wts kinase complex. In particular, Wts protein negatively regulated Yki by phosphorylating it at Ser168 (Huang et al., 2005). The antagonistic effect on Yki, upon phosphorylation, occurred due to the binding of the inhibitor 14-3-3 which, in turn, led to cytoplasmic retention of the protein (Oh and Irvine, 2008). Accordingly, eye-specific overexpression of Yki, mutated in the phosphorylation site Ser 168, ($Yki^{S168A}$), led to an overgrowth of the *Drosophila* eye. This elicited the role of Yki as an oncogene (Dong et al., 2007) (Figure 1.5.A).

***Hippo pathway in Mammals***

The core kinase cascade of the Hippo pathway in *Drosophila* is conserved throughout the eukaryotic kingdom, including mammals. The mammalian homologs of the core kinase cascade are Hpo: MST1 and MST2, Sav: Sav1 or WW45, Wts: LATS1 and LATS2 and Mats: MOB1. These components were able to functionally rescue the respective Drosophila mutants *in vivo*, indicating evolutionary conservation of a functional hierarchy between the fruit fly and mammals including humans (Edgar, 2006). As seen in Drosophila, MST1/2, SAV1, LATS1/2 and MOB1 form a core kinase cassette and transduce signal to phosphorylate YAP which is a mammalian homolog of Yki. Similarly, YAP's phosphorylation by LATS1/2 on Ser 127 site enables binding of 14-3-3 which in turn blocks nuclear translocation of YAP (Zhao et al., 2007) (Figure 1.5.B).

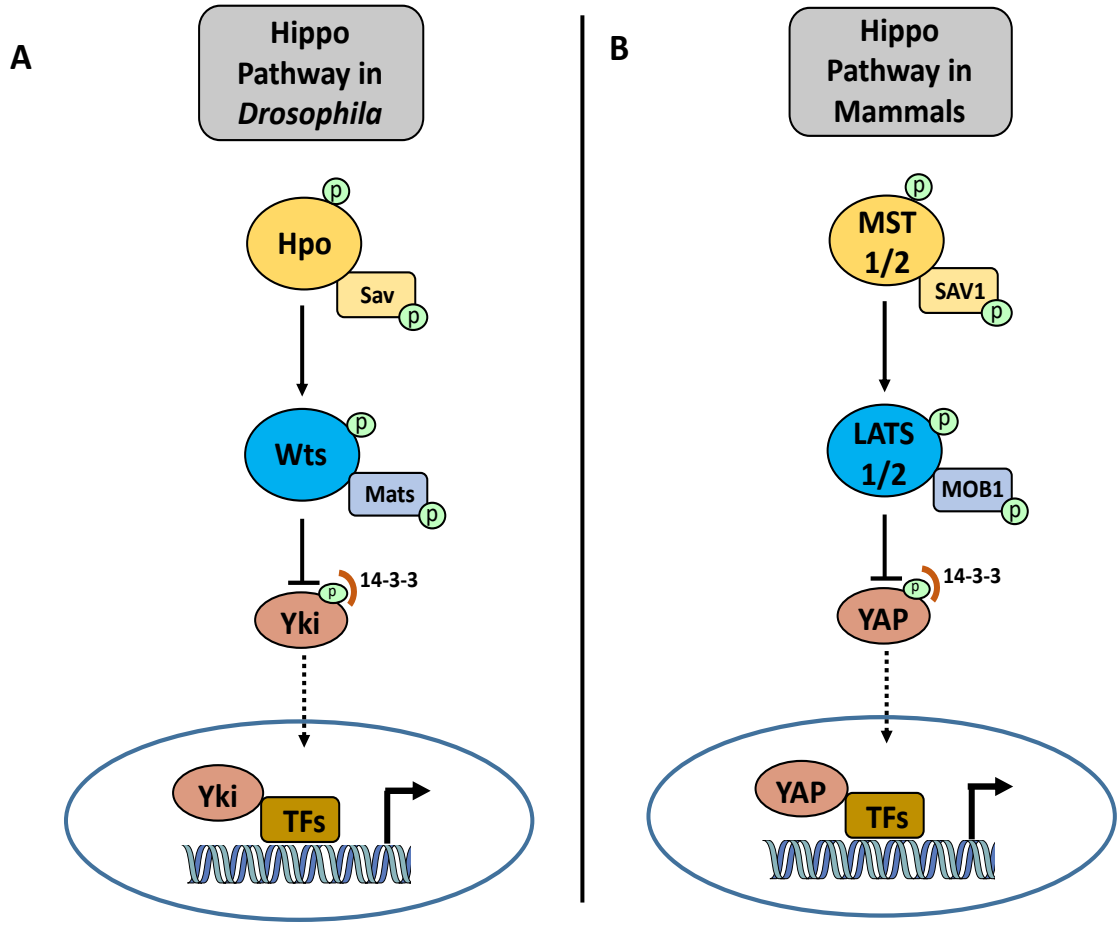


**Figure 1.5. Simplified overview of the core components of Hippo pathway in (A) Drosophila and (B) Mammals**. Activation of the Hippo pathway due to the upstream regulators, including NF2 and RASSF1A, stimulates MST1/2 kinase activation in mammals and Hpo in *Drosophila*. This, in turn, phosphorylates and activates LATS1/2 and Wts respectively. As a result, LATS1/2 phosphorylates YAP on Ser 127 while Wts phosphorylates Yki on Ser 168. The phosphorylation allows the inhibitory protein, 14-3-3, to bind to YAP(Yki) proteins and retain them in the cytoplasm. In cancers, the inactivation of Hippo pathway prevents LATS1/2 (Wts) from negatively regulating YAP (Yki), which is then translocated into the nucleus to activate several transcription factors including TEAD (Scalloped in *Drosophila*). Consequently, this results in a number of cellular effects such as cell proliferation, survival and anti-apoptosis. Figure modified from (Taha et al., 2018).

### *Introduction to YAP*

YAP was first identified as a novel transcriptional co-activator by Yagi et al in 1999. This study demonstrated that YAP contains a WW domain which binds strongly to the PY motif of the transcriptional factors and activates the transcription of several target genes (Yagi et al., 1999). YAP is a candidate gene driving the chromosome 11q22 amplicon in human

cancers (Overholtzer et al., 2006). Sudol in 1994 first characterised YAP as a novel protein that bound to Src homology domain 3 (SH3) of Yes proto-oncogene product. Moreover, the protein was identified to have a molecular mass of 65 kiloDalton (kDa), hence the name was given as Yes-Associated Protein of 65 kDa (YAP65). Subsequently, YAP65 (referred as YAP in this thesis) was found to bind to other SH3 domain containing molecules including Non-catalytic region of tyrosine kinase protein adaptor 1 (Nck), CT10 Regulator of Kinase (Crk), Abelson murine leukemia viral oncogene homolog (Abl) and GTPase activating protein (GAP) (Sudol, 1994).

The amplification of 11q22 amplicon, which resides the YAP gene locus, has previously been identified in PDAC (Bashyam et al., 2005). YAP is also emerging as a key player in the neoplastic development of pancreatic exocrine cells (Kapoor et al., 2014; Zhang et al., 2014). The deletion of YAP's expression, using Cre-lox system, in adult mouse pancreas demonstrated YAP to be dispensable in the normal development of the pancreas. While this YAP deletion, alongside concomitant expression of mutated *Kras* in the pancreas, was also shown to be inessential in the initiation of ADM, it led to complete abrogation of PanIN lesions development and PDAC formation. This indicated that YAP might be absolutely critical in the progression of PanIN lesions to PDAC (Zhang et al., 2014).

Kapoor and colleagues in 2014 demonstrated a critical role for YAP in the progression of PDAC that is independent of constitutive activation of mutated *KRAS*. In *Kras* $^{G12D}$ inducible mouse model, primary tumours regressed after the withdrawal of oncogenic *Kras* induction. This was, however, followed by tumour relapse in some tumours. Intriguingly, these tumours were devoid of mutated KRAS expression and canonical downstream MAPK signalling. Instead YAP was revealed to be crucial in the relapse and progression of these oncogenic KRAS independent tumours (Kapoor et al., 2014). Similarly, *in vitro* studies using

human PDAC cell lines also demonstrated YAP's ability to replace oncogenic function of KRAS (Shao et al., 2014). Of note, both studies suggested YAP interaction with transcription factors to be context dependent. Proteins belonging to TEAD family members (TEAD1-4) are one of the best characterised binding transcription factors of YAP (Vassilev et al., 2001). The promoter binding activity of YAP/TEAD complex enables various cellular phenotypes including cell proliferation, survival, oncogenic transformation and epithelial-to-mesenchymal transition (EMT) (Camargo et al., 2007). As a result, YAP regulates transcription of a myriad of target genes including *CTGF* (Zhao et al., 2008), *AREG*(Zhang et al., 2009), *MYC* (Neto-Silva et al., 2010) and *AXL* (Xu et al., 2011). In a differing cellular context, however, a tumour-suppressive role of YAP has also been reported (Kim et al., 2018). Severe cellular stress due to DNA damage induces c-ABL activation which, in turn, phosphorylates YAP on Tyrosine 357 (Y357). Subsequently, the phosphorylated YAP proteins (Y357) translocate into the nucleus and interact with p73. The YAP/p73 complex, as a result, activates transcription of pro-apoptotic genes including BAX and PIG3, enhancing the tumour suppressive mechanism of YAP in a different cellular context (Cottini et al., 2014; Keshet et al., 2015; Levy et al., 2008).

Moreover, this context dependency of YAP seemed to go beyond transcription factors and appeared to be involved in the molecular subtypes of PDAC. Accordingly, highly activated YAP was involved in the progression of squamous subtype of PDAC. Notably, the squamous subtypes displays a more aggressive phenotype clinically, in comparison to other PDAC subtypes including a pancreatic progenitor class. Furthermore, YAP also played a role in elevating the malignancy of progenitor subtype by enabling their switch into the squamous PDAC subtype (Tu et al., 2019).

Importantly, YAP's role in embryogenesis was highlighted through embryonic lethal phenotype in mice with homozygosity for the *Yap*$^{tm1Smil}$ allele (*Yap*$^{-/-}$) (Morin-Kensicki et al., 2006). Additionally, YAP has been identified as a prognostic marker in pancreatic cancer patients. Importantly, YAP target genes – including *Areg*, *Notch2*, *Ccnd1*, *Cdk6*, *Ajuba* and *Serp1* – along with inducers of YAP activation, such as growth factors: TGFa and HBEGF growth factors, integrin: ITGA2, receptors: $P2Y_2R$ and GPR87 and mucin: MUC1, have all been associated with poor survival outcome of PDAC patients. Likewise, the increased expression of several components that are known to inhibit YAP activation, including AMPK, STRAD, MARK1, PKA and TSC1/TSC2, has been associated with favourable prognosis for PDAC patients (Rozengurt et al., 2018).

***Introduction to TAZ***

Besides YAP, TAZ (also known as WWTR1) is also phosphorylated by LATS1/2 in mammals (Lei et al., 2008). Indeed, TAZ protein is a paralog of YAP which was first identified as a WW domain-containing protein (Kanai *et al.* 2000). The WW-domain allows TAZ to bind to the PPxY motif of transcriptional factors, enabling the protein to enact as a transcriptional co-activator. Likewise, TAZ was also shown to be negatively regulated by 14-3-3 which binds to the protein upon phosphorylation on Ser89, equivalent to Ser127 of YAP. 45% of amino acid sequence homology was identified between human YAP and TAZ (Kanai et al., 2000). Structurally, two tandem WW domains present in human YAP is reduced to one WW domain in human TAZ protein (Figure 1.6). Similar to YAP, TAZ was also demonstrated to interact with TEAD for nuclear activity enhancement and oncogenic transformation (Chan et al., 2009). Expectedly, TAZ expression was elevated in human PDAC (Morvaridi et al., 2015).

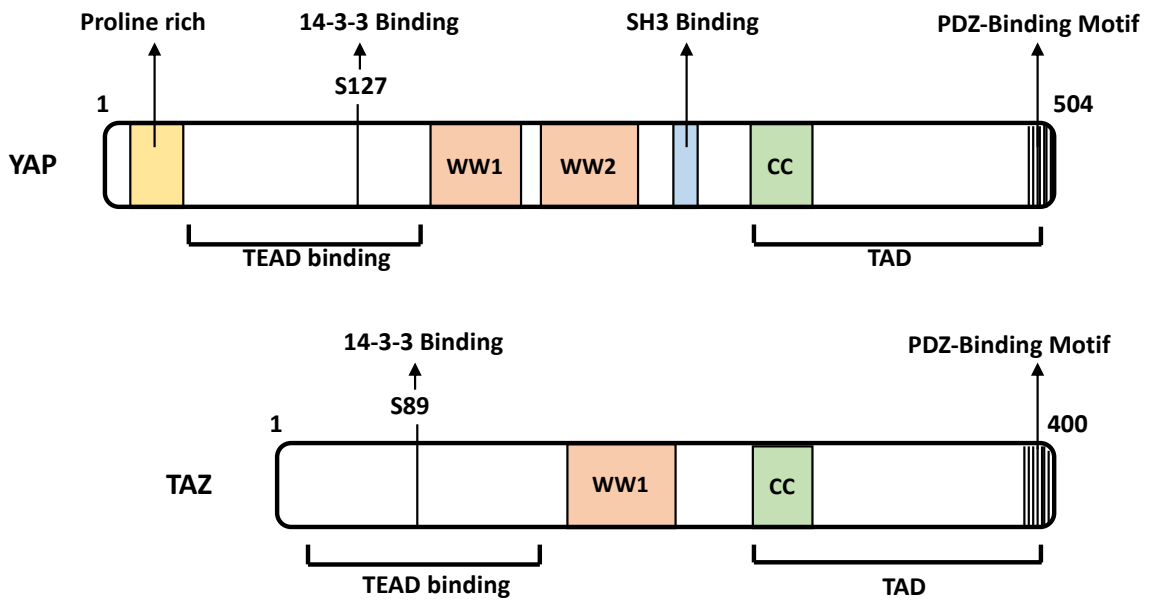


**Figure 1.6. Hippo pathway effectors, YAP and TAZ share 45% sequence homology.** Both YAP and TAZ contain important domains and regulatory modifications including WW domains ( two in YAP and one in TAZ, coiled-coin (CC) domain, TEAD binding domain, transcriptional activation domain (TAD) and PDZ-binding motif. YAP also contains SH3-binding domain. Phosphorylation in Ser127 in YAP and Ser89 in TAZ present as a binding site for 14-3-3 which leads to cytoplasmic retention. Figure modified from (Varelas, 2014)

### *NF2 in Hippo pathway*

NF2 is a well-known bona fide tumour suppressor gene and an upstream activator of the Hippo pathway. NF2 is clinically significant, with mutation of its gene leading to autosomal dominant disorder, Neurofibromatosis type 2 (Rouleau et al., 1993). During this condition, there is a development of multiple benign schwannomas which are associated with other brain-related tumours including meningiomas and ependymomas (McClatchey and Giovannini, 2005; Yu and Guan, 2013). The *NF2* gene, that lies in chromosome 22q12, encodes for the protein product Merlin. It is a 587 amino acid protein that belongs to the FERM (4.1, Ezrin, Radxin and Moesin) superfamily of proteins (Trofatter et al., 1993). Loss of heterozygosity in the *NF2* locus leads to the formation of a range of tumours including osteosarcoma, lymphoma, lung adenocarcinoma, hepatocellular carcinoma and fibrosarcoma with highly metastatic phenotype Initially identified as a tumour suppressor

gene (Rouleau et al., 1993; Trofatter et al., 1993), NF2 is primarily localised in the plasma membrane: cytoskeleton interface. Consequently, it is involved in the regulation of several biological processes including cell-cell communication, contact-dependent cell death or inhibition of proliferation, receptor trafficking via endocytosis, actin cytoskeleton remodelling and membrane organisation (McClatchey and Giovannini, 2005). Interestingly, the association of NF2 with the plasma membrane occurs at the apical surface of polarised epithelial cells (Bretscher et al., 2002). Furthermore, NF2 is involved in the regulation of cell-proliferation and apoptosis. This particularly occurs as the protein acts as an upstream regulator of the Hippo pathway. In *Drosophila*, NF2 promotes Wts phosphorylation and, as a result, controls Yki activity. Similarly, the NF2-mediated activation of Hippo signalling is highly conserved in mammals (Zhang et al., 2010). In the context of PDAC tumourigenesis, NF2's role is prominent and there is a loss of expression of the protein product in PDAC cell lines. Similarly, the exogenous expression of NF2 attenuated pancreatic cell growth, migration and invasion *in vitro,* along with tumorigenicity and metastasis of PDAC *in vivo* (Quan et al., 2015).

***RASSF1A in Hippo pathway***

*RASSF1* (Ras association domain family 1) is a gene located in 3p21.3 region of the human genome. The RASSF1 gene in this region produces eight isoforms — amongst these, transcripts A (RASSF1A) and C (RASSF1C) are ubiquitously expressed in normal tissues (Dammann et al., 2000). Interestingly, the expression of RASSF1A was shown to be lost in number of cancer cell lines, including breast, non-small lung and pancreatic cancer, highlighting tumour suppressive role of the protein (Burbee et al., 2001; Dammann et al., 2000). Similarly, functional inactivation of RASSF1A through complete genetic knockout led to spontaneous tumour formation *in vivo* including lung adenoma, lymphoma and breast

adenocarcinoma (Tommasi et al., 2005). Allelic imbalances of RASSF1A locus at 3p21.3 have been reported in a plethora of tumours including lung, breast, ovary, thyroid, brain, prostate and head and neck tumours (Donninger et al., 2007). Besides, epigenetic factors are shown to be mostly involved in the inactivation of RASSF1A, with most tumours presenting high percentage of hypermethylation of the RASSF1A promoter (Agathanggelou et al., 2001). Importantly, RASSF1A methylation provides significant clinical utility as it presents poor prognosis and associates with aggressive tumour phenotype in different cancer types (Grawenda and O'Neill, 2015).

Of note, Hippo pathway has been shown to elicit the tumour suppressive function through RASSF1A. RASSF1A is known to interact with the MST1 to induce apoptosis (Oh et al., 2006). Additionally, RASSF1A, by interacting with SAV1 proteins, induces MST2 autophosphorylation and ultimately leads to LATS1 phosphorylation. This complex, observed initially in *Drosophila*, enables cell cycle control and apoptosis, and is highly conserved among mammalian cells (Guo et al., 2007; Matallanas et al., 2007; Pefani et al., 2016). Similarly, there is a high loss of RASSF1A expression in human PDAC samples. This diminished expression of RASSF1A was highly correlated with frequent methylation of the gene promoter in PDAC (Amato et al., 2016). Intriguingly, high *KRAS* mutation has been shown to be associated with PDAC exhibiting unmethylated *RASSF1A*. The inactivation of *RASSF1A*, indeed, appeared to be mutually exclusive with mutated *KRAS* in PDAC (Dammann et al., 2003). This postulates a possible role of RASSF1A-related pathways in mediating KRAS signalling during PDAC tumourigenesis.

## 1.4 Models to study PDAC development

### 1.4.1 Genetically engineered mouse models (GEMMs) in PDAC

A novel mouse strain that could conditionally express mutated *Kras* was developed in 2001. In this, a mouse carrying a conditional $Kras^{G12D}$ knocked-in allele was used. The mutated allele was silenced due to the insertion of the STOP transcriptional cassette, flanked by two LoxP sites, into the endogenous locus upstream of the modified exon 1 for G to A transition in codon 12. Following the use of AdenoCre, the STOP element was removed. As a result, the homologous recombination led to the endogenous expression of oncogenic KRAS in the mouse lung adenocarcinoma (Jackson et al., 2001). This endogenous expression of mutant KRAS under physiological conditions was utilised by Hingorani *et al.* in 2003 to create a genetically engineered mouse model that faithfully recapitulated stepwise natural progression of human PDAC. This model was generated by crossing mice harbouring $Kras^{LSL.G12D/+}$ knocked-in allele with a transgenic strain that expresses a bacterial Cre recombinase under the control of the pancreatic specific promoters, *Pdx1* or *Ptf1a/P48* (Figure 1.7). Consequently, the mutated KRAS oncogene is expressed in all pancreatic lineages during embryonic development of the resulting strains (Guerra and Barbacid, 2013; Hingorani et al., 2003). The $Kras^{LSL.G12D+/-}$*; Pdx-Cre* mice (hereafter termed as KC mice) were born with normal pancreatic histology and architecture and displayed complete penetrance of PanIN lesions that were histologically identical to that in human PDAC. Of note, such mice displayed initial stages of PanIN lesions (PanIN-1A) as early as two-weeks old. Subsequently, the frequency and grade of PanIN lesions increased with the increase in mice age (Guerra and Barbacid, 2013). A full spectrum of PanIN lesions developed in the mouse model with a long latency for PDAC formation and median survival of 14 months. The KC model was, indeed, important in providing evidence of *Kras* mutation as an

initiating event in the development of pancreatic cancer (Hingorani et al., 2003; Westphalen and Olive, 2012).

The long latency to PDAC development in KC mouse model was overcome by additional inactivation of tumour suppressor genes including *Trp53*, *Cdkn2a* and *Smad4*. Amongst these, a mouse model harbouring *Trp53* inactivation caused by a point mutation ($Trp53^{R172H}$) in the pancreas along with concomitant *Kras* mutation (hereafter termed as KPC model) is one of the most frequently used models to analyse preclinical therapeutic agents (Gopinathan et al., 2015). The prenatal mouse models, albeit useful, present variation in the etiology of PanIN lesions and PDAC development with that of human counterparts. This is because PDAC is not a paediatric but rather an older age-related disease. Similarly, KRAS mutations are most likely to occur sporadically in selected cell types in PDAC patients rather than the entire pancreas. Hence, second generation GEM models were generated by crossing $Kras^{LSL.G12Vgeo}$ knockin strain with transgenic mice that express Cre under the control of *Elastase* promoter in a tet-off system (Elas-tTA; Tet-O-Cre). The selective expression of mutated $Kras^{G12V}$ led to the development of full spectrum of PanIN lesions with similar latencies to that of KC mouse model (Guerra and Barbacid, 2013). Furthermore, GEMMs to study hereditary pancreatic cancer have been generated by crossing the KC strain with mice that comprise germline *Brca2* heterozygosity caused by truncated *Brca2* allele (Skoulidis et al., 2010).

Besides PanIN lesions, human PDAC consists of other types of precursor lesions including IPMNs and MCNs. Hence, GEMMs recapitulating the progression of these precursor lesions are also necessary. Accordingly, mouse models displaying formation of IPMNs (Bardeesy et al., 2006) and MCNs (Izeradjene et al., 2007), upon the deletion of *Smad4* in the pancreatic compartment of KC mice, have been generated. Similarly, due to increasing

speculations in regard to the cell of origin of PDAC, GEMM models with cell-type specific expression of mutated *Kras*$^{G12D}$ have also been developed and will be discussed in the next section of this chapter. Briefly, the GEM model with acinar cell specific *Kras*$^{G12D}$ mutation led to the development of full spectrum of PanIN lesions and invasive ductal adenocarcinoma. In contrast, a ductal cell derived *Kras*$^{G12D}$ model presented precursor lesions with more hyperplastic phenotype (Ferreira et al., 2017) and were less reminiscent of low-grade PanIN lesions (Lee et al., 2018). Furthermore, additional deletion of *Pten* tumour suppressor gene alongside *Kras*$^{G12D}$ activation, specifically in ductal cells, led to the formation of IPMNs (Kopp et al., 2018). Taken together, the utilisation of GEMM is useful in understanding the genetics and biology of PDAC development and progression. Besides, these models also present as critical platform for target validation and preclinical studies (Gopinathan et al., 2015).

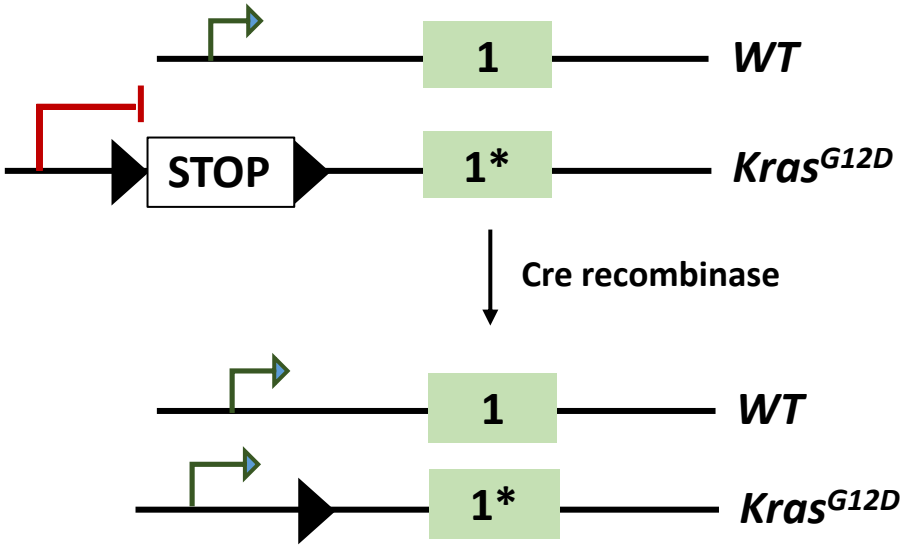


**Figure 1.7. Schematic diagram representing conditional *LSL-KRAS*$^{G12D}$ allele to generate KC mice.** Lox-STOP-Lox construct was inserted upstream of exon 1, engineered to contain G to A transition, in codon 12 . Cre-mediated recombination led to the expression of KRAS G12D which are heterozygous for the wild-type allele. Under pancreas specific promoters, Pdx1 or P48, the homologous recombination led to the generation of *Kras*$^{G12D+/-}$*; Pdx-Cre* (KC) mice. Figure modified from (Hingorani et al., 2003).

***Intratumoural heterogeneity of murine PDAC***

PDAC is a highly heterogeneous disease. GEMMs harbouring activating *Kras* mutations alongside additional inactivation of *Trp53* or *Cdkn2a* displayed intertumoural and intratumoural heterogeneity within their genomic landscape (Chung et al., 2017). Hingorani et al., when characterising the KPC model for the first time, also referred to heterogeneity in the molecular expression of ERRB1/EGFR and ERRB2/HER2 among PanIN lesions within the same pancreatic tissue (Hingorani et al., 2005). Similarly, primary PDAC tumours comprise extensively of subclones within the pancreatic tissue with varying genetic and phenotypic properties (Maddipati and Stanger, 2015). The PDAC heterogeneity could arise from various factors including cell of origin and stromal response to tumour microenvironment (Chung et al., 2017). This thesis will focus on exploring the cell of origin in relation to PDAC heterogeneity.

## 1.4.2 3D organoids

The most commonly use models to study PDAC tumorigenesis include 2-dimensional (2D) cell culture and genetically engineered mouse model (GEMM). These systems have been very useful for studying the pathophysiology of PDAC progression. Nevertheless, they have their own limitations; the culture of cancer cells in 2D surface were, particularly, shown to be physiologically irrelevant when modelling human disease progression. Moreover, they were deemed unsuitable in predicting therapeutic response (Boj et al., 2016). The necessity for an alternative model accurately modelling the human disease led to the development of an organoid model. Organoid can be defined as a group of derived epithelial cells, grown in a 3-dimensional (3D) structure, with physiological and molecular properties resembling the tissue of origin. The organoid model systems more closely represent human physiological conditions as they overcome attachment of the cells on the flat surface.

Different techniques have been applied to model pancreatic organoids. In brief, tissue disintegration is initially achieved by either applying mechanical force or by using collagenase. Following this, the cells can be cultured in suspension. Alternatively, they can also be grown on top or embedded into the matrix including collagen and matrigel. Morphologically, when cultured in Matrigel, organoids from the pancreas grow as a layer of polarised epithelial cells surrounding a hollow lumen in the centre. As the expansion of organoids occur, their cystic structures begin to fold and bud off (Baker et al., 2016; Hohwieler et al., 2019; Huch et al., 2013) (Figure 1.8). An advantageous feature of the pancreatic organoid model over 2D cell culture is the possibility to grow normal ductal epithelium from healthy pancreas along with ductal structures from pancreatic tissues with neoplastic PanIN lesions and malignant tumours. The ability of the organoids to grow continuously, from both normal and neoplastic tissues, is primarily attributed to their self-renewal and self-organisation capacities (Moreira et al., 2017). These are speculated to be mediated by pancreatic progenitors, including LGR5 and DCLK1, which are known cancer stem cell markers in the intestine (Hirsch et al., 2014; Rao and Mohammed, 2015; Yui et al., 2012). Notably, only the ductal epithelial cells were able to form the organoid structure. This indicates the residence of the pancreatic progenitors within the ductal compartments of pancreas (Carpino et al., 2016; Hohwieler et al., 2019).

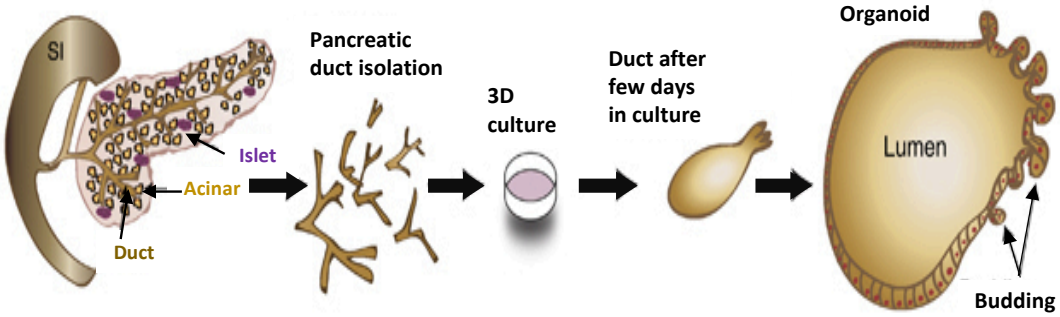


**Figure 1.8. Schematic diagram demonstrating the process of ductal isolation from mouse pancreas to their growth in culture as organoids.** The adult mouse pancreas is digested, following which ductal cells are picked and embedded in matrigel for their growth in a 3D system. Few days after the ducts are isolated and grown in culture, they adapt cystic-like structures. These cystic structures expand after several days in culture, with epithelial cells encapsulating a hollow lumen. As the organoids grow further, they start to fold and bud off, leading to the multiplication of the organoid structures. Figure reprinted from (Huch et al., 2013) and is an open access under the Creative Commons Attribution License.

## 1.5 Cell-type origin of PanIN lesions and PDAC

***PDAC's origin – acini or ducts?***

Pancreatic ductal adenocarcinoma, as its name suggests, was initially speculated to originate from the pancreatic ducts due to its ductal, glandular morphology (Bailey et al., 2014; Xu et al., 2019). Moreover, Brembeck *et al.* targeted ductal cells by expressing mutated $Kras^{G12V}$ in the promoter region of the ductal marker, Cytokeratin-19 (CK19). This ductal specific oncogenic *Kras* expression led to the formation of ductal hyperplasia in the pancreata of transgenic mice and were described to resemble PanIN lesions in human counterparts (Brembeck et al., 2003; Ray et al., 2011). The use of specific markers, particularly mucins in later studies, however, rarely detected PanIN lesions in the pancreata of a ductal cell specific model (Kopp et al., 2012). Interestingly, many investigations have reported formation of PanIN lesions as a result of acini specific point mutations of *Kras*, particularly $Kras^{G12V}$ (Guerra et al., 2007) or $Kras^{G12D}$ (Carrière et al., 2009; DeFeo et al., 1981; Habbe et al., 2008; Morris et al., 2010). This observation was

indeed fascinating considering the initial assumption that PanIN lesions and PDAC were derived from the ducts (Hruban et al., 2000). Commenting on the research published by Guerra *et al.* 2007 in Cancer Cell, Murtaugh and Leach named PDAC origin "as a case of mistaken identity" (Guerra et al., 2007; Murtaugh and Leach, 2007). Of note, initial studies establishing transgenic mouse models, with *Kras* mutation in the pancreas, focused primarily on the expression of the mutated oncogene in all of the pancreatic cell types, with less emphasis on the origin of PDAC (Hingorani et al., 2003; Hingorani et al., 2005).

***Role of ADM as origin of PDAC***

With the higher susceptibility of acinar cells to oncogenic insults (as mentioned in Section 1.2.6 of this chapter), many studies have postulated a working model of PDAC originating from the process of acinar-to-ductal metaplasia or ADM, in which acinar cells transdifferentiate and adapt the morphology of ductal cells (Guerra et al., 2007; Kopp et al., 2012). Furthermore, external stimuli, such as tissue damage due to inflammatory condition (chronic pancreatitis), can lead to the transformation of ADM to form the full spectrum of PanINs and PDAC in adult mice (Guerra et al., 2007). Similarly, Kopp *et al.* 2012 demonstrated that the reprogramming of $Kras^{G12D}$ expressing acinar cells ($Ptf1a^{CreER}$; $Kras^{G12D}$) into the ductal ones (Kopp et al., 2012) and subsequent PanIN lesion formation is dependent on the induction of *Sox9* gene. Indeed, Sox9 is known as a critical regulator of ductal cell development (Kopp et al., 2012; Shih et al., 2012). Strikingly, earliest studies using *in vitro* system described transdifferentiation of acinar into ductal structures in pancreas of different species including mouse (De Lisle and Logsdon, 1990), rat and guinea pig (Arias and Bendayan, 1993) and human (Hall and Lemoine, 1992). Strobel *et al.* in 2007 showed direct evidence for the transdifferentiation of acinar to ductal cells in adult pancreas by using Cre-LoxP-based lineage tracing *in vivo* (Strobel et al., 2007). Oncogenic

*Kras* mediated ADM has largely been known as an irreversible process. Some studies, however, indicated reversal of PanIN lesions formed due to the progression of transdifferentiated ductal cells back to acini, both in *in vitro* and *in vivo* systems (Wong et al., 2016). This conversion was shown to primarily occur either through the use of inhibitors of MAPK signalling, PD325901 (Collins et al., 2014) and Exendin-4, or genetic manipulation of Dickkopf-3 (DKK-3) (Zenzmaier et al., 2012) and E47 that inhibit Wnt Signalling and control cell cycle respectively (Kim et al., 2015) .

***Cell-type specific models for PanIN lesions and IPMNs***

Even if acinar cells are the putative origin of PanIN lesions, the exact role of ducts in PDAC progression remains unclear. Currently, the model to study cell of origin of PDAC has mostly been carried out in genetically engineered mice. Particularly, the expression of mutated KRAS oncogene is introduced by utilising Cre-LoxP system. In this, Cre recombinase expression is directed by promoters specific to markers either in acinar cells including *Ela*, *P48* and *Mist1* or ductal cells including *Sox9*, *Ck19* and *Hnf1a* (Xu et al., 2019). There is evidence to indicate derivation of IPMNs from ductal cells (von Figura et al., 2014). Accordingly, concomitant activation of $Kras^{G12D}$ along with the loss of a tumour suppressor gene, *Pten*, specifically in the ductal cells, led to the formation of IPMNs in the mouse pancreas (Kopp et al., 2018). Similarly, ductal cell regulated *Kras* mutation along with the deletion of another tumour suppressor gene, *Fbw7*, led to the bypass of PanIN lesions and formation of carcinoma *in situ* (Ferreira et al., 2017). Additionally, another study using a ductal cell specific mouse model presented pancreata that were devoid of low-grade PanIN lesions. These mice were mostly present with invasive high-grade PanIN lesions which progressed rapidly to aggressive PDAC phenotype, and developed distant metastasis (Lee et al., 2018). Collectively, these findings indicate a potential lack of dependency of ductal

cells on low-grade PanIN lesion formation during tumourigenesis. Moreover, PanIN lesions and IPMNs can also occur concordantly in tissue samples from human PDAC, implying the need to further unravel the questions regarding cellular origin of precursor lesions and PDAC (Xu et al., 2019).

***Importance of understanding PDAC's cell of origin***

One of the notable features of normal pancreatic cells is to maintain a high level of plasticity of the epithelium. This quality is inherited during PDAC development, and possibly enables the heterogeneity within the tumour environment. There is also a need to investigate cellular origin of PDAC in order to better understand the disease for improved diagnosis. This can, in turn, facilitate in providing new therapy for PDAC patients based on the cellular lineage (Xu et al., 2019). Acini, the most abundant cell type in the pancreas, have been conjectured to be the direct progeny of embryonic multipotent progenitor cells in adult pancreas (Zhou et al., 2007; Ziv et al., 2013). Notwithstanding this, the inability of acini to form other precursor lesions such as IPMNs, upon the concomitant *Kras* mutation and *Pten* deletion, unlike ductal cells (Kopp et al., 2018) highlights the necessity to investigate the underpinnings of the development of different types of precursor lesions and PDAC in the context of cell-type. Using lineage-tracing studies, PDAC in human patients displayed heterogeneity in terms of cell of origin, exhibiting regions with both acinar and ductal origins within the tumour region (Xu et al., 2019). Despite the limitations in models and techniques that have been developed hitherto, the necessity of understanding mechanisms underlying cellular origin of PDAC is crucial. There is, therefore, an expanding need to develop new approaches to further explore the cellular route of PDAC initiation.

## 1.6 Aims of the project

The main aim of this project is to investigate pro-tumourigenic effects of YAP when it translocates into the nucleus and activates transcription of genes involved in the enhancement of cell proliferation, growth and survival. In particular, we are interested to explore if YAP directly regulates KRAS-mediated MAPK signalling pathway in PDAC progression. In order to investigate this, I will first deplete the expression of YAP in pancreatic cancer cell lines and assess any changes in the components of MAPK pathway. Also, to investigate if the active role of YAP contributes in the progression of low-grade PanIN lesions into PDAC, I will examine the pancreatic tissue from genetically engineered mouse model. In particular I will analyse the nuclear expression of YAP in varying grades of PanIN lesions in *Kras*$^{LSL.G12D+/-}$*; Pdx*-Cre (KC) mice. Furthermore, I will explore the involvement of the tumour suppressor Hippo pathway in regulating YAP activation by looking at the two upstream regulators of the Hippo pathway, NF2 and RASSF1A. I will investigate the role of NF2 by depleting the protein's expression in pancreatic cancer cells and subsequently looking at any effects on the activation of YAP and MAPK pathway. Similarly, I will examine the role of RASSF1A in PDAC progression in *in vivo* settings. I will analyse any association between RASSF1A and YAP in the PanIN lesions of KC mice. Also, to see if RASSF1A is involved in the tumourigenic process of *Kras*-mutated PDAC, I will crossbreed the KC mice with *Rassf1a* A133S SNP (rs2073498A SNP) mice and monitor for any changes in the mice survival and tumour phenotype in the mouse pancreas.

Secondly, I will investigate the cell of origin of PanIN lesions and PDAC in relation to the nuclear expression of YAP. I will use Alcian blue, which is a known marker of PanIN lesions, to distinguish between acinar-derived and ductal-derived precursor lesions in KC mice and PDAC in human patient samples. I will then correlate the positivity of Alcian blue with

nuclear YAP expression to determine for any association between the two stainings. This will enable to determine for any possible role of YAP as a distinct marker for a particular phenotype in early precursor lesions and PDAC.

Finally, I will use a more complex 3D pancreatic organoids system to study cell of origin of the precursor lesions and PDAC and YAP's involvement during this process. The ductal cells will be isolated from KC mouse pancreas and manipulated for the expression of YAP. I aim to orthotopically inject the YAP-depleted organoids into normal mouse pancreas after the establishment of the technique in our laboratory. Establishing these models will enable to study the role of YAP in the molecular pathogenesis of PDAC in relation to cell of origin.

The data generated in this thesis will give an insight to the mechanisms through which YAP acts as a critical player in the advancement of early-stage precursor PanIN lesions into aggressive form of tumour in pancreas.

# Chapter 2 Materials and Methods

## 2.1 Materials

### 2.1.1 Mouse strains

Genetically modified conditional *Kras*$^{LSL.G12D+-}$*; Pdx-1-Cre* (KC) mice were previously described (Hingorani et al., 2003). Male KC mice and female *Pdx-Cre* only mice were kindly provided by Dr Paul Miller from Prof Xin Lu's laboratory at Ludwig Cancer Research Institute, University of Oxford for crossbreeding. Similarly, KC pancreatic tissue sections were also provided by Dr Paul Miller during initial analysis. All animal studies were performed, in accordance with the UK Animals (Scientific Procedures) Act of 1986, under licences approved by the UK Home Office and with the University of Oxford ethical review committee. Animals were housed in environmentally enriched IVC cages. This included activity wheel or crawl ball, nesting material and chew sticks with a group of 5 mice per cage. The animal house was maintained in a 12-h day-night cycle facility at 22°C and in 50% humidity. All mice had *ad libitum* access to certified food and tap water.

### 2.1.2 Patient Materials

Formalin fixed paraffin embedded (FFPE) tissue blocks were obtained from the Department of Pathology archive together with clinical follow-up data and diagnostic images at the Oxford University Hospital NHS Trust. Patients had previously provided an informed consent. The present study was approved by the Oxford Radcliffe Biobank, University of Oxford (Project: OCHRe 14/A176). 4 µm FFPE sections on glass slides were used for histochemical analysis of Alcian blue and YAP staining.

### 2.1.3 General Laboratory Reagents

All chemicals were purchased from either Sigma-Aldrich or Thermo Fisher and used according to manufacturer's guidelines, unless stated otherwise. Tissue culture plastic was purchased from Corning and Sarstedt. Glassware was purchased from VWR and Fisher.

**Table 2.1: List of chemical reagents.**

| Name | Provider |
|---|---|
| 1 Kb Plus Ladder | Invitrogen |
| 2-Propanol | Fisher Scientific |
| Agarose | Sigma-Aldrich UK |
| Bovine serum albumin (BSA) | Thermo Fisher |
| Dimethyl sulfoxide (DMSO) | Sigma-Aldrich UK |
| Dithiothreitol (DTT) | Sigma-Aldrich UK |
| Ethanol (EtOH) | Fisher Scientific |
| Ethylenediaminetetraacetic acid (EDTA) | Sigma-Aldrich UK |
| Formaldehyde (PFA) | Thermo Fisher |
| Glycine | Fisher Scientific |
| Methanol (MeOH) | Fisher Scientific |
| Milk powder | Marvel |
| NP40 | Sigma-Aldrich UK |
| NuPAGE MOPS SDS Running Buffer (20X) | Thermo Fisher |
| PageRuler™ Prestained Protein Ladder | Thermo Fisher |
| Phosphatase inhibitors | Roche |
| Phosphate buffered saline (PBS) tablets | Oxoid |
| PIPES | Sigma-Aldrich UK |
| Protease inhibitors | Roche |
| Sodium chloride | Fisher Scientific |
| Sodium deoxycholate | Sigma-Aldrich UK |
| Sodium dodecyl sulphate (SDS) | Sigma-Aldrich UK |
| Sodium hydroxide | Sigma-Aldrich UK |
| Tris base | Fisher Scientific |
| Triton-X 100 | Sigma-Aldrich UK |
| Tween-20 | Sigma-Aldrich UK |

### 2.1.4 Genotyping primers and probes

| **Table 2.2: Primers and probes used for genotyping for the study.** | | | |
|---|---|---|---|
| **Gene** | **5' -> 3' Sequence** | **Provider** | |
| Actin | Forward: GGTGTCATGGTAGGTATGGGT<br>Reverse: CGCACAATCTCACGTTCAG | Sigma-Aldrich UK | |
| Cre | Forward: CATTTGGGCCAGCTAAACAT<br>Reverse: ATTCTCCCACCGTCAGTACG | Sigma-Aldrich UK | |
| Kras | Forward Wildtype:<br>CTAGCCACCATGGCTTGAGT<br>Forward Mutant:<br>ATGTCTTTCCCCAGCACAGT<br>Reverse Common:<br>TCCGAATTCAGTGACTACAGATG | Sigma-Aldrich UK | |
| **TaqMan Assay** | **5' -> 3' Sequence** | **Provider** | **Assay ID/Catalog No** |
| RASS1 mouse _A133S | Context sequence:<br>GCGGGAGACACCNGATCTTTCTCAA[G/T]TG AGACTGAGCAGAAAATCAAGGAC<br>FAM probe: TCAGTCTCAGATTGAG<br>VIC probe: CTCAGTCTCAGCTTGAG<br>Forward primer:<br>GTCTTTCAGGATGAGGCTGTAGAG<br>Reverse primer:<br>GGCCATTGTAGTCCTTGATTTTCTG | Thermo Fisher (TaqMan® SNP Genotyping Assay) | ANU62ZX / 4332077 |

### 2.1.5 Antibodies used

| **Table 2.3: Primary and Secondary antibodies for IHC. Table also indicates antigen retrieval conditions used for each primary antibody.** | | | | | |
|---|---|---|---|---|---|
| **Antibody** | **Provider** | **Catalogue No.** | **Dilution** | **Antigen Retrieval Buffer** | **Antigen Retrieval (Boiling/Sub-boiling temperature)** |
| GFP | Cell Signalling Technology | 2956 | 1:100, | Citrate Buffer pH6 | 110°C, 2 min/ 85°C, 1 min |

| | | | | | |
|---|---|---|---|---|---|
| pERK (T202/Y204) | Cell Signalling Technology | 4370 | 1:300, | Citrate Buffer pH6 | 110°C, 2 min/ 85°C, 1 min |
| pYAP | Cell Signalling Technology | 4991 | 1:100, | Citrate Buffer pH6 | 110°C, 2 min/ 85°C, 1 min |
| RASSF1A | Protein Atlas | HPA040735 | 1:100, | Citrate Buffer pH6 | 110°C, 2 min/ 90°C, 1 min |
| YAP | Cell Signalling Technology | 4912 | 1:100, | Citrate Buffer pH6 | 110°C, 2 min/ 85°C, 1 min |
| **Secondary Antibody** | **Provider** | **Catalogue No.** | | | |
| HRP labelled Polymer anti-Rabbit | Dako EnVision+ System | K4003 | | | |

**Table 2.4: Primary and Secondary antibodies for Western Blot and IF.**

| **Primary Antibody** | **Provider** | **Catalogue No.** | **Dilution** |
|---|---|---|---|
| Actin | Santa Cruz | Sc-1616 | 1:100, WB |
| E-cadherin (G-10) | Santa Cruz | sc-8426 | 1:100, IF |
| ERK1/2 | Cell Signaling Technology | 4696 | 1:500, WB |
| GAPDH | Cell Signaling Technology | 97166S | 1:1000, WB |
| pERK (T202/Y204) | Cell Signaling Technology | 4370S | 1:500, WB |
| RAS | Cell Signaling Technology | 3965S | 1:500, WB |
| YAP | Cell Signaling Technology | 4912 | 1:100, IF |
| YAP (63.7) | Santa Cruz | sc-101199 | 1:500, WB |
| **Secondary Antibody** | **Provider** | **Catalogue No.** | **Dilution** |
| Alexa fluor® goat anti-mouse 594 nm | Invitrogen, Life Tech | A-11005 | 1:500, IF |
| Alexa fluor® goat anti-rabbit 488 nm | Invitrogen, Life Tech | A-11008 | 1:500, IF |
| HRP conjugated anti-Mouse | Cell Signaling Technology | 7076 | 1:5000, WB |
| HRP conjugated anti-Rabbit | Cell Signaling Technology | 7074 | 1:5000, WB |

### 2.1.6 Cell lines and cell culture reagents used

**Table 2.5: List of the cell lines used in this study. Table indicates cell line, tissue of origin and mutation status of KRAS and TP53.**

| Name | Origin | Source | KRAS | TP53 |
|---|---|---|---|---|
| KPC | Mouse pancreatic ductal adenocarcinoma | Prof Jennifer Morton, Beatson Institute of Cancer Research, University of Glasgow | G12D | 270H |
| MiaPaCa-2 | Human pancreatic ductal adenocarcinoma | Remko Prevo, Department of Oncology, University of Oxford | G12C | 248W |
| Panc-1 | Human pancreatic ductal adenocarcinoma | Remko Prevo, Department of Oncology, University of Oxford | G12D | 273H |
| PanO2 | Mouse pancreatic ductal adenocarcinoma | Dr Emmanouil Fokas, Department of Oncology, University of Oxford | WT | WT |
| Psn-1 | Human pancreatic ductal adenocarcinoma | Remko Prevo, Department of Oncology, University of Oxford | G12R | 132Q |
| HEK 293T | Human embryonic kidney | ATCC | WT | WT |

**Table 2.6: List of the cell culture reagents and supplements**

| Name | Provider |
|---|---|
| DMEM | Life Technologies |
| Glutamine | Life Technologies |
| Opti-MEM | Life Technologies |
| Penicillin/Streptomycin | Life Technologies |
| RNAiMAX | Thermo Fisher |
| Trypsin-EDTA | Life Technologies |

| **Table 2.7: List of reagents and supplements for Mouse Complete Feeding Media to culture organoids** | | | |
|---|---|---|---|
| **Mouse Complete Feeding Media Components** | **Provider** | **Final Concentration** | Mouse Complete Feeding Media Components |
| 1M HEPES (100X) | Sigma-Aldrich | 1X | 1M HEPES (100X) |
| A83-01 (TGF-β inhibitor) | TOCRIS | 0.5 µM (0.21 µg/mL) | A83-01 (TGF-β inhibitor) |
| Advanced DMEM/F-12 | Thermo Fisher | 1X | Advanced DMEM/F-12 |
| B27 supplement 50X (serum-free) | Thermo Fisher | 1X | B27 supplement 50X (serum-free) |
| EGF Recombinant Mouse Protein | Thermo Fisher | 0.05 µg/mL | EGF Recombinant Mouse Protein |
| Gastrin I | TOCRIS | 0.01 µM (0.021 µg/mL) | Gastrin I |
| GlutaMAX Supplement (100X) | Thermo Fisher | 1X | GlutaMAX Supplement (100X) |
| mNoggin | Peprotech | 0.1 µg/mL | mNoggin |
| N-Acetylcysteine | Sigma-Aldrich | 1.25 mM (0.2 mg/mL) | N-Acetylcysteine |
| Nicotinamide | Sigma-Aldrich | 10 mM (1.22 mg/mL) | Nicotinamide |
| Penicillin/Streptomycin (100X) | Thermo Fisher | 1X | Penicillin/Streptomycin (100X) |
| R-spondin-conditioned media | TREVIGEN® | 10% | R-spondin-conditioned media |
| Recombinant Human FGF-10 | Peprotech | 0.1 µg/mL | Recombinant Human FGF-10 |

### 2.1.7 RNAi interference and Lenti-viral shRNA vectors for knockdown

**Table 2.8: siRNAs and shRNAs used for the study**

| **Target gene** | **siRNA target sequence** | **Provider** |
|---|---|---|
| siLuciferase | GCCAUUCUAUCCUCUAGAGGAUG | Eurofins MWG |
| siNF2 human (siGenome SMARTpool) | ACGCCGAGAUGGAGUUCAA (1)<br>CUUACGCCGUCCAGGCCAA (2)<br>AGAAGCAGAUUUUAGAUGA (3)<br>AGGAAGCAACCCAAGACGU (4) | Thermo (Dharmacon) |
| siNT (Non-Targetting) | UAAGGCUAUGAAGAGAUAC | |
| siYAP human | CUGGUCAGAGAUACUUCUU | Eurofins MWG |
| siYAP mouse | CTGGTCAAAGATACTTCTTAA | Qiagen |
| **Target gene** | **shRNA target sequence** | **Provider** |
| shRNA Control | CCGGCAACAAGATGAAGAGCACCAACTCGAGTTGGT GCTCTTCATCTTGTTGTTTTT | Sigma MISSION SHC002 |
| shYAP human #1 | GCCACCAAGCTAGATAAAGAA | Addgene |
| shYAP human #2 | CCCAGTTAAATGTTCACCAAT | Addgene |
| shYAP mouse | CCGGGAAGCGCTGAGTTCCGAAATCCTCGAGGATTT CGGAACTCAGCGCTTCTTTTTG | Sigma MISSION |

## 2.2 Methods

### 2.2.1 Generation of a mouse model harbouring A133S SNP within the *Rassf1* gene

The mice harbouring *Rassf1* A133S SNP (hereafter referred as rs2073498 SNP) were generated by Dr Ben Davies at the Wellcome Trust Centre, University of Oxford and provided by Michael Eyres in our laboratory. In this mouse model, genetic knockin of the

point mutation G to T was mediated through Crispr/Cas9 nuclease. The nuclease was directed against exon 3 sequence of the *Rassf1* gene, encompassing the target site Alanine 133. The site-specific double strand break into the genome is presented as a template for homology directed repair (HDR). During this, a single stranded oligonucleotide (ssODN) comprising the G to T point mutation, leading to the alteration of Alanine codon at 133 to Serine, acts as the donor DNA. Besides, the ssODN also harboured silent mutation that marked the mutated allele by including a BglII restriction site. Collectively the Crispr/Cas9 reagents and ssODN were injected into mouse embryonic stem (ES) cells. Transfected cells were transiently selected with puromycin, following which individual clones were isolated and expanded on a 96-well plate. The target locus was amplified by PCR and digested with BglII in order to reveal Crispr/Cas-9 knock-in clones (Appendix, Figure 7.1.A ) The DNA sequencing of one clone was identified to harbour a perfect knock-in of the point mutation (SNP) and the silent mutation, that is used to mark the mutated allele with an BglII restriction site (Appendix, Figure 7.1.B). These cells were then further injected into the cystic cavity of blastocysts from albino mice. Ultimately, they were implanted into the uteri of 2.5-day pseudopregnant foster mice. The resulting chimeras presented 40-99% contribution from the injected ES cells. The chimera with the highest ES contribution was then selected for further breeding which then generated rs2073498 SNP mice through the successful germline transmission of the SNP allele.

### 2.2.2 Genotyping

For genotyping, genomic DNA was extracted from ear notch using HOTSHOT method. 50 µl of Alkaline Lysis Reagent [25 mM (w/v) NaOH, 0.2 mM (w/v) EDTA] was added to 1-2 mm of ear notch and incubated at 95°C for at least 15 min. Following this, the sample was

kept on ice and mixed with 50 µl of Neutralisation Reagent [40 mM (w/v) Tris-HCl, pH 6.5]. After mixing the sample well with the Neutralisation Reagent, 1 µl of the extracted DNA was used for genotyping.

To genotype for *Kras* mutation in *Kras$^{LSL.G12D/+}$; Pdx-1-Cre* (KC) mice, HotStart PCR was performed using KAPA Taq HotStart PCR Kit (KAPA Biosystems). The PCR master mix was prepared in a 200 µl PCR tube and included 12.5 µl of KAPA2G Fast HotStart Genotyping Mix, 1.25 µl of Forward wild type primer (that anneals exclusively to the Wild-type allele), 1.25 µl of Forward mutant primer (that anneals exclusively to the mutant allele), Common reverse primer (that pairs two allele-specific primers), 1 µl of extracted DNA and 7.75 µl of nuclease-free water in order to get a total volume of 25 µl ( See Table 2.2 for the primers used). The tubes were then transferred to a thermal cycle (My Cycler, Bio-Rad) following the protocol: Initial Denaturation (1X cycle at 95°C for 4 min), Denaturation (30X cycles at 95°C for 15 sec), Annealing (30X cycles at 60°C for 30 sec), Extension (30X cycles at 72°C for 15 sec), Final Extension (1X cycle at 72°C for 1 min) and Hold at 4°C. The PCR mix was then run on a 1.5% agarose gels. For this 1.5 g agarose was added to 100 ml of 1x TAE buffer [40 mM (w/v) Tris, 18 mM (v/v) Glacial acetic acid, 1 mM (w/v) EDTA pH 8] and microwaved for approximately 3 min for complete dissolving of the agarose. Following this, SYBR® Safe DNA Gel Stain (Invitrogen) was added to the agarose mixture and poured into a Bio-Rad tank. The solution mixture was left at room temperature for approximately 30 min to solidify and form gel. The gel was then covered with 1x TAE Buffer. The PCR mix was then loaded into the wells along with 1 Kb Plus Ladder (Invitrogen). The gel was run at 100 Volts for approximately 45 min. The bands were then detected using Gel doc™ XR+ (Bio-Rad) and images analysed using Image Lab™ Software (Bio-Rad) (Appendix, Figure 7.2.A).

To genotype for *Rassf1* SNP allele, TaqMAN SNP Genotyping Assay was used. Reaction mix was prepared in a MicroAmp™ Optical 96-Well Reaction Plate (Life Technologies) for PCR amplification by adding 5 µl of 2X TaqMAN Genotyping Master Mix (Thermo Fisher) with 0.25 µl 40X TaqMan Probe (See Table 2.2 for the probe used). 1 µl of the extracted DNA using the HOTSHOT method was added to the mixture and brought to a final volume of 10 µl per reaction by adding 3.75 µl of nuclease-free water. The plate was then covered with MicroAmp Optical Adhesive Film (Life Technologies) and centrifuged briefly to spin down the mixture and eliminate any air bubbles from the solutions. The PCR reaction was run in StepOnePlus™ Real-Time PCR machine (Thermo Fisher). The reporter dyes were manually linked as VIC® dye to the Wild-type allele and 6FAM™ to the SNP allele. The thermal cycling conditions were applied as: AmpliTaq Gold, UP Enzyme Activation (HOLD at 95°C for 10 min), Denaturation (40X cycles at 95°C for 15 sec) and Annealing and Extension (40X cycles at 60°C for 1 min). After PCR amplification, an allelic discrimination read was performed on the real-time PCR instrument. The plate read document was analysed and manually verified for the allele types (Appendix, Figure 7.2.B).

### 2.2.3 Immunohistochemical Staining (IHC)

For immunohistochemical analysis, formalin-fixed, paraffin-embedded (FFPE) tissue sections were deparaffinised in Citroclear and rehydrated in graded alcohol concentrations (100%, 90%, 70%, and 50%) for 3 min each, followed by two washes in PBS. The unmasking of the antigen was performed using Citrate buffer, pH 6.0, 10x (Sigma-Aldrich). The boiling temperature for the retrieval of antigen was optimised. The slides were maintained at an optimised sub-boiling temperature (Table 2.3 for the antigen retrieval conditions used). The deparaffinised, rehydrated sections were subjected to incubation with $H_2O_2$ to block

endogenous peroxidase activity. Blocking of non-specific antibody was carried out using dual endogenous enzyme block (Dako EnVision) for 1 h. Primary antibodies were diluted appropriately (after optimisation) in an antibody diluent (Abcam) (See Table 2.3 for the list of antibodies and dilution used). Tissues were incubated in primary antibody overnight in a moist chamber at 4°C. Following day, slides were washed with PBS to remove any unbound antibody and then incubated in HRP labelled secondary antibody conjugated to anti-rabbit immunoglobulins (Dako EnVision) for at least 30 min. The staining in the tissues were developed by adding the mix of DAB chromogen in DAB substrate buffer in 1:50 dilution (Dako EnVision). The slides were then counterstained with aqueous haematoxylin for nuclear staining. The sections were dehydrated by transferring them to 50% (v/v) ethanol, 70% (v/v) ethanol, 100% ethanol and 100% Xylene. The slides were mounted by applying DPX mounting medium (Sigma-Aldrich) to a glass coverslip and then placing it onto the dehydrated tissue sections. IHC images were obtained using Aperio Slide scanner Software (Leica Biosystems).

### 2.2.4 Haematoxylin and Eosin Staining (H&E)

Tissue slides were deparaffinised and rehydrated following the same conditions as for the IHC staining. The slides were then placed in freshly filtered Harris Haematoxylin for 5 min, followed by 5 min wash under running tap water. To remove any non-specific background noise, the sections were then differentiated with 2 dips in acid alcohol solution [ 1% (v/v) HCl in 70% (v/v) ethanol]. The slides were washed in water with 5-10 dips. To achieve blueing up of the tissues more quickly, the slides were then placed in Scott's tap Water Substitute Solution [20g (w/v) $MgSO_4.7H_2O$ and 3.5 g (w/v) $NaHCO_3$ in 1L tap water] with 10 dips. The blueing process is further accelerated by placing the slides in 0.5% (v/v) lithium

carbonate solution with 10 dips. The slides were again washed well under running tap water for 3 min and dehydrated by placing them through the ethanol gradient, starting with 10 dips in 50% (v/v) ethanol. The process was then repeated in 70% (v/v) ethanol and 100% ethanol before placing the slides in the Eosin solution for 3 min. The slides were then washed in 100% ethanol with 10 dips to remove excess eosin. Finally, the slides were placed in Xylene for 1 min before applying DPX mounting medium in a glass coverslip to mount the tissue sections.

### 2.2.5 Alcian blue Staining (AB)

Tissue sections were firstly deparaffinised and rehydrated following the previously used protocol for IHC and H&E stainings. Alcian blue staining was then performed using the Alcian blue pH 2.5 Stain Kit from Abcam. The protocol included incubation of the tissue sections in Acetic Acid Solution, following deparaffinisation and rehydration process, for 3 min. Tissue sections were then incubated in Alcian blue (pH 2.5) solution for 30 min at room temperature (RT). After incubation, the Alcian blue was removed and tissue sections were briefly rinsed in Acetic acid solution to further remove any excess Alcian blue. The slides were then washed in running tap water for 2 min, followed by a brief wash in distilled water. The sections were then stained in Safranin O Solution for 5 min. Again, the slides were washed in running tap water for 2 min, followed by a brief wash in distilled water. As previously for IHC and H&E stainings, the sections then went through the dehydration process with 50% (v/v), 70% (v/v) and 100% ethanol before being placed in Xylene. The mounting was again carried out by applying DPX mounting medium to a glass coverslip and then onto the tissue sections.

### 2.2.6 Cell Culture

Pancreatic cancer cell lines KPC, MiaPaCa-2, Panc-1, PanO2 and Psn-1 were cultured in Dulbecco's Modified Eagle Medium (DMEM) supplemented with 10% Fetal Bovine Serum (FBS), 2 mM Glutamine, and Penicillin/Streptomycin (Pen-Strept) (100 U/ml) [Complete DMEM]. Cells were cultivated in a cell culture incubator at 37°C and 5% $CO_2$. Cells stored in liquid nitrogen were defrosted by placing them in a 37°C water bath for 2 min. Once thawed, cells were resuspended in Complete DMEM. To remove leftover Dimethyl sulfoxide (DMSO) from freezing media, cells were centrifuged at 250 x g for 5 min. Cell pellets were then resuspended in 10 mL of the Complete DMEM and seeded into a T75 flask. The cell culture work was performed under a laminar flow hood and materials were disinfected using 70% (v/v) ethanol. The media and buffers were warmed up in a 37°C water bath. Cells were sub-cultured approximately at 80% confluency. To passage cells, they were first washed with Phosphate Buffered Saline (PBS) to remove any leftover media and cellular debris. Cells were then trypsinised with the 0.25% Trypsin-EDTA solution. Trypsinised cells were resuspended in Complete DMEM and reseeded into new tissue culture flasks as required by the experiments – for usual passaging cells were split at a 1:10 ratio. Cells were routinely frozen down in freezing media [ 90% (v/v) FBS, 10% (v/v) DMSO]. To freeze the cells down, cells were washed in PBS, trypsinised and centrifuged at 250 xg for 5 min. After the removal of supernatant, the cell pellets were resuspended in freezing media and transferred into cryovials (>1x$10^6$ cells in 1 mL freezing media/vial). Cryovials were frozen using a Nalgene® Mr Frosty at RT containing 200 mL isopropanol and placing them at -80°C for 24 h. Freezing vials were then transferred into vapour phase nitrogen in liquid nitrogen tanks for long term storage.

### 2.2.7 Organoid Isolation

Organoids were manually isolated from small intralobular ducts. After the dissection of pancreas, it was immediately brought to the tissue culture hood to start the digestion procedure. The pancreas was minced in a Petri dish in Mouse Wash Media (DMEM supplemented with 1% FBS, 2 mM Glutamine and Penicillin/Streptomycin (100 U/ml). After the pancreas had been minced and broken into pieces of up to approximately 1-2 mm size, they were transferred to 15 mL Falcon Tube containing 5 mL of the Mouse Wash Media. The tube was then left at RT for 1 min to allow the pancreas to settle at the bottom. Most of the supernatant, that would contain fat, was discarded, leaving approximately 1 mL of the Mouse Wash media with pancreas. The pancreas pieces were then subjected to digestion by the addition of 10 mL of Mouse Digestion Media [ 0.125 mg/mL (w/v) Collagenase Crude Type XI (Collagenase from *Clostridium histolyticam* (Sigma-Aldrich)], and 0.125 mg/mL (w/v) Dispase II (Thermo Fisher) in DMEM with 1% FBS, 1% Pen-Strept and 1% Glutamine. The pancreas was then left to digest in the Mouse Digestion Media by incubating at 37˚C for 20 min, with constant shaking at 450 rpm. Digested pancreas was removed from the heat shaker and pipetted up and down with 10 mL pipette to break up pieces. The tube was then left for 1 min to allow the pancreas pieces to sink at the bottom. 8.5 mL of supernatant was transferred to a petri dish containing the Mouse Wash Media. Meanwhile 8.5 mL of fresh Mouse Digestion Media was added to the remaining pancreas pieces and incubated at 37˚C for 10 min, with gentle agitation at 450 rpm. The Petri dish containing supernatant after the first round of digestion was visualised under bright field microscope to look for the presence of ducts. The ducts appear like small chains of cells under 10X objective, when the phase contrast is on. These ducts were picked using P20 that has been set to 10 µL. The pipette plunger was pushed to first stop, following which it

was brought closer to ducts as visualised under the microscope. The plunger was then released to suck up the duct. This process of pulling up the ducts was continued until the plunger has been released all the way. The ducts in the pipette was then dispelled into the 15 mL tube containing 5 mL of the Mouse Wash Media. Simultaneously, the pancreas in the digestion media was removed after 10 min incubation at 37˚C with gentle agitation. The pancreas was again pipetted up and down to break up the pieces and left for 1 min for the pieces to settle down. The same process of transferring the supernatant to petri dish with the Mouse Wash Media to pick up the ducts was continued. Meanwhile the remaining pancreas was again added with the Mouse Digestion Media and incubated at 37˚C for 10 min, with gentle agitation at 450 rpm. This cycle was continued at least until the eighth wash until no ducts could be detected in the washes anymore. This was done to ensure as many ducts were picked up as possible. Following this, the 15 mL Falcon Tube containing the picked-up ducts were spun down at 145 xg for 5 min. Since the pellets were very small, supernatant was aspirated off, leaving around 16 µL with the pellet. This was then resuspended in 34 µL Matrigel. Following this, the total volume of 50 µL was plated into a well of pre-warmed 24-well plate and was allowed to form a dome. The plate was then placed back carefully into 37˚C incubator for the Matrigel to harden. After approximately 15 min incubation at 37˚C, the dome was covered with 500 µL of Mouse Complete Feeding Media (See Table 2.7 for the complete reagents and supplements used) and was supplemented with Rho Kinase Inhibitor Y-27632 (Sigma-Aldrich) at the final concentration of 10.5 µM.

### 2.2.8 Organoid passaging and culture

To passage the organoids, the Mouse Complete Feeding Media that provide essential components for the organoid growth was removed. The Matrigel comprising organoids in each well was dislodged and broken up by adding ice-cold Splitting media [ Advanced DMEM/F-12 supplemented with 1 M (w/v) Hepes, GlutaMAX and Penicillin/Streptomycin (100 U/ml)] directly on top of the organoids following which they were centrifuged at 200 xg for 5 min. Using a 23-gauge needle attached to a 5 mL syringe, the organoid pellet resuspended in the Splitting media was pulled up and pushed back few times in order to enable dissociation of the organoid structures. The organoid suspension was then added to a larger volume of ice-cold Splitting media and centrifuged at 300 xg for 5 min. After spinning, the pellet was then suspended in ice-cold Matrigel diluted in Splitting Media (3:1). As previously, 50 µl of the mixture was then added to a well of a 24-well plate to form a Matrigel dome and overlaid with pre-warmed Mouse Complete Feeding Media after allowing the Matrigel to harden in a 37°C tissue culture incubator for approximately 15 min. Fresh Complete Feeding Media was added to the well every two days.

### 2.2.9 Transient knockdown using RNAi interference

***2D cells***

Downregulation of YAP and NF2 expression was performed in human pancreatic cancer cells using Lipofectamine™ RNAiMAX. Cells to be subjected to transfection were seeded in culture dishes for 24 h in Complete DMEM. On the day of transfection, siRNA and Lipofectamine™ RNAiMAX were simultaneously diluted in OptiMEM (See Table 2.8 for the siRNAs used). After 5 min of incubation, diluted siRNA was mixed with diluted RNAiMAX reagent at a 1:1 ratio and incubated for 15 min at RT. siRNA-lipid complexes were then

added onto the fresh culture media [DMEM supplemented with 10% FBS and 2 mM Glutamine] with the final concentration of the siRNA at 20 nM. After 6 h of transfection, the culture media was replaced with fresh Complete DMEM. Cells were cultured for either 24- or 48 h in Complete DMEM following transfection according to the experimental requirements.

***3D organoids***

siRNA-mediated YAP knockdown was carried out in 3D organoids isolated from mouse pancreas. The organoids were grown up to 80-90% confluency in a 24-well plate. On the day of transfection, ice-cold Splitting media was added onto the Matrigel containing the organoids. The organoids were scrapped and pipetted up and down using a P1000 pipette. Following this, the organoids were centrifuged at 200 xg for 5 min at RT. After centrifugation, supernatant was removed and 2 mL of 0.25% Trypsin-EDTA solution added to the cell pellet. Cells were vigorously pipetted up and down and incubated at 37°C for 5 min. The trypsinisation of the organoids were routinely checked every 2 min using a bright-field microscope. Once satisfied that the majority of organoids (90-95%) were dissociated as single cells, the trypsinisation process was stopped by using ice-cold Splitting media. The cells were then centrifuged at 300 xg for 5 min. After the removal of supernatant, cell pellet was resuspended with 450 µL of Complete Feeding media. To this, 50 µl of siRNA:Lipofectamine mixture was added. This mixture was prepared simultaneously during trypsinisation of the organoids. Similar to 2D cells, siRNA and Lipofectamine™2000 was diluted separately with OptiMEM for 5 min. Diluted siRNA and Lipofectamine™2000 were then mixed at a 1:1 ratio and incubated for 15 min at RT. 50 µL volume containing siRNA-lipid complexes added to the 450 µL of single cell suspension of organoids contained siRNA at a final concentration of 20 nM. 500 µL of cell mixture with siRNA-lipid complexes was

then transferred to a well of a 24-well plate. The plate was centrifuged at 32°C at 600 xg for 1 h. After centrifugation, the plate was incubated in a tissue culture incubator at 37°C for 4 h. Following the 4h incubation, the transfection mixture was centrifuged at 400 xg for 5 min at RT. The supernatant was then removed, and the cell pellet was embedded in Matrigel and cultured in a 24 well plate at 37°C tissue culture incubator as described previously.

### 2.2.10 Stable knockdown using lentiviral shRNA vectors

Stable knockdown of YAP was achieved through the infection of human cell lines MiaPaCa-2, Panc-1 and Psn-1 and mouse cell lines PancO2 and KPC with shRNA lentivirus. To perform this, pLKO.1-puro-shRNA constructs targeting human YAP (Addgene) and mouse YAP (Sigma) was used. Similarly, pLKO.1-puro Non-Target control shRNA (Sigma) was used as the control (See Table 2.8 for the shRNAs used). The lentiviral constructs were generated by transfecting HEK 293T cells with the shRNA vector along with second generation lentivirus packaging vectors, psPAX1 (Addgene) and pMD2.G (Addgene). X-tremeGene9 (Sigma-Aldrich) was used as the transfection reagent. The transfection mix was incubated for 20 min before mixing them with HEK 293T cells that have been trypsinised and suspended as single cells in the Complete DMEM. After 24 h of incubation in 37°C tissue culture incubator, the transfected cells were added with fresh Complete DMEM. Following this, the transfected HEK 293T cells were then cultured for further 24 h. The virus-containing supernatant was then harvested and filtered through 0.45 μM filter. The preparation of viral particles and infection of 2D cells and 3D organoids were carried out as described below.

***2D cells***

For 2D cells, the lentiviral particles produced by transfecting HEK 293T cells were diluted 1:2 in Complete DMEM and made into aliquots of 0.25 mL. To infect the cell lines, 8 mg/mL (w/v) of Polybrene (Hexadimethrine bromide) (Sigma) was added to an aliquot of the lentiviral particles at a dilution of 1:1000 and incubated for 10 min. The suspension mix was then added into the recipient cells and incubated at 37°C overnight. After 24 h, the process of cell infection with lentiviral particles was repeated to increase the efficiency. Again, the cells were incubated for 24 h, following which the media containing the virus supernatant was removed and washed ten times with 1X PBS. The cells were then trypsinised and replated into fresh flasks. Accordingly, the cells were cultured in Complete DMEM supplemented with 3 µg/mL (w/v) of puromycin for selection. The media with puromycin was changed every two days until the satisfied selection had occurred. Finally, the cells were expanded and cultured in the Complete DMEM without puromycin and cells were harvested for further analysis.

***3D organoids***

For 3D organoids, the harvested viral supernatant was added with Lenti-X Concentrator (Clontech) at a ratio of 3:1. This mixture of viral particles and supernatant was incubated at 4°C overnight and then centrifuged next day at 1500 xg for 45 min at 4°C. The pelleted virus was resuspended at 1 mL of Splitting Media and aliquotted at a volume of 0.25 mL. For infection of organoids, the 3D organoids were first dissociated as single cells from their dome-shaped structure embedded in Matrigel using the same protocol as described earlier of breaking up and trypsinisation of the organoids. After the quenching of the trypsinisation process by adding DMEM (supplemented with 5% FBS, 1% P/S and 2mM Glutamine), the cells were centrifuged at 200 xg for 5 min at 4°C. The resuspended pellets were then added with 0.25 mL viral aliquots. Similar to 2D cells, the viral aliquots were also

incubated in 8 mg/mL (w/v) of Polybrene before mixing with the organoid pellets. The suspension of single cells with viral particles was transferred to 48-well culture plate and centrifuged at 600 xg for 1 h at RT. The centrifuged plate was then incubated at 37°C in a tissue culture incubator for 6 h. Following incubation, the organoids, incubated with viral particles, were centrifuged at 120 xg for 5 min at 4°C. The pellets were again resuspended in the Matrigel as described previously and overlaid with the Mouse Feeding Media after the Matrigel dome had solidified. 10 µM of Rho Kinase Inhibitor, Y-27632, was added to the Feeding Media at 1:1000 concentration. After 48 h of incubation of the cells at 37°C tissue culture incubator, the media was changed to fresh Feeding Media containing 3 µg/mL Puromycin for selection. Again, similar to 2D cells, the Feeding Media with puromycin was changed every two days until the occurrence of satisfied selection. Following this, the organoids were expanded and harvested for further analysis.

### 2.2.11 Protein extraction from cell lines and organoids

The cells from both cancer cell lines and organoids were harvested using radioimmunoprecipitation assay (RIPA) buffer [150 mM (w/v) NaCl, 5mM EDTA, pH 8.0, 1M Tris, pH 8.0, 1.0% NP-40, 0.5% (w/v) sodium deoxycholate, 0.1% (w/v) SDS] with cOmplete™ protease and PhosSTOP™ phosphatase inhibitor cocktails (Roche). For 2D cells, the culture media was removed and washed once with ice-cold 1X PBS. RIPA lysis buffer, with freshly added protease and phosphatase inhibitors, was added onto the tissue culture plate with the cells. Cells were then scraped down using a rubber policeman and lysed with RIPA buffer. Furthermore, the cells were sonicated at 20% vibration amplitude at the pulses of 2 seconds for 10-20 cycles depending on the cell density on a sonicator (Model 300 V/T, Ultrasonic homogenizer, Biologics Inc.). The lysed cells were then centrifuged at

4°C for 10 min at the highest speed (13,000 xg) and supernatant containing extracted proteins was collected.

Similarly, for the extraction of proteins from organoids, the organoids embedded within the Matrigel dome in a well of a 24-well plate was washed with ice-cold 1X PBS following the removal of Mouse Complete Feeding media. Approximately 500 µL of BD Cell Recovery Solution (Corning) was then added onto the Matrigel dome. The organoids within the layer of the gel were then transferred along with the Recovery Solution into a 15 ml tube and left on ice for 1 h to allow the release of the organoid from the Matrigel. The tube was then centrifuged at 300 xg for 5 min following which the pellets were washed with ice-cold 1X PBS. RIPA lysis buffer, freshly supplemented with protease and phosphatase inhibitors, was added to the pellet. Subsequently, rest of the steps were followed as before for the protein extraction from cell lines.

Following protein extractions, protein concentrations were determined using Pierce BCA (bicinchoninic acid) Protein Assay Kit (Thermo Fisher) for the colourimetric detection. The BCA reagents, Reagent A and B, were mixed in a ratio of A: B = 50:1. The absorbance at 562 nm allows this assay to provide linear increment with the ascending concentration of proteins. Bovine Serum Albumin (BSA) (Thermo Fisher) at varying concentrations of 20-2,000 µg/mL was used to generate standard curve. Protein amounts were normalised by resuspending in NuPAGE LDS Sample Buffer (Thermo Fisher) and boiled at 95 °C for 10 min.

### 2.2.12 Western blotting

Equal amounts of protein samples were loaded on NuPAGE® 10% Bis-Tris Gel 1.5 mm (Life Technologies). Gels were generally run at 120 V in NuPAGE® MOPS SDS running buffer (Life Technologies) for 2 h. Separated protein samples were then transferred onto PVDF

membrane (GE Healthcare Whatman™) at 100 V for 90 min in transfer buffer [25mM (w/v) Tris-HCl, 190 mM Glycine, 20% (v/v) methanol]. Western blot membranes were blocked in either 5% (w/v) non-fat milk or 5% (w/v) BSA and PBS/0.01% Tween-20 (PBS-T) for 1 h. The membranes were then incubated in primary antibodies overnight at 4°C. Following this, membranes were washed with PBS-T and incubated in secondary antibodies, conjugated to horseradish peroxidase (HRP) (See Table 2.4 for the list of antibodies and dilution used). Enhanced chemiluminescence (ECL) (Thermo Fisher) or Millipore Immobilon Western Chemiluminescent HRP Substrate (Merck Millipore) was used for protein detection. Blotted proteins were visualised using X-ray Film (Fujifilm).

### 2.2.13 Immunofluorescent staining of organoids

Organoids were embedded in a 50 µL of the Matrigel in a well of a 8-well chamber-slide (Thermo Fisher). For fixation, 300 µL of freshly prepared 4% (v/v) paraformaldehyde (PFA) [16% (v/v) PFA in PME buffer] were added to the organoids and incubated for 20 min at RT. PME buffer was prepared as 10X stock solution by mixing 500 mM (w/v) PIPES, 25 mM $MgCl_2$ and 50 mM EDTA. After 20 min of fixation, the PFA solution was removed, and organoids were washed with IF buffer [ 0.2% (v/v) Triton X-10 and 0.05% (v/v) Tween diluted in PBS]. Following this, the organoids in the well were permeabilised for 20 min by adding 300 µL of Permeabilisation Solution [0.05% (v/v) Triton X-100 in PBS]. The organoids were washed with IF buffer and incubated in Blocking Solution [1% (v/v) BSA in IF buffer] for 30 min at RT. Primary antibodies were diluted in blocking solution, with 150 µL of the final volume added to each well. (See Table 2.4 for the list of antibodies and dilution used). The chamber-slide was placed in a large humidified chamber and incubated in primary antibody overnight at 4°C. Next day, the well was washed with 300 µL IF buffer, by placing

it on a benchtop orbital shaker during each wash. Subsequently, the organoids were incubated in secondary antibodies diluted in Blocking Solution at a final volume of 150 µL for 1 h at RT. DAPI was also added to the secondary antibody solution at a dilution of 1:1000 to visualise nuclei. After the secondary antibody incubation, the well was washed with 300 µL IF buffer. The chamber was detached from the slide using the removal kit. A small amount of Prolong® Gold antifade reagent (Thermo Fisher) was applied over each sample and a 24 x 60 mm cover glass (VWR) was placed over each slide, avoiding bubbles. The sides of the cover glass to the slide was sealed with a clear nail polish and kept in RT in the dark to harden. Confocal microscopy was done using Andor Dragonfly microscope and image analysis carried out using Fiji software.

### 2.2.14 Orthotopic Injection of organoids into mouse pancreas

Pancreatic organoids were first dissociated into single cells. For this, organoids in Matrigel were harvested using Splitting Media containing 4 mg/mL Dispase II (Thermo Fisher) and rocked at 600 rpm in a thermomixer at 37°C for 30 min. The cells were then centrifuged at 200 xg for 5 min. After ensuring the complete removing of the Matrigel, cells were trypsinised by using 3 mL of 0.25% Trypsin-EDTA solution with 10 µL of 10 mg/mL DNase I (Sigma-Aldrich). The organoids in the trypsin solution were incubated at 37°C for 15-30 min, with occasional vortexing, until sufficient single cell dissociation was achieved. Following this, cells were again centrifuged at 200 xg for 5 min and then washed in Phenol Red Free (PRF) Splitting Media (+++). The dissociated cells were then counted and diluted in 50% Matrigel/PRF+++ such that 10 µL volume would contain desired number of cells.

During the surgical procedure, mouse was anaesthetised with 4% Isoflurane/Oxygen. The mouse was then transferred to the nose cone, where the Isoflurane was reduced to 2%.

Eye gel was applied in order to avoid dryness in the eyes. Analgesics – 5 mg/kg dosage of Metacam and 0.1 mg/kg of Vetergesic – was administered into the scruff of the mouse neck. Fur which would cover a reasonable area of the wound site in the abdomen was removed using hair clipper. Following this, a small incision (around 1 cm) was made in the skin of the left abdominal side. An even smaller incision was then made through the peritoneum in the same orientation. Using forceps, the spleen was exteriorised along with the pancreas attached to it. 10 uL of Matrigel/PRF+++ containing organoids were then injected into the tail portion of the pancreas using a Hamilton syringe with 26 gauge needle. The formation of a bubble intact at the injection site indicated successful injection with no possible leakage through pancreatic capsule. The needle was then slowly retracted, and the spleen and pancreas gently moved back into the peritoneal cavity. The peritoneum was sutured using a 4.0 Vicryl (Ethicon) and the skin was closed with a 7 mm clip applier. The mouse was then kept at 37°C recovery chamber and placed back to IVC upon fully waking up. The mouse was monitored closely after surgery.

### 2.2.15 MRI Scanning

One-week post-surgery, the mouse underwent MRI scan to monitor any possible tumour growth in the pancreas. Prior to scanning, the mouse was anaesthetised with 1.5-3% Isoflurane/Oxygen following which it was positioned into a custom-made, 3D printed, multimodality cradle. The MRI scanning of the abdominal region of the mouse in the cradle was performed using a 4.7 T 310 mm horizontal bore Biospec AVANCE III HD preclinical imaging system equipped with 114 mm bore gradient insert (Bruker BioSpin GmbH, Germany). The mouse body temperature was maintained at 36°C by monitoring rectal temperature using an optical system (ACS-P4-N-62SC and OTP-M, Opsens Inc., Quebec,

Canada). Using a pneumatic balloon (VX010, Viomedex Ltd, UK), respiration was monitored and maintained at 40-60 breaths/min. The balloon was placed against the animal's chest and coupled to a pressure transducer. The respiration signal was then passed to a custom-built gating device to generate a threshold-based respiration gating control signal. In the respiratory gating method, an additional duration of about 150 ms was set to last until after the completion of each breath. This allowed acquisition of fully relaxed slices during inter-breath periods. As a result, efficient multi-slice scanning of the mouse was obtained with reduced sensitivity to respiratory motion of the free breathing animal (Kinchesh et al., 2019).

### 2.2.16 Image and statistical analyses

Pancreatic Intraepithelial Neoplasia (PanIN) lesions were identified based on cytological and architectural features as described in Section 1.2.6 of this thesis and confirmed by Prof Robert Goldin at the Ludwig Institute for Cancer Research, University of Oxford. Immunoreactivity for pERK and YAP was, at first, assessed by using Aperio ImageScope software to determine nuclear intensity signals. Number of positive nuclear for each intensity signal (3 = strong, 2 = medium, 1 = weak and 0 = negative) was then quantified manually. This was verified by using the analysis tool in Aperio ImageScope software. Besides, the ImageScope software was also used to determine percentage of intensity of RASFF1A and pYAP signals in the apical region of PanIN lesions. Regression analysis was carried out to determine correlation coefficient, *R*, and p-value.

Densitometry for Western Blot images was quantified by calculating mean grey value in Fiji (ImageJ) software. For all the densitometries from Western Blot experiments and the correlation study between Alcian blue and nuclear YAP in PanIN lesions of KC mice,

statistical analysis was carried out using two-tailed Student's t-test and calculated on Microsoft Excel or GraphPad Prism 7.0. Mean $\pm$ standard deviation (S.D) was calculated for the error bars. Chi-squared independence test was carried out to compare the distribution of categorial variables – in this study the staining intensity for nuclear YAP – between two human PDAC groups of high and low Alcian blue. The p-value for the Chi-square test was calculated in Microsoft Excel. For the Kaplan-Meier curves, R Survival package was used to generate Kaplain-Meier survival curve. In all statistical analyses, $p \leq 0.5$ was considered statistically significant and $p \leq 0.1$ was considered to indicate high statistical significance.

# Results I

# Chapter 3 Role of YAP in KRAS-mediated progression of PDAC

## 3.1 Introduction

### 3.1.1 Role of YAP and TAZ in PDAC

YAP, a downstream target of the Hippo pathway, is a well-known oncogene in many cancers including pancreatic ductal adenocarcinoma (PDAC) (Zanconato et al., 2016). Besides, YAP's close paralog TAZ is also a main effector of the Hippo tumour suppressor pathway and plays an important role in tissue development in mammals along with stem cell differentiation and renewal (Zhou et al., 2011). Indeed, Zhang et al. suggested YAP's critical role during the neoplastic progression of PDAC (Zhang et al., 2014). The tumour regions from PDAC patients presented higher expression of YAP proteins when compared to the adjacent normal ductal epithelium (Diep et al., 2012). A similar observation was also made at the mRNA level. Despite this, at the single cell level, the protein expression of YAP within the individual tumour cell was similar to that of normal ductal epithelium. Hence, the overall increase in YAP expression in the PDAC regions was reasoned to occur due to the proliferation of neoplastic cells rather than the increase in mRNA transcript and protein levels (Zhang et al., 2014).

Similarly, pancreatic tissues from mouse model with endogenous *Kras* mutation, *Kras*$^{LSL.G12D/+;}$ *Pdx-Cre* (KC) as well as human PDAC displayed elevated expression of TAZ in

the nuclei of PanIN lesions. This indicated significance of TAZ alongside YAP in PDAC tumourigenesis (Morvaridi et al., 2015). Besides pancreas, an active role of YAP and TAZ has been correlated with their malignant features in the tumour derivatives of other tissues including breast, lung and liver. These findings are significant given the non-essential role of these proteins in normal homeostasis of several adult organs and their very weak presence in the normal acinar cells of the pancreas (Zanconato et al., 2016).

### 3.1.2 Crosstalk between different components of Hippo and MAPK pathway

Previous studies reported that the elevated expression of YAP in the PDAC regions were localised mostly in the tumour nuclei. This presence of functionally activated YAP, as indicated by the protein's nuclear localisation, revealed significant role of upstream regulators of the Hippo pathway in PDAC development (Diep et al., 2012). Hence, the contribution of the upstream Hippo pathway should be considered while investigating YAP's role during PDAC progression. The study by Garcia-Rendueles et al. was of particular interest. In this, they demonstrated that the loss of NF2, which is an upstream regulator of Hippo pathway, led to an increased activation of YAP/TEAD in thyroid cancer. This, in turn, promoted transcription of oncogenic and wild type RAS, ultimately resulting in the augmentation of MAPK output (Garcia-Rendueles et al., 2015). In contrast, Zhang et al. reported YAP as the downstream effector of KRAS/MAPK pathway in the event of PDAC progression. They exhibited that the KRAS mediated MAPK pathway enhanced transcriptional activity of YAP. In turn, YAP augmented proliferation of epithelial cells in the PanIN lesions by expressing secretory factor-encoding genes. This ultimately enabled the progression of the neoplastic cells into PDAC (Zhang et al., 2014). This posed the

question whether there is a feedback mechanism that regulates the crosstalk activity between YAP-related, NF2-mediated Hippo pathway and KRAS-related MAPK pathway. While this still remains to be fully elucidated, previous studies have reported the negative feedback mechanism of YAP activation. This occurs via YAP's involvement, as a transcriptional co-activator, to induce the expression of its direct upstream inhibitor, LATS2 (Park et al., 2016). Furthermore, YAP is also involved in transcriptionally regulating the expression of NF2. Consequently, this allows further activation of LATS1/2, which in turn negatively affects YAP's activity (Dai et al., 2015; Moroishi et al., 2015).

## 3.2 Aims

We speculated that the mechanism of YAP-driven PDAC progression would involve the proteins' activation, regulated by upstream Hippo pathway, to be associated with other cell signalling pathways. Given the importance of MAPK pathway in cancer progression and high percentage of *KRAS* mutations in PDAC patients, in this chapter, I aim to study the association of YAP activation with the MAPK pathway signalling in pancreatic cancer cells. Furthermore, in order to characterise the phenotypic changes by which YAP contributes in the progression of precursor lesions to form aggressive PDAC, I aim to investigate the activation of YAP, by analysing its nuclear localisation, and associating the observation with the activation of MAPK signalling in the precursor lesions. In order to investigate these, I will be using pancreatic tissue from *Kras*-mutated mice with varying grades of PanIN lesions in this study.

## 3.3 Results

### 3.3.1 Transient YAP knockdown alters activation of ERK in pancreatic cancer cell lines

Previous work by Garcia-Rendueles et al. demonstrated YAP's transcriptional activity to regulate the expression of RAS in thyroid cancer cells (Garcia-Rendueles et al., 2015). We were curious to see if a similar mechanism, by which YAP and pERK proteins would associate, was observable in our *in vitro* models. Accordingly, I selected two human PDAC cell lines, MiaPaCa-2 ($KRAS^{G12C}$) and Panc-1 ($KRAS^{G12D}$), to carry out *in vitro* analyses. The molecular properties and phenotype of these cell lines have been well established and described to have high potential for tumourigenicity and invasion (Deer et al., 2010). In this study, I utilised the pancreatic cancer cell lines to transiently knock down the expression of YAP. Transfection was performed using siRNA technology against YAP and cells were harvested 24 h post transfection. Subsequently, I confirmed the knockdown in YAP's protein expression and evaluated its effect on MAPK pathway through western blot analyses (Fig 3.1).

Our data revealed reduced activation of ERK upon YAP silencing in the *KRAS* mutated cancer cells, Panc-1 and MiaPaCa-2 (Figure 3.1.A). Similarly, the densitometric analysis also confirmed a significant decrease in pERK levels in both cell lines, Panc-1 (n = 3, $P = 0.0007$) and MiaPaCa-2 (n = 3, $P = 0.001$) (Figure 3.1.B). Furthermore, a decrease in RAS expression was observed in Panc-1 cells (Figure 3.1.1A). The quantitative measurement revealed a trend of depletion in RAS levels, despite with no significance, in Panc-1 cells (Figure 3.1.B). On the other hand, the expression level of RAS proteins was unaffected upon YAP knockdown in MiaPaCa-2 cells (Figure 3.1.A) and was corroborated by quantitative

densitometric analysis that displayed only a slight fold decrease in RAS levels when YAP was knocked down (Figure 3.1.B). Importantly, the RAS protein here represents all three isoforms: KRAS, HRAS and NRAS. Hence, investigating expression level of specific RAS isoforms during YAP knockdown would be more informative in future.

In order to examine if the effect of YAP on MAPK pathway could be sustained, I transfected Panc-1 cells with YAP siRNA and harvested the cells 48 h post transfection. Paradoxically, the western blot analyses demonstrated a trend of increase in pERK levels, albeit being statistically non-significant, in Panc-1 cells ($P = 0.06$) (Figure 3.2.A and 3.2.B). RAS proteins, on the other hand, decreased significantly ($P = 0.001$) upon YAP knockdown in Panc-1 cells for 48 h. The effects of siRNA-mediated YAP knockdown in the activation of ERK for cells harvested 48 h post transfection presented contrasting results from the earlier observations for 24 h. While the observations for 48 h transfection will need to be validated in MiaPaCa-2 cell lines for further confirmation, these indicate potential activation of downstream MAPK activity, independent of RAS, when the depletion of YAP is prolonged. To validate this using a better approach, I carried out stable knockdown of YAP in the next step.

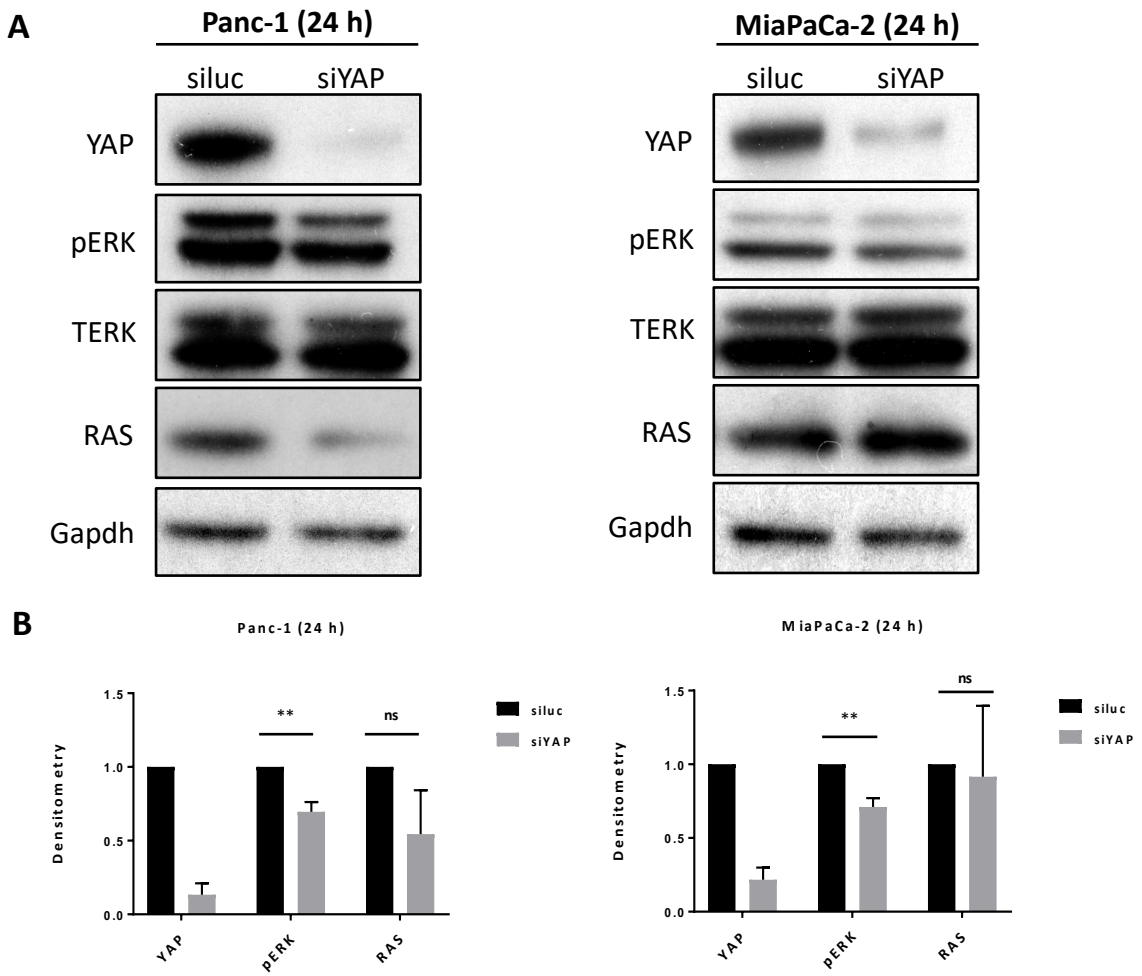


**Figure 3.1: Transient transfection of YAP for 24 h depletes MAPK/pERK signalling.** Panc-1 and MiaPaCa-2 cells were transfected with YAP siRNA (siYAP). siRNA against luciferase (siluc) was used as a control. (A) After 24 h of transfection, protein lysates were extracted using RIPA buffer and assessed by SDS-PAGE/Western Blot. The membranes were probed with phospho- and total ERK1/2 and RAS antibodies, while YAP antibody was used as an internal control. GAPDH acted as a loading control. (B) Protein levels were quantified by densitometry. Data are represented as mean ± SD from three independent experiments. $*P \leq 0.05$, $**P \leq 0.01$, $***P \leq 0.001$, $^{ns}P > 0.05$, two- tailed Student's *t* test.

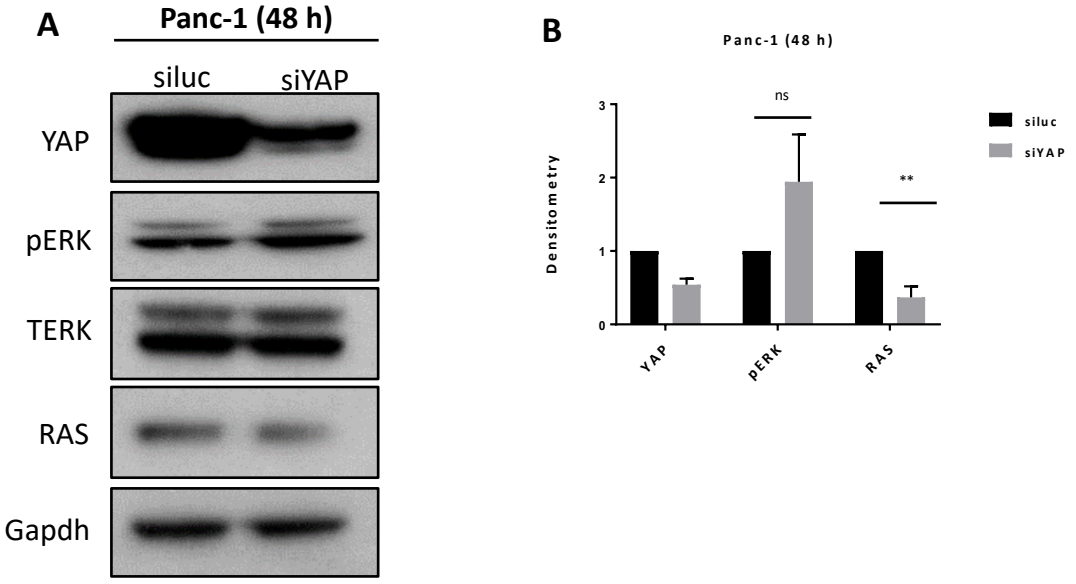


**Figure 3.2: Transient transfection of YAP for 48 h enhances ERK1/2 activation.** Panc-1 cells were transfected with YAP siRNA (siYAP). siRNA against luciferase (siluc) was used as a control. (A) After 48 h of transfection, protein lysates were extracted using RIPA buffer and assessed by SDS-PAGE/Western Blot. The membranes were probed with phospho- and total ERK1/2 and RAS antibodies, while YAP antibody was used as an internal control. GAPDH acted as a loading control. (B) Protein levels were quantified by densitometry. Data are represented as mean ± SD from three independent experiments. $*P \leq 0.05$, $**P \leq 0.01$, $***P \leq 0.001$, $^{ns}P > 0.05$, two- tailed Student's *t* test.

### 3.3.2 Stable YAP knockdown alters pERK and TAZ levels in pancreatic cancer cell lines

Earlier results demonstrated discrepancy in the levels of pERK after the harvesting of Panc-1 cells was prolonged from 24 to 48 h post transfection with YAP siRNA (Figure 3.1 and Figure 3.2). This led to investigate the long-term effects of stable YAP knockdown on the components of the MAPK pathway. For this, I used short hairpin (shRNA) for YAP (shYAP) in both mouse and human pancreatic cancer cell lines. Alongside, non-targetting shRNA (shCtrl) was used as a control. The two mouse cancer cells used in this study were PanO2 and KPC. PanO2 cell lines were established from induced tumour in C57BL/6 mouse and were devoid of mutations in *Kras* or other additional genes including *Egfr*, *Pik3ca* or *Braf* (Agalioti et al., 2017; Corbett et al., 1984). KPC cell lines were derived from tumour in a

genetically modified mouse developed due to Cre-mediated concomitant expression of mutated *Kras*$^{G12D}$ and *Trp53*$^{R172H}$ in a pancreas-specific manner (Torres et al., 2013). Lentiviruses were utilised for the delivery of shRNA into the cells. The cells were then harvested to confirm the knockdown of YAP and analyse subsequent effect on pERK level as a MAPK pathway output through western blot. Contrasting previous results in human PDAC cells harvested 24 h post transfection with siRNA (Figure 3.1), our data demonstrated an increase in the activation of ERK upon stable knockdown of YAP in both mouse cell lines (Figure 3.3.A). Quantitative analysis, however, indicated this difference to be statistically significant only in PanO2 cells (n = 2, $P$ = 0.005) (Figure 3.3.B). Likewise, I repeated the shRNA transfection of YAP in two human cell lines, MiaPaCa-2 and Panc-1, that were used previously for the siRNA experiments (Figure 3.4). A similar trend for ERK activation was again detected where stable YAP knockdown led to an overall increase in the protein's expression level (Figure 3.4.A). Of note, only MiaPaCa-2 cell lines displayed a significant change in the levels of pERK across three independent experiments when YAP was knocked down (n = 3, $P$ = 0.02), though the fold increase was less in comparison to Panc-1 cells (Figure 3.4.B).

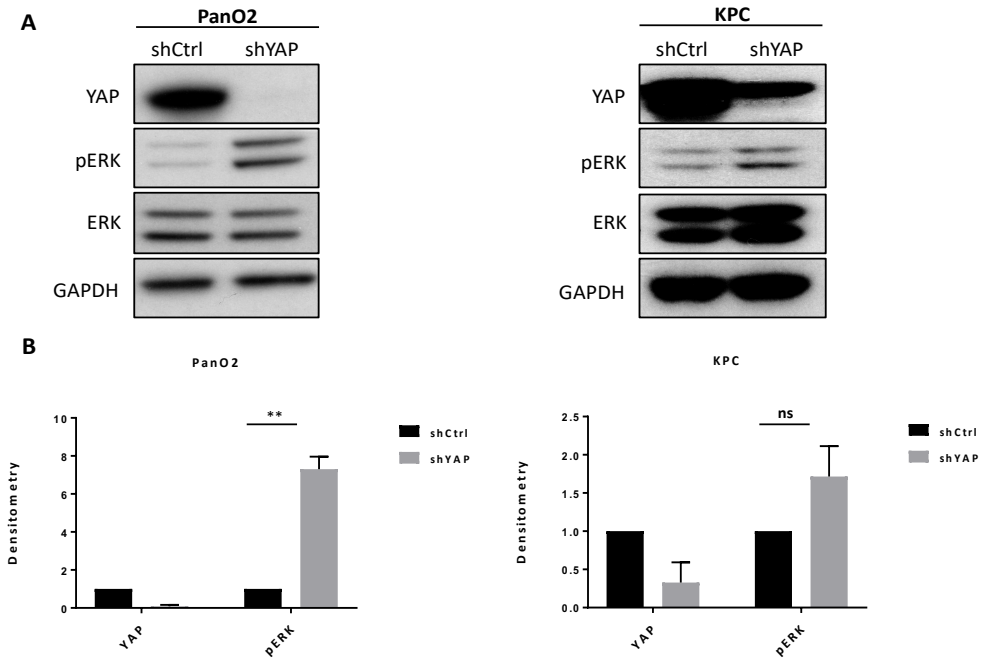


**Figure 3.3: Stable knockdown of YAP in mouse PDAC cell lines increases pERK levels.** Mouse pancreatic cancer cells, PanO2 and KPC, were subjected to shRNA-mediated knockdown of YAP. Non-Target shRNA (shCtrl) was used as a control. (A) After selection with puromycin, transfected cells were harvested using RIPA buffer and proteins assessed by SDS-PAGE/Western Blot. The membranes were probed with phospho- and total ERK1/2 antibodies, while YAP antibody was used as an internal control. GAPDH acted as a loading control. (B) Protein levels were quantified by densitometry. Data are represented as mean ± SD from two repeats of cell harvesting experiment. $*P \leq 0.05$, $**P \leq 0.01$, $***P \leq 0.001$, $^{ns}P > 0.05$, two- tailed Student's *t* test.

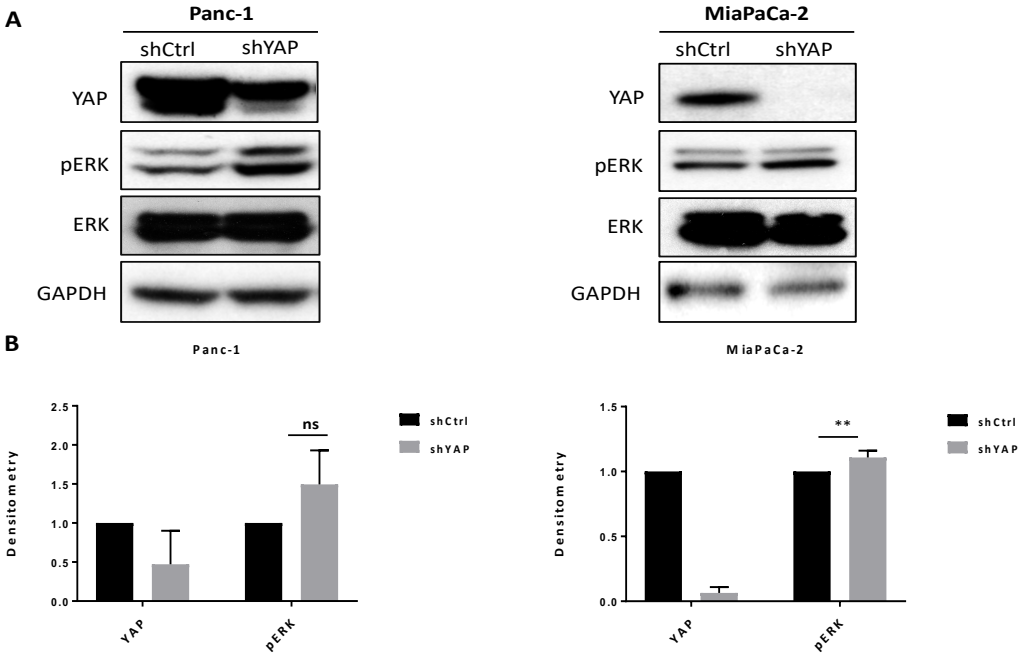


**Figure 3.4: Stable knockdown of YAP in human PDAC cell lines increases pERK levels.** Human pancreatic cancer cells, Panc-1 and MiaPaCa-2, were subjected to shRNA-mediated knockdown of YAP. Non-Target shRNA (shCtrl) was used as a control. (A) After selection with puromycin, transfected cells were harvested using RIPA buffer and proteins assessed by SDS-PAGE/Western Blot. The membranes were probed with phospho- and total ERK1/2 antibodies, while YAP antibody was used as an internal control. GAPDH acted as a loading control. (B) Protein levels were quantified by densitometry. Data are represented as mean ± SD from three technical repeats of cell harvesting experiment. $*P \leq 0.05$, $**P \leq 0.01$, $***P \leq 0.001$, $^{ns}P > 0.05$, two- tailed Student's *t* test.

I then investigated if the increment of pERK in shRNA-mediated YAP knocked down cells occurred due to the presence of serum in the culture. Serum stimulation results in the activation of ERK. A previous study using serum-starved HEK 293 cells displayed a peak in pERK level within 5 min of serum stimulation and was sustained at least until 30 min (Abkhezr et al., 2010). Hence, in this study, I cultured KPC cells that had been transfected with either shCtrl or shYAP. During this, I serum starved the cells by depleting the concentration of FBS to 0.1% in the culture media (DMEM) for 18 h. Next, I stimulated the cells with serum by replacing the media with 10% FBS. The KPC cells were stimulated for different time periods – 5, 10, 15 and 30 min. After this, the cells were harvested and analysed by western blot. The results displayed a gradual increase in pERK levels as the duration of serum stimulation prolonged in both shCtrl and shYAP transfected KPC cells (Figure 3.5.A). Similarly, comparative analysis between shCtrl and shYAP transfection displayed an increased activation of ERK upon YAP knockdown at each time point of serum stimulation. This was confirmed by the densitometric analysis (Figure 3.5.B). Despite the general trend of increased ERK activity upon stable YAP knockdown, the difference was significant only at 15 min of serum stimulation. (n = 2, $P = 0.007$). Taken together, our data indicate a paradoxical increase in pERK levels when YAP's depletion is prolonged in mouse and human pancreatic cancer cells. The presence of serum did not appear to regulate this effect on the MAPK component due to depletion of YAP.

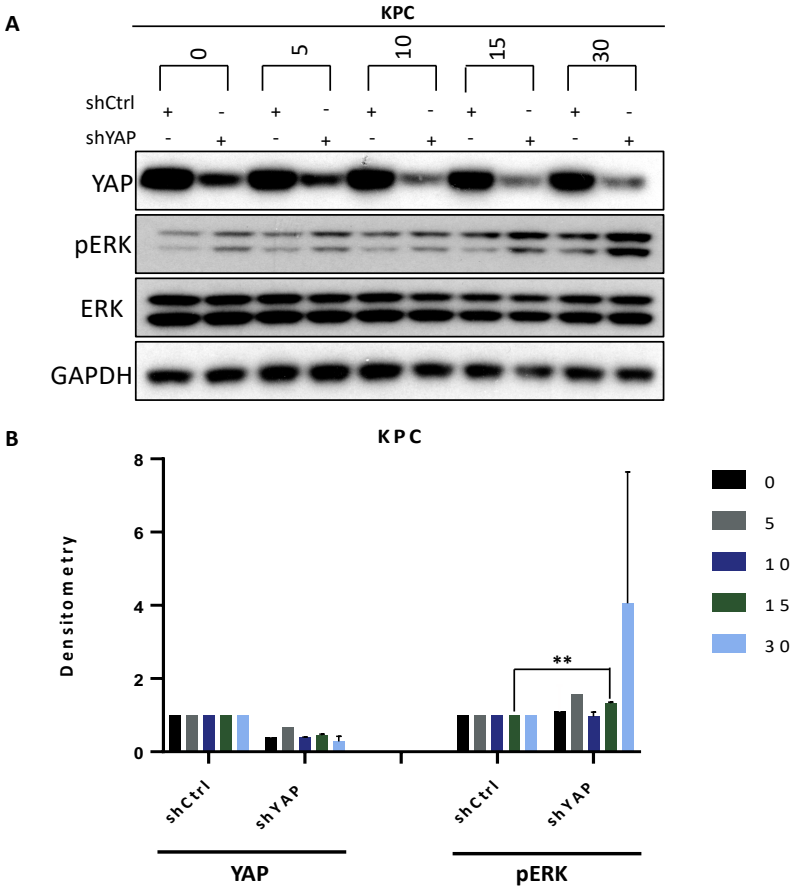


**Figure 3.5: Time-dependent stimulation of shYAP transduced KPC cells with serum.** KPC cells, that were transduced with Non-Target shRNA (shCtrl) and YAP shRNA (shYAP), were grown in serum free media (0.1% FBS in DMEM) for 18 hr. Following this, the stably transfected KPC cells were replaced by serum (10% FBS in DMEM). (A) Cells were harvested at different time points (5-30 min) using RIPA buffer. Proteins were then assessed by SDS-PAGE/Western Blot. The membranes were probed with phospho- and total ERK1/2 antibodies, while YAP antibody was used as an internal control. GAPDH acted as a loading control. (B) Protein levels were quantified by densitometry. Data are represented as mean ± SD from two technical repeats of serum stimulation and cell harvesting experiments. $*P \leq 0.05$, $**P \leq 0.01$, $***P \leq 0.001$, $^{ns}P > 0.05$, two- tailed Student's *t* test.

Next, I investigated if TAZ, which is a paralog of YAP, would play any role in enhanced activation of ERK observed in human and mouse pancreatic cell lines with stable knockdown of YAP. Previous studies have suggested a compensatory role of TAZ in YAP knockout conditions (Guo and Zhao, 2013; Miesfeld et al., 2015). Based on these, I speculated that TAZ could be providing a similar compensatory mechanism in stably YAP knocked down pancreatic cancer cells in this study. An increase in TAZ expression level was observed when YAP was stably depleted in mouse cell lines, PanO2 and KPC (Figure 3.6.A),

and human cell lines, Panc-1 and MiaPaCa-2 (Figure 3.7.A). Densitometric analysis corroborated this observation of increasing trend in TAZ levels, though the data were statistically non-significant (Figures 3.6.B and 3.7.B). Nevertheless, given the seeming trend of TAZ elevation, the possible role of the protein in compensating for the loss of YAP, by enhancing ERK activation, should not be ruled out. Combined deletion of both YAP and TAZ is required before any conclusion can be drawn.

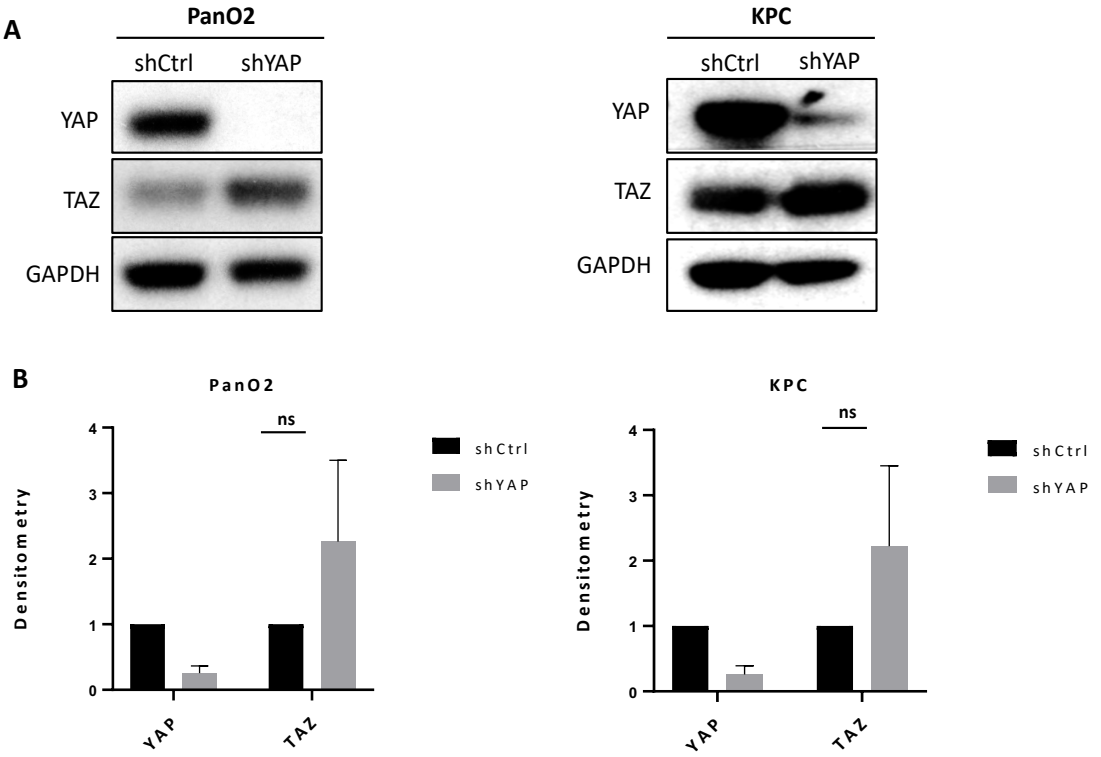


**Figure 3.6: Stable knockdown of YAP in mouse PDAC cell lines increases TAZ levels.** Mouse pancreatic cancer cells, PanO2 and KPC, were subjected to shRNA-mediated knockdown of YAP. Non-Target shRNA (shCtrl) was used as a control. (A) After selection with puromycin, transfected cells were harvested using RIPA buffer and proteins assessed by SDS-PAGE/Western Blot. The membranes were probed with TAZ antibody, while YAP antibody was used as an internal control. GAPDH acted as a loading control. (B) Protein levels were quantified by densitometry. Data are represented as mean ± SD from two technical repeats of cell harvesting experiment. $*P \leq 0.05$, $**P \leq 0.01$, $***P \leq 0.001$, $^{ns}P > 0.05$, two- tailed Student's *t* test.

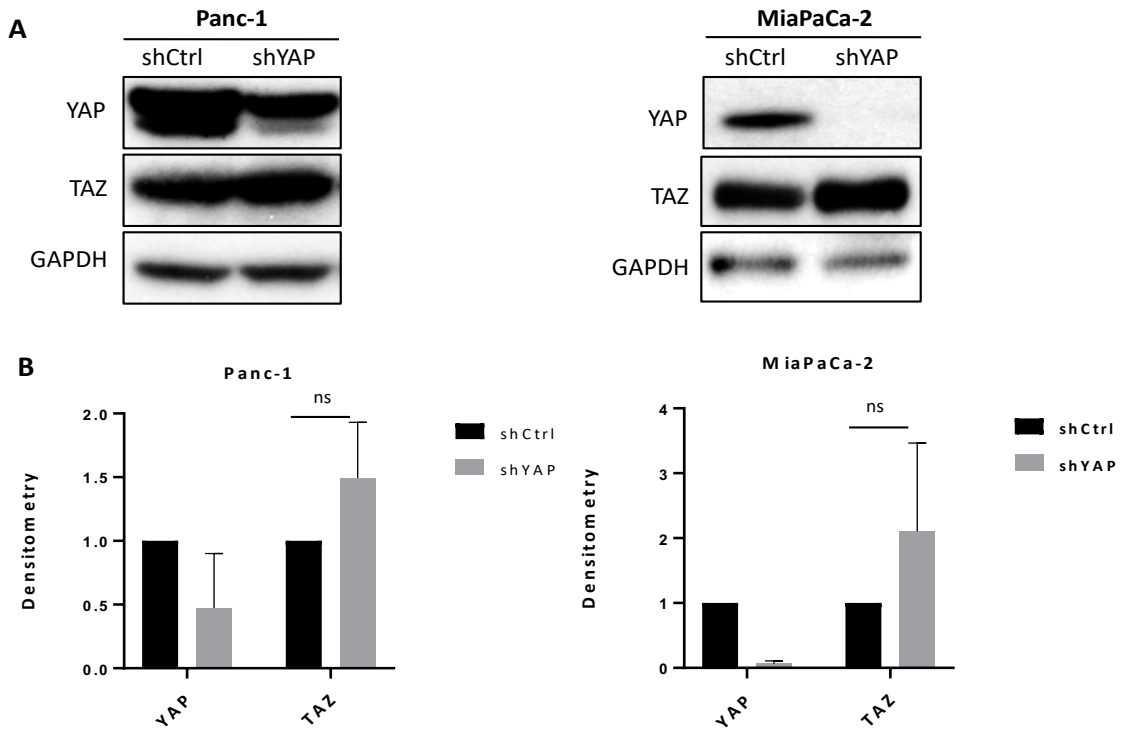


**Figure 3.7: Stable knockdown of YAP in human PDAC cell lines increases TAZ levels.** Human pancreatic cancer cells, Panc-1 and MiaPaCa-2, were subjected to shRNA-mediated knockdown of YAP. Non-Target shRNA (shCtrl) was used as a control. (A) After selection with puromycin, transfected cells were harvested using RIPA buffer and proteins assessed by SDS-PAGE/Western Blot. The membranes were probed with TAZ antibody, while YAP antibody was used as an internal control. GAPDH acted as a loading control. (B) Protein levels were quantified by densitometry. Data are represented as mean ± SD from three technical repeats of cell harvesting experiment. $*P \leq 0.05$, $**P \leq 0.01$, $***P \leq 0.001$, $^{ns}P > 0.05$, two- tailed Student's *t* test.

### 3.3.3 Role of upstream regulator of Hippo pathway, NF2, in the regulation of MAPK pathway in PDAC

I next focussed to investigate if the upstream regulators of the Hippo pathway, particularly NF2, would produce any downstream effect on YAP and MAPK activity in the context of PDAC. To address this, I firstly examined the expression levels of NF2 and YAP in the publicly accessible PDAC gene expression datasets. I used web-based resource, cBioPortal for Cancer Genomics (http://www.cbioportal.org/) (Cerami et al., 2012; Gao et al., 2013), and then explored the dataset in the resource provided by The Cancer Genome Atlas (TCGA). The TCGA dataset, based on RNA-Seq results, provide gene expression in individual PDAC sample (Williams et al., 2014). The TCGA cohort analyses, that included 149 PDAC patient

samples, did not demonstrate any obvious correlation in the mRNA expression of YAP and NF2 genes [ Pearson coefficient = -0.19, Spearman coefficient = -0.20, p-value= 0.0134] (Figure 3.8.A). Given the weakness of correlation between YAP and NF2 at the mRNA level, the impending question to the mechanism by which the tumour suppressor Hippo pathway regulates YAP during PDAC tumorigenesis remained unanswered. To further investigate this, I altered the expression of NF2 gene by using siRNA technology. For this, an additional cell line, Psn-1, was used besides previously used MiaPaCa-2 cells. Psn-1 cells were derived from human PDAC tissue and characterised to contain activated $Kras^{G12C}$ mutation, which was amplified in the same degree as the original tumours (Yamada et al., 1986). siRNA-mediated depletion of NF2 led to the increment of pERK levels in both MiaPaCa-2 and Psn-1 cells when harvested 48 hours post transfection (Figure 3.8.B). I had postulated that any change in pERK level would occur due to the upstream regulation by the Hippo pathway. Surprisingly, pYAP expression was unaltered upon knockdown of NF2 in both cell lines. (Figure 3.3.1B). These observations are very preliminary (n=1). Hence, solid conclusions can only be drawn after further repeats. The preliminary data, so far, indicate NF2 to contribute in ERK1/2 activation through a different mechanism and is independent of the Hippo pathway-mediated regulation.

Taken together, our investigation in pancreatic cancer cells displayed YAP's involvement in contributing MAPK signalling. While the mechanism appeared to be affected by the presence of TAZ in the cancer cells, our data highlights the importance of YAP in PDAC. Accordingly, our results from the *in vitro* experiments enabled us to further explore the association of Hippo-pathway regulated YAP activation with the activation of MAPK signalling in the pre-invasive neoplastic lesions of pancreas. To study this, I used pancreata

from *Kras*$^{LSL.G12D/+}$*; Pdx-Cre* (KC) mice that has been characterised to display a spectrum of PanIN lesions at different grades (Hingorani et al., 2003).

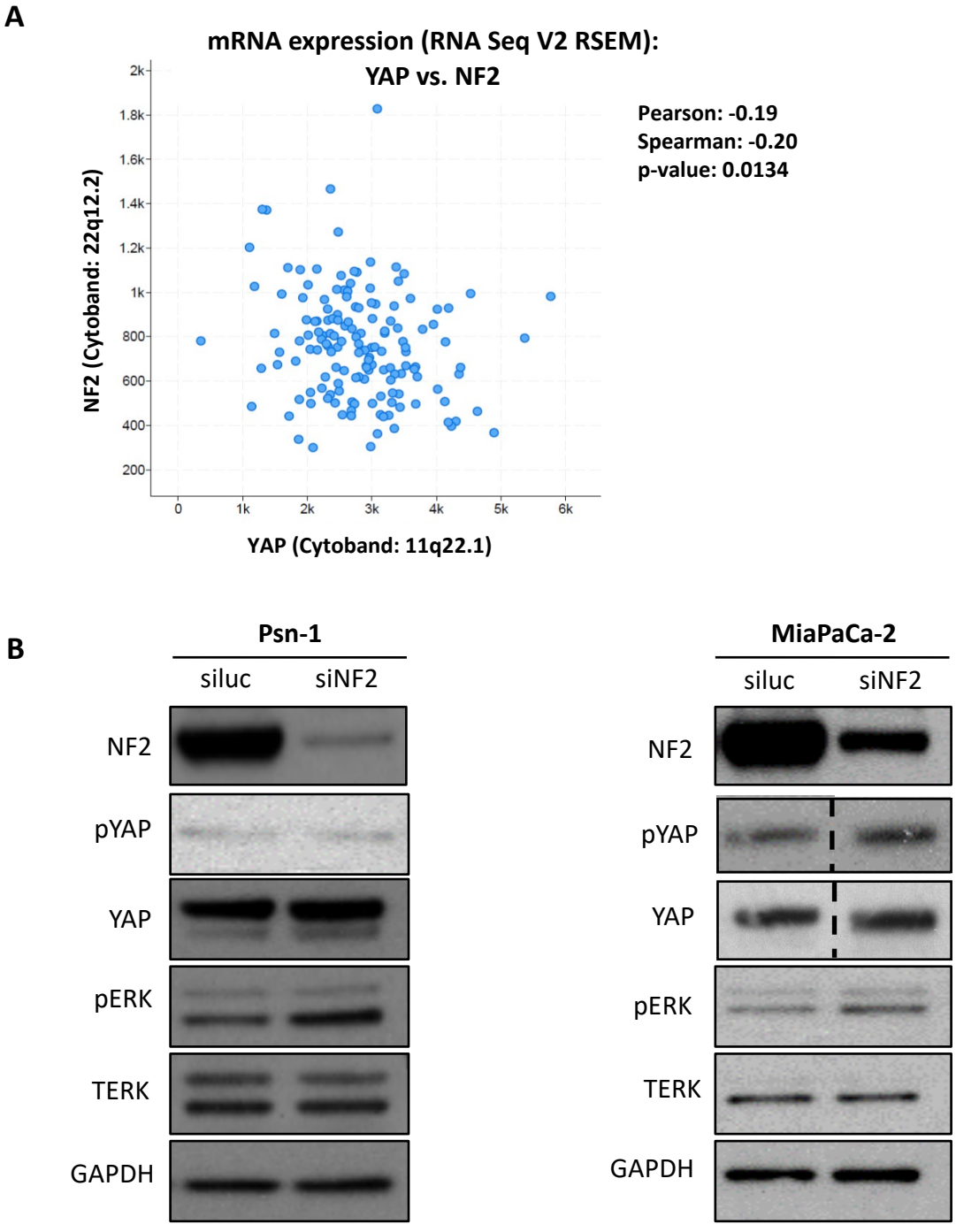


**Figure 3.8: Transient knockdown of NF2 enhances pERK levels but has no effect in YAP activation.** (A) RNA Seq data from 149 PDAC patients in TCGA displayed no correlation between NF2 and YAP mRNA levels. Analysis was performed using cBioportal (http:// cbioportal.org) (B) Psn-1 and MiaPaCa-2 cells were transfected with NF2 siRNA (siNF2). siRNA targetting luciferase (siluc) was used as a control. (B) After 48 h of transfection, protein lysates were extracted using RIPA buffer and assessed by SDS-PAGE/Western Blot. The membranes were probed with phospho- and total YAP and phospho- and total ERK1/2 antibodies, while NF2 antibody was used as an internal control. GAPDH acted as a loading control. Data are represented from one experimental repeat.

### 3.3.4 Histological characterisation of normal exocrine structure and precursor lesions (PanINs) in the KC mouse model in our study

Pancreatic Intraepithelial Neoplasia (PanIN) lesions undergo multiple stages of progression before developing into aggressive form of tumour. These several stages were earlier described as PanIN-1A/B, PanIN-2 and PanIN-3 which then ultimately progress into PDAC. The precursor lesions were classified based on their morphological and cytological features (Hruban et al., 2004). Recently, the classification system of PanIN lesions was re-evaluated and re-grouped into high- and low-grade lesions (Basturk et al., 2015). For the purpose of this study, I will classify the PanIN lesions into PanIN-1, -2 and -3 lesions. This is mainly due to our interest in investigating the molecular mechanisms of YAP during very early stages of PanIN-lesion development. Moreover, this will be useful in getting detailed molecular analyses of YAP as PanIN lesions acquire several other genetic alterations during their further progression into later stages of development.

At first, I characterised if the morphology and cytology of PanIN lesions hold true in the *Kras*$^{LSL.G12D/+}$*; Pdx-Cre* (KC) mouse model used in this study too. The H&E staining exhibited normal acinar and ductal structures in the exocrine region of the mouse pancreas. Expectedly, acini were arranged abundantly in a “berry-like clusters” manner (Figure 3.9i) whereas the intralobular duct represented classical cuboidal epithelium structure (Figure 3.9ii). Ducts, together with acini, constructed the normal region of the pancreas of the *Kras*-mutated mice. In regard to the pancreatic region affected by *Kras* mutation, a reactive area of ADM, where acinar cells appeared to undergo differentiation to form ductal structures, was observed (Figure 3.9iii). As described previously (Chapter 1, Section 1.2.6), PanIN-1 lesions were identified as the columnar cells with basally located nuclei. The

subdivisions, PanIN-1A and -1B, were grouped together and were generally referred as PanIN-1 lesions (Figure 3.9iv). Similarly, the transition to PanIN-2 lesions were mostly distinguished by common features including papillary structure, moderate nuclear atypia and loss of nuclear polarity that enables the nuclei localised in the basement membrane to migrate towards the apical region (Figure 3.9v). PanIN-3 lesions displayed mostly advanced features of the PanIN-2 lesions along with "budding off" of the cluster of epithelial cells into the lumen (Figure 3.9vi). Finally, PDAC, as by definition, presented invasion of basement membrane and arrangement of ductal structures, in a haphazard pattern, within the stroma (Figure 3.9vii). Overall, the identification of various structures – including normal: duct and acini, neoplastic: ADM and PanIN, and tumour – in the exocrine region of KC mouse pancreas is important. This, in turn, would enable us to further investigate the role of YAP in the multi-step progression of PanIN lesions into aggressive PDAC.

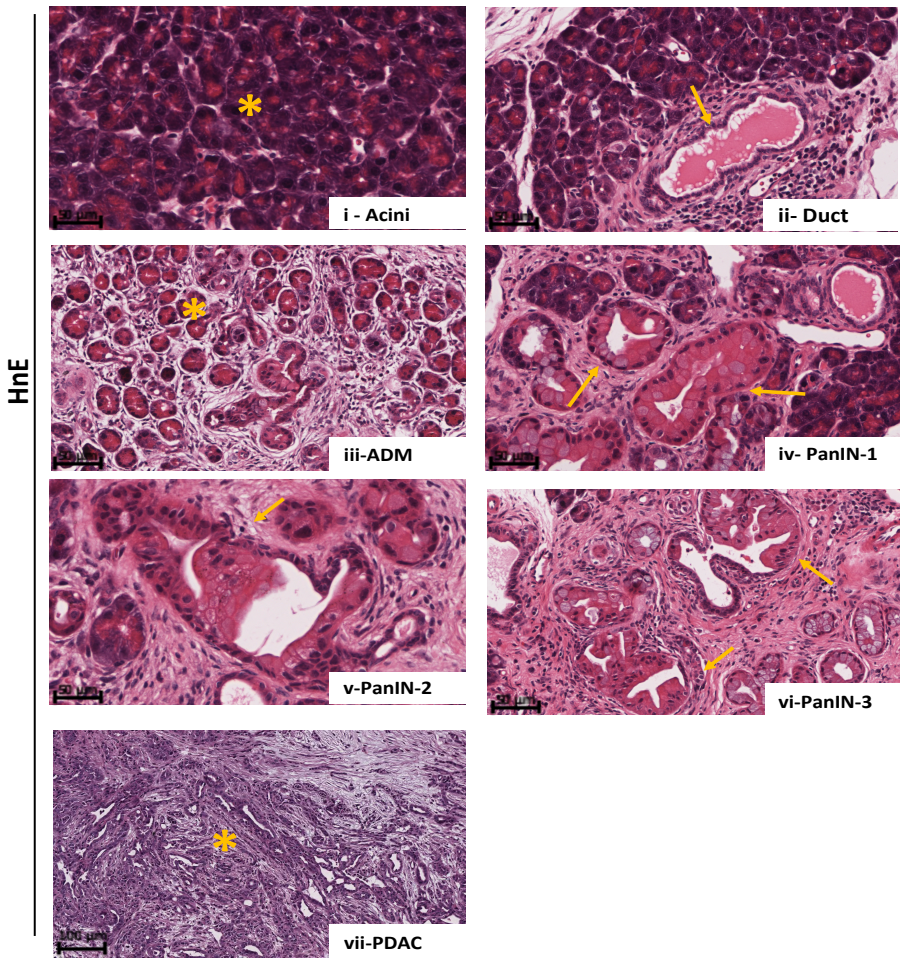


**Figure 3.9: Histological assessment of pancreatic tissue from *Kras*$^{LSLG12D/+}$; *Pdx-1-Cre* (KC) mouse displays a spectrum of PanIN lesions.** (i) Most of the normal pancreatic region comprises of acini(asterisk) which arrange as "berry in a cluster". (ii) Interlobular duct (arrow) displays cuboidal epithelium surrounding a lumen. (iii) Reactive region of acinar cells (asterisk) undergoing ADM form ductal epithelial-like structure. These metaplastic cells acquire luminal structures. Additionally, some of them also contain eosinophilic granules in the cytoplasm, reminiscent of acinar cells. (iv) PanIN-1 lesions (arrows) consist of columnar cells with basally located nuclei. (v) PanIN-2 lesion (arrow) showcases loss in nuclear polarity in the papillary structure and are pseudostratified. (vi) High-grade PanIN-3 lesions (arrows) display complete loss of nuclear polarity, with the cellular epithelium budding off into the lumen. (vii) An area of invasive ductal adenocarcinoma (asterisk) reveals haphazard arrangement of glands within desmoplastic stroma. Scale bars: i-vi = 100 µm and vii = 50 µm

### 3.3.5 YAP expression in the *Kras* mutated PanIN lesions

The Hippo pathway, by negatively regulating YAP-mediated proliferation, tightly controls the development of mammalian pancreas (George et al., 2012). YAP's localisation and stability plays an important role during this process. During embryonic development in mouse, there is a high nuclear expression of YAP proteins – they are mostly localised in the nuclei of pro-ductal cells and cytoplasm in acinus-fated cells. In the adult mouse pancreas,

however, this YAP expression is hugely reduced. Particularly, YAP was noted to mostly confine within the ductal compartment and only weakly present in the cytoplasm of acini. Human pancreas recapitulated this expression pattern of YAP in mice and presented positive nuclear staining of the protein in the ducts (George et al., 2012; Morvaridi et al., 2015).

To begin with, I investigated the expression pattern of YAP in KC mouse pancreas that endogenously expresses mutant *Kras*. YAP was present in the nuclei of the ductal epithelium of the KC mice (Figure 3.10.A). Moreover, this strong nuclear YAP in the ducts was consistently present in KC mice at different age (Appendix, Figure 7.3). In view of YAP's role during neoplastic progression of PDAC (Zhang et al., 2014), I also evaluated the presence of YAP in different stages of PanIN lesions in KC mice. Although YAP was strongly expressed in the nuclei of individual cells of normal ducts, given previous observations of YAP's strong presence with increased cell number in PDAC (Morvaridi et al., 2015), I postulated an increment in the overall expression of YAP within PanIN lesions of KC mice. Accordingly, I closely examined any alteration in nuclear YAP expression during multi-step progression of PanIN lesions into PDAC. Unexpectedly, nuclear YAP did not appear to increase proportionally as PanIN lesions progressed into later stage. In contrast, the observed PanIN lesions in KC presented both loss as well as retention of YAP in the nuclei (Figure 3.10.B). Indeed, the expression pattern of nuclear YAP in PanIN lesions was more complex and unpredictable within a given mouse. The representative image of a KC mouse pancreatic tissue displayed focal regions with differing intensities for YAP staining. There was heterogeneity in the expression of nuclear YAP, ranging from negative to strong positive signals among different grades of PanIN lesions (Figure 3.10.C). Interestingly, in the case of PDAC in KC mice, the tumour regions were mostly positive for nuclear YAP

expression (Figure 3.10.B). Given the heterogeneity, we next analysed hybrid epithelial structures that had properties common to both normal duct and PanIN lesions. Similar to previous observation, the immunostained images again exhibited two different scenarios – either loss of nuclear YAP expression or retention of nuclear YAP expression as the normal ductal cells transited into neoplastic lesions (Figure 3.10.D). Intriguingly, YAP's presence in the apical region of these PanIN lesions persisted even when the protein expression was lost from the nuclei (Figure 3.10.B and Figure 3.10.D).

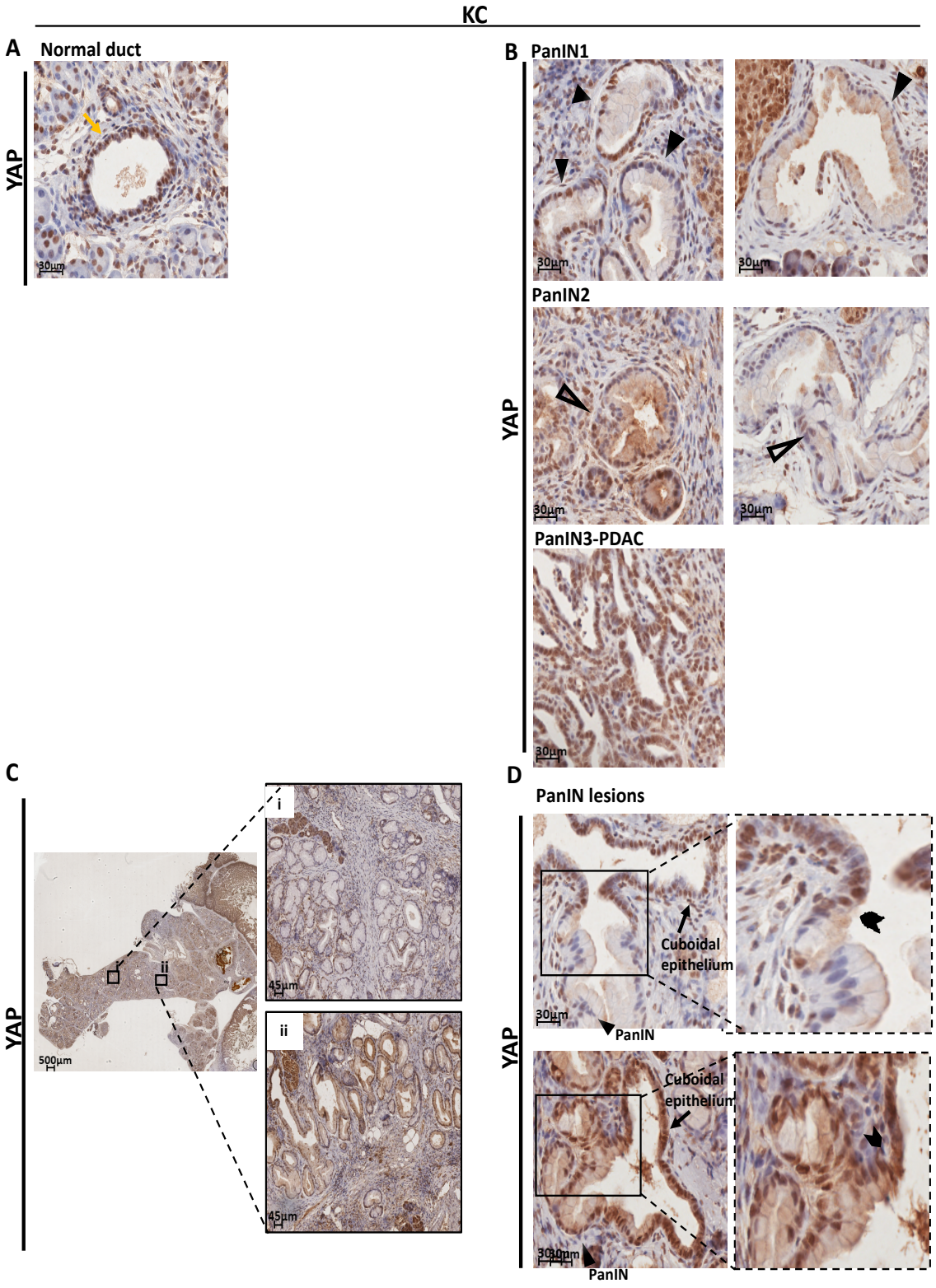


**Figure 3.10: Immunohistochemical analysis of YAP in PanIN lesions of KC mouse pancreata display heterogeneity.**
(A) Representative image of YAP in normal ductal epithelium (arrow) of *Kras*$^{LSL.G12D/+}$*;Pdx-1-Cre* (KC) mice . Scale bar = 30 µm (B) IHC staining for YAP in varying grades of PanIN lesions and/or PDAC. Black arrowheads: PanIN-1; Empty arrowheads: PanIN-2. Scale bar = 30 µm (C) Whole pancreatic section revealing immunohistochemical staining for YAP (left). Scale bar = 500 µm. Two different focal regions with PanIN lesions of the pancreatic tissue are magnified (right) and display negative (i) and positive (ii) for nuclear YAP in the PanIN structures. Scale bar = 45 µm (D) IHC staining for YAP in hybrid structures highlighting both normal ductal epithelium and PanIN lesions in KC mouse pancreata (left). Arrows: Normal epithelium; Black arrowheads: PanIN lesions. Scale bar = 30 µm. The region showcasing transition from normal duct to PanIN was cropped and magnified (right). Chevrons: Transition point. Data for PanIN lesions are representative of at least six mice (n=6).

### 3.3.6 pERK levels in the *Kras* mutated PanIN lesions

Activating mutations of *KRAS* occur at the earliest stage of low-grade PanIN lesions, PanIN-1, and are found in almost 90-95% of PDAC cases (Kanda et al., 2012; Kent, 2018). In order to study activation of KRAS-mediated MAPK pathway, I investigated the expression of phosphorylated ERK (pERK) as an output signal of the pathway (Moodie et al., 1993; Vojtek et al., 1993). In our study, weak-to-moderate staining of pERK mostly dominated ductal epithelium of KC pancreas (Figure 3.11.A). Besides, there was a small number of epithelial cells that displayed strong pERK signal. ERK1/2 is a master regulator of G1- to S- phase transition and crucial in cell growth and proliferation (Meloche and Pouyssegur, 2007) (William and Holtz 2017). Hence, the presence of pERK in normal ductal epithelium of KC could be reasoned due to the presence of mutated *Kras* in the pancreas. This oncogenic KRAS would enable sustained pERK activity and ultimately lead to aberrant proliferation and transformation of ductal cells into PanIN lesions.

To confirm this, I analysed for the presence of pERK in the PanIN lesions at different grades. As seen in Figure 3.11.B, pERK was present with medium to strong intensity among the entire spectrum of PanIN lesions as well as PDAC. Given the expression of mutated KRAS in the PanIN lesions, this observation was predictable as it leads to constitutive activation of KRAS/MAPK/pERK pathway. To closely examine the status of pERK signal, I looked at the hybrid structure transitioning from normal duct to PanIN lesions (Figure 3.11.C). Again, there was a shift in pERK intensity to stronger signal as the normal ductal epithelium transformed into PanIN lesions. Importantly, this increase in pERK level was prevalent in both the cytoplasm and nuclei of the PanIN lesions. Interestingly, when the presence of pERK specifically in the nuclei of PanIN lesions was considered, the consistent increase in the pERK levels was lost (Figure 3.11.C). I hypothesised this inconsistent expression pattern

of pERK in the nuclei might potentially associate with heterogeneously expressed nuclear YAP.

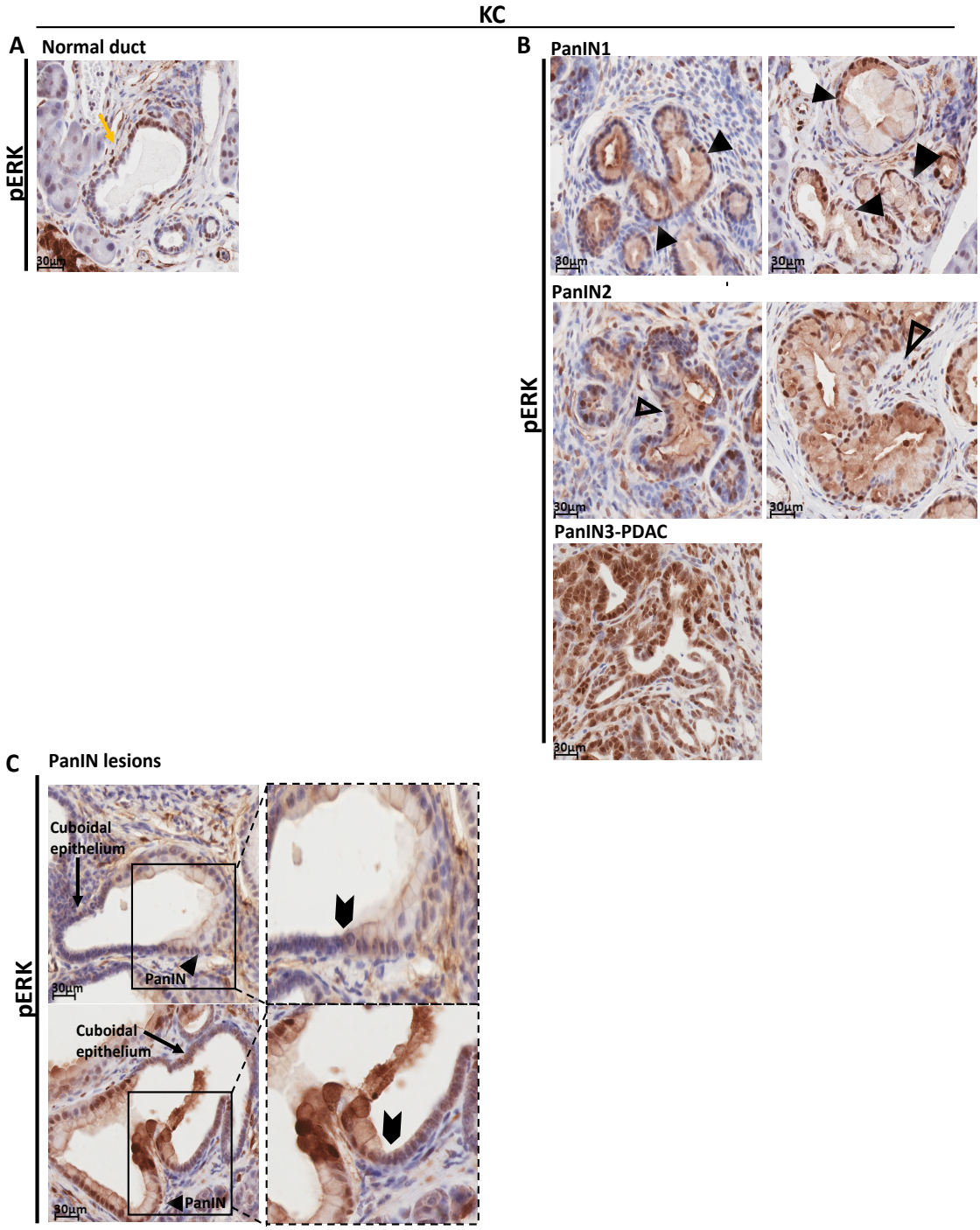


**Figure 3.11: Immunohistochemical analysis reveals strong levels of pERK in PanIN lesions of KC mouse pancreata.** (A) Representative image of pERK in normal ductal epithelium (arrow) in *Kras*$^{LSL.G12D/+}$*;Pdx-1-Cre* (KC) mice. Scale bar = 30 µm (B) IHC staining for pERK in varying grades of PanIN lesions and/or PDAC. Black arrowheads: PanIN-1; Empty arrowheads: PanIN-2. Scale bar = 30 µm (C) IHC staining for pERK in hybrid structures highlighting both normal ductal epithelium and PanIN lesions in KC mouse pancreata (left). Arrows: Normal epithelium; Black arrowheads: PanIN lesions. Scale bar = 30 µm. The region showcasing transition from normal duct to PanIN was cropped and magnified (right). Chevrons: Transition point. Data for PanIN lesions are representative of at least six mice (n=6).

### 3.3.7 YAP's activity in relation to pERK in the *Kras* mutated PanIN lesions

Given the heterogeneity in the nuclear expression of YAP (Figure 3.10) and pERK (Figure 3.11) among PanIN lesions, I next asked if there is an association between activated YAP and pERK within the same PanIN lesion. To address this, I examined any correlation between nuclear expression levels of YAP and pERK when matched PanIN lesions were taken into account. Firstly, I obtained serial sections from KC mouse pancreas and stained them for YAP and pERK. I then identified matching PanIN lesions in corresponding regions of these serial sections differently stained with YAP and pERK antibodies. Indeed, our qualitative analysis demonstrated YAP and pERK to follow similar nuclear immunoreactivity pattern within the same PanIN lesion. For lesions with low nuclear YAP expression, pERK positive nuclei in the corresponding lesion also appeared to be weak (Figure 3.12.A). Following a similar trend, lesions with strong nuclear YAP activity presented higher levels of pERK in the nuclei of matched lesions (Figure 3.12.B). Additionally, I examined this correlation of nuclear intensities between YAP and pERK quantitatively. PanIN lesions (n=22) from KC mice displaying both high and low intensities for nuclear YAP positivity were considered, irrespective of the grade of lesions. The intensity of the pERK nuclear signal in the corresponding lesions stained for YAP was also quantified. Our data indeed indicated a correlation between the nuclear expression of YAP and pERK in PanIN lesions of KC mice ($R$ =0.5, $P$ =0.012) (Figure 3.12.C). The data suggested presence of two types of PanIN lesions in the KC mice – PanIN lesions with high expression of nuclear YAP and pERK and PanIN lesions with low expression of nuclear YAP and pERK. Moreover, it established a possible link between Hippo pathway and MAPK pathway which could be useful in the advancement of *Kras* mutated PanIN lesions in KC mouse pancreata.

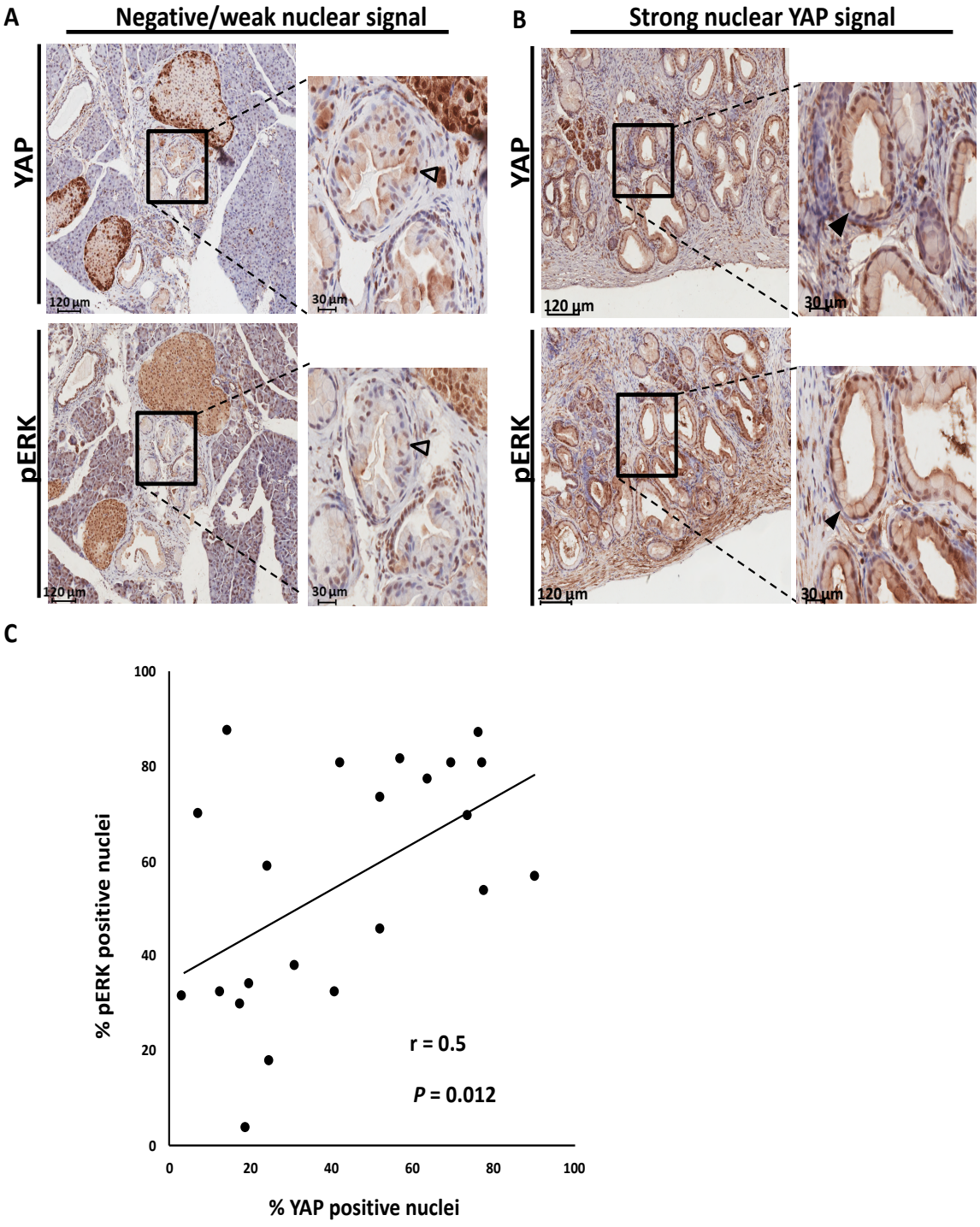


**Figure 3.12: Expression of YAP positively correlates with pERK levels in the nuclei of corresponding PanIN lesions of KC mouse pancreata.** IHC images representing corresponding regions in serial sections from *Kras*$^{LSL.G12D/+}$;*Pdx-1-Cre* (KC) mice stained with YAP and pERK (left). Scale bar = 30 µm. Magnified image showcasing corresponding PanIN lesions differently stained with YAP and pERK (right). Black arrowheads: PanIN-1; Empty arrowheads: PanIN-2. Scale bar = 120 µm. The PanIN lesions display both negative/weak signals (A) and strong signals (B) in the nuclei for the two antibodies. (B) Quantitative analysis demonstrates correlation between percentage of pERK positive nuclei and YAP positive nuclei in corresponding PanIN lesions (n =22). PanIN lesions included in the analysis were derived from pancreata of two KC mice at similar ages (40-42 weeks). *r* =0.5, *P* = 0.012.

## 3.4 Discussion

In this chapter, I investigated the potential role of YAP in the progression of early PanIN lesions during PDAC tumourigenesis. Indeed, our data from the spectrum of PanIN lesions within the pancreata of KC mice revealed heterogeneity in the nuclear expression of YAP (Figure 3.10). This observation potentially highlights the need to consider the risks associated with PanIN lesions based on their nuclear expression of YAP oncogene. It would also provide some explanation behind the failure of all PanIN lesions developing into invasive tumour despite being highly prevalent in most adult pancreas. Similarly, Hingorani et al. in 2003 demonstrated that not all mice developed invasive carcinoma in their pancreatic ducts in their KC mouse model (Hingorani et al., 2003). Therefore, understanding the molecular mechanism of nuclear YAP would be potentially useful in assessing the severity of individual PanIN lesions. This, in turn, would be useful in making therapeutic decisions in patients with a spectrum of these lesions.

Intriguingly, we observed a strong presence of nuclear YAP in the normal ductal epithelium of KC pancreas (Figure 3.10.A). Previously, a study reported that the presence of YAP in the small ducts of normal pancreas potentially plays a role in the maintenance of tissue homeostasis (Diep et al., 2012). YAP plays a crucial role in regulating progenitor cells in the pancreas (George et al., 2012), and the progenitor cell subpopulation has been long assumed to reside in the ductal compartment. From the nuclear localisation of YAP in the ductal epithelium in this study, we can speculate that YAP may be involved in maintaining stemness in the pancreas (Bonner-Weir et al., 2004; Lian et al., 2010; Voltes et al., 2019). Furthermore, the PanIN lesions that lost YAP in the nuclei were still able to retain the protein in the apical membrane (Figure 3.10.B and Figure 3.10.D). The upstream regulators

of the Hippo pathway kinases have been shown to recruit the core kinase cascade of the pathway to the apical membrane for activation (Yu and Guan, 2013). Hence, we can assume an active role of the Hippo pathway to regulate YAP's phosphorylation and localisation in the apical region of the PanIN lesions which are in nuclear expression of YAP. Hingorani et al. presented high heterogeneity in the expression of ERBB2/HER2 among the PanIN lesions in KPC mice. Interestingly, the heterogeneously expressing ERBB2/HER2 proteins exhibited strong positive correlation with pERK in these KPC mice (Hingorani et al., 2005). In our study of KC mice, the pERK signal was also shown to be inconsistent in the nuclei of PanIN lesions (Figure 3.11). This nuclear translocation of pERK has been known to be essential in G1 to S transition and consequently in cell proliferation (Mebratu and Tesfaigzi, 2009). From this, we can speculate that the PanIN lesions expressing higher levels of pERK in the nuclei would proliferate more and potentially progress faster during tumourigenesis.

In Figure 3.12, we demonstrated an association between heterogeneously expressing nuclear YAP with that of pERK in the nuclei of PanIN lesions. Similarly, through *in vitro* analyses, we presented the modulation of KRAS/MAPK signalling pathway output regulated by upstream YAP activation (Figure 3.1). Taken together, we propose a potential role of YAP to control the proliferative fate of PanIN lesions via MAPK/pERK pathway. Furthermore, our results also revealed that YAP might not be the sole player in modulating MAPK pathway activation in PDAC. Paradoxically, the stable knockdown of YAP in pancreatic cancer cells demonstrated an increased activation of ERK (Figure 3.3 and 3.4). Concomitantly, we also saw a trend of upward shift in TAZ expression level, albeit statistically insignificant, when YAP was stably depleted in these cancer cells (Figure 3.6 and Figure 3.7). The mechanism by which YAP negatively regulates the expression of TAZ

has been previously described: YAP targets TAZ for proteasomal degradation through its downstream effectors, heat shock protein 90 (Hsp90) and glycogen synthase kinase 3 (GSK-3α/β) (Finch-Edmondson et al., 2015).

Indeed, the important role of TAZ alongside YAP has been highlighted by Gruber et al. in 2016. In this study, the co-deletion of YAP and TAZ led to the failure in ADM formation, both *in vitro* and *in vivo* (Gruber et al., 2016). This is interesting as YAP was previously shown to be dispensable in ADM formation (Zhang et al., 2014). Similarly, this co-deletion of YAP and TAZ along with concomitant activation of oncogenic $Kras^{G12D}$ led to the arrest of PanIN lesions formation in the mouse model (Gruber et al., 2016).

In our study, we speculate a compensatory role of TAZ that could lead to the rescue of YAP phenotype upon its stable knockdown. Previously, the compensatory role of TAZ has been shown in zebrafish. It was shown that the knockout of *Taz* ($taz^{-/-}$) was required in *Yap* knockout ($Yap^{-/-}$) embryos for the complete loss of retinal pigment epithelium (RPE) formation during eye development. Similarly, the change in TAZ due to *Yap* knockout was shown to occur at the post-transcriptional level (Miesfeld et al., 2015). This could provide an alternative explanation for the increase in TAZ protein level due to stable depletion of YAP in our study. Further repeats, however, would need to be carried out to ensure the increase in TAZ expression levels is significant. Based on these, future experiments to explore the potential role of TAZ can be conducted by carrying out combined deletion study of YAP and TAZ.

Furthermore, I attempted to recapitulate the effect of NF2-mediated Hippo pathway in MAPK activation in thyroid cancer (Garcia-Rendueles et al., 2015). The results in this study in pancreatic cancer cells (Figure 3.8) indicated possible impact on the activity of pERK upon NF2 knockdown. This appears to occur via different mechanism and is independent

of Hippo-mediated pathway as there was no change in YAP activation. These observations are, however, preliminary and require further investigation. Given the important role of TAZ in PDAC and our observations of the TAZ's possible compensatory role upon prolonged depletion of YAP, it would be interesting to also investigate the protein level of TAZ when NF2 is depleted in pancreatic cancer cells.

In a previous study by Diep et al in human pancreatic cancer cells revealed low-to-moderate YAP staining in the nuclei of Panc-1 cells. Similarly, the effects of proliferation, apoptosis and anchorage independent growth in this cell line were also explored to establish the oncogenic role of YAP (Diep et al., 2012). Nevertheless, it is crucial to consider possible discrepancies while interpreting results linking our *in vivo* and *in vitro* models. Particularly, an *in vitro* system that recapitulates normal and early neoplastic ductal epithelium would be more useful while elucidating the possible association between YAP and ERK1/2 activation in the precursor lesions of KC mice.

In summary the work in this chapter presents heterogeneity in YAP's nuclear expression in PanIN lesions of KC mice. YAP appears to be associated with MAPK in these *Kras*-mutated mouse tissue and pancreatic cancer cells. Since, the MAPK output, pERK, plays a critical role in proliferation, YAP could contribute in the progression of these PanIN lesions into an aggressive form of tumour. While the contribution of YAP seems critical in PDAC progression, some of the lesions were devoid of nuclear YAP. We suspect that these lesions are in fact at low risk of aggressively developing into PDAC. Besides examining the downstream effects of YAP, it would be interesting to see the cause of this heterogeneity. While the mechanistic question regarding the Hippo pathway regulation still needs to be addressed, the observed phenotypic effects possibly – due to the cell of origin – could be investigated during the tumourigenic process in PDAC.

# Results II

# Chapter 4 Aggressive phenotype in PDAC in relation to cell of origin

## 4.1. Introduction

Morphological features are predominantly used to describe different stages of PanIN lesions. Nonetheless, they are insufficient while specifying their cell of origin. Although the exact lineage of cellular origin of PanIN lesions and, ultimately, PDAC still remains to be discovered, several studies in the past few years have supported the statement that PDAC originates from the acini. A recent study by Lee et al. used mouse models to concomitantly drive the expression of $Kras^{G12D}$ and ablate that of *Trp53*, specifically in the acini or the ducts using *Ptf1a* and *Sox9* promoter respectively. Ductal-derived PDACs mostly developed from high-grade PanIN lesions, which were move invasive and progressed faster to acquire aggressive PDAC phenotype, whereas acinar-derived PDACs maintained molecular properties of low-grade PanIN lesions. Comparatively, the acinar-specific mouse model took much longer to induce tumours in their pancreata. (Lee et al., 2018). Another study led by Ferreira et al. also exhibited a difference in tumour aggressiveness between PDAC of different cell of origin. They generated mouse models that expressed Cre-inducible $Kras^{G12D}$ allele in the acini, via Elastase-1 promoter, or in the ducts, via Ck19 promoters, alongside concomitant inactivation of tumour suppressors such as *Trp53* or *Fbw7*. The development of mucinous PanIN lesions derived from acini was similarly demonstrated, in a stepwise manner, before culminating into PDAC. In contrast, ductal-derived PDAC

formation did not depend on the progression of PanIN lesions but rather evolved faster from non-mucinous carcinoma in situ (Ferreira et al., 2017). Both of these studies displayed shorter median survival in mice with ductal-derived PDAC in comparison to the acinar-derived ones.

Previous studies have demonstrated abundant expression of mucins in PanIN lesions including MUC1, MUC2, MUC4, MUC4, MUC5AC and MUC6. The expression patterns for each of these mucins vary depending on different stages of development of PanIN lesions. Mucins are large *O*-glycoproteins comprising of a long peptidic chain called apomucin. They are secreted by epithelial cells, leading to the formation of viscoelastic gels (Jonckheere et al., 2010). This, in turn, allows the epithelial surfaces to remain protected. Interestingly, changes in the expression and glycosylation of mucins have been associated with several diseases including cancer (Dong et al., 2012). Alcian blue, a phthalocyanine dye, has been utilised to detect the presence of acidic mucins (Scott, 1996; Steedman, 1950). For this reason, Alcian blue has been used as a positive marker for the production of mucins in PanIN lesions (He et al., 2018). The acidic mucins are composed of carbohydrates with carboxylate ($CO_2^-$) or sulphanate ($SO_3^-$) groups, giving them an overall negative charge (Bansil and Turner, 2006). On the other hand, the molecular structure of the phthalocyanine in Alcian blue contains copper in the center, along with four basic isothiouronium groups, providing a positive charge to the molecule. As a result, Alcian blue molecule gets attracted to the anionic sites in mucin molecules and ultimately leads to the formation of blue colour when stained for acidic mucins (Kiernan, 2006).

Alcian blue staining is present in low-grade PanIN lesions and duct-like lesions devoid of neoplastic features whereas it is absent from high-grade PanIN lesions (Kopp et al., 2013). Given the association of Alcian blue positive low grade PanIN lesions in PDAC of acinar-cell-

, but not ductal-cell-, derived mouse models in previous studies (Ferreira et al., 2017; Lee et al., 2018), the application of Alcian blue in our study presented to be an important tool to determine precursor lesions and PDAC from different cell of origin. Regardless of several studies indicating putative ADM giving rise to PanIN lesions which ultimately progress to PDAC, the derivation of PDAC from ducts is still possible. This might, however, entail more complex, if not different, process for the progression of ductal cells into PDAC.

## 4.2 Aims

In this study, I intend to investigate the role of cell of origin by examining precursor lesions in pancreatic tissue from *Kras$^{LSL.G12D/+}$; Pdx-Cre* (KC) mouse model and PDAC from human patient cohort. For this, I firstly aim to establish if Alcian blue is, indeed, a valid method to differentiate cell of origin of precursor lesions and PDAC. Subsequently, I would like to optimise the quantification of Alcian blue in the PDAC region of human samples in order to analyse the trend of survival in patient samples stratified based on their expression level of Alcian Blue. Ultimately, I intend to investigate any association of Alcian blue staining with that of nuclear YAP in the precursor lesions and PDAC regions. Our observations in the previous chapter indicated heterogeneity in nuclear expression of YAP in the precursor lesions of KC mice. Hence, by correlating this heterogeneously expressed nuclear YAP with Alcian blue, I aim to further investigate if nuclear YAP expression coincided with precursor lesions and PDAC originated from a specific cell type.

## 4.3 Results

### 4.3.1. Establishment of Alcian Blue as a method for determining the origin of precursor lesions

Normal pancreatic ducts are devoid of Alcian blue positive ($AB^+$) mucins, and only stain for Periodic Acid-Schiff (PAS) – which stains for polysaccharides and neutral mucins. PanIN lesions, on the other hand, are positive for Alcian blue mucinous expression, indicating an early sign of metaplasia (Strobel et al., 2010). Furthermore, Kopp et al. indicated that this positivity for Alcian blue staining are generally limited to low-grade PanIN lesions whereas the high-grade lesions are mostly negative for Alcian blue (Kopp et al., 2012). To determine if this was also true in our study, I carried out immunohistochemical staining with Alcian blue in the pancreata of KC mice. Similarly, serial sections from the pancreatic tissue were used for H&E staining to determine the architecture of various cellular types and tissues. Consistent with previous studies, Alcian blue staining was absent in the ductal regions of these mice (Figure 4.1.Ai). Similarly, acini in these pancreatic tissues also stained negatively for Alcian blue. Likewise, the KC mice pancreata contained focally localised precursor lesions, with morphological features similar to pancreatic intraepithelial neoplasia. These lesions, which were positive for Alcian blue staining (Figure 4.1.A.ii), were herein termed as PanIN-like lesions. Most of the PanIN-like lesions appeared to be of low-grade (PanIN-1 and PanIN-2) lesions. The data is, indeed, consistent with previous studies that have defined Alcian blue as a marker of low-grade lesions. Interestingly, our images from Alcian blue staining also revealed incidence of negatively stained precursor lesions (Figure 4.1.Aiii). Although these precursor lesions also resemble the morphology of PanIN lesions – particularly PanIN-2 – previous literatures classified these precursor lesions to be

independent of low-grade lesions (Ferreira et al., 2017; Lee et al., 2018). Henceforth, I referred these structures that were negative for Alcian blue staining as hyperplastic lesions — a term used in the previous study (Ferreira et al., 2017). Of note, the classification of the precursor lesions and Alcian blue analysis was cross validated with the help of a histopathologist, Professor Robert Goldin. Similarly, the structures that underwent the process of acinar-to-ductal metaplasia (ADM) appeared to lack the expression of mucins, as indicated by the negative staining for Alcian blue ($AB^-$) (Figure 4.1.B). Upon overall observation, the frequency of these $AB^-$ precursor lesions were less in comparison to the $AB^+$ lesions in the pancreatic tissue. In spite of this, the evident heterogeneity in the Alcian blue staining led us to question its relevance in relation to invasive phenotype of the premalignant lesions. To unravel this further, I analysed tumour in human PDAC that were stained with Alcian blue in the next section.

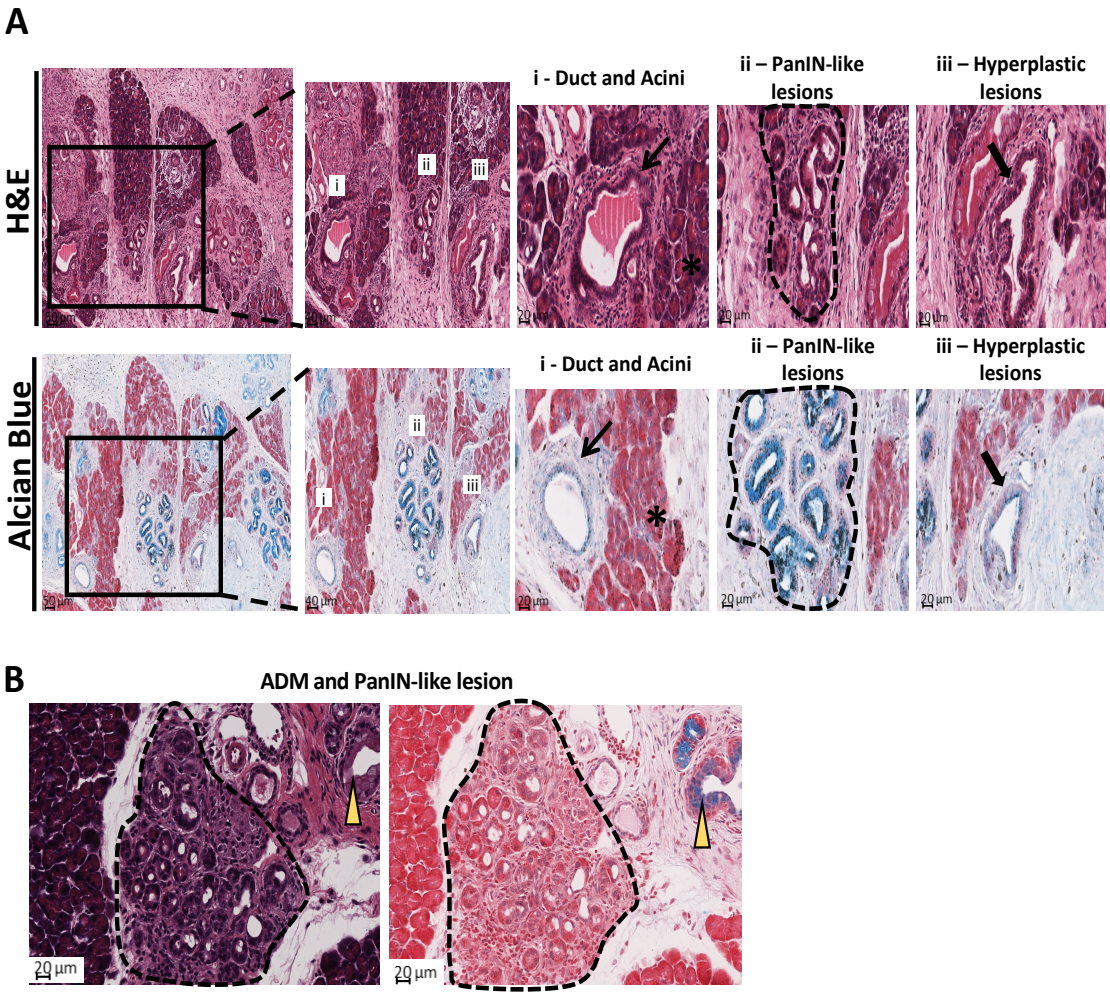


**Figure 4.1: Alcian Blue as a method to determine cell of origin in murine pancreatic precursor lesions**. (A) Representative images showcasing histological analysis on serial sections of *Kras*$^{LSL.G12D/+}$*;Pdx-1-Cre* (KC) mouse pancreas, stained with H&E (Top Panel) and Alcian blue (Bottom Panel). (i) Arrow indicates duct; Asterisk indicates acinar region. (ii) Dotted area includes PanIN-like lesions. (iii) Block arrow indicates hyperplastic lesions. Scale bars: 1$^{st}$ column = 50 µm, 2$^{nd}$ column = 40 µm, 3$^{rd}$-5$^{th}$ columns = 20 µm(B) Representative images of H&E (Top Panel) and Alcian blue (Bottom Panel) of KC mouse pancreas. Dotted area includes ADM; Yellow arrowhead indicates PanIN-like lesion. Scale bar = 20 µm. Data for the duct, acini and neoplastic lesions are representative of at least six mice (n=6).

### 4.3.2. Optimisation to quantify Alcian Blue staining in pancreatic tissues from a cohort of PDAC patients

The phenotype of PDAC region in pancreata of both GEMMs and human tissues displays a glandular form. The PDAC structure is comprised of disorganised duct-like structures, in varying degrees of differentiation, and surrounded by extensive desmoplastic stroma (Gopinathan et al., 2015; Han et al., 2018). In the previous section, I established Alcian blue staining as a method of determining cell of origin in precursor lesions. Following this, I applied the Alcian blue staining technique in pancreatic tissue samples from a cohort of PDAC patients (n = 76). Through this I intended to investigate if the further progression of precursor lesions to PDAC could be associated with the cell of origin. Next, I attempted to quantify the Alcian Blue staining in PDAC regions. Unlike our binary classification for Alcian blue staining in the precursor lesions of KC mice, human PDAC cohort proved to be rather challenging — particularly due to larger area of the tissue samples. Hence, establishment of a methodology to quantify Alcian blue staining in human PDAC cohort was required. To address this, all of the patient samples in the cohort were analysed by Professor Robert Golding to determine tumour regions and exclude healthy tissue area (Figure 4.2.A). Subsequently, I divided the identified tumour region into small square boxes of 4 $mm^2$ (Figure 4.2.B). I then carried out two different approaches to quantify Alcian Blue staining in the PDAC regions. The first method included automated digital analysis. In this approach, I utilised the annotation feature of the Aperio ImageScope software. I manually annotated all of the structures resembling duct-like epithelial phenotype in each square box, as shown in Figure 4.2.Bii. This illustration ensured the exclusion of stromal cells from the analysis. The software provided a value, in $\mu m^2$, for the area of each annotated region (Figure 4.3.A).

Following the software analysis to obtain the area of the annotated structures, they were finally classified as either positive or negative for Alcian blue staining – similar to the previously applied Alcian blue classification technique for precursor lesions in KC mine. While the structures identified as Alcian blue positive were given distinct labels in the "Text" columns (annotated with a blue box in Figure 4.3.A), Alcian blue negative structures were labelled by "n" (annotated with a red box in Figure 4.3.A). Based on this classification for Alcian blue and the area in $\mu m^2$ generated by the software for the annotated structures, I quantified percentage of Alcian blue positive area in ductal structures in each of the small square boxes (Figure 4.3.B). Taken together, this provided an overall percentage of Alcian blue positivity in the epithelial cells of the tumour region within the tissue sample.

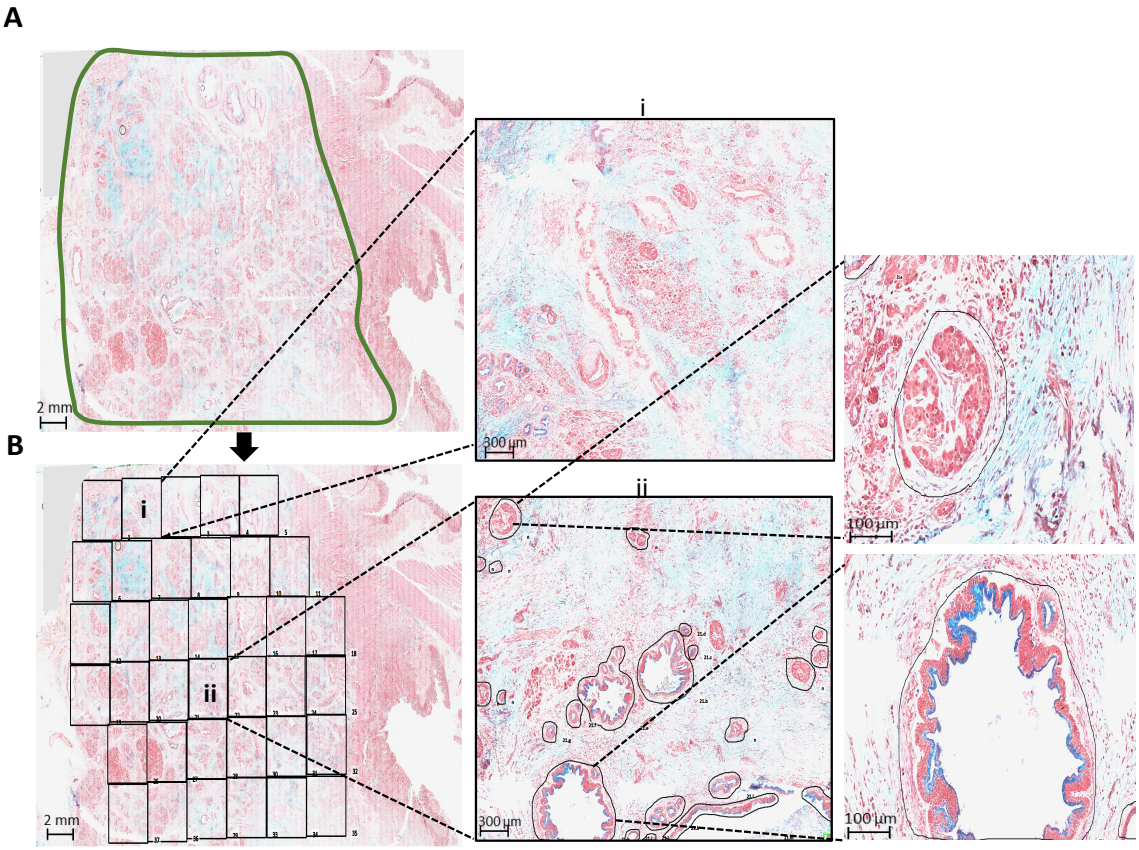


**Figure 4.2: Quantification of Alcian Blue Staining in human PDAC samples.** (A) Representative image of pancreatic tissue from human cohort. Green marked area includes tumour region. Scale bar = 2 mm. (B) Tumour region was divided into black square boxes of 4 $mm^2$ and numbered. Black boxes (i) and (ii) indicate magnified regions of two of the square boxes. Scale bars as indicated in the images. The black square box of 4 $mm^2$ in (ii) shows the annotation of structures displaying duct-like epithelial phenotype. Two of these duct-like epithelial structures in the tumour region are magnified and displayed in the right. Scale bars: 1$^{st}$ column = 2 mm, 2$^{nd}$ column = 300 µm, 3$^{rd}$ column = 100 µm.

**A**

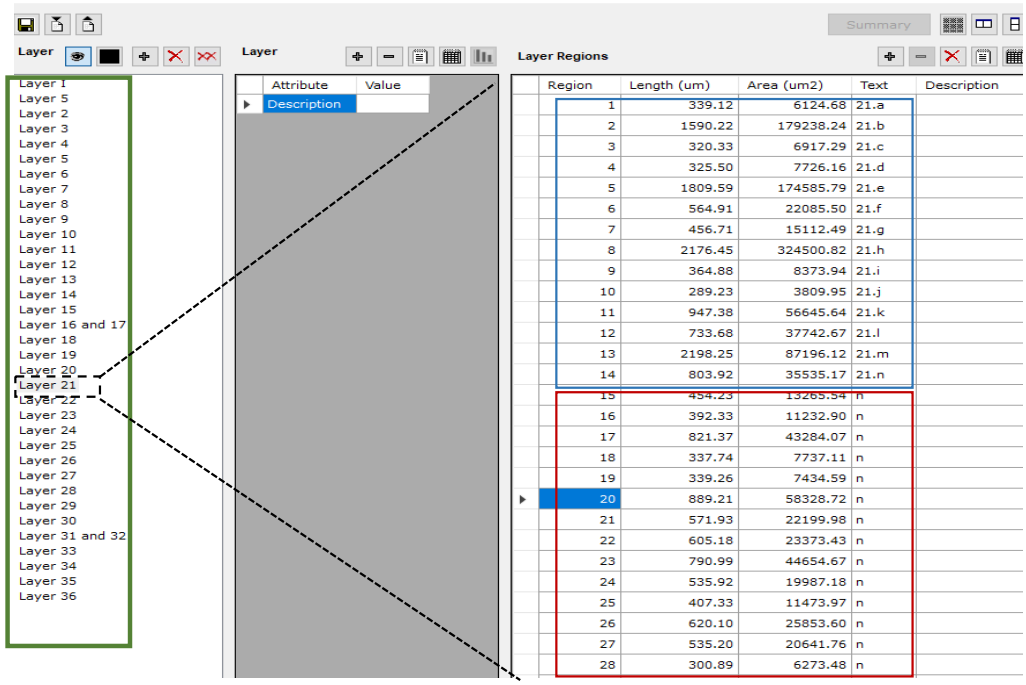


**B**

| Layer | | Area of Alcian Blue postive lesions | | Area of Alcian Blue negative lesions |
|---|---|---|---|---|
| 1 | 1.a | 18727.96 | n | 10712.38 |
| | 1.b | 8672.48 | n | 2114.81 |
| | 1.c | 3789.88 | n | 27860.37 |
| | 1.d | 5685.54 | n | 17823.66 |
| | 1.e | 17337.74 | n | 6373.94 |
| | 1.f | 9024.85 | n | 49439.61 |
| | | | n | 170515.39 |
| | | | n | 141007.36 |
| | | | n | 32981.31 |
| | | | n | 26615.71 |
| | | | n | 28568.8 |
| | | | n | 36854.11 |
| | | | n | 8555.3 |
| | | | n | 54374.87 |
| | | | n | 12099.07 |
| | | | n | 3756.09 |
| | | | n | 14506.5 |
| | | | n | 19597.51 |
| | | | n | 4236.02 |
| | | | n | 20016.88 |
| | | | n | 10918.32 |
| | | | n | 8672.48 |
| | | | n | 10976.83 |
| | | | n | 5564.23 |
| | | | n | 145423.3 |
| | | | n | 71583.21 |
| Total | | 63238.45 | | 941148.06 |
| Total area of positive and negative regions | | 1004386.51 | | |
| % of positive Alcian Blue regions | | 6.296226539 | | |

| Layer | | Area of Alcian Blue postive lesions | | Area of Alcian Blue negative lesions |
|---|---|---|---|---|
| 2 | 2.a | 37186.83 | n | 6099.07 |
| | 2.b | 6985.8 | n | 63594.95 |
| | 2.c | 39759.58 | n | 48539.71 |
| | 2.d | 15863.02 | n | 21418.68 |
| | 2.e | 14960.2 | n | 197157.42 |
| | 2.f | 33976.59 | n | 46931.85 |
| | | | n | 95573.34 |
| | | | n | 52917.11 |
| | | | n | 105654.33 |
| | | | n | 97894.42 |
| | | | n | 40618.96 |
| | | | n | 26591.91 |
| | | | n | 17899.69 |
| | | | n | 137224.94 |
| | | | n | 48472.62 |
| | | | n | 24070.67 |
| | | | n | 93828.86 |
| | | | n | 33271.46 |
| | | | n | 7349.03 |
| | | | n | 12825.68 |
| | | | n | 3706.84 |
| | | | n | 7200.76 |
| | | | n | 6286.54 |
| | | | n | 6459.59 |
| | | | n | 15142.52 |
| Total | | 148732.02 | | 1216730.95 |
| Total area of positive and negative regions | | 1365462.97 | | |
| % of positive Alcian Blue regions | | 10.89242427 | | |

| Layer | | Area of Alcian Blue postive lesions | | Area of Alcian Blue negative lesions |
|---|---|---|---|---|
| 3 | 0 | 0 | n | 204950.76 |
| | | | n | 40219.35 |
| | | | n | 175497.88 |
| | | | n | 77650.06 |
| | | | n | 205070.96 |
| | | | n | 34030.23 |
| | | | n | 336537.97 |
| | | | n | 68138.66 |
| | | | n | 5987.75 |
| | | | n | 229922.15 |
| | | | n | 416385.25 |
| | | | n | 175329.07 |
| Total | | 0 | | 1969720.09 |
| Total area of positive and negative regions | | 1969720.09 | | |
| % of positive Alcian Blue regions | | 0 | | |

| Layer | | Area of Alcian Blue postive lesions | | Area of Alcian Blue negative lesions |
|---|---|---|---|---|
| 4 | 0 | 0 | n | 2780193.57 |
| | | | n | 2865572.32 |
| | | | n | 19760.99 |
| | | | n | 37980.8 |
| | | | n | 188378.8 |
| | | | n | 8438.59 |
| | | | n | 13604.82 |
| Total | | 0 | | 5913929.89 |
| Total area of positive and negative regions | | 5913929.89 | | |
| % of positive Alcian Blue regions | | 0 | | |

| Layer | | Area of Alcian Blue postive lesions | | Area of Alcian Blue negative lesions |
|---|---|---|---|---|
| 5 | 0 | 0 | n | 26041.58 |
| | | | n | 26684.21 |
| | | | n | 291599.17 |
| | | | n | 12926.44 |
| | | | n | 65768.06 |
| | | | n | 18788.67 |
| | | | n | 13198.06 |
| | | | n | 20182.35 |
| | | | n | 129125.72 |
| | | | n | 43761.62 |
| | | | n | 133254.46 |
| | | | n | 250998.72 |
| | | | n | 26415.7 |
| | | | n | 30641.28 |
| | | | n | 16789.49 |
| | | | n | 27673.35 |
| | | | n | 27700.82 |
| | | | n | 46822.58 |
| | | | n | 8798.42 |
| Total | | 0 | | 1217170.7 |
| Total area of positive and negative regions | | 1217170.7 | | |
| % of positive Alcian Blue regions | | 0 | | |

**Figure 4.3: Quantification of Alcian Blue Staining in human PDAC using automated digital analysis.** (A)The numerically labelled small square boxes 4 $mm^2$ are divided as layers in the Aperio ImageScope Software (indicated by green box on the left). Each layer includes all the annotated structures within the square box and provides area in $\mu m^2$ for each structure. The image shows the annotated structures as regions for square box 21 (Layer 21 in Aperio ImageScope). Each annotated structure within the box/layer that stains positive for Alcian Blue is given a distinct label that corresponds to the number of the layer (indicated by blue box on the right), whereas the structures negatively stained Alcian Blue are labelled as "n" (indicated by red box on the right). (D) Quantification method displaying the mean of the area of the annotated structures calculated for each small square box. Percentage of positive Alcian Blue regions was quantified for each square box and the total average of all the boxes was obtained for the tumour sample.

Although this method of automated digital analysis seemed robust, it proved to be highly time consuming and labour intensive. Hence, I limited this quantification approach to only 2 out of 76 human PDAC samples. In order to quantify more efficiently, I tested a second approach using visual assessment. This method entailed “eyeballing” to visually estimate Alcian blue positivity in each of the small 4 $mm^2$ boxes within the PDAC region. The number of square boxes analysed were limited down to 10 and were randomly selected. Since each of the boxes were assigned a number, the 10 boxes were randomly generated online ( https://www.randomizer.org/). (Figure 4.4.A). Following this, I scored the percentage of Alcian Blue positive region in each of these randomised boxes using “eyeballing” technique (Figure 4.4.B). In order to ensure that the “eyeballing" method was indeed reliable and reproducible, I also carried out the visual assessment process in one of the PDAC samples for a total of five times. 10 square boxes were randomly selected during each time of quantification. Interestingly, I observed a standard deviation of 5.78 among these five quantifications for the overall average Alcian blue positivity of 15.78% (Appendix, Figure 7.4). This standard deviation seemed acceptable given the uneven expression of Alcian blue staining in randomly selected boxes from different regions of PDAC during each analysis. Thereupon, I used the second method of visual assessment to quantify Alcian blue staining in all PDAC samples, including the two PDAC samples that had been previously analysed using the first method of digital analysis, in our cohort for further analysis.

A

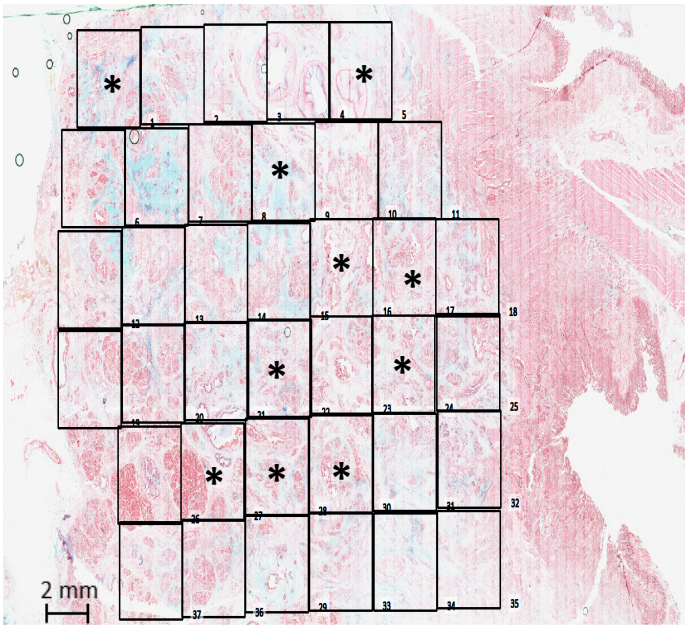


B

| Region label | % of Alcian blue positive region |
|---|---|
| 1 | 10 |
| 5 | 2 |
| 8 | 10 |
| 15 | 40 |
| 16 | 5 |
| 21 | 50 |
| 23 | 0 |
| 27 | 30 |
| 28 | 20 |
| 30 | 10 |
| Average | 17.7 |

**Figure 4.4: Quantification of Alcian blue staining in human PDAC using visual assessment.** (A) Representative image of pancreatic tissue from human cohort showcasing tumour regions divided into small square boxes of 4 $mm^2$ which have been numerically labelled. Asterisks indicate the boxes that were selected during randomisation. Scale bar = 2 mm. (B) Table highlights the percentage of Alcian Blue positive region obtained through the eyeballing method for ten random square boxes.

### 4.3.3. Survival curve analysis in PDAC patient cohort with Alcian blue staining

Published studies, using mouse models with Cre-driven PDAC from specific cell type, demonstrated that the Alcian blue staining was inversely correlated with the aggressive phenotype of the disease (Ferreira et al., 2017; Lee et al., 2018). Following the establishment of Alcian blue quantification method in human PDAC, I was curious to further explore any potential clinical significance of this Alcian blue measurement in our cohort of human PDAC. To examine this, I, at first, decided to stratify the data sets into two groups: patients with high positivity for Alcian blue and patients with low positivity for Alcian blue. To correctly stratify PDAC patients with high and low Alcian blue, an optimal cut-off point was required. For this, I distributed the datasets of Alcian blue positive region

by binning the continuous values into a series of equally sized range of intervals. The representative histogram displayed data distribution for the Alcian blue staining as multimodal (Appendix, Figure 7.5). Given that the median for this distribution is at 23.9%, I firstly used the median as the cut-off point for further analysis. Kaplan-Meier curves were generated using the R survival package. The data revealed PDAC patients with high Alcian blue to have relatively higher overall survival rate (median survival = 2 years) in comparison to low Alcian blue patients (median survival = 1 year), even if the difference was not significant ($P$ = 0.2) (Figure 4.5.A). A similar trend with no significance was also observed for metastasis-free survival ($P$ = 0.2); median survival for high Alcian blue group was 1.6 years and low Alcian blue group was 1.2 years. Interestingly, there was no difference observed between high and low Alcian blue groups for disease-free survival (median survival for both was approximately 1.6 years; $P$ = 0.6). Secondly, I also utilised the quartiles to find the top 25% and bottom 25% of Alcian blue positive regions among the 66 PDAC samples. The low Alcian blue group was based on the first quartile (8.45%) and high Alcian blue group on the third quartile (35.2%). This stratification, however, also displayed similar results as for the cut-off based on median —a trend of higher overall survival ($P$ = 0.5) and metastasis-free survival ($P$ = 0.2) was observed in patient group with high Alcian blue but with no significance (Figure 4.5.B). Similarly, there was again no difference in the disease-free survival between patient groups with high and low Alcian blue ($P$ = 1). Despite several limitations – including sample size, appropriate statistical test to determine cut-off point and no statistical significance between the two groups – the difference in the overall and metastasis-free survival hints a relationship between Alcian blue staining and the disease phenotype in PDAC patient samples in the cohort.

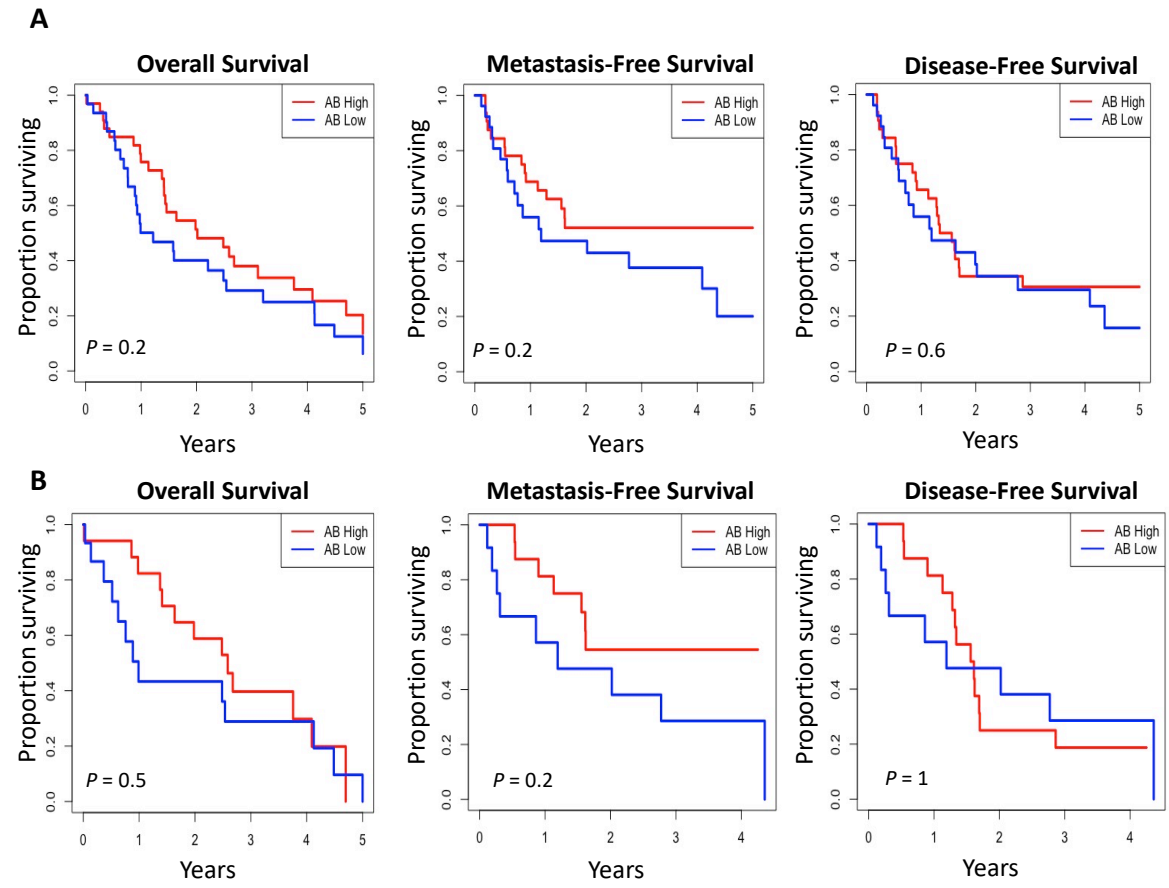


**Figure 4.5: Five-year relative survival in PDAC patients based on the staining of Alcian Blue.** Kaplan-Meier survival analysis stratified using Alcian Blue tumour signature; high and low for human PDAC samples. The curves show overall survival, metastasis-free survival and disease-free survival. (A) The cut-off value for the stratification of two groups was determined at median of 23.9% for the distribution of Alcian Blue positive region among the PDAC samples, n=66. (B) The Alcian blue high and low groups were based on the first (8.45%) and the third (35.2%) quartiles for the distribution of Alcian blue positive region among the PDAC samples, n=66.

### 4.3.4. Quantification of corresponding precursor lesions stained with Alcian Blue and nuclear YAP staining in KC mice

In view of our investigation of Alcian blue as a potential prognostic marker in PDAC, I attempted to analyse if varying Alcian blue staining was related with nuclear YAP expression, in both precursor lesions and PDAC. Based on this, I also aimed to determine if YAP could be used as a marker for either acinar or ductal derived precursor lesions and PDAC. To address this, I firstly examined pancreatic tissue from KC mouse model and investigated for any correlation between Alcian blue staining and nuclear YAP expression

when matched lesions were taken into account (Figure 4.6). I identified the same regions in the serial sections of the pancreatic tissue stained for mucins (Alcian blue) and YAP (IHC).

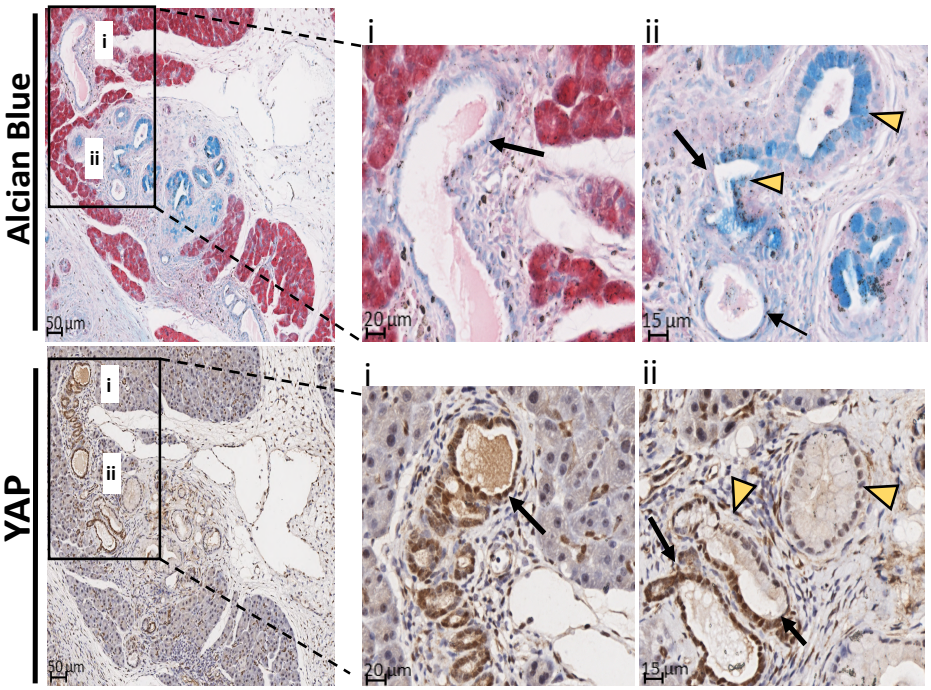


**Figure 4.6: Comparative analysis between Alcian Blue and YAP staining in the ductal region and precursor lesions of KC mice.** Representative images of pancreatic tissue from *Kras$^{G12D/+}$;Pdx-1-Cre* (KC) mice. Consecutive sections were stained with H&E (Top Panel) and YAP (Bottom Panel). Corresponding areas of the tissue sections are represented in the smaller boxes. Black arrow indicates duct. Yellow arrowhead indicates PanIN-like lesions. Scale bars: 1$^{st}$ column = 50 µm, 2$^{nd}$ column = 20 µm and 3$^{rd}$ column = 15 µm.

Subsequently, corresponding precursor lesions in the matched regions were considered. Indeed, qualitative analysis displayed negative correlation between the two stainings (Figure 4.7). PanIN-like lesions, that were positive for Alcian Blue Staining, displayed low nuclear immunoreactivity for YAP (Figure 4.7.A). Morphologically, these PanIN-like lesions mostly represented the described features of PanIN-1 lesions. Conversely, Alcian blue negative hyperplastic lesions demonstrated high nuclear YAP expression (Figure 4.7.B). The

morphology of these hyperplastic lesions closely resembled to that of PanIN-2 lesions. However, this correlation was not 100% exclusive since there was a very small percentage of precursor lesions that exhibited positive correlation between Alcian Blue and nuclear YAP staining (Appendix Figure 7.6). I then analysed Alcian Blue and nuclear YAP staining in the precursor lesions of KC mice quantitatively. In order to achieve this, I evaluated the precursor lesions over five pancreatic tissue samples from KC mice (overall number of lesions = 122). For each lesion structure, at first, I manually counted the number of nuclei based on the intensity of YAP staining and grouped: no reaction and weak staining for YAP as YAP negative (YAP -ve), and moderate and strong staining for YAP as YAP positive (YAP +ve) lesions ( Figure 4.7 and 4.8) . The nuclei intensity was assessed visually through the "eyeballing" method. Collectively, this provided overall status of nuclear YAP expression for each precursor lesion. Separately, serial sections stained with Alcian blue were analysed visually and assorted as either positive or negative for the stain (Figure 4.7 and 4.8.A). Figure 4.8.B indicated that Alcian blue positive ($AB^+$) PanIN-like lesions (approximately 85%) were predominantly YAP negative (negative or weak for nuclear YAP) with high significance ($P = 7.8 \times 10^{-8}$). On the other hand, Alcian blue negative ($AB^-$) hyperplastic lesions mostly comprised of YAP positive nuclei (approximately 75%). The high expression of nuclear YAP in these $AB^-$ lesions was also observed to be statistically significant ($P = 0.09$). Of note, the data in Figure 4.8.B represents the average percentage of positive and negative nuclear YAP in a precursor lesion that is either Alcian blue positive ($AB^+$) or negative ($AB^-$). When the absolute number of precursor lesions were taken into account, the presence of $AB^+$ PanIN-like lesions were highly predominant (n = 105) in Figure 4.8.B in comparison to $AB^-$ hyperplastic lesions (n = 17). Nevertheless, the data in Figure 4.8 overall suggests that PanIN-like precursor lesions, with high Alcian blue staining, could be derived

from acini and have low nuclear YAP expression. Conversely, low Alcian blue displaying precursor (hyperplastic) lesions could develop from ducts. Moreover, high nuclear YAP expression in these hyperplastic lesions could suggest for a potential ability of these lesions to progress faster into invasive cancer during tumourigenesis.

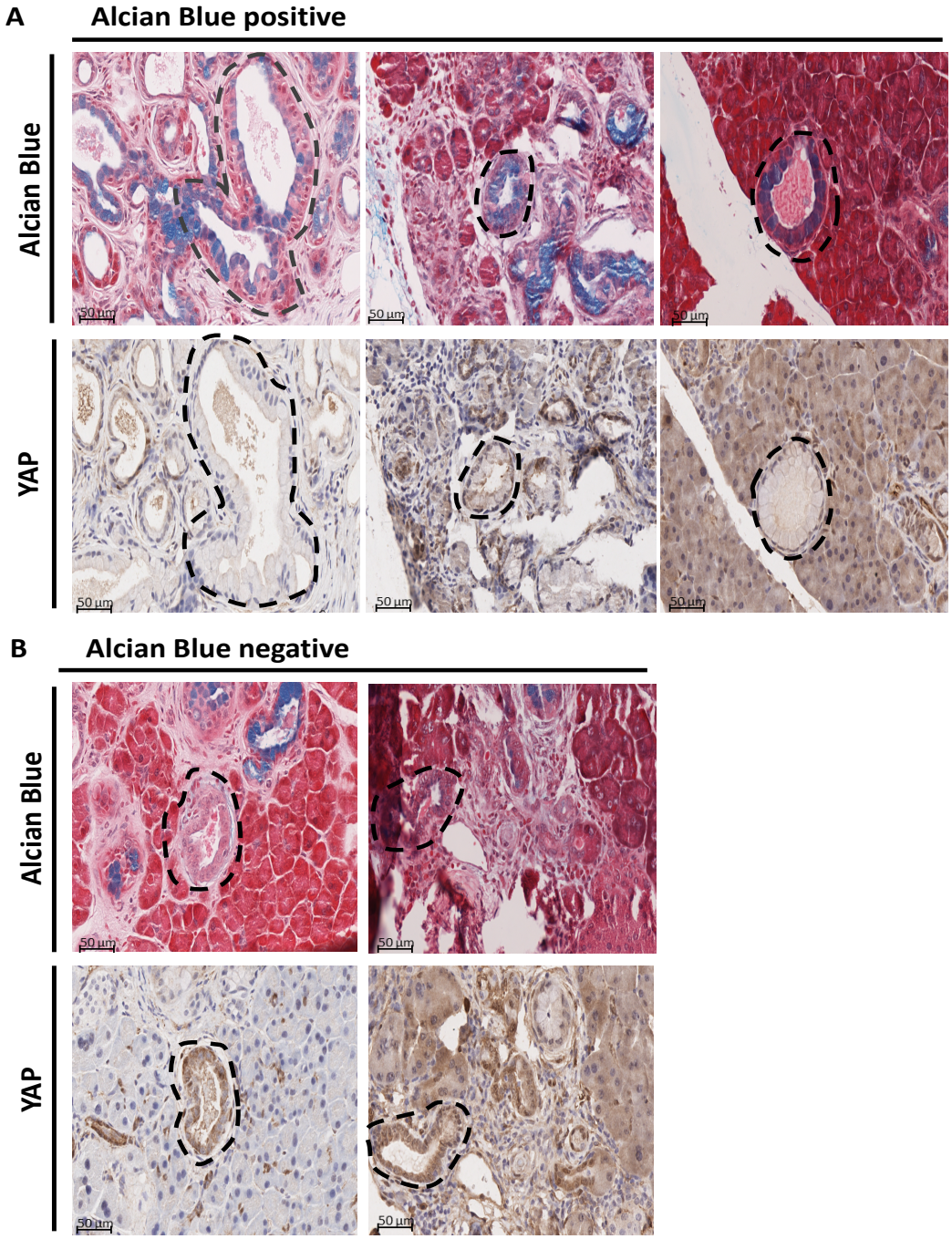


**Figure 4.7: Establishment of the quantification method for the correlation between Alcian Blue and YAP staining in the precursor lesions of KC mice**. Representative images of pancreatic tissue from *Kras*$^{G12D/+}$*;Pdx-1-Cre* (KC) mice stained with H&E (Top Panel) and YAP (Bottom Panel). Precursor lesions were identified as either (A) positive or (B) negative for Alcian blue. Corresponding lesions stained for YAP were identified separately and quantified for nuclear YAP. Corresponding PanIN lesions are included within the dotted region. Scalebars for all images = 50 µm.

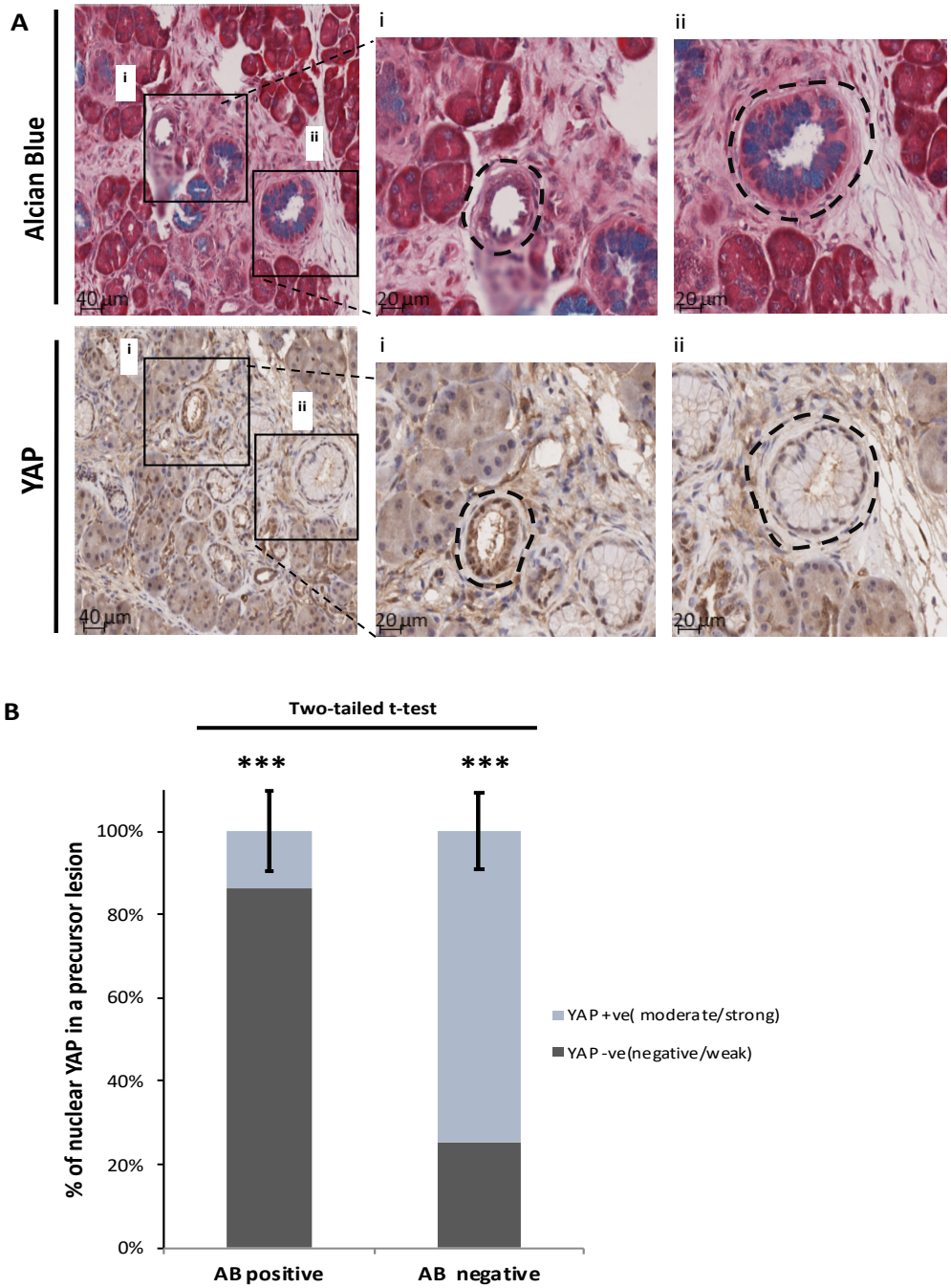


**Figure 4.8: Lower expression of nuclear YAP in a PanIN-like precursor lesion of KC mice.** (A) Histological analysis of *Kras*$^{G12D/+}$*;Pdx-1-Cre* (KC) mice pancreas with Alcian blue stain and IHC stain for YAP. Nuclear expression of YAP was quantified based on the intensity. Each precursor structure was manually calculated for the number of nuclei displaying YAP positivity (moderate and strong nuclear expression) or YAP negativity (weak and negative nuclear expression). Scale bars: 1$^{st}$ column = 40 µm and 2$^{nd}$-3$^{rd}$ columns = 20 µm.(B) Quantification shows percentage of nuclear YAP in a AB positive or negative precursor lesion. Pancreatic tissues from at least five KC mice were used and 122 precursor lesion structures were analysed in total. Among these, 105 precursor lesions were categorised as Alcian blue positive and 17 precursor lesions as Alcian blue negative. *$P \leq 0.05$, **$P \leq 0.01$, ***$P \leq 0.001$, $^{ns}P > 0.05$, Student's two- tailed *t* test.

### 4.3.5. Quantification of corresponding PDAC regions with Alcian Blue and nuclear YAP staining in patient cohorts

Following the analysis of Alcian blue and nuclear YAP staining in the precursor lesions of KC mice, I expanded this investigation to include data from the human PDAC cohort available in our laboratory. There were 66 samples in the cohort and were matched for two variables, Alcian blue stain and nuclear YAP expression. In this analysis, PDAC regions comprising epithelial structures with duct-like phenotype were considered and have been described previously in this Chapter (Figure 4.2). The methodology to quantify the positivity of Alcian blue staining in human PDAC samples were also developed (Figure 4.2). In regard to the YAP staining in human PDAC cohort, immunohistochemical staining was performed by Aline Herbert and the scoring for nuclear YAP positivity was carried out by Prof Robert Goldin. The scoring entailed providing an intensity value for nuclear YAP staining, and included no reaction (0), weak (1), moderate (2) and strong (3). Additionally, this intensity was considered at an observed percentage of positive tumour cells over total cells in the PDAC regions (Fedchenko and Reifenrath, 2014). Indeed, our qualitative analysis displayed inverse correlation in corresponding tumour regions stained for YAP and Alcian Blue (Figure 4.9.A). Likewise, the quantitative analysis also reflected this negative correlation with significance ($P$ = 0.003) (Figure 4.9.B). A percentage of PDAC samples exhibiting moderate-to-strong nuclear YAP appeared to belong to low Alcian blue (60% out of 33 low Alcian blue samples). Conversely, a large number of PDAC samples, displaying weak or negative stain for nuclear YAP, were noted to belong to the group displaying high Alcian blue staining (85% out of 33 high Alcian blue samples) (Figure 4.9.B).

This comparison between Alcian blue and nuclear YAP is important given the growing understanding of the role of active YAP in PDAC tumourigenesis (Rozengurt et al., 2018). Briefly, YAP's activity, controlled by inhibitory Hippo signalling pathway, is enhanced as it translocates into the nucleus and acts as a transcriptional regulator (Zhao et al., 2007). In accordance, tissue samples from the PDAC patient cohort stained for YAP was retrieved and stratified, by Michael Eyres, into four groups of YAP staining: nuclear enrichment, cytoplasmic enrichment, no enrichment and YAP negative. The datasets were subsequently run through the R survival package in order to generate survival curve. As expected, the Kaplan-Meier curve demonstrated lowest overall survival for the PDAC patient group with nuclear enrichment for YAP (Appendix, Figure 7.7). Moreover, this observation and recent studies using cell-type specific tumour in mouse model (Ferreira et al., 2017; Lee et al., 2018) further support our data to suggest YAP's possible contribution to predict aggressive phenotype of PDAC based on cell of origin.

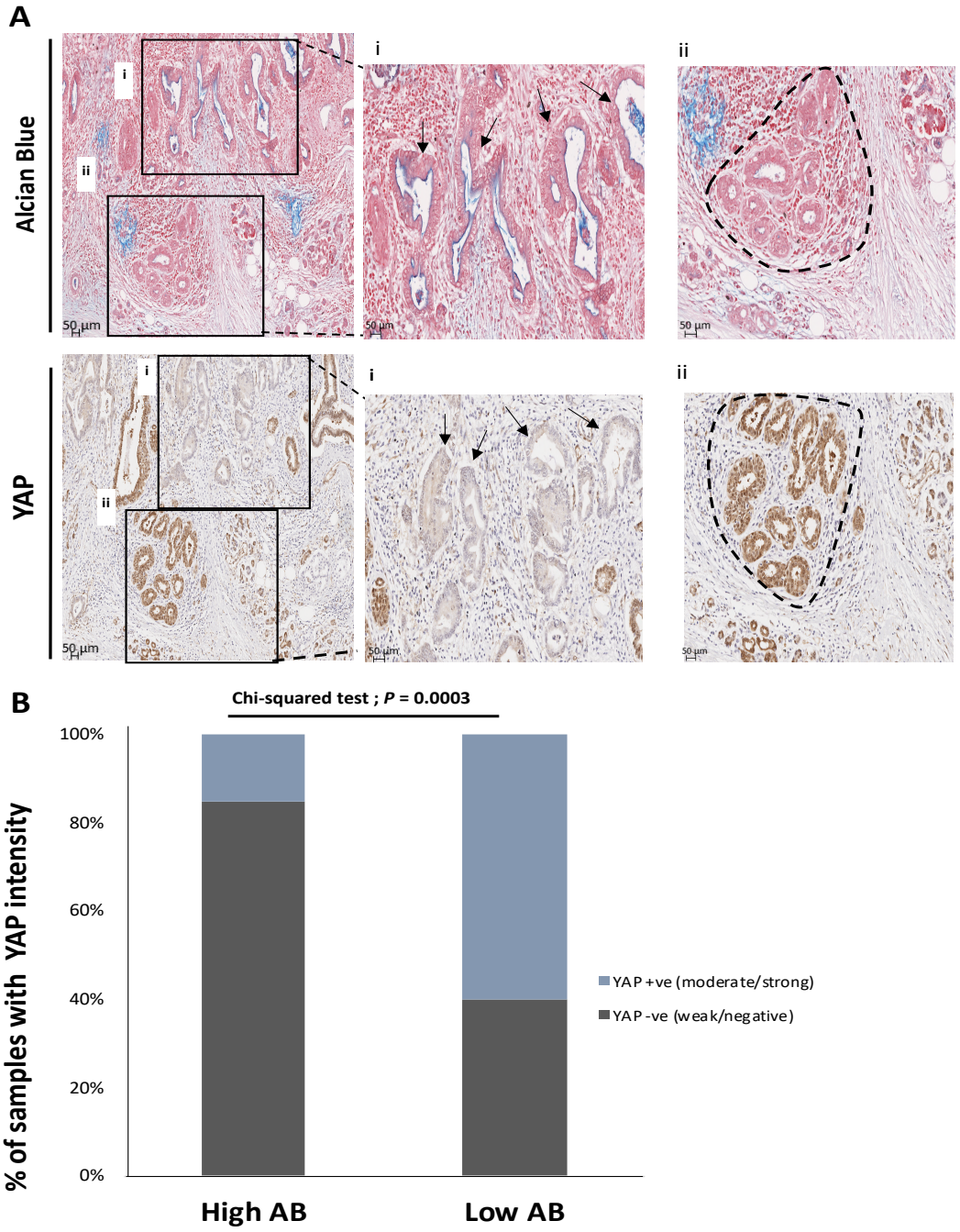


**Figure 4.9: Comparative analysis between Alcian Blue and YAP in the PDAC region of human cohort.** (A) Representative histological (H&E) (top panel) and IHC analysis for YAP (bottom panel) in the tumour region of human PDAC cohort. Corresponding regions from consecutive sections were used for comparative analysis and are represented in small boxes. (i) Black arrows indicate corresponding structures comprising of ductal epithelial phenotype in the PDAC region and display positive staining for Alcian blue and negative staining for nuclear YAP. (ii) Black dotted regions indicate corresponding epithelial structures in the tumour region that display negative staining for Alcian blue and positive staining for nuclear YAP. Scale bars = 50 µm(B) Quantification of negative nuclear YAP staining (weak/negative YAP) and positive nuclear YAP staining (moderate/strong nuclear YAP) in PDAC human tissues that were matched for Alcian blue staining. PDAC samples were divided either as high Alcian blue (n=33) or low Alcian blue (n=33) samples after determining the cut-off value at 23.9% for the distribution of percentage of Alcian blue positivity. 66 matched samples were used in total for the analysis. The p-value was calculated using Chi-squared test.

## 4.4 Discussion

The initial assumption that PDAC was derived from ductal cells (Hruban et al., 2000) was recently challenged. Several studies highlighted the importance of metaplastic process that acinar cells undergo. The acinar cells form a ductal-like phenotype, which further develops into PanIN lesions (Guerra et al., 2007; Kopp et al., 2012). Under oncogenic conditions and environmental stress, the lesions ultimately progress to PDAC. The controversy surrounding the cell of origin of PDAC, however, still prevails. Recent studies have suggested models and markers based on the cell of origin (Ferreira et al., 2017; Lee et al., 2018), expanding our view of PDAC initiation process. Given the heterogeneity in nuclear YAP expression in the precursor lesions of KC mice in our study (Chapter 3, Figure 3.10), I investigated if this heterogeneity of YAP was interlinked with the lesions' cell of origin.

I, at first, validated Alcian blue staining as a tool for investigating cell of origin of both precursor lesions (Figure 4.1) and PDAC (Figure 4.2). Kopp et al. used Alcian Blue Staining as a method to measure PanIN lesions frequency in *Ptf1a$^{CreER}$; Kras$^{G12D}$; R26R$^{YFP}$* (acinar-specific *Kras* activated) and *Sox9CreER; Kras$^{G12D}$; R26R$^{YFP}$* (duct-specific *Kras* activated) mice. This was based on the previously known molecular feature of PanIN lesions for high acidic mucin production, detected histologically by Alcian blue (Kopp et al., 2012). Interestingly, the retention of PanIN properties in PDAC derived from acinar-specific promoter was lost in the ductal-derived PDAC (Lee et al., 2018). Correspondingly, Ferreira et al. described the Alcian Blue positive lesions, that were observed primarily in the acinar derived mouse model, as PanIN lesions. On the other hand, they referred the Alcian blue negative lesions, that were found mostly in ductal specific KRAS activated pancreas, as

hyperplastic lesions. These hyperplastic lesions were demonstrated to bypass the transitioning stages of PanIN formation and progress rapidly to PDAC (Ferreira et al., 2017). Interestingly, we observed heterogeneity in Alcian blue staining in the precursor lesions of KC mouse pancreas (Figure 4.1.A). This could potentially lead to intertumoural heterogeneity in PDAC due to different cell of origin, as previously reported in the mouse models (Lee et al., 2018; Xu et al., 2019).

Next I investigated any association between Alcian blue and nuclear YAP expression in the tissue samples from KC mice and human PDAC. Our results revealed low nuclear YAP expression in the PanIN-like precursor lesions that were positive for Alcian blue (Figure 4.7 and 4.8). Conversely, a negative correlation was, again, true for the Alcian blue negative hyperplastic precursor lesions as they displayed high nuclear immunoreactivity for YAP. This inversely related correlation between Alcian blue and nuclear YAP was also established in tumour regions of human PDAC (Figure 4.9). Collectively, our results suggest a potential role of YAP to mark cell of origin and enable risk-stratification of both precursor lesions and PDAC.

Similarly, I selected a visual assessment method, after optimising quantification method, to analyse Alcian blue positivity in human PDAC regions. However, there is some discrepancy between the quantification method for Alcian blue positivity and nuclear YAP staining in human tissues. Mainly, the method of visual assessment for Alcian blue quantification is not entirely consistent with the method utilised by the pathologist to visually score the intensity of nuclear YAP expression in a positively stained area within the entire PDAC. Also, the visual assessment for Alcian blue quantification is limited by the absence of double-blind score which would provide more reproducible, reliable results to our analysis.

Published studies described low-grade PanIN lesions as derivation of acinar cells, with positive staining for Alcian blue. Alcian blue negative ducts, on the other hand, were suggested to form PanIN-independent precursor lesions. Whilst our data displayed Alcian blue negative precursor lesions that were reminiscent of PanIN lesions morphology, these were mostly present at PanIN-2 stage. This advanced stage of PanIN lesion could result from higher activity of nuclear YAP in the ductal cells. Of note, the strength of the negative correlation between Alcian blue positivity and nuclear YAP expression was not perfect. This indicates for the presence of some Alcian blue negative precursor lesions that lack nuclear YAP expression. The occurrence of these lesions could be justified as bystander lesions due to nearby *Kras* activated focal region of PanIN lesions. This adds another layer of complexity in distinguishing "true" PanIN lesions (Ferreira et al., 2017).

Taken together, the work in this chapter addressed the unresolved question of cell of origin of PDAC. By using Alcian blue staining, both precursor lesions from KC mice and PDAC from patient samples could be categorised based on their origin from either acinar or ductal cells. Similarly, nuclear YAP – observed to be expressed heterogeneously in the precursor lesions of KC mouse pancreas in our study – is associated inversely with the Alcian blue staining. Thus, nuclear YAP expression could be associated with a distinct cell of origin. This is interesting since the importance of YAP oncogene in the advancement of PDAC formation is emerging (Kapoor et al., 2014; Shao et al., 2014; Zhang et al., 2014). Moreover, cell of origin has been shown to provide source of intertumoural heterogeneity in PDAC patients (Lee et al., 2018). The observation highlights the necessity of PDAC patient stratification based on the cell of origin. The results elucidate the potential significance of nuclear YAP as a marker to predict the rate by which precursor lesions would progress into invasive tumour based on their cell of origin. Similarly, in terms of PDAC, linking YAP with

the cell of origin could be advantageous in making decision for effective treatment in PDAC patients.

# Results III

# Chapter 5 Generation of a genetically engineered mouse model, 3D organoids and an orthotopic model to study PDAC tumourigenesis

## 5.1 Introduction

### 5.1.1 Role of RASS1A in PDAC progression

Previous studies have demonstrated loss of RASSF1A expression in human PDAC samples (Amato et al., 2016; Dammann et al., 2003). RASSF1A, as a tumour suppressor gene, has been shown to play a crucial role in microtubule stabilisation (van der Weyden et al., 2005), maintenance of genomic stability (Vos et al., 2004) control of cell cycle components including cyclin D1 (Shivakumar et al., 2002), regulation of apoptosis (Vos et al., 2000) and promotion of differentiation (Papaspyropoulos et al., 2018). Indeed, the loss of tumorigenicity upon RASSF1A expression highlights its significance in regulating cellular biology of cancer. Despite this, mutations in RASSF1A are rare. Most commonly, epigenetic silencing, due to hypermethylation of CpG islands within the promoter of *RASSF1A* gene, leads to the loss of RASSF1A expression in many human cancers (Agathanggelou et al., 2001; Dammann et al., 2000). The silencing of *RASSF1A* was demonstrated to correlate inversely with *KRAS* activation in PDAC (Dammann et al., 2003). Interestingly, several polymorphisms have also been reported for the gene, including the best characterised single nucleotide polymorphism (SNP), *RASSF1 c.397G>T* (rs2073498), which is highly prevalent in European and Asian populations.

The SNP leads to the conversion of the amino acid Serine (Ser) at residue 133 to Alanine (Ala) (RASSF1A p.133Ser), disrupting the protein's secondary structure. In turn, the closely located putative Ataxia Telangiectasia Mutated (ATM) substrate site at Ser131 is perturbed. This attenuates phosphorylation of RASSF1A p.133Ser by ATM. The inability of RASSF1A p.133Ser to activate MST/LATS-mediated Hippo pathway, as a result, leads to decreased apoptosis upon DNA damage (Yee et al., 2012). While the RASSF1A p.133Ser has been associated with its reduced ability to regulate G1 to S transition during cell cycle (Shivakumar et al., 2002), it has also been linked to increased risk of many cancers including breast cancer (Donninger et al., 2011; Gao et al., 2008), lung cancer (Zhou et al., 2013), hepatocellular cancer (Bayram, 2012) along with soft tissue sarcoma (Yee et al., 2012).

Previously, a *Rassf1a* knockout mouse model was created by deleting the exon 1-alpha of the *Rassf1* gene. The specific loss of *Rassf1a gene (Rass1a*$^{-/-}$*)* led to spontaneous tumourigenesis in adult mice including lung adenomas, lymphomas and breast adenocarcinomas (Tommasi et al., 2005). However, the lack of *Rassf1a* in these knockout mice appeared to be compensated by its closest homologue *Rassf5* (49% identity) (Papaspyropoulos et al., 2018; Zhang et al., 2016). Meanwhile, a mouse model with rs2073498 SNP has not been described in the literature yet. The creation of the mouse model in our laboratory has led to phenotypic effects in different organs including lung tumorigenesis, cyst in the kidney and clear cell carcinoma-like cells (not published yet).

### 5.1.2 The application of 3D organoids and orthotopic model for the study of PDAC development

Besides the genetically engineered mouse model (GEMMs), organoids hold a great promise in PDAC study. This is due to the ability of cells from normal and neoplastic human tissue to grow in an *in vitro* system that resembles the genetic and phenotypic state of the original human PDAC. Huch et al. first described the use of an organoid model in the pancreatic tissue by isolating duct cells expressing stem cell marker, LGR5 (Huch et al., 2013). Since then, different pancreatic model systems have been developed to study PDAC development and treatment. Our study utilised the model by Boj et al. that first cultured 3D organoid from mouse and human pancreatic adenocarcinoma (Boj et al., 2015b). In this model, which is based on the protocol from Clevers and Tuveson's laboratory, pancreatic ducts isolated from mouse and human tissues are embedded into matrigel. The matrigel, in turn, presents an extracellular basement membrane-like matrix containing several components such as laminin, collagen and proteoglycans (Hohwieler et al., 2019). Importantly, the self-renewal capability in this organoid model system is maintained by feeding the media with R-Spondin 1 (RSPO1). RSPO1, an agonist for Wnt signalling, stimulates the pathway and ultimately leads to the activation of the target gene *Lgr5*. The culture medium of the pancreatic organoids in our study are supplemented with several additional components. These components, along with their role, are described as: Noggin and A83-01 inhibit TGF-beta signalling, recombinant EGF and FGF-10 provide growth signalling, N-acetylcysteine and B27 lead to retinoic acid activation, nicotinamide inhibits poly(ADP-ribose) polymerases (PARP-1) and promotes endocrine lineage, and

gastrin I hormone stimulates acinar cells to secrete digestive enzymes (Boj et al., 2015b; Hohwieler et al., 2019). Besides the pancreatic organoid model from Clevers and Tuveson's laboratory, several other studies have described complex 3D organoid systems including co-culture of primary human tumour cells with stromal and immune cells. By incorporating representative tumour microenvironment, these models might be more accurate for clinical applications including drug testing and examining immunotherapeutic effects (Baker et al., 2016; Hohwieler et al., 2019; Tsai et al., 2018). Boj et al. also demonstrated recapitulation of pathophysiological development of neoplastic lesions into PDAC by orthotopic transplantation of the organoids into syngeneic or Nu/Nu mice (Boj et al., 2015b). While the ex-vivo model of organoid itself is useful in predicting drug response, the orthotopic transplantation of these 3D cultured cells enable more accurate and detailed understanding of the disease progression. This is owed to the fact that organoids maintain the identity of the tissue of origin. Besides, data from the orthotopic model is obtained much more quickly in comparison to genetically engineered mouse model. The application of this preclinical model can be very useful in the context of patient derived tumour samples or biopsies as these tissues can be isolated to form organoids and their progression monitored by transplanting them orthotopically into mouse pancreas (Hohwieler et al., 2019). Intriguingly, the ductal morphology in the human tumour-derived organoids closely resemble PanIN structures in human PDAC (Boj et al., 2015a). As a result, the generation of 3D organoid culture from human samples and their orthotopic transplantation could be utilised to make accurate and quicker decision for personalised treatment.

## 5.2 Aims

Our preliminary results in the previous chapter (Chapter 3, Figure 3.8) indicated a role of NF2 in regulating ERK1/2 activation in pancreatic cancer cells. This effect, however, appeared to be independent from the Hippo pathway since NF2 did not impact YAP's activity. Nevertheless, from our analysis of PanIN lesions *in vivo*, we were able to establish an association between YAP and pERK. This led us to speculate whether a different upstream regulator, RASSF1A, could be involved in the Hippo pathway-mediated YAP's activation. This could then potentially result in cell proliferation through the MAPK/pERK pathway during PDAC development. Hence, in this chapter I aim to study the role of the upstream regulator of the Hippo pathway, RASSF1A, in the progression of PDAC. I particularly focus on looking at the phenotypic changes during PDAC tumourigenesis. For this purpose, I utilised mouse with rs2073498 SNP as another mouse model, besides the previously used *Kras$^{G12D/+}$; Pdx-Cre* (KC) model in our study. The rs2073498 SNP mouse model was created by Dr Ben Davies from the Wellcome Trust Centre, Oxford. Previous study has shown an inverse correlation between *RASSF1A* silencing and *KRAS* activation. Hence, I intend to study the effect of RASSF1A p.Ser131 in the context of oncogenic KRAS which is a well-established initiator and driver of PDAC.

I also aim to establish 3D organoid system isolated from both WT and KC mice in our laboratory and carry out genetic manipulation of YAP expression. Similarly, I aim to establish the protocol of the orthotopic injection of pancreatic organoids in our laboratory. Ultimately, this would enable transplantation of YAP depleted pancreatic organoids into the mouse pancreas and in turn would to allow to observe any

phenotypical and functional consequences in the progression of PDAC due to these genetically variant models.

## 5.3 Results

### 5.3.1 Investigation of RASSF1A in the progression of PanIN lesions using GEMMs

Given the high loss of RASSF1A expression in PDAC samples (Amato et al., 2016), I investigated the possible mechanism by which the tumour suppressor gene contributes to the tumorigenesis in PDAC. To investigate this, I used *in vivo* models rather than *in vitro* settings, given the lack of RASSF1A expression in most of the pancreatic cancer cells (Dammann et al., 2003). Firstly, I examined the expression pattern of the RASSF1A protein in the early precursor lesions, PanINs, in *Kras*$^{LSL.G12D/+}$*; Pdx-Cre* (KC) mouse pancreas. Simultaneously, I also looked at the possible association of RASSF1A with YAP activation. I carried this out by analysing the expression of phosphorylated YAP (pYAP) in the corresponding lesions of the consecutive sections which were obtained through serial sectioning. Interestingly, RASSF1A expression complemented with that of pYAP, with both proteins expressed mostly in the apical region of the PanIN lesions (Figure 5.1.A). The observation was corroborated by quantitative analysis that demonstrated positive correlation in the expression of RASSF1A and pYAP ($R$ = 0.52, $P$ = 0.02) in the apical region of PanIN lesions (n=19) in KC mice (Figure 5.1.B). Moreover, the expression of total YAP proteins was also analysed. The positive staining for total YAP in the apical membrane possibly represents the phosphorylated form of the protein.

Likewise, total YAP demonstrated positive immunoreactivity in the nuclei of the ductal structure that displays transition from the normal ductal epithelium to PanIN lesion Notably, the overall nuclear intensity of total YAP was weaker in the PanIN lesion when compared to the normal ductal epithelium in the transitioning structure (Figure 5.1.A).

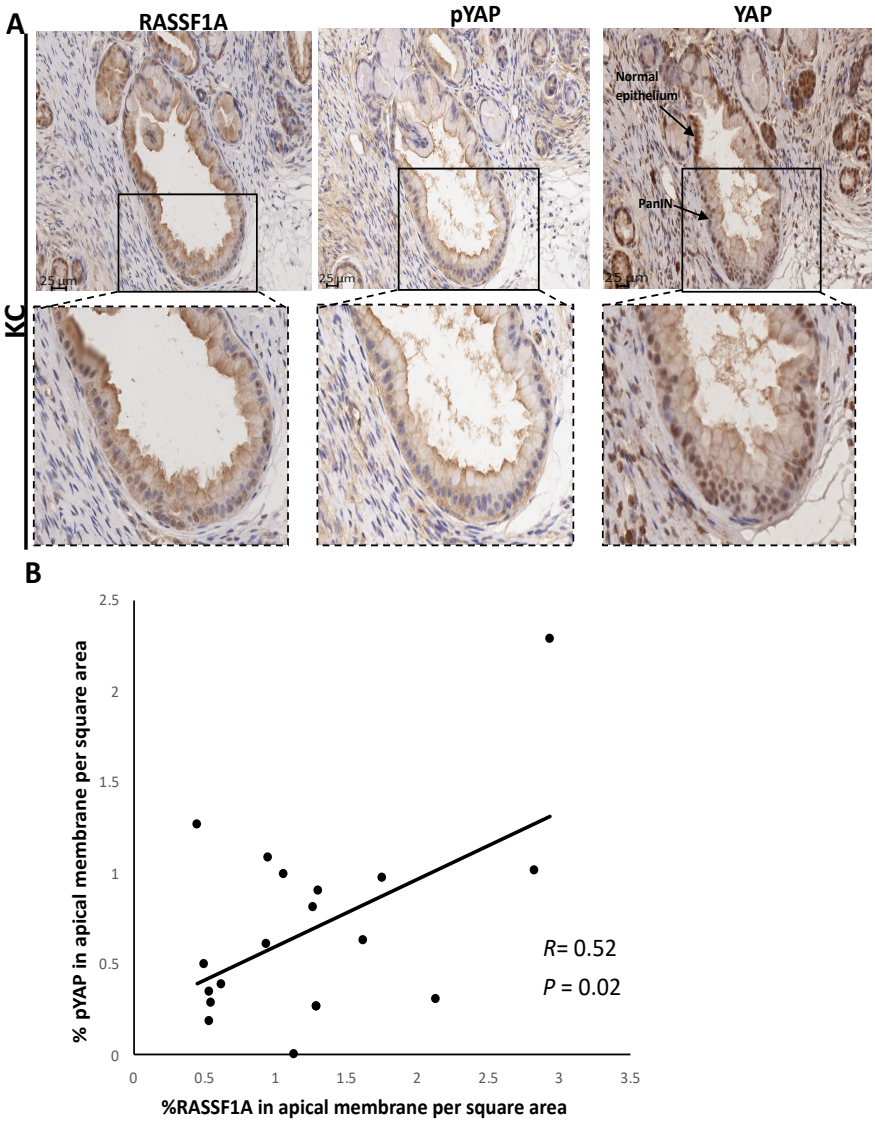


**Figure 5.1: Association between RASSF1A and phosphorylated YAP in the apical membrane of PanIN lesions in KC mouse pancreata.** Representative images of immunohistochemical stainings of RASSF1A, phosphorylated YAP (pYAP) and total YAP (YAP) in the pancreata of *Kras*$^{LSL.G12D/+;}$*Pdx-Cre* (KC) mice. Scale bars = 25 µm. Bottom panel shows the cropped and magnified region of the PanIN lesions. µm. (B) Quantitative analysis demonstrates correlation between percentage of pYAP and RASSF1A in the apical region of corresponding PanIN lesions (n =19). PanIN lesions included in the analysis were derived from pancreata of two KC mice at similar ages (40-42 weeks). *R* =0.52, *P* = 0.02.

Next, given the association between YAP and pERK in our previous observations (Chapter 3, Figure 3.12), I explored the effect of RASSF1A in the background of *Kras* mutation. For this, I utilised the *Rassf1* A133S SNP (rs2073498 SNP) mouse model that was developed by Dr Ben Davies. This was generated by genetically knocking in point mutation G to T through Crispr/Cas9 nuclease directed against exon 3 sequence of the *Rassf1* gene in mouse embryonic stem cells and subsequently carrying out germline transmission of the *Rassf1* SNP allele in mice. I crossbred the rs2073498 SNP mice comprising heterozygous SNP allele, ($Rassf1^{SNP/+}$, hereafter referred to as R1-Het), with the previously described $Kras^{LSL.G12D/+}$*; Pdx-Cre* (KC) mice (Hingorani et al., 2003) (Figure 5.2.A). The Pdx-Cre driven $Kras^{G12D}$ expression in the progenitor cells would lead to the confinement of the *Kras* mutation, mostly, in the pancreas of KC mice. On the other hand, RASSF1A p.133Ser would be present in several organs of adult R1-Het mice. Consequently, the generation of transgenic offspring, $Kras^{LSL.G12D/+}$*;Pdx-Cre;*$Rassf1^{SNP/+}$ (hereafter referred to as KCR1-Het) would exhibit RASSF1A p.133Ser in adult mouse pancreas in the background of activating mutations of *Kras*.

In our GEMM model of KCR1-Het, RASSF1A p.133Ser in pancreas expressing oncogenic KRAS did not appear to have any additional adversity in the mice health than expected. Our survival curve analysis of up to 30 weeks revealed no significant difference, albeit seeming trend of less favourable outcome in the survival of KCR1-Het mice when compared to the combined survival of KC only or R1-het only mice (Figure 5.2.B). A few of the KCR1-Het mice (6 out of total of 14 KCR1-Het mice), between the age of 20-32 weeks, were euthanised since they displayed more than mild discomfort and distress. The necroscopy of these mice revealed absence of any tumour in the pancreas. Importantly, the cause of distress in these six mice mostly included keratoacanthomas

of the vulva and oral mucosae which were larger in size. These are, however, the commonly observed effects which occur due to the leakiness of Pdx-Cre, in KC mice around that age (Westphalen and Olive, 2012).

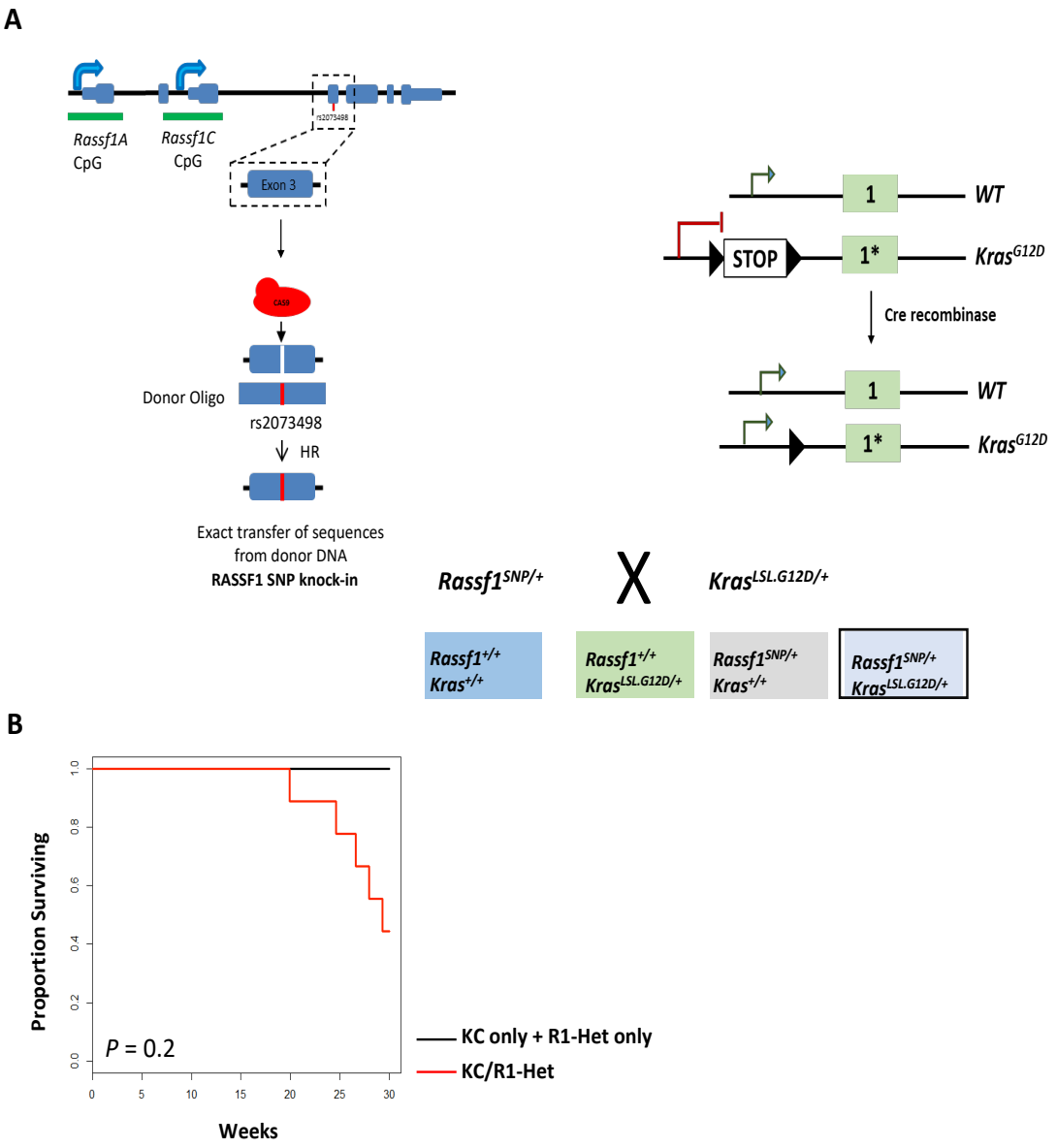


**Figure 5.2: Generation of genetically engineered *Rassf1* SNP mice with *Kras* mutation in pancreas.** (A) The rs2073498 SNP is integrated into CRISPR/Cas9 induced double strand break (DSB) by homologous recombination from a donor oligo. The resulting strain, RASSF1A-p.133Ser mice, that are heterozygous for the SNP allele were crossed with *Kras*$^{LSL.G12D/+}$*;Pdx-Cre* mice to generate transgenic strain *Rassf1*$^{SNP/+}$*; Kras*$^{LSL.G12D/+}$*;Pdx-Cre* mice. (B) Survival of *Rassf1*$^{SNP/+}$*; Kras*$^{LSL.G12D/+}$*;Pdx-Cre* mice is decreased with no significance. Kaplan-Meier curves demonstrate lower survival of triple mutant mice, *Rassf1*$^{SNP/+}$*; Kras*$^{G12D}$*;Pdx-Cre*(KCR1-Het) mice (n=14), represented by red line, compared with the combined survival of *Rassf1*$^{SNP/+}$ (R1-Het) mice (n=15) and *Kras*$^{LSL.G12D/+}$*;Pdx-Cre* (KC) mice (n=8), represented by black line, up to 30 weeks. Culled R1-Het and KC mice, that were included in this group, were categorised as healthy as they did not show any sign of sickness during their endpoint. The lower proportion of survival in KCR1A-Het group are indicated by mice that were culled due to sickness (n=6). *P* = 0.2. Kaplan Meier Curve was performed using R survival package by Michael Eyres.

Furthermore, I histologically assessed the pancreatic architecture of the KCR1-Het mice. I was interested to see if the addition of *Rassf1* SNP, besides the mutation of *Kras*, would cause any effect in the cellular pathology and ductal phenotype in KCR1-Het pancreas. As shown in Figure 5.3, the pancreata from these mice displayed stochastic presence of a spectrum of PanIN lesions of varying grades. This morphology closely resembled the pancreata of KC mice of similar age-group. These results thus suggested that the heterozygous SNP of RASSF1A in *Kras*-mutated pancreas did not distinctly impact in the phenotype of precursor lesions during PDAC tumourigenesis.

Taken together, RASSF1A appeared to associate with YAP's phosphorylation in early PanIN lesions of KC mice. This suggests possible involvement of the canonical Hippo pathway in monitoring early stages of PDAC development. Moreover, the results deduced from the KCR1-Het mice study revealed that while the heterozygosity in the *Rassf1* SNP allele may not have a profound effect in the formation of KRAS-mediated PDAC, it needs to be further investigated with the homozygous *Rassf1* SNP allele and investigate for any distinct changes affecting PDAC development.

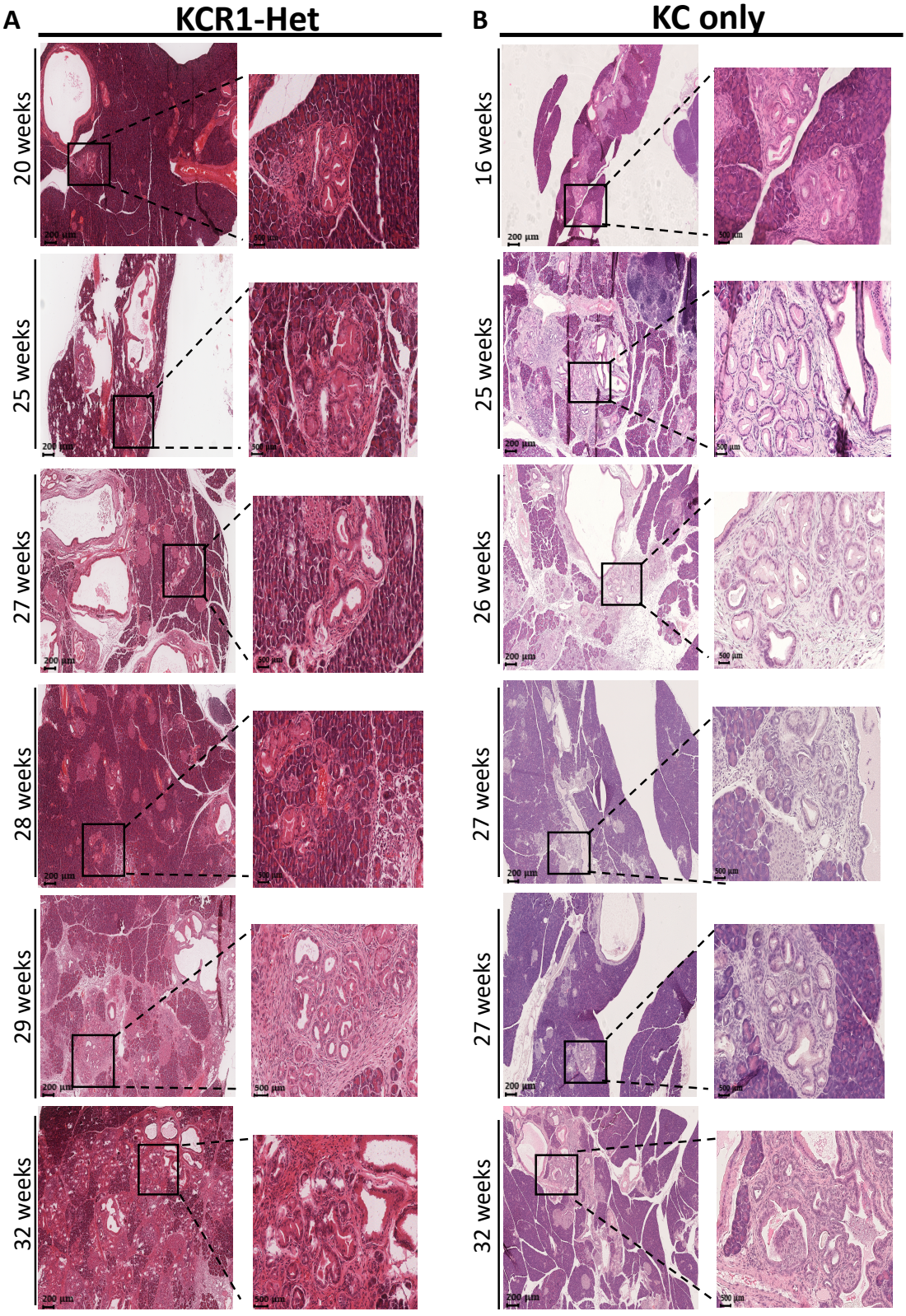


**Figure 5.3: Heterozygous RASSF1A SNP in mice with *Kras* mutated pancreas revealed no distinct phenotype.** (A) Histological analysis of mouse pancreata obtained through H&E staining in *RASSF1*$^{SNP/+}$; *Kras*$^{G12D}$;*Pdx-Cre*(KCR1-Het) mice up to 32-weeks old. Staining was performed in collaboration with Simone Lanfredini. Scale bars: 1$^{st}$ column = 200 µm, 2$^{nd}$ column = 500 µm. (B) H&E stained images from *Kras*$^{LSL.G12D/+;}$*Pdx-Cre*(KC) mice of similar ages were used as controls. H&E images were provided by Paul Miller. Scale bars: 1$^{st}$ column = 200 µm, 2$^{nd}$ column = 500 µm.

### 5.3.2 Establishment of 3D pancreatic organoids

To study the biology of PDAC development, we established a 3D pancreatic organoid protocol in our laboratory with the help of Jelte van daar Vaart, a Master's student and Fiona Bangs, a postdoctoral researcher in our laboratory. During the establishment process, we isolated small intralobular ducts from the pancreatic tissues of C57Bl/6 mice (Isolation protocol explained in detail in Chapter 2, Materials and Methods). The genetic backgrounds of these mice consisted of Wild type (WT) with normal pancreatic tissue and *Kras*$^{LSL\text{-}G12D/+}$*; Pdx1-Cre* (KC) with PanIN lesions. Following the isolation, the ductal cells were embedded in matrigel and cultured as organoids. These cultures were supplemented with the Complete Feeding Media (Chapter 2, Materials and Methods) every two days. The pancreatic organoids in our study, based on the Clevers and Tuveson's protocol (Boj et al. 2015), could grow more than 20 passages (Appendix, Figure 7.8.). The continuously proliferating cells in the organoids, possibly due to pancreatic progenitors residing in the ductal compartment (Carpino et al., 2016; Yamaguchi et al., 2015), led to a growth in the organoid size (Appendix, Figure 7.9).

Next, our interest in studying YAP's role during PDAC progression led us to analyse the protein's expression in this 3D setting of organoids. In order to do so, I firstly carried out immunofluorescence staining of pancreatic organoids derived from the Wild-type (WT) and *Kras*$^{LSL.G12D+/-}$*;Pdx-Cre* (KC) mice. Alongside, I also examined the epithelial structure of the organoids by staining for E-cadherin. The qualitative analysis displayed a uniform expression of YAP in both WT and KC organoids. The YAP proteins were localised in both the cytoplasm and nuclei of these organoids (Figure 5.4). Similarly, the presence of the epithelial marker, E-cadherin indicated the maintenance of the epithelial structure in these organoids. Qualitatively, YAP localisation in the nuclei

appeared to be more prominent in the KC organoid. This observation is, however, preliminary and insufficient to establish any comparative analysis of YAP expression and localisation between WT and KC organoids. Nevertheless, these data indicate the presence of YAP in organoids derived from both WT and KC mice. Overall, we were able to establish a 3D culture system using mouse pancreas that are more physiologically relevant to study PDAC tumorigenesis than 2D pancreatic cancer cell lines.

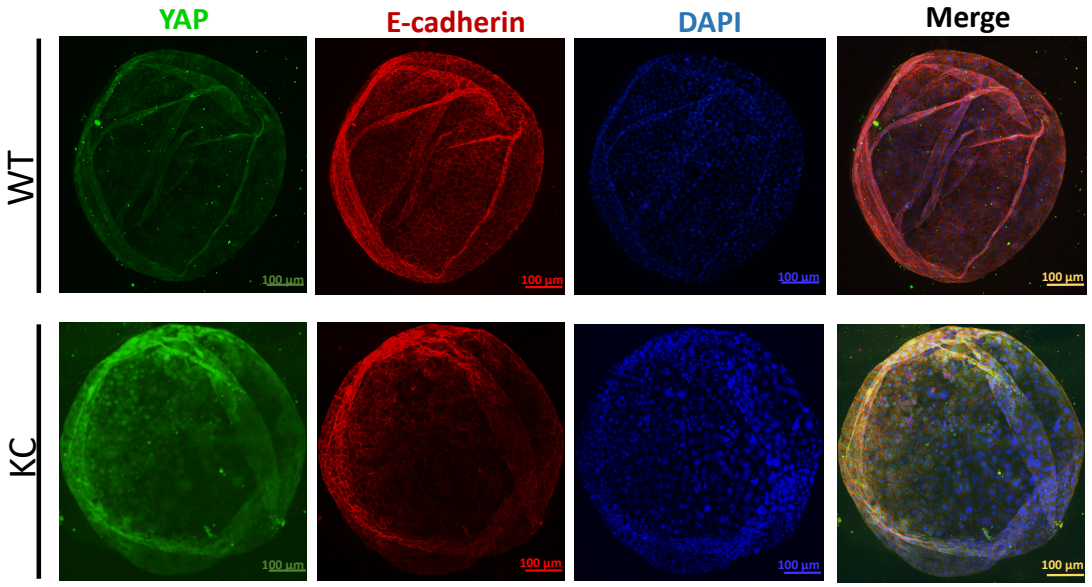


**Figure 5.4: Expression of YAP in 3D organoids from mouse pancreas. I**mmunofluorescence images of pancreatic organoids from Wild-type (WT) and KC mice stained with YAP (green), E-cadherin (red) and DAPI (blue) for nuclei. Scale bar = 100 µm.

### 5.3.3 Orthotopic injection of organoids into the mouse pancreas

Current advancement in PDAC treatment includes the use of patient derived organoids for genomic, transcriptomic and therapeutic profiling, which in turn, has shown promising results of precision medicine to PDAC patients (Tiriac et al., 2018). Prior to this, the study of pancreatic organoids derived from GEMMs were utilised to study the

molecular pathogenesis of PDAC *in vivo* by transplanting them back into mouse pancreas (Boj et al., 2015). The use of the orthotopic model in the study was significant as normal ductal architecture was regenerated in the pancreas upon the injection of organoids. Similarly, the injection of tumour organoids in the study led to the formation of both early-stage and late-stage PanIN lesions alongside PDAC. This orthotopic model in pancreas was demonstrated as early as 1989 (Vezeridis et al., 1989). In this study, Vezeridis et al. harvested pancreatic tumour developed in xenograft mouse models and transplanted them orthotopically into the pancreas of nude mice to study spontaneous metastatic process, that would closely resemble to that in human counterparts. Following this, the orthotopic model – transplanting pancreatic cancer cell lines into mouse pancreas – has been utilised in several studies for preclinical study and for understanding the process of pancreatic tumourigenesis (Mohammad et al., 1998; Morton et al., 2007; Tseng et al., 2010). The transplantation of normal and neoplastic ductal cells from 3D organoids, however, leads to more accurate and detailed analysis of molecular pathways involved in PDAC progression. Hence, we attempted to employ this technique with the goal of ultimately evaluating the detailed role of our protein of interest, YAP, in the orthotopic model.

Firstly, we standardised the technique of orthotopic injection in our laboratory settings. For this, I worked in collaboration with Simone Lanfredini, a postdoctoral researcher in the laboratory, and injected KPC cell lines into syngeneic C57BL/6 mice (500 cells per animal). After optimising the protocol of surgery, the tumour growth was monitored using repetition time (TR) multi-slice magnetic resonance imaging (MRI) of the mice abdomen. This was performed on a high-field 4.7 T (Tesla) preclinical imaging system for detailed anatomical and pathophysiological information in mice. Images obtained

from the MRI scanning showed growth in the tumour volume after segmentation (Appendix, Figure 7.10.A). Tissues including pancreas were harvested 5 weeks after injection or after the tumour volume has reached 800 $mm^3$ to gain histological, genetic and immunophenotypic information (Appendix, Figure 7.10.B). The histological analysis displayed formation of tumour in the pancreas injected with KPC cells (Appendix, Figure 7.10.C). Similarly, other tissues including liver, spleen, left kidneys and liver were also harvested to examine any offsite tumours or metastases.

After the establishment of the orthotopic model, I attempted to inject pancreatic organoids into the mouse pancreas (Fig 5.5.A), along with the help of Simone Lanfredini for the surgery, to see if we could also recapitulate the retention of normal ductal architecture into the host pancreas as observed previously by Boj et al. (Boj et al., 2015). At first, I used organoids derived from *Kras$^{G12D+/-}$; Pdx-Cre* mouse (KC organoids) only (n=3) to examine the feasibility and viability of the experiment. We initially injected 500 ductal cells from the KC organoids per mouse since this was the number used for cell line injections. Following this, I monitored growth of injected cells after surgery for four weeks, using preclinical high-field MRI 4.7T and obtained images every week. As shown in Figure 5.5.B, the images displayed anatomical features of the animal including pancreas, spleen, intestines, left and right lung, right kidney and stomach. Similarly, the site of injection in the pancreas was also accurately identified with matrigel showcased as the bright region (Figure 5.5.B).

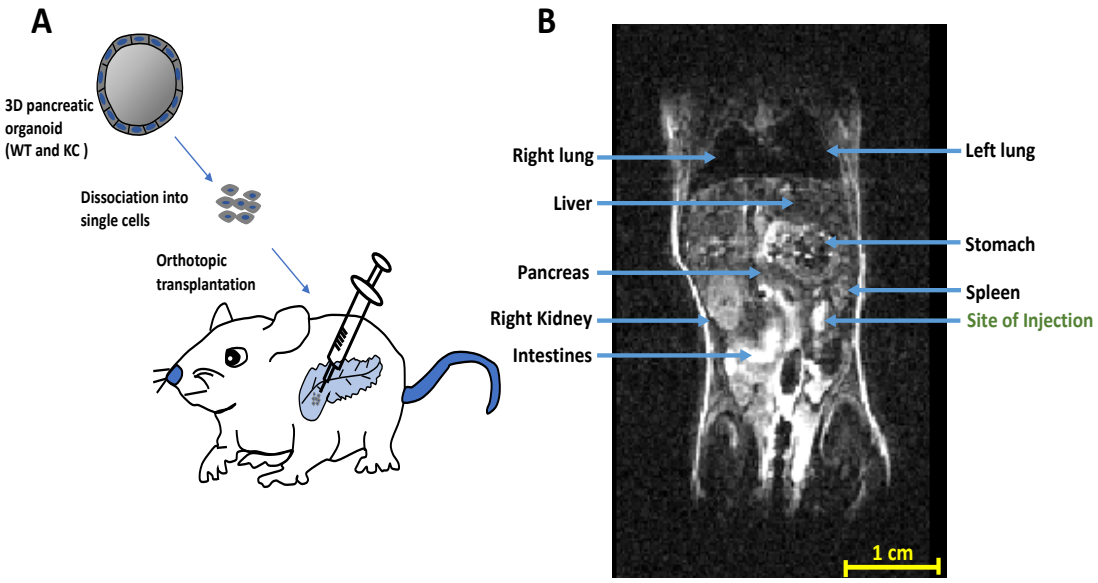


**Figure 5.5: Orthotopic injection of pancreatic organoids into mouse pancreas.** (A) Schematic representation of the orthotopic transplantation approach. Organoids derived from either Wild-type (WT) or *Kras*$^{LSL.G12D/+}$*;Pdx-Cre* (KC) mice are dissociated into single cells and injected orthotopically into syngeneic mouse pancreas. (B) Cross-sectional anatomy of mice abdomen obtained through respiratory gated MRI images in mouse that had been orthotopically injected with matrigel. Scale bar, 1 cm

In contrast to cell line growth, our orthotopic injection of 500 ductal cells from KC organoids did not indicate any rapid cell growth in the pancreata of all three mice over the course of four weeks (Figure 5.6). Although unsuccessful, this original experiment allowed us to optimise the methodology of single cell isolation from the organoids (Explained in detail in Chapter 2, Materials and Methods) and injection of these ductal cells into the mouse pancreas. In subsequent experiments, 10,000 ductal cells were injected per mouse. This cell number could not be exceeded due to the limitation in our project licence approved by the Home Office.

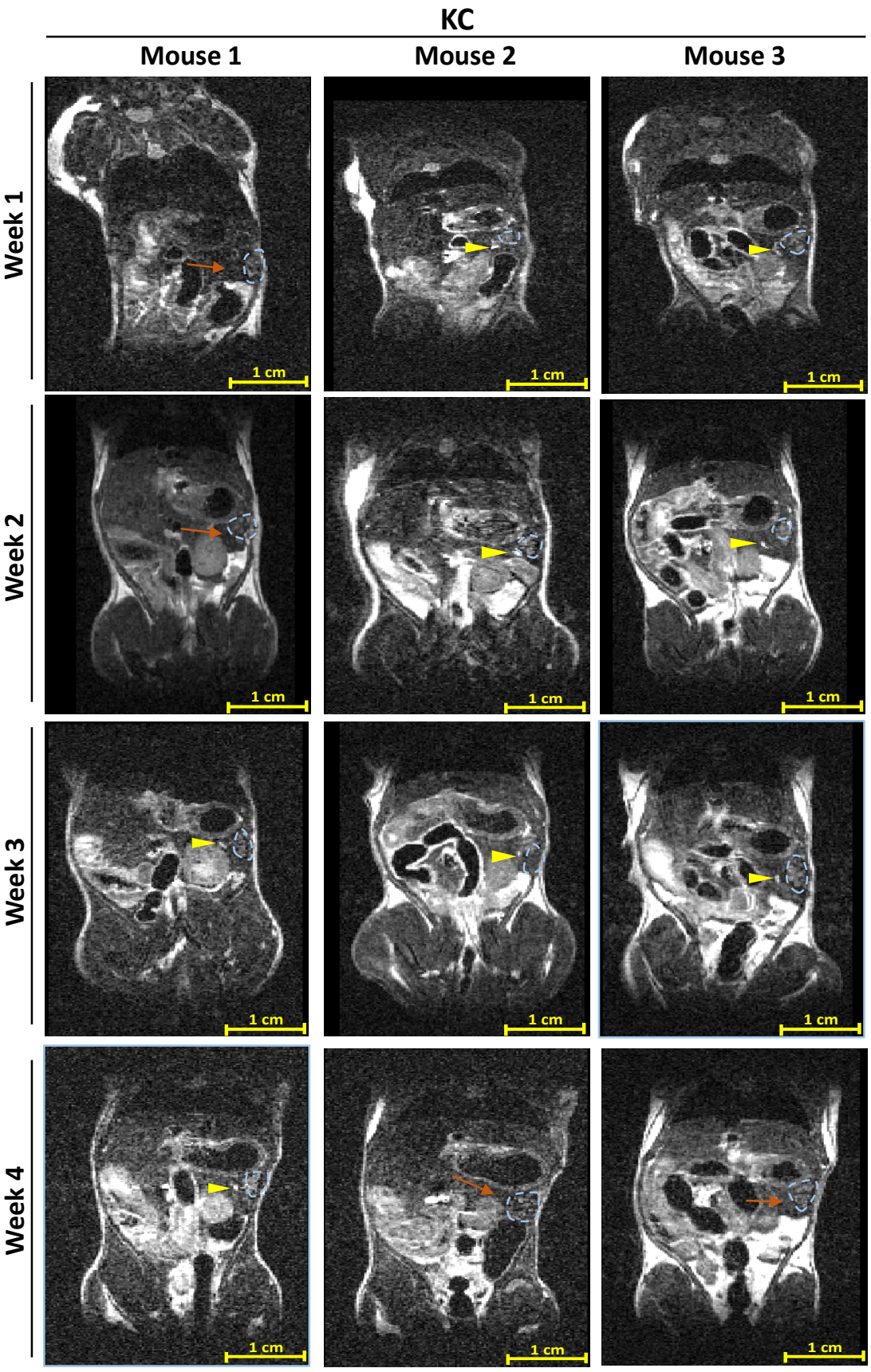


**Figure 5.6: *In vivo* MRI images of mice abdomen analysed each week after orthotopically injected with pancreatic organoids.** Mice with injection of 500 cells from *Kras*$^{LSL.G12D/+}$*;Pdx-Cre* (KC) organoids analysed up to four weeks before harvesting the pancreas. Blue dotted region indicates spleen. Yellow arrowhead indicates site of injection of Matrigel. Orange arrow indicates an area of pancreas, next to the spleen, with possible site of injection Scale bars = 1 cm.

In the following experiment, I included organoids from Wild type mouse (WT organoids) (n=3) as control alongside YFP-transduced KC organoids (*Kras$^{LSL.G12D+/-}$; Pdx-Cre; Rosa YFP)* (n=3). This enabled comparison of any changes in the mouse pancreas that were injected with ductal cells from differing genetic backgrounds of either Wild type (WT) or *Kras* mutation (KC). Since the cells were diluted in the matrigel for injection, control mice (n=3), injected just with the matrigel (matrigel only), were also included. In the study by Boj et al., orthotopic injection of normal organoids led to the formation of ductal structure for up to one month, which could not be sustained after two months. On the other hand, the research group demonstrated the formation of dysplastic cells upon orthotopic injection of PanIN organoids, which prevailed even after two months (Boj et al., 2015). Based on the study, I harvested pancreatic tissue two months after the injection of organoids in our study. Over the course of two months, I examined any occurrence of overproliferation of the injected cells through the MRI scanning. Image analysis of the MRI scans obtained at the eighth week did not indicate any signs of aberrant cell proliferation in the mice pancreata (Figure 5.7). This was, indeed, expected as the organoid cells that were injected comprised of normal and neoplastic ductal cells. Hence, there is a possibility of formation of normal or dysplastic architecture in the host pancreas. This, however, is unlikely to be succeeded by PDAC formation unless tumour organoids are injected into the pancreas (Boj et al., 2015). Nevertheless, I carried out MRI imaging to ensure animal welfare and avoid any risk of failure in tumour detection that could potentially harm animal's health.

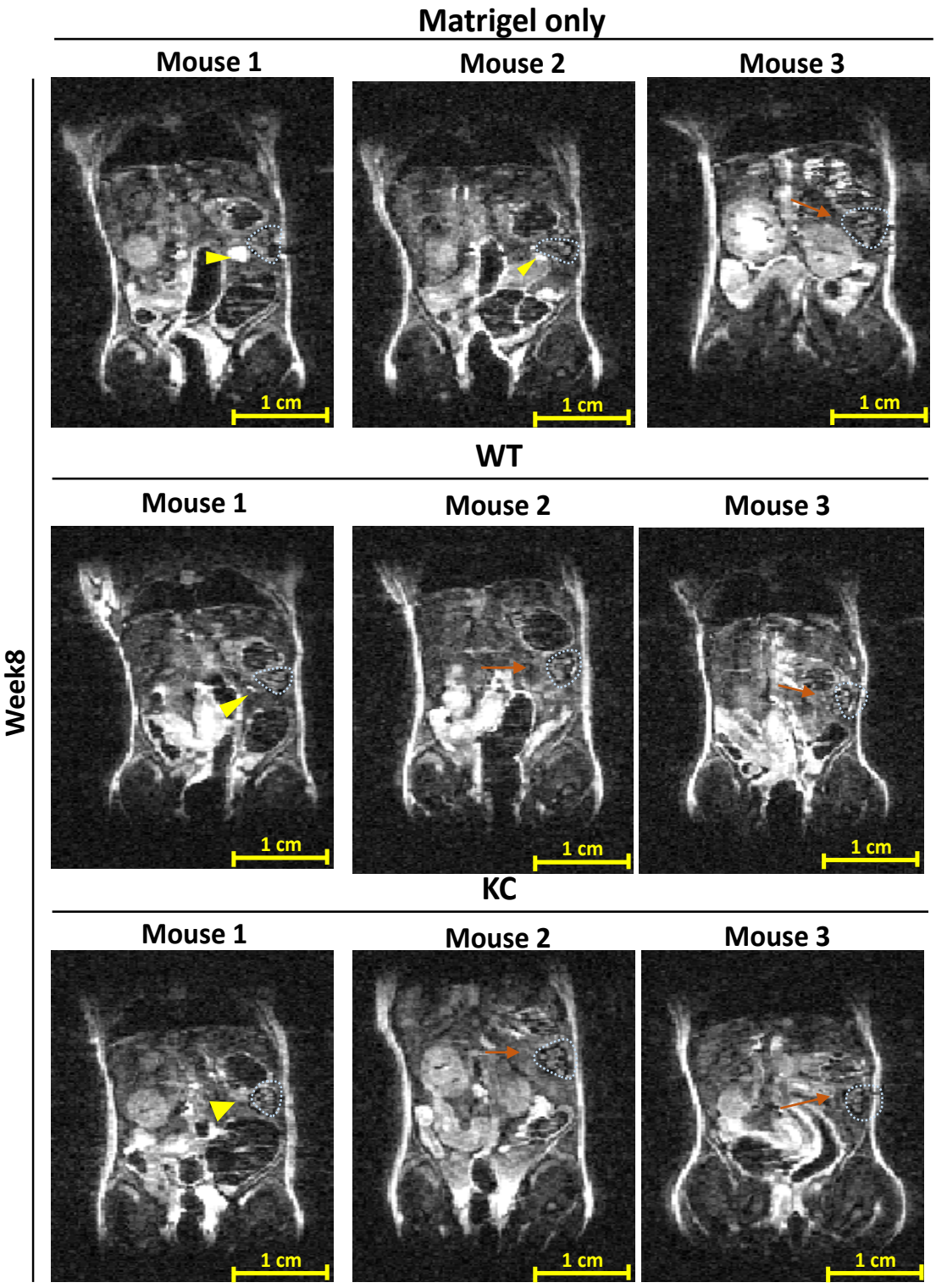


**Figure 5.7: *In vivo* MRI images of mice abdomen orthotopically injected with pancreatic organoids analysed before the harvesting of pancreas.** MRI images acquired at eighth week before harvesting the mice injected with 1 x $10^4$ cells from Wild-type (WT) and KC pancreatic organoids. Matrigel only was injected as a control. Blue dotted region indicates spleen. Yellow arrowhead indicates site of injection of Matrigel. Orange arrow indicates an area of pancreas, next to the spleen, with possible site of injection. Scale bars = 1 cm.

### 5.3.4 Histological assessment of orthotopic model of pancreatic tissue

I speculated that our orthotopic injection of ductal cells from the Wild type (WT) and *Kras$^{LSL.G12D/+}$; Pdx-Cre; Rosa YFP* (hereafter referred to as KC-YFP+ve) mice would lead to the formation of dysplastic cells that recapitulates early PanIN lesions in murine and human disease model. As a result, I harvested pancreas two months after the WT and KC-YFP+ve organoids had been injected into the mouse pancreas (n=3 for each) along with matrigel only (n=3) as the experimental control (explained previously in Section 5.3.3). In order to identify any distinct morphological features that may resemble PanIN structure, I performed H&E staining of the tissues. Alongside, I also evaluated pancreatic tissue from WT mouse that had not undergone any surgical procedure as a control to deduce any morphological difference. Overall, the H&E images displayed presence of structures with ductal architecture in the pancreata of the orthotopic model (Figure 5.8.A). I was, however, unable to determine distinct structures that fit our morphological description of mouse PanIN lesions.

Next, I evaluated any ductal structures present around the vicinity of site of injection. The caveat to this was that I was able to identify the site of injection only in some tissues. In the tissues where the site of injection was identified, there was no presence of distinct dysplastic structures around these regions (Appendix, Figure 7.11). Further sectioning of the tissues, however, needs to be carried out to ensure focal regions with dysplasia were not missed by chance. Moreover, to confirm any presence of PanIN disease state, I stained the pancreata obtained from the orthotopic model along with the tissue from WT mouse for Alcian blue (Figure 5.8.C and Figure 5.8.D). Our observation of the absence of morphologically distinct PanIN-like lesion structures was further supported by the negative staining in the ductal structures for Alcian blue.

Although there was a presence of blue staining in the ductal structure of KC-YFP+ve orthotopic model (Figure 5.8.C), the intensity of the staining was very low. In comparison, the Alcian blue staining of PanIN lesions from genetically modified KC mouse tissue was more prominent (Appendix, Figure 7.12). Additionally, the intensity of Alcian blue staining in the ducts of both orthotopic mice model (Figure 5.8.C) and normal WT pancreas (Figure 5.8.D) was similar. This suggests that the Alcian blue staining observed in the ductal structures of our orthotopic model could be the result of non-specific background noise. The production of mucins, which can be determined by Alcian blue, is a feature of low-grade PanIN lesions (He et al., 2018). Appropriately, the normal ductal epithelium that lacks mucin production is stained negative for Alcian blue (Strobel et al., 2010). I, therefore, speculate that the ductal structures in KC-YFP+ve tissue, as shown in Figure 5.8.A, are non-neoplastic epithelium based on low staining for Alcian blue. To confirm this further, staining of the orthotopic model with MUC5AC can be useful.

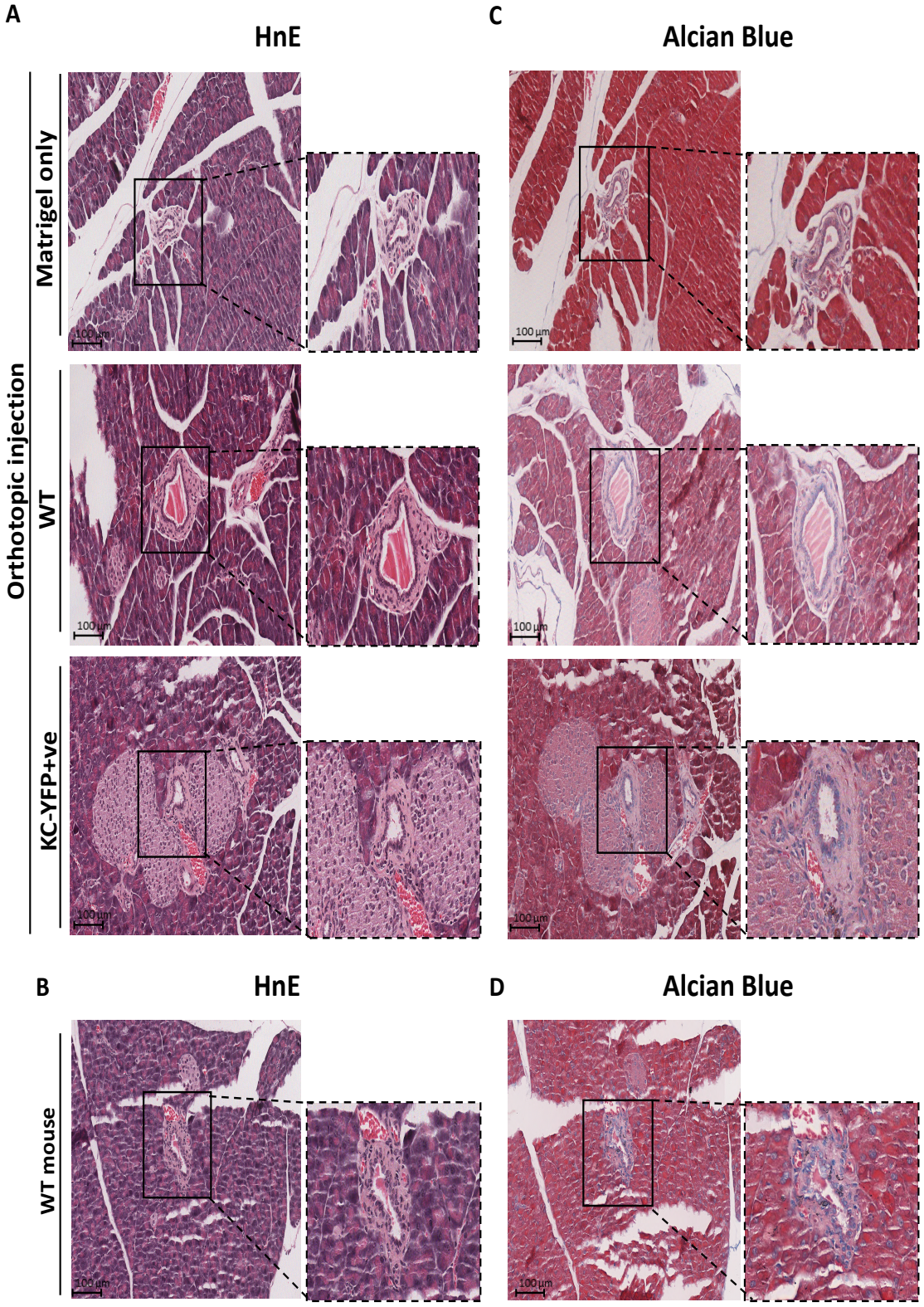


**Figure 5.8: Ductal structures in pancreas with orthotopically injected organoids resembled normal ductal epithelium.** (A) Histological analysis of mouse pancreata obtained through (A) H&E staining and (B) Alcian blue staining after 8-weeks of orthotopic injection with Wild-type (WT) and *Kras*$^{LSL.G12D/+}$*; Pdx-Cre; Rosa YFP* (KC-YFP+ve) organoids displayed normal ductal architecture. Matrigel only was injected as a control. Wild-type mouse pancreas with no orthotopic injection were also stained with (C) H&E and (D) Alcian blue as controls. Scale bars for all images = 100 µm. Images within the dotted box on the right were cropped and magnified region to highlight the ductal structures.

### 5.3.5 GFP staining in the pancreatic tissue from the orthotopic model and KC-YFP+ve mouse

The histological assessment through haematoxylin and eosin (H&E) staining and mucin detection through Alcian blue staining failed to demonstrate the presence of neoplastic structures in our orthotopic model (Figure 5.8.B). To further confirm if these results are truly representative, I investigated YFP expression in the pancreata injected with KC-YFP+ve organoids. For this, immunohistochemical staining of the pancreata was carried out using a GFP antibody to detect the expression of YFP. Firstly, I verified for the presence of the lineage tracing marker, YFP, in the pancreata of *Pdx-Cre; LSL-Kras*$^{G12D/+}$*; Rosa26 YFP* (KC-YFP+ve) mouse from which KC-YFP+ve organoids were derived. Upon histological examination of the pancreas from the 17-week old KC-YFP+ve mouse, normal architecture was visible from the different pancreatic regions (Figure 5.9.A). I had speculated the presence of, at least, early PanIN lesions in this *Kras*-mutated pancreas based on literature (Hingorani et al., 2003) and our previous observations in KC mice of similar age (Chapter 3). There was no detection of any morphologically distinct neoplastic structures in this 17-week old mouse. While any positivity for YFP protein would indicate the presence of recombined cells harbouring Cre expression, it does not indicate for the expression of oncogenic *Kras* mutations. Nevertheless, I carried out immunohistochemical analyses to look for the expression of YFP proteins by using a GFP antibody. During this, different conditions were applied for the optimisation process – antigen retrieval using citrate buffer at pH 6, boiled at two different temperatures of 110°C and 125°C, and GFP antibody concentrations at 1:100 and 1:200. In order to rule out any background staining, consecutive sections for each

condition were also stained with only HRP-conjugated rabbit secondary antibody only. The IHC analyses presented positivity for the GFP staining in all of these four conditions (Figure 5.9.B). The expression of Pdx-1 occurs around E8.5 during embryonic development. These progenitor cells expressing Pdx-1 give rise to all mature cells and ultimately is confined to pancreatic islets in the mature adult mouse (Hingorani et al., 2003). In accordance with this, our cell-lineage tracing with GFP antibody demonstrated YFP expression in all pancreatic cell types of the KC-YFP+ve mouse. This, in turn, indicated stochastic Cre expression, driven by Pdx, that would result in YFP expression. The GFP staining, however, does not indicate the concomitant expression of oncogenic KRAS given the lack of detection of PanIN lesions in the pancreas of KC-YFP+ve mouse before utilising the tissue for organoid isolation. The genetic background of this mouse should be reconfirmed through genotyping to ensure that the mouse had indeed harboured *Kras*$^{LSL.G12D/+}$ knocked-in allele.

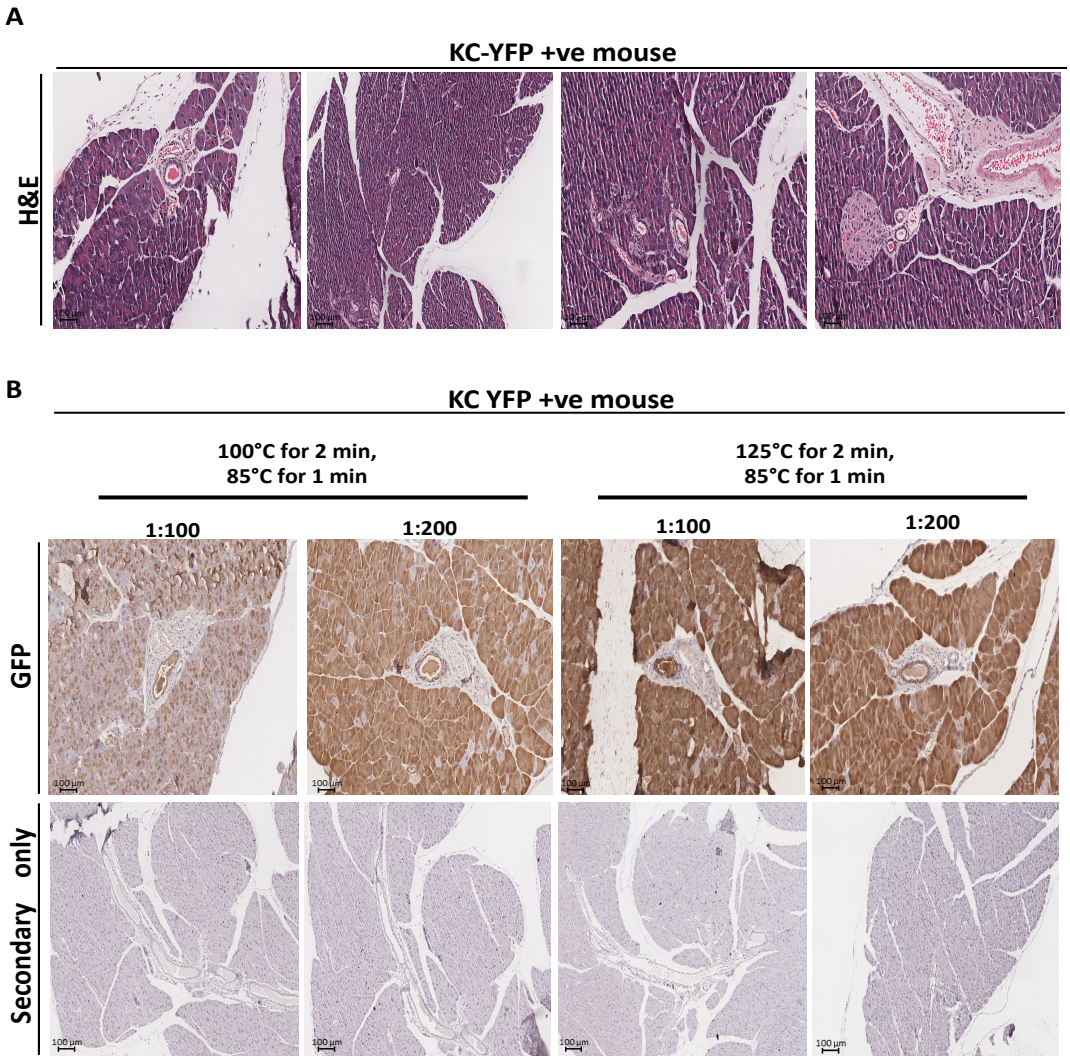


**Figure 5.9: YFP expression in the pancreas of KC-YFP+ve mouse.** (A) Representative H&E images of *Kras*$^{LSL.G12D/+}$*; Pdx-Cre; Rosa YFP* (KC-YFP+ve) mouse pancreas. (B) The tissue sections were stained with GFP antibody to detect for the presence of YFP. The staining conditions were optimised using different conditions for antibody concentration and antigen retrieval. HRP-conjugated anti-rabbit secondary antibody only was used as control. Scale bar for all images = 100 µm.

Subsequently, I stained the orthotopic model injected with KC-YFP +ve organoids for GFP to trace any Cre positive cells in the pancreas (Figure 5.10.A). During this, the optimised condition for GFP - antigen retrieval with citrate buffer at pH 6, boiled at 110°C for 2 min and heated at 85°C for 1 min and GFP antibody concentration at 1:100 – was applied due to its better signal (Figure 5.9.B). The Wild-type (WT) organoids, injected into the orthotopic model, were used as a negative control for YFP expression (Figure 5.10.A). Additionally, other control samples were also included: pancreas with matrigel only injection (Figure 5.10.A) and WT pancreas with no injection (Figure 5.10.B) were used as negative controls while the pancreas from KC-YFP+ve mouse was used as a positive control (Figure 5.10.C). Alongside these, I stained the tissue samples with secondary antibody only in order to negate any background staining. Our immunohistochemical analyses did not demonstrate any presence of YFP expression in the orthotopic model injected with KC-YFP+ve organoids. From this, it is most likely that the orthotopic injection of organoids was unsuccessful in our study – presumably due to the organoid cells dying off either during the process of dissociation into single cells or during the procedure of orthotopic transplantation.

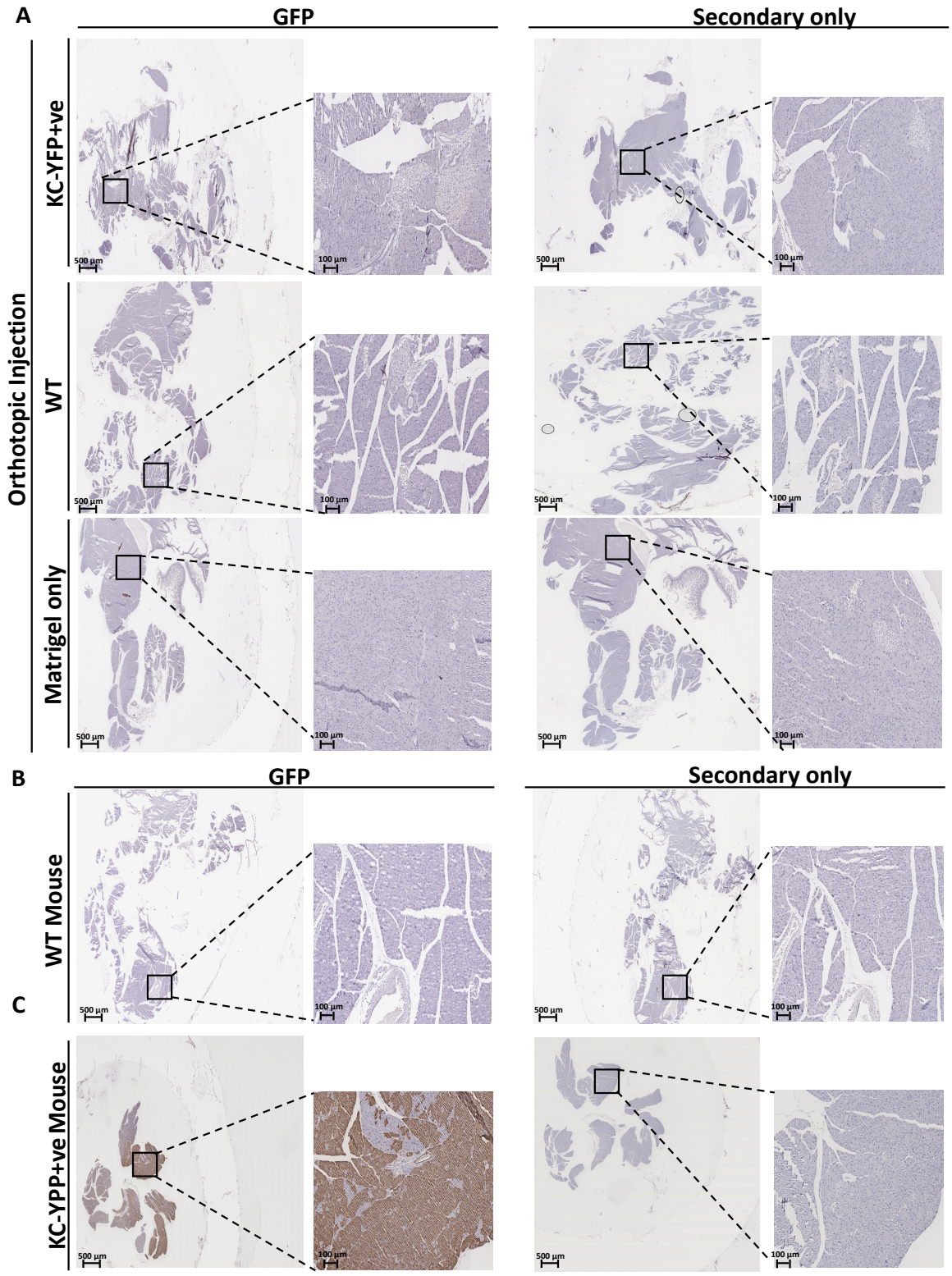


**Figure 5.10: Investigation for YFP expression in mice injected with organoids isolated from KC-YFP+ve mouse.** (A) Representative IHC images of GFP antibody in mouse pancreas orthotopically injected with *Kras*$^{LSL.G12D/+}$*; Pdx-Cre; Rosa YFP* (KC-YFP+ve) organoids to look for the expression of YFP. Mice injected with Wild-type (WT) organoids and Matrigel only were used as control (left panel). The tissue sections were consecutively stained with HRP-conjugated anti-rabbit secondary antibody only as a control for the staining (right panel). Scale bars: 1$^{st}$ and 3$^{rd}$ rows = 500 µm, 2$^{nd}$ and 4$^{th}$ rows = 100 µm (B) Pancreas from a WT mouse and a KC-YFP+ve mouse, that had not been orthotopic injection, were also stained with GFP antibody (left panel) and HRP-conjugated anti-rabbit secondary antibody only (right panel) as controls. Staining experiment was performed with the kind help of Sophie Hughes and Frances Willenbrock. Scale bars: 1$^{st}$ and 3$^{rd}$ columns = 500 µm, 2$^{nd}$ and 4$^{th}$ columns = 100 µm.

### 5.3.6 Stable YAP knockdown in KC organoids

Despite the difficulties so far in establishing the orthotopic injection of organoids into mouse pancreas in our laboratory, previous studies have demonstrated the development of normal and neoplastic lesions upon the transplantation of normal and PanIN organoids (Boj et al., 2015). I aimed to investigate if this phenotypic progression of PanIN lesions would be altered if YAP knocked down organoids were injected instead into the mouse pancreas.

The previous findings in this study indicated YAP's differing role in the regulation of KRAS/MAPK pathway in transiently and stably knocked down pancreatic cancer cells. Alongside we also observed heterogeneity in YAP expression in the precursor lesions of *Kras*-mutated mouse pancreas (Chapter 3, Figure 3.10). Based on these observations, I manipulated the expression of YAP in order to investigate any contribution of the protein in activating MAPK pathway in terms of 3D system. Firstly, I attempted to transiently knockdown YAP's protein level using siRNA technology in KC organoids. Using the KC organoids, I primarily wanted to validate if siRNA-mediated YAP knockdown could be performed in the 3D system. The protocol involved mechanical disruption of the organoids into single cells for transfection, following which they were embedded again into the matrigel for the organoid re-growth. The transient transfection of YAP using siRNA, however, proved rather difficult despite repeated attempts (n=3) (Figure 5.11.A). Indeed, previous studies have mostly been unsuccessful in the *in situ* delivery of siRNA to organoids using lipofectamine-based transfection techniques (Morgan et al., 2018). Alternatively, given the well-established protocols to stably silence protein expression in organoids, I carried out lentiviral transduction of KC organoids using shRNA for YAP (shYAP) (Explained in detail in

Chapter 2, Materials and Methods). The vector containing a shRNA insert that does not target any known gene (shCtrl) was used as a negative control.

I then validated the efficiency of the stable transfection through western blot analyses. Indeed, our results showed a depletion in YAP's protein level in the organoids transfected with shRNA for YAP (n=2) (Figure 5.11.B and 5.11.C). Given the increased level of pERK and TAZ in pancreatic cancer cells with stable knockdown in our earlier observations (Chapter 3, Figure 3.3 to Figure 3.7), it would be interesting to see the effect on the proteins in the 3D organoid system. Nevertheless, the 3D organoids would present as a better model than 2D pancreatic cancer cells to study neoplastic progression of PDAC through orthotopic injection into mouse pancreas. Taken together, our ability to manipulate YAP in the 3D organoids can be used as a genetically traceable model to directly explore YAP's contribution in PDAC progression *in vivo*.

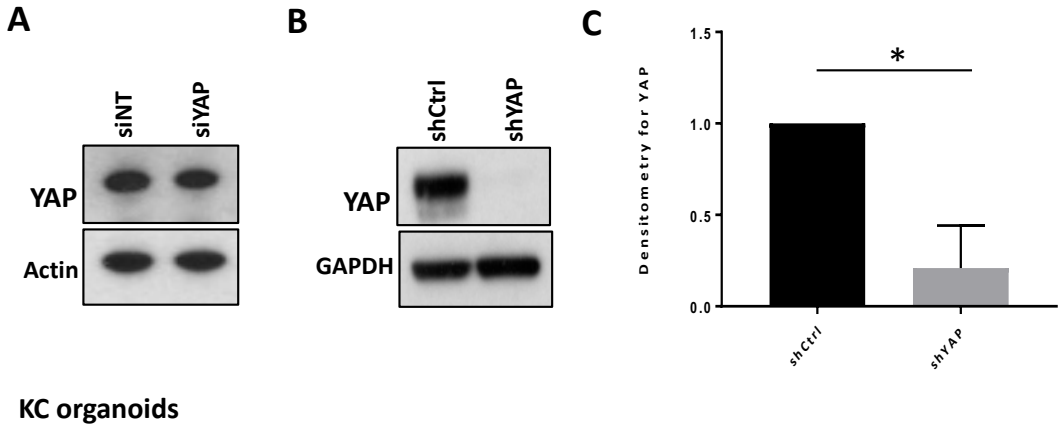


**Figure 5.11 : Depletion of YAP expression in organoids isolated from KC mouse pancreas.** (A) siRNA-mediated transfection was unable to knockdown YAP expression in *Kras*$^{LSL.G12D/+}$*;Pdx-Cre* (KC) organoids (n=3) (B) Lentiviral vectors were used to transduce KC organoids with either non-targeting shRNA (shCtrl) or YAP shRNA (shYAP). Organoids were treated with puromycin to select organoids that integrated shRNA plasmids. After selection with puromycin, transfected organoids were harvested using RIPA buffer and proteins assessed by SDS-PAGE/Western Blot. The membranes were probed with YAP to confirm the knockdown. GAPDH acted as a loading control. The blots are represented from one technical experiment (C) Protein levels of YAP due to shRNA-mediated knockdown was confirmed through densitometry. Data are represented as mean ± SD from two technical repeats of cell harvesting experiment. *$P \leq 0.05$, **$P \leq 0.01$, ***$P \leq 0.001$, $^{ns}P > 0.05$, Student's two- tailed t test.

## 5.4 Discussion:

Our preliminary findings to explore any potential tumour suppressive role of NF2 in PDAC progression, via MAPK pathway, revealed no change in YAP phosphorylation in pancreatic cancer cell lines (Chapter 3, Figure 3.8). We thus explored the possible contribution of RASSF1A in PDAC progression. The role of the tumour suppressor, RASSF1A, to promote apoptosis through the Hippo pathway has been previously documented (Oh et al., 2006). While the loss of RASSF1A and increased YAP activation in PDAC have been previously shown (Amato et al., 2016; Dammann et al., 2003; Kapoor et al., 2014; Shao et al., 2014; Zhang et al., 2014) , the possible linkage due to RASSF1A induced Hippo pathway signalling to control YAP activation is yet to be established in PDAC. In our study, we observed an association between RASSF1A and phosphorylated YAP expression in early precursor lesions (Figure 5.1). Both of these proteins, RASSF1A and pYAP, were localised in the apical membrane - a region where Hippo pathway core kinases are recruited for activation (Yu and Guan, 2013). Interestingly, the lower expression of nuclear YAP in the PanIN lesions in comparison to normal duct appeared to be in concomitant with higher expression of pYAP and RASSF1A in the corresponding PanIN lesions (Figure 5.1.A). This suggests possible role of the Hippo pathway inhibiting YAP activity in the PanIN lesions that exhibit low expression of nuclear YAP.

Additionally, in order to understand the mechanism through which RASSF1A could potentially impact PDAC progression, we utilised GEM models which are more representative of the human disease state. During this, I crossbred *Rassf1*$^{SNP/+}$ (R1-Het) mice with *Kras*$^{LSL.G12D/+}$*; Pdx-Cre* (KC) mice. The resulting transgenic offspring -

*Kras*$^{LSL.G12D/+}$*; Pdx-Cre; Rassf1*$^{SNP/+}$ (KCR1-Het) – displayed a trend of low survival, albeit insignificant, when compared to KC and R1Het alone (Figure 5.2.B). The histological analysis also displayed no aggressive phenotype formation in the pancreas of KCR1-Het mice in comparison to KC only mice, suggesting no pathological aberrations (Figure 5.3).

Despite the RASSF1A SNP – that reduces the ability of ATM to phosphorylate RASSF1A-p.133Ser upon DNA damage (Yee et al 2012) – rendering no difference in KRAS-mediated PDAC advancement (Figure 5.3), further investigation would be useful. This is particularly of our interest given the trend of lower survival rate of KCR1-Het mice (Figure 5.2.B). The data was deduced from six mice that were euthanised as they displayed signs of more than mild discomfort and distress. While this mostly occurred due to facial papilloma – an effect of the Pdx-Cre leakiness – it would be worthy to make a record of the degree of severity of papilloma in these mice when compared to age-matched KC mice. Furthermore, the effect of RASSF1A in PDAC needs to be corroborated by exploring any effect of homozygous SNP for *Rassf1* in the background of *Kras* mutation in the pancreas.

Additionally, in this study, with the help of Jelte Van der Vaart and Fiona Bangs, we were able to successfully establish 3D organoid culture system from both WT and KC mouse pancreas based on Clevers and Tuveson's protocol (Figure 5.4). While these organoids were derived from the ductal cells of the pancreas, the possible residence of progenitor cells in these ductal compartments present them with self-proliferating capacity (Huch et al., 2013). Consequently, it will be useful to confirm this proliferative state in the organoid system and any difference in the organoids derived from mice with two different genetic backgrounds by using a proliferative marker, such as Ki67.

Our next attempt was to establish orthotopic model with organoids injected into the mouse pancreas. The orthotopic injection of cancer cells, which had been standardised in our laboratory, resulted in high rate of tumour formation in the pancreas (Appendix, Figure 7.10.C). Our interest in examining early stages of tumourigenesis led us to extend our investigation by using 3D organoid system instead of 2D culture for the orthotopic injection. Our MRI analysis presented site of injection in some but not all pancreas that had undergone surgery (Figure 5.6 and 5.7). While this indicates potential error in successfully transplanting cells into the pancreas, it is inconclusive as rapid cell proliferation of normal and neoplastic organoids were not expected, unlike the KPC cancer cells, when injected into mouse pancreas.

It is well-appreciated from the literature that the organoid recapitulates the tissue of origin. Moreover, Boj et al. demonstrated that only the metastases-derived organoids lead to rapid tumour formation. On the other hand, the transplantation of PanIN or tumour organoids had a much slower rate of growth during the multi-phase progression from early stage to PDAC, usually taking longer than two months (Boj et al., 2015). Based on this study, we expected to detect the formation of early PanIN lesions, and not aggressive tumour phenotype, in our orthotopic model.

Morphologically, the ductal structures in our orthotopic model of KC organoids were very similar to the ones displayed by Boj et al. from their orthotopic injection of PanIN organoids (Boj et al., 2015). We were, however, unable to detect any morphological change in these structures that fitted the definition of early PanIN lesions (Figure 5.8.A). Moreover, our Alcian Blue staining to confirm the disease state of PanIN lesions displayed negative staining in the ductal regions of the orthotopic model (Figure 5.8.B). This needs to be further confirmed by carrying out Alcian blue staining in the

orthotopically injected pancreata alongside a positive control of an older KC mouse pancreas (25-40 weeks old) that has previously been confirmed to display low-grade PanIN lesions (Chapter 3 and Chapter 4). Other specific markers that determine PanIN disease state can also be used including MUC5AC, MUC6 and TFF1 (Boj et al., 2015). Moreover, the absence of any PanIN lesions in the 17-week old KC-YFP+ve mouse pancreas (Figure 5.9) could also explain the failure of neoplastic formation in the orthotopic model following the injection of organoids from the KC-YFP+ve mouse. Indeed, the mouse might not have harboured *Kras*$^{LSL.G12D/+}$ knocked-in allele and needs to be confirmed through genotyping.

The IHC staining with GFP antibody failed to show YFP expression in the orthotopic model derived from *Kras*$^{G12D+/-}$*; Pdx-Cre; Rosa YFP* (KC-YFP+ve) pancreas (Figure 5.10). The lack of YFP expression indicates possibility of the organoid cells dying off during the orthotopic injection. This could arise due to the prolonged incubation period of the organoids in trypsin during their dissociation into single cells, which could potentially kill the cells. The absence of viable cells during injection could, in turn, explain failure in formation of PanIN-like structures and thus their lack of detection in our orthotopic model. In order to ensure that our single cell dissociation procedure is not affecting the cells' viability, carrying out cell viability assay following the dissociation process will be useful. Similarly, increasing the number of ductal cells injected would be ideal to truly recapitulate the protocol carried out in the previous study (Boj et al., 2015).

We were able to successfully knock down YAP expression, using shRNA technology, in our KC organoids (Figure 5.11). We, however, need to repeat this further by using our WT organoid model to make any fair and complete comparison. Ultimately, these YAP depleted organoids can be transplanted to mouse pancreas to directly analyse any

effect of YAP by exploring phenotypic changes in the formation of precursor lesions during PDAC tumourigenesis. This can be performed following the optimisation of the orthotopic model.

While the cell of origin for PDAC still remains controversial, our findings in this study indicated the possibility of PDAC origin from both acinar and ductal cell types (Chapter 4). The organoid model would also present a very useful tool to investigate cell of origin in our study. Using the organoids from ductal cells with conditional Adeno-Cre driven $Kras^{G12D}$ expression, Boj et al. reported the ability of ductal cells to form PanIN lesions (Boj et al., 2015). This can be incorporated into our future investigations by manipulating YAP expression in the organoids with conditional $Kras^{G12D}$ expression. The resulting observation could allow us to gain more insight into the association of YAP with the cell of origin during PDAC development.

Taken together, the utilisation of 3D organoid has the potential to be a better, quicker and more convenient model to understand the role of YAP in relation to cell of origin and aggressive phenotype of precursor lesions.

# Chapter 6 Discussion

## 6.1 Background Summary

Pancreatic ductal adenocarcinoma is a lethal disease, with only 3% of patients attaining the 5-year survival period (Bardeesy and DePinho, 2002). This is mainly attributed to the lack of early diagnosis — by the time patients are diagnosed with PDAC, they are presented at the late stage with metastatic disease. The only curative treatment available so far for PDAC patients involves surgical resection, with the eligibility limited to very few percentage (10-20%) of patients. Palliative chemotherapy is provided as the first-line therapy for the PDAC patients at the advanced stage (Abbassi and Algul, 2019). This highlights the necessity to diagnose PDAC at a pre-invasive stage. The process of PDAC progression involves multiple stages before the disease develops into the malignant form. This multi-step progression of PDAC is initiated by neoplastic precursor lesions. Amongst different types, the most common precursor lesions are the microscopic, non-invasive epithelial neoplastic lesions known as Pancreatic Intraepithelial Neoplasia (PanIN) (Brat et al., 1998; Klimstra and Longnecker, 1994). A classification system divided PanIN lesions into different grades; low-grade lesions consist of PanIN-1 and PanIN-2 whereas the high-grade of PanIN-3 lesions. This classification is based on the degree of cytological and architectural changes (Basturk et al., 2015; Hruban et al., 2004).There are, however, no specific molecular markers that distinctively separate each stage of PanIN lesions. Importantly, despite the role of PanIN lesions as preinvasive neoplasia, around 40% of adult individuals harbouring PanIN-1 lesions never develop into invasive adenocarcinoma in their lifetime. PanIN-3

lesions are rarely observed in these pancreata (<5%). On the other hand, 30% to 50% of pancreata with invasive behaviour also have PanIN-3 lesions (Hruban et al., 2004). This, indeed, posed the question whether some PanIN lesions had aberrant changes at the molecular level and thus were at a higher risk of developing into invasive adenocarcinoma, in comparison to others. The primary tumour in PDAC, similar to many cancers, consists of several subclones with genetic diversity. These subclones are generated as the cancer cells proliferate uncontrollably and outgrow surrounding cells to form clonal populations. Another level of complexity arises as the multifocal regions of PDAC consist of both acinar- and ductal-derived cell, at least in the KPC model (Ferreira et al., 2017). Although PDAC were initially speculated to originate from the ducts due to its glandular and ductal morphology (Bailey et al., 2014; Xu et al., 2019), subsequent studies demonstrated the ability of acinar cells to undergo metaplasia and transform into ductal cells. During this process, the acinar cells gain structures and markers reminiscent of the ducts. The structures due to acinar-to-ductal metaplasia (ADM) are identified to emanate PanIN lesions formation which eventually develop into PDAC (Guerra et al., 2007; Kopp et al., 2012). This revelation, however, questioned the true origin of PDAC. More recent studies have showcased that both acinar and ductal cells give rise to PDAC. The molecular mechanism through which these two cell types develop into tumour is distinct which, in turn, determines the degree of aggressiveness of the PDAC disease (Ferreira et al., 2017; Lee et al., 2018).

## 6.2 Final Discussion of Chapter 3

### 6.2.1 Mechanisms by which YAP contribute to drive PDAC progression

Zhang et al. in 2014 presented YAP as the first molecule to be absolutely critical in the neoplastic progression of *Kras*-mutated pancreas (Zhang et al., 2014). Hence, I first investigated the role of YAP oncogene in PanIN lesions of KC mouse pancreas, with the speculation that YAP's activation would proportionally increase with the increasing grade of PanIN lesions. The immunohistochemical staining revealed the presence of nuclear YAP in the normal ductal epithelium (Figure 3.10.A) which would be necessary for the maintenance of tissue homeostasis (Diep et al., 2012). Unexpectedly in some cases, the expression of nuclear YAP was lost as the normal ductal epithelium transitioned into low-grade PanIN lesions. There was indeed heterogeneity since there were also few other PanIN lesions present that were able to retain nuclear YAP expression (Figure 3.10.B to Figure 3.10.D). Given the known contribution of YAP in PDAC progression (Kapoor et al., 2014; Shao et al., 2014; Zhang et al., 2014), the variation of nuclear YAP in the PanIN lesions could be associated with their risk of progression into PDAC.

Furthermore, to link YAP's cellular effects with PDAC development, I investigated for any association of YAP with that of phosphorylated ERK (pERK) in the nuclei of *Kras*-mutated lesions. The activated ERK1/2 is known as a master regulator in G1 to S phase transition of cell cycle and thus enhances cell proliferation (Mebratu and Tesfaigzi, 2009). I demonstrated a positive correlation between YAP and pERK levels in the nuclei of PanIN lesions (Figure 3.12). This indicates YAP's possible role in the constitutive activation of ERK and uncontrolled cell proliferation in the PanIN lesion structures. As

a result, PanIN lesions with high nuclear YAP – indicating the protein's functionally activated role – could potentially enable the lesions to progress into malignant derivatives. A previous study demonstrated that YAP lies downstream of MAPK/pERK in *Kras*-mutated pancreatic cancer cells and, in turn, induces secretory proteins for cell proliferation (Zhang et al., 2014). Another study showed that the downregulation of Hippo pathway led to activate YAP activation in thyroid cancer. Activated YAP, in turn, transcriptionally regulated the increased expression of KRAS expression and, as a result, augmented MAPK pathway (Garcia-Rendueles et al., 2015). Based on these findings, I speculated the presence of a positive feedback loop between the Hippo/YAP pathway and the KRAS/MAPK/pERK pathway. Hence, to understand YAP's potential to act as an upstream regulator of KRAS/MAPK pathway and enhance pERK activity, I manipulated the expression of YAP using an *in-vitro* system. I depleted expression of YAP in pancreatic cancer cells to investigate the possible mechanism by which YAP could regulate the KRAS/MAPK pathway. Transient depletion of YAP expression for 24 hours by using siRNA against YAP displayed a decrease in ERK1/2 activation (Figure 3.1). On the other hand, prolonging the transfection period to 48 hours led to a paradoxical increase in pERK levels (Figure 3.2). When stable knockdown of YAP was performed, similar results of an increase in pERK was observed in the pancreatic cancer cells (Figure 3.3 to Figure 3.5). Alongside this, a trend of increasing TAZ protein levels was also observed upon stable knockdown of YAP (Figure 3.6 and Figure 3.7). This enabled us to speculate the compensatory role of TAZ in regulating growth-promoting cellular effects by enhancing the activity of MAPK pathway upon YAP's depletion. The impairment of cell growth and survival due to high levels of TAZ expression was shown previously (Kanai et al., 2000). Similarly, the important role of TAZ, alongside YAP, was also

highlighted by Gruber et al in 2016. In this study, the co-deletion of YAP and TAZ demonstrated failure in ADM formation induced by oncogenic *Kras$^{G12D}$ in vitro* and by caerulin induced pancreatitis *in vivo* (Gruber et al., 2016). This observation is fascinating since YAP alone was previously shown to be dispensable in ADM formation (Zhang et al., 2014). Although the study by Gruber et al. showed reduced ability of ADM formation by *Kras$^{G12D}$* in the acinar cells when only YAP was deleted, the complete failure in ADM formation was observed only in double mutant acinar cells for *Yap/Taz*. Similarly, PanIN lesion formation was arrested when YAP and TAZ were co-deleted in mice with pancreas-specific *Kras$^{G12D}$* mutation (Gruber et al., 2016). Interestingly, depletion of TAZ in hepatocellular carcinoma – that predominantly expresses TAZ compared to YAP – enabled compensatory YAP expression to incur (Hayashi et al., 2015). Despite the importance of the paralog TAZ coming into play, YAP's potential role as an important marker to stratify patients with early precursor lesions that are at high-risk of developing into invasive adenocarcinoma is still relevant and needs further investigation.

The Hippo pathway is an important regulator of pancreas development which occurs through inactivation of YAP (George et al., 2012). In pancreatic cancer, the Hippo pathway is inactivated and plays an important role in the tumourigenic process (Ansari et al., 2019). Similarly, loss of NF2, which is an upstream activator of the Hippo pathway, has also been associated with the progression and development of PDAC (Quan et al., 2015). In order to investigate if NF2-mediated Hippo pathway was involved in the regulation of YAP activity in our study, I carried out transient knockdown of the protein in pancreatic cancer cells. From the preliminary results presented, NF2

did not appear to contribute in the regulation of YAP activation, though there was an increase in ERK1/2 activation (Figure 3.8). This indicates that the effect of NF2 inactivation in MAPK activity could possibly occur through a different mechanism. One possible explanation is due to the activation of Wnt/β-catenin signalling, which is attenuated by NF2, during pancreatic tumour growth (Quan et al., 2015). As a result, Wnt signalling, which has previously been identified as a positive regulator of the MAPK pathway in pancreatic cancer cells (Zhang et al., 2013), could be a potential contributor to the increase in pERK levels in our preliminary observations.

### 6.2.2 Future research

Given the possible role of TAZ in compensating YAP's depletion, it would also be useful to investigate TAZ's expression level in early precursor lesions in KC mice in future. Similarly, investigating TAZ's association with pERK in these PanIN lesions would be useful in understanding the collaborative mechanism through which YAP and TAZ paralogs would contribute in PDAC development. Besides, the role of TAZ can be investigated using *in vitro* settings. TAZ expression can be depleted in stably YAP knocked down cancer cells and the downstream effects on MAPK can be explored for any possible compensation by TAZ.

It would be also be beneficial to analyse the survival curve in PDAC patients with differing levels of YAP and TAZ expression using cohort from publicly available database as well as RNA-Seq data from the PDAC cohort available in our laboratory. This would provide a clinical insight into the role of YAP and TAZ in maintaining the disease malignancy of PDAC.

Taken together, our data in this chapter presented YAP's contribution in regulating ERK1/2 activation in pancreatic cancer cells *in vitro* and the association of YAP with that of pERK in the nuclei of PanIN lesions *in vivo*. It would be interesting to investigate the mechanisms by which YAP increases phosphorylation of ERK1/2 and hence regulates MAPK signalling pathway. One possibility is through YAP acting as a transcriptional co-activator to induce the expression of KRAS and amphiregulin (AREG) (Figure 6.1). AREG, which is a ligand for EGF receptor and a known transcriptional target of YAP, has been previously identified as an important prognostic biomarker in PDAC patients (Wang et al., 2016; Yotsumoto et al., 2010; Zhang et al., 2009). In future, the potential transcriptional activation of AREG, due to YAP regulated by the upstream Hippo-pathway, and subsequent augmentation of the MAPK pathway could be explored in our study. Similarly, activation of KRAS could also be investigated in our system by monitoring GTP-KRAS levels during YAP deletion.

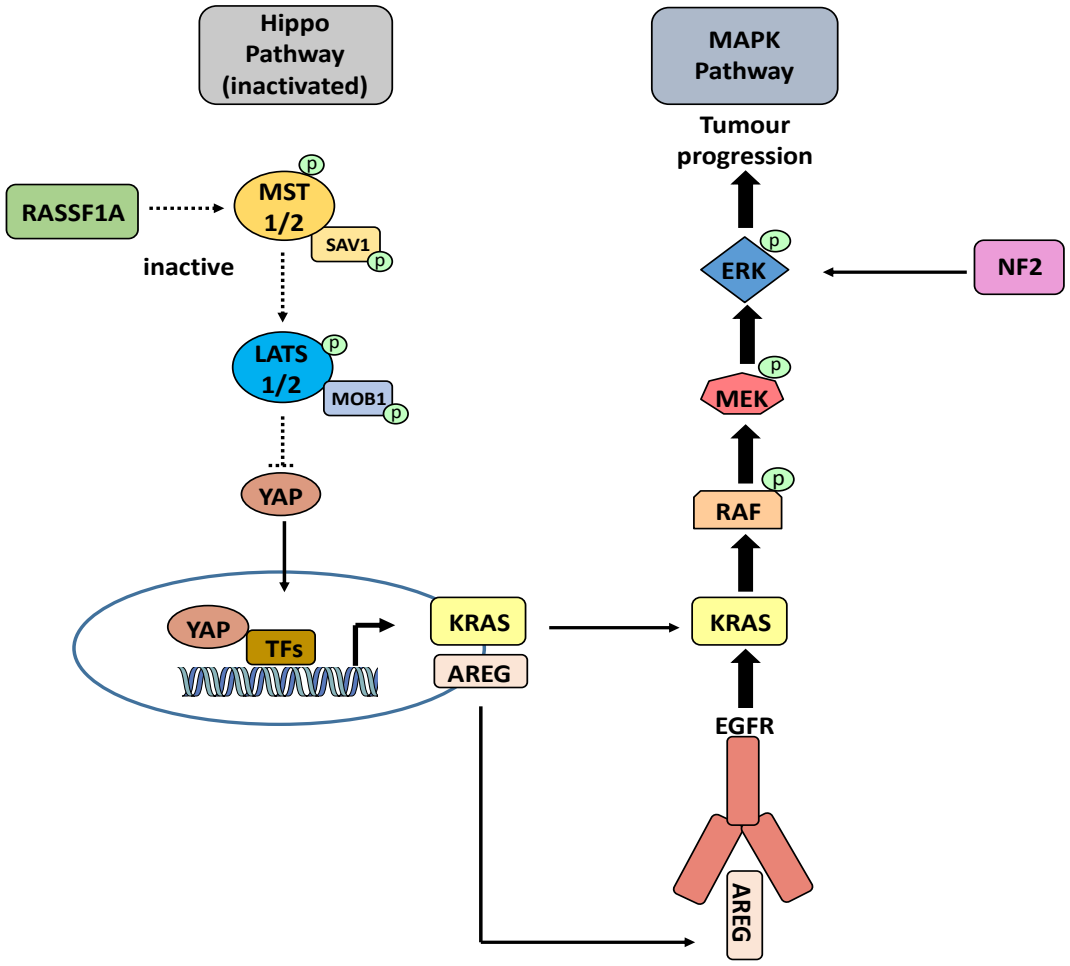


**Figure 6.1: Proposed mechanism by which YAP activation leads to increased MAPK signalling in PDAC.** The inactivation of RASSF1A which is an upstream regulator of the Hippo signalling pathway causes the pathway to turn off. As a result, negative regulation of YAP activation due to phosphorylation by LATS1/2 is abrogated. The unphosphorylated YAP translocate into the nucleus and, in complex with TEAD or other transcription factors (TFs), potentially leads to increased transcription of KRAS genes. Besides, amphiregulin (AREG), a known transcriptional target of YAP, is also a possible candidate in PDAC. Consequently, the increased expression of AREG and KRAS could drive MAPK pathway by increasing output signalling of pERK and, in turn, could enable progression of tumour. Similarly, NF2, which is a known upstream regulator of the Hippo pathway, was observed to influence pERK levels, independent of Hippo-mediated activation in PDAC cell lines in our study.

## 6.3 Final Discussion of Chapter 4

### 6.3.1 The association of nuclear YAP expression with cell of origin of precursor lesions and PDAC

Due to a display of heterogeneous nuclear YAP expression in the precursor lesions of KC mice in the previous chapter, I speculated whether this could be associated with the cell of origin. Indeed, analysis of the human PDAC samples from the cohort in our laboratory presented negative staining for YAP in some of the tissue samples (Appendix, Figure 7.7). Here, I explored the cell of origin of PanIN lesions in KC mice and PDAC in human cohorts and attempted to link this with the expression level of YAP. For this, I applied Alcian blue, that stains for mucins, in the pancreatic tissue from KC mice and human cohorts. Since PanIN lesions are known to abundantly express mucins, Alcian blue has been commonly used in previous studies to mark for PanIN lesions (Jonckheere et al., 2010). Interestingly, previous studies using a cell type specific mouse model reported that the PanIN lesions and PDAC formed in acinar-derived model were positive for Alcian blue. On the other hand, Alcian blue negative PanIN lesions, that were more hyperplastic in nature, along with PDAC were derived from the ducts (Ferreira et al., 2017; Lee et al., 2018). In our study, there was an inconsistent pattern of Alcian blue staining among the PanIN lesions that had been identified based on their morphological and cytological features (Figure 4.1). Given the findings in previous studies, I classified the Alcian blue negative precursor lesions to be derived from the ductal epithelium whereas the Alcian blue positive lesions to be derived from the acini which would then undergo metaplasia to gain ductal phenotype before transforming into neoplastic lesions. Intriguingly, our data demonstrated an inverse correlation

between nuclear YAP expression and Alcian Blue staining, both in the precursor lesions of KC mice (Figure 4.8) and PDAC of human samples (Figure 4.9). Similarly, previous studies using the cell-type specific mouse model revealed ductal-derived PDAC to develop faster than the acinar-derived ones (Ferreira et al., 2017; Lee et al., 2018). These findings are indeed complemented by our study in which we observed an association of negative Alcian blue staining with high nuclear YAP expression in the precursor lesions. Similarly, the percentage of positive Alcian blue staining in PDAC samples were quantified. Based on this, the patient samples in our PDAC cohort were stratified into high Alcian blue and low Alcian blue. Intriguingly, the patient group with low Alcian blue presented higher nuclear YAP expression and displayed a trend of lower overall survival (Figure 4.5). Furthermore, the analysis of overall survival of PDAC patients based on YAP expression presented the patient-group with elevated nuclear YAP to have the least favourable survival outcome (Appendix, Figure 7.7). This postulates nuclear YAP as a marker for aggressive PDAC phenotype. Overall, the presence of YAP in the nuclei of precursor lesions which are negative for Alcian blue – suggesting they are derived from the ducts – elucidates the possible role of YAP in facilitating faster progression of duct-derived lesions into invasive PDAC.

### 6.3.2 Future research

Our conclusion largely depended on previous observations that showcased a difference in Alcian blue staining in precursor lesions and PDAC derived from different cell types (Ferreira et al., 2017; Lee et al., 2018). Based on these, I compared the origin of both of these precursor lesions and PDAC with nuclear YAP expression. The major caveat in our study is the use of KC mouse model instead of cell-type specific mouse models. Using mouse models that express mutated *Kras* specifically in acinar or ductal cells,

would present a robust platform to explore YAP's potential in inducing precursor lesions to aggressive tumour phenotype. Concomitant with *Kras* mutation, YAP expression can be deleted in these cell-type specific models to further examine its role in enhancing the PDAC's invasiveness. Besides these, the role of acinar and ductal cells, under genetic and epigenetic settings along with environmental insults, could also be considered. Recent works have highlighted the importance of focusing on genetic status while investigating the role of cell of origin in PDAC development and phenotype. Alongside *Kras* mutation, the inactivation of other genes, including *Trp53*, *Fbw7*, *Brg1* and *Arid1a*, in different cell types have also shown to contribute in PDAC formation. PDAC developed through these genetic alterations in different cell types also presented varying routes of precursor lesions development –either through PanINs or IPMNs depending on the cell of origin. As a result, differing latency and survival rates were displayed in these mouse models (Kimura et al., 2018; Tsuda et al., 2018; von Figura et al., 2014; Xu et al., 2019)

Cell-type specific mouse models, nonetheless, have their own drawbacks. It is mostly constrained due to imbalance in the abundance ratio of acinar in comparison to ductal cells in pancreas. This raises concerns about bias in experiments with cell type specific alterations of oncogenes and tumour suppressor genes (Ziv et al., 2013) . The KC mouse model might be useful in this context as it expresses *Kras* mutation in all pancreatic lineages, reducing cell type specific bias (Hingorani et al., 2003).

The cell type specific mouse model by Ferreira et al. described Anterior gradient protein 2 (AGR2) as a potential marker for duct derived PDAC. Importantly, the study showed heterogeneous expression of AGR2, with multifocal regions either strongly positive or negative for the protein, within the PDAC region from KPC mouse model. Additionally,

the heterogeneity in AGR2 expression also persisted in tissue microarray from human PDAC (Ferreira et al., 2017). Our KC model corroborates this observation by displaying heterogeneous YAP expressing multifocal lesions in the pancreata. Hence, it would be interesting to explore for any link between AGR2 and nuclear YAP expression in the future.

The application of Alcian blue staining in this chapter is useful due to its quick, cheap and easy protocol. This makes the technique quite convenient to be used by pathologists for diagnostic purposes. The method could be useful in predicting prognosis for patients at risk of developing PDAC. Alcian blue technique, however, is not robust enough as it stains all the mucins present, including the ones in the stroma. A better method would include immunohistochemical staining of mucin markers that are specifically upregulated in PanIN lesions such as MUC5AC. Furthermore, a more complex model would be essential to further substantiate our findings, which we investigate in the final results chapter.

## 6.4 Final Discussion of Chapter 5

### 6.4.1 3D organoids as a model to understand YAP's role in PDAC from different cell of origin

In view of the need for a better model to further investigate the relation of cell of origin with YAP activation, I attempted to use a 3D organoid system in this study. We were able to establish 3D organoid culture isolated from C57Bl/6 mice with either Wild type (WT) or *Kras*-mutated (KC) genetic backgrounds in our laboratory (Figure 5.4). Besides, I was able to stably deplete the expression level of YAP in the KC organoids (Figure 5.11). The establishment of this 3D culture would be beneficial to study the

physiological effects *in vitro* using a more complex system. Furthermore, these organoids can also be transplanted into mouse pancreas. Although the orthotopic transplantation of WT and KC organoids into mouse pancreas have yet to be established successfully, orthotopic injection of pancreatic cancer cells grown in 2D culture has already been optimised in our laboratory (Appendix, Figure 7.10.A-B). This orthotopic transplantation of 2D cancer cells demonstrated continuous growth of tumour volume in the pancreatic region due to the injection (Appendix, Figure 7.10.C). Previously, Boj et al. had demonstrated that orthotopic injection of neoplastic organoids from KC mouse pancreas form PanIN lesions. These PanIN lesions ultimately progressed into invasive adenocarcinoma (Boj et al., 2015). Given this evident formation of PanIN lesions in an orthotopic model and the already standardised orthotopic injection technique in our laboratory, our future work would involve further optimisation of the injection of organoids — particularly by ensuring that the single cells dissociated from the organoids are viable and also by increasing the number of cells injected. Following the establishment of orthotopic injection of organoids, we can subsequently include YAP-depleted organoids in the orthotopic transplantation and monitor any change in the formation of PanIN lesions in the host pancreas. The organoids established in our study are isolated from ductal cells which proliferate continuously in the 3D culture. This could potentially occur due to the progenitors residing in the ductal compartment (Carpino et al., 2016; Yamaguchi et al., 2012). As a consequence, manipulating YAP in these organoids that are derived from ductal cells can present as a suitable model to study the role of YAP in relation to cell of origin.

### 6.4.2 Future research

The use of organoids provides a more efficient platform to study the disease progression and test for personalised medicine, in comparison to primary 2D cell lines from tumours, which often fail during isolation, or even more sophisticated patient-derived xenograft, which normally take 6-12 months to establish with sufficient maturation. Most PDAC patients, however, do not survive until this time period. Despite the organoid providing promising avenues to better understand PDAC progression and as a platform to test drug treatment, it is yet to fully incorporate stromal and immune components (Hohwieler et al., 2019). Despite this, a human derived organoid model would be useful as they better represent human disease state. Indeed, the morphology of ductal structures following the orthotopic transplantation of human organoids more closely resembled human PanINs (Boj et al., 2015). Hence, using patient-derived organoids in future would be more informative to fully understand the mechanism by which PanIN lesion progress to PDAC in future. Given that only a very low percentage of PDAC patients are eligible to undergo surgical resection, biopsies from PDAC patients can be utilised to grow as organoids. With the organoids closely resembling the molecular and phenotypic properties of tissue of origin (Boj et al., 2016), the 3D culture derived from patients' biopsies would enable longitudinal study of the course of disease from each patient. Moreover, the status of YAP expression can be investigated in each of the patient's derived organoids to get a better understanding of the risk of the disease developing into the more advanced stage.

### 6.4.3 The generation of GEMMs to study upstream regulator of the Hippo pathway in PDAC

The preliminary study in Chapter 3 demonstrated that the effect of NF2 on MAPK activity in pancreatic cancer cells was not mediated by Hippo pathway regulated YAP activation. To analyse the application of GEMM in understanding the involvement of Hippo pathway in PDAC progression, I explored the role of a tumour suppressor gene, RASSF1A, which is a known upstream regulator of the Hippo pathway (Guo et al., 2007; Matallanas et al., 2007; Oh et al., 2006; Pefani et al., 2016). In our study, localisation of both RASSF1A and phosphorylated YAP (pYAP) was observed in the apical regions of the corresponding PanIN lesions in KC mice (Figure 5.1.A). This was corroborated by our quantitative analysis which revealed positive correlation between the expression level of the proteins in the apical membrane (5.1.B). RASSF1A inactivation is frequently found in many human cancers including PDAC. This loss of expression is commonly attributed to hypermethylation of CpG islands within the promoter of *RASSF1A* (Amato et al., 2016; Dammann et al., 2003). Previous studies using a *Rassf1a* knockout mouse model demonstrated formation of lung adenomas, lymphomas and breast adenocarcinomas (Tommasi et al., 2005). However, the absence of RASSF1A appeared to be compensated by RASSF5 in this knockout model (Papaspyropoulos et al., 2018; Zhang et al., 2016). I, therefore, utilised rs2073498 SNP (*RASSF1 c.397G>T*) mouse model generated by Dr Ben Davies. This genetically engineered mouse model was generated by crossbreeding heterozygous *Rassf1* A133S SNP mice (R1-Het) with mice harbouring *Kras*-mutation in the pancreas (KC mice). The resulting transgenic strain, $Kras^{LSL.G12D/+}$*; Pdx-Cre;* $RASSF1^{SNP+/-}$ (KCR1-Het), presented a trend towards lower overall

survival, albeit non-significant, in comparison to KC or R1-Het mice alone (Figure 5.2). While this data seems promising, examination of pancreatic tissues from KCR1-Het mice that were culled due to ill-health did not present any distinct phenotype than that from KC mice. The pancreatic tissue presented a full spectrum of PanIN lesions that were reminiscent of age-matched KC mice. A better model is therefore needed to fully understand the impact of the loss of RASSF1A in *Kras*-mediated PDAC progression. This could potentially involve generating a homozygous *Rassf1* SNP allele in *Kras* mutated background – $Kras^{LSL.G12D/+}$; *Pdx-Cre*; $RASSF1^{SNP/SNP}$ (KCR1-Hom).

## 6.5 Final Conclusion

We see heterogeneity in YAP expression in the nuclei of PanIN lesions. YAP, as an oncogene, is associated with the MAPK pathway in these lesions of *Kras*-mutated mice and pancreatic cancer cells. Given the critical role of pERK– which is an output signal of MAPK – in cell proliferation, YAP's contribution to the progression of the PanIN lesions into malignant tumour could be deduced. While the role of YAP seems essential in PDAC progression, some of the lesions were devoid of nuclear YAP. This allows us to predict that the PanIN lesions with low nuclear YAP expression were associated with low risk behavior whereas the ones with high nuclear YAP expression presented high risk of aggressively developing into invasive adenocarcinoma. Similarly, we associate this heterogenous expression of nuclear YAP in the precursor lesions with their cell-of-origin. High nuclear YAP expression correlated with low Alcian blue staining in both pre-malignant lesions and malignant tumours. This highlights possible contribution of active YAP in driving ductal-derived cell to invasive cancer (Figure 6.2). Furthermore, YAP is also presented as a potential marker for PDAC originated from a distinct cell

type, i.e. ductal epithelium. This finding is useful as it signifies the importance of analysing YAP expression in patient biopsies and serum, which in turn would allow to predict the aggressive nature of the disease in PDAC patients. Finally, our establishment of a more complex 3D organoid system demonstrated a promising, despite challenging, technique which would aid in our understanding of YAP's role during early diagnosis. These organoids closely resemble the tissue from which they were isolated, both genetically and phenotypically. The orthotopic injection of these organoids into mouse pancreas still needs to be refined in our study. Nevertheless, the model presents a platform to elucidate the role of active YAP in facilitating PDAC progression in terms of cell of origin. This can further be associated with the intertumoural heterogeneity of primary PDAC tumour. Accordingly, PDAC patients can be stratified into different groups based on their cell of origin. This, ultimately, can be beneficial in providing better prognosis and effective therapy tailored to each patient group.

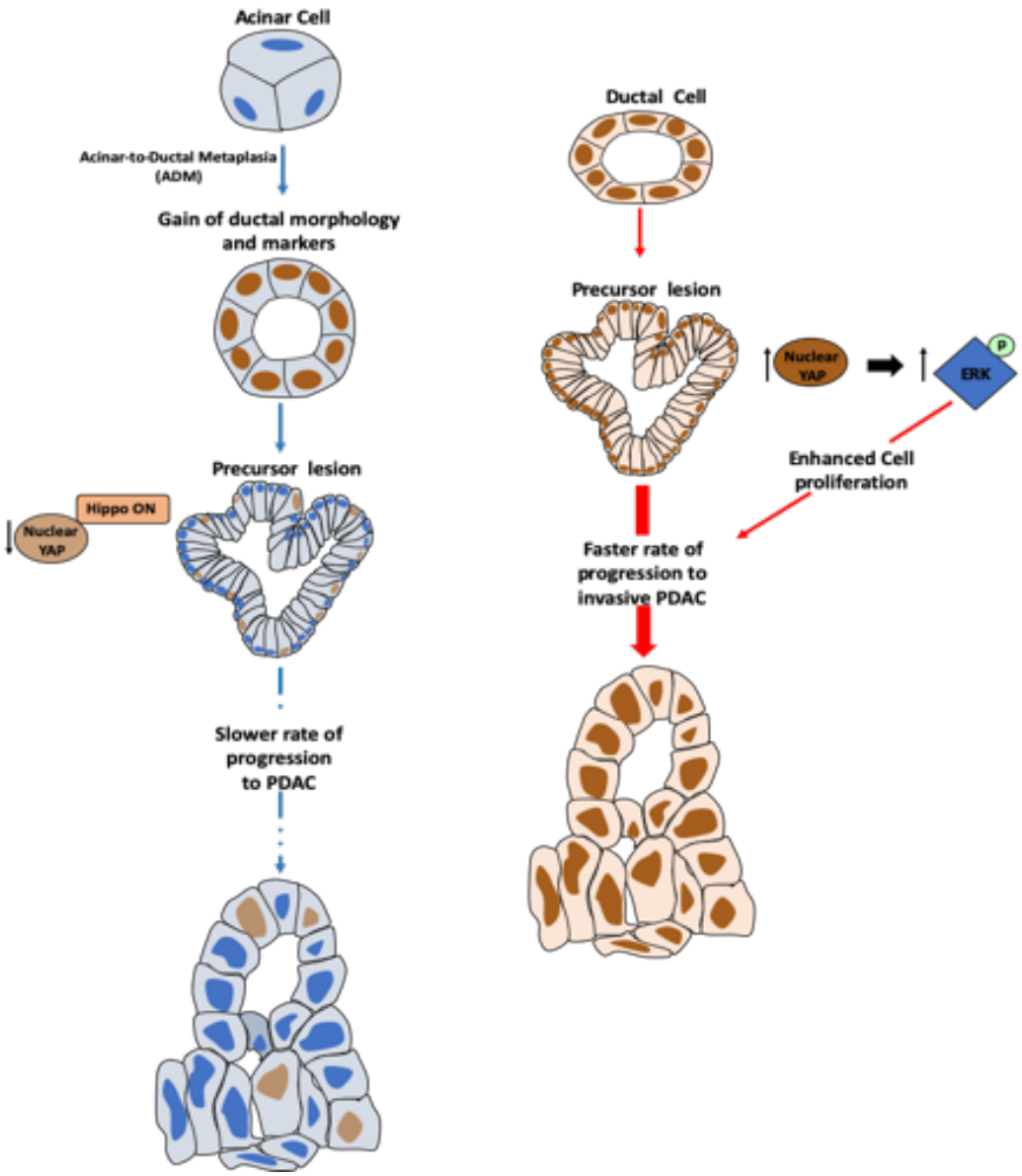


**Figure 6.2. Working model illustrating role of YAP in the progression of neoplastic lesions to PDAC in relation to cell of origin based on the data in this thesis.** Normal ducts display relatively high level of nuclear YAP in the pancreas. When the ductal epithelium transits into precursor lesions i.e. PanIN lesions during the multi-step process of tumorigenesis, YAP is either retained or lost from the nucleus. This heterogeneity of nuclear YAP presents two different types of PanIN lesions and could vary due to their differing cell of origin. PanIN lesions with low nuclear YAP appears to originate from acinar cells that undergo metaplastic process and gain the phenotype of ductal cells before developing into PanIN lesions. The decrease in nuclear YAP could potentially occur due to the activation of upstream Hippo pathway. On the other hand, the PanIN lesions with high expression of nuclear YAP appears to be derived from the ducts. These lesions are more hyperplastic in nature and progress faster to invasive ductal adenocarcinoma. This could be attributed to enhanced pERK signals due to high levels of YAP transcriptionally activating components of MAPK signalling pathway. Enhanced ERK1/2 activation could potentially contribute to G1-to-S transition, hence increasing cell proliferation. As a result, epithelial cells in the ductal-derived neoplastic lesions proliferate quickly to form more aggressive tumour in comparison to the acinar-derived ones.

# Appendix A Appendix

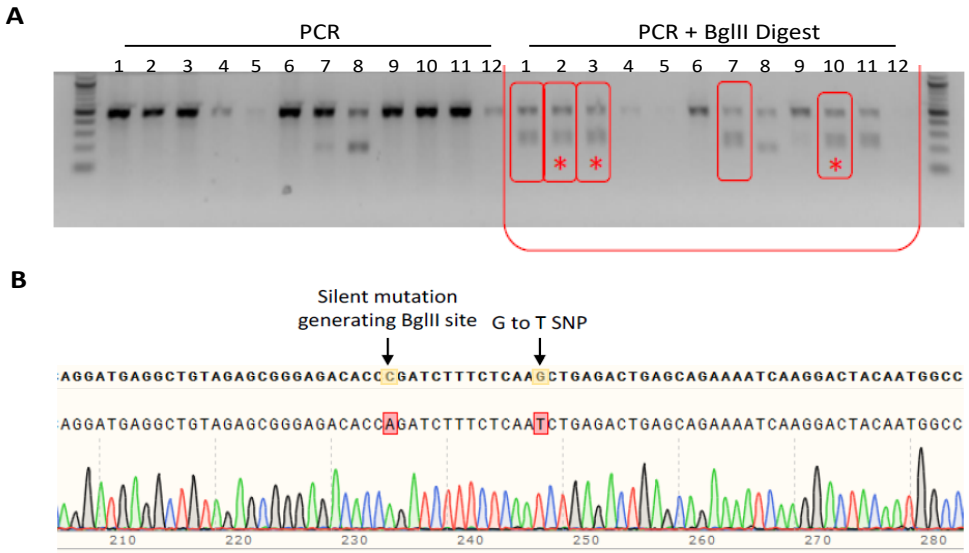


**Figure 7.1: Generation of the rs2073498 SNP Mouse. A**) Screening of ES cells following CRISPR/Cas9 knock-in. A silent mutation that generated a BglII site was introduced along with the SNP. PCR amplification of the SNP region (left) and BglII digested PCR products (right) are shown. Putative knock-in clones are shown in red. Starred samples were taken forward for sequencing. **B**) Sequencing read of homozygous knock-in clone. Mice generated and figures provided by Dr Ben Davies.

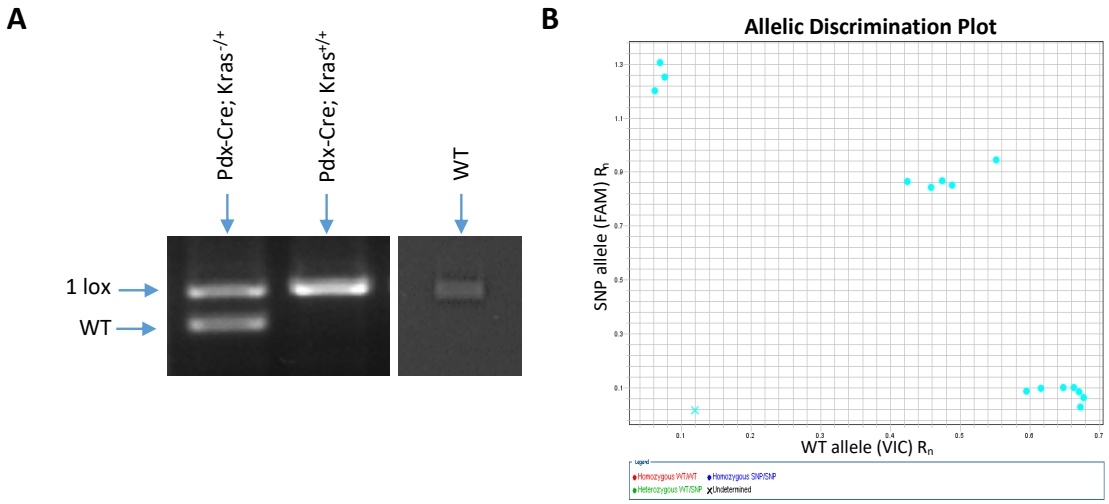


**Figure 7.2: Genotyping for *Kras* mutation and *Rassf1* SNP allele.** (A) DNA extracted from mouse ear notch was analysed through PCR for mutated *Kras* alleles. PCR distinguishes presence of recombined allele from WT allele. (B) Extracted DNA was analysed for *Rassf1* SNP allele using TaqMan assay,with VIC® probe detecting for Wild-type allele and 6FAM™ for the *Rassf1* SNP allele. Allelic Discrimination Plot shown in the figure displays variation in clustering due to the genotype of the target allele.

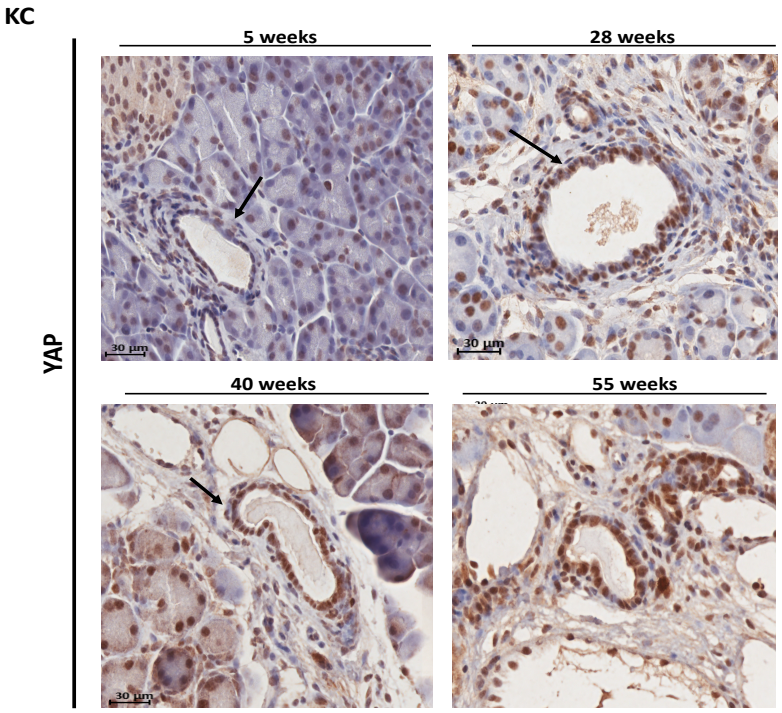


**Figure 7.3: Active YAP in normal ducts with increasing age of mice genetically modified to recapitulate early stages of PDAC.** Representative images of IHC staining for YAP in pancreatic tissue sections from *Kras*$^{LSL.G12D/+}$*; Pdx-1-Cre* mice of indicated ages. Arrows: normal ducts. Scale bars = 30 µm.

| n=1 | | n=2 | | n=3 | | n=4 | | n=5 | |
|---|---|---|---|---|---|---|---|---|---|
| Region label | % of Alcian blue positive region | Region label | % of Alcian blue positive region | Region label | % of Alcian blue positive region | Region label | % of Alcian blue positive region | Region label | % of Alcian blue positive region |
| 1 | 10 | 2 | 20 | 8 | 5 | 3 | 2 | 4 | 10 |
| 5 | 2 | 3 | 2 | 10 | 5 | 6 | 10 | 11 | 2 |
| 8 | 10 | 7 | 20 | 17 | 10 | 10 | 20 | 12 | 5 |
| 15 | 40 | 9 | 5 | 20 | 10 | 13 | 10 | 14 | 2 |
| 16 | 5 | 11 | 20 | 22 | 5 | 17 | 20 | 15 | 15 |
| 21 | 50 | 27 | 40 | 24 | 10 | 19 | 40 | 23 | 2 |
| 23 | 0 | 28 | 20 | 31 | 40 | 21 | 60 | 25 | 15 |
| 27 | 30 | 29 | 40 | 32 | 30 | 24 | 15 | 27 | 20 |
| 28 | 20 | 30 | 15 | 33 | 2 | 28 | 20 | 32 | 10 |
| 30 | 10 | 32 | 20 | 36 | 2 | 34 | 10 | 33 | 3 |
| Average | 17.7 | Average | 20.2 | Average | 11.9 | Average | 20.7 | Average | 8.4 |

**Total Average of percentage of Alcian blue positive region from five randomisations = 15.78**

**Standard deviation = 5.4**

**Figure 7.4: Repeat of visually quantified Alcian blue staining in a human PDAC sample.** Each table highlights the percentage of Alcian blue positive region obtained through the eyeballing method for ten randomly selected square boxes. The process of randomisation and visual assessment was carried out five times for the human PDAC sample as represented by the "n" number for the tables. Standard deviation from the five repeats were calculated, SD = 5.4 for the total average of 15.78% for Alcian blue positive region.

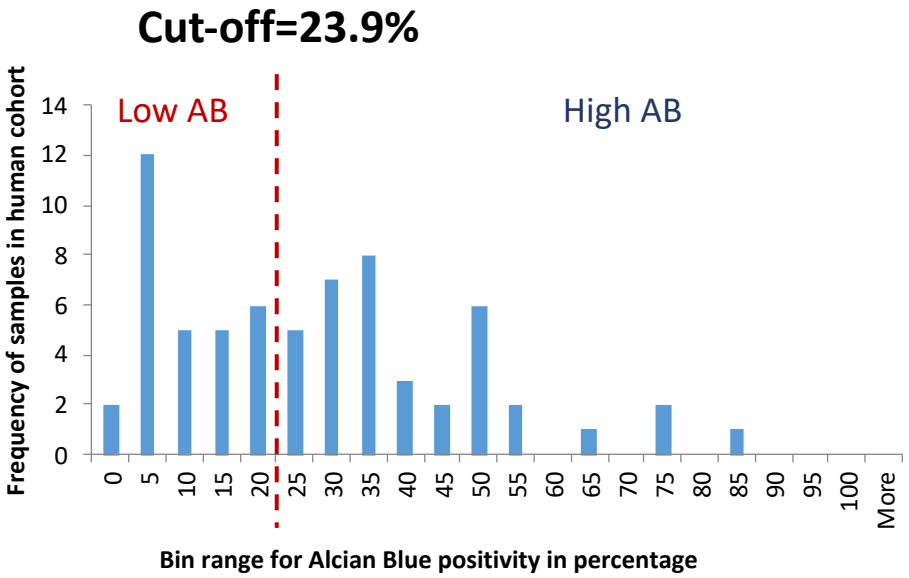


**Figure 7.5: Determination of cut-off point to stratify PDAC patients into high and low Alcian blue.** Human PDAC samples were distributed by binning the percentage of Alcian blue positivity into a continuous range of interval of 5. The cut-off value at 40% was determined based on the median value of 23.9%.

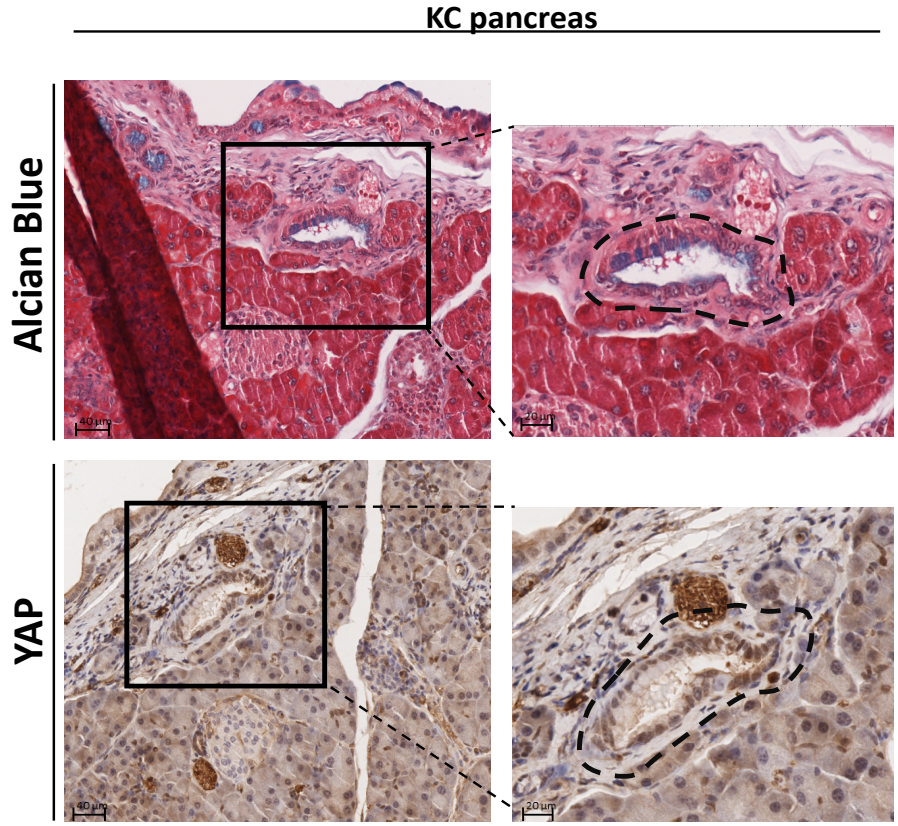


**Figure 7.6: A precursor lesion in KC mice demonstrated positive correlation between the staining of Alcian blue and nuclear YAP.** Histological analysis of *Kras*$^{LSL.G12D/+}$*;Pdx-1-Cre* (KC) mouse pancreas presented a rare occurrence of precursor lesion displaying positive correlation between Alcian blue and nuclear YAP staining. Nuclear expression of YAP was quantified based on the intensity. Scale bars: 1$^{st}$ column = 40 µm, 2$^{nd}$ column = 20 µm.

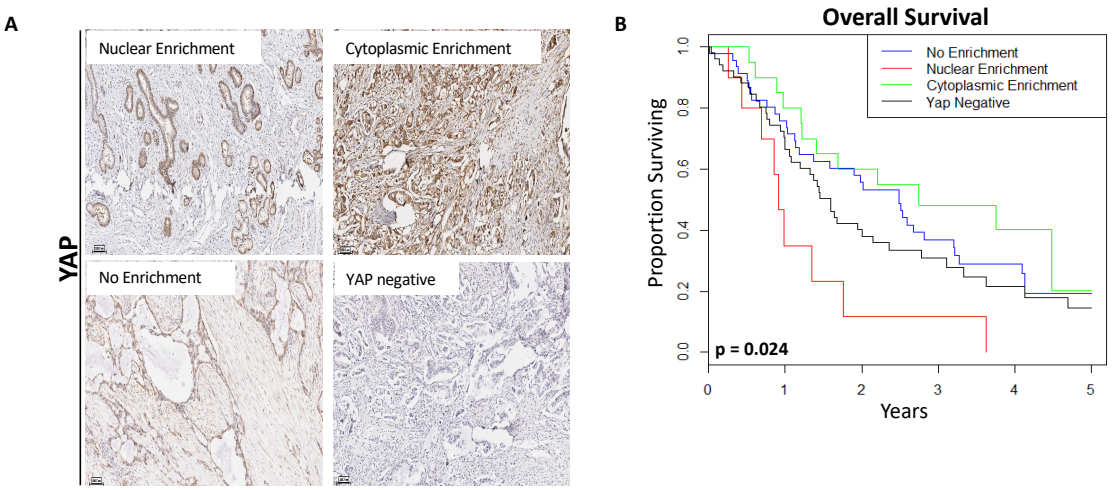


**Figure 7.7: Nuclear expression of YAP associates with aggressive PDAC phenotype.** (A) Representative IHC stain in pancreatic tissue sections from human PDAC cohort. Differential expression pattern of YAP is detected in tissue samples, including either nuclear or cytoplasmic enrichment, no enrichment and negative expression of YAP. (B) Kaplan-Meier survival curve of overall survival among 143 PDAC patients. The five-year survival rate observed among PDAC samples with enrichment for YAP in nucleus or cytoplasm, no YAP enrichment or negative expression for YAP. Figures for YAP staining and Kaplan-Meier survival curve, generated using R survival package, were provided by Michael Eyres. YAP scoring was done by Prof Robert Goldin.

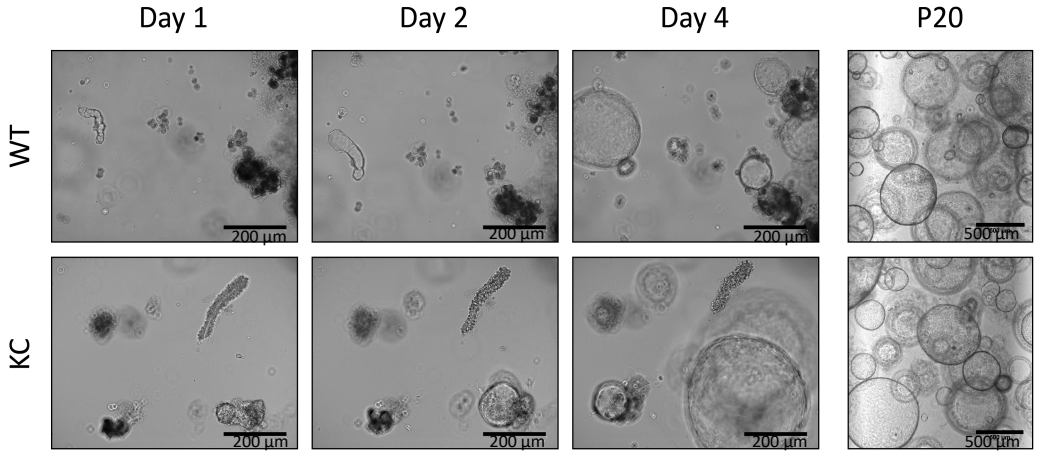


**Figure 7.8: Establishment of pancreatic organoids.** Representative images showing growth of organoids established from C57Bl/6 mice with two genetic backgrounds, Wild type (WT) mice and *Kras*$^{LSL.G12D/+}$*;Pdx-Cre* (KC) mice. Scale bar = 200µm. Representative images of WT and KC organoids after 20 passages (4$^{th}$ column). Scale bar = 500µm. Organoid isolation was done in collaboration with Jelte van der Vaart and Fiona Bangs. Figure is adapted from Jelte van der Vaart's Master's thesis.

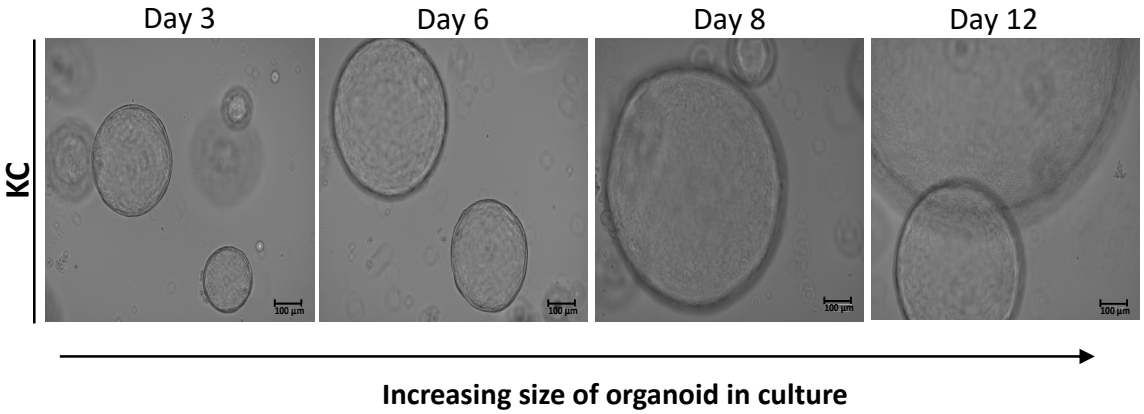


**Figure 7.9: Proliferation of ductal pancreatic organoids in culture.** Brightfield images displaying pancreatic organoids isolated from *Kras*$^{LSL.G12D/+}$*; Pdx-Cre* (KC) mouse pancreas with increasing size when grown in culture. Scale bar = 100 µm.

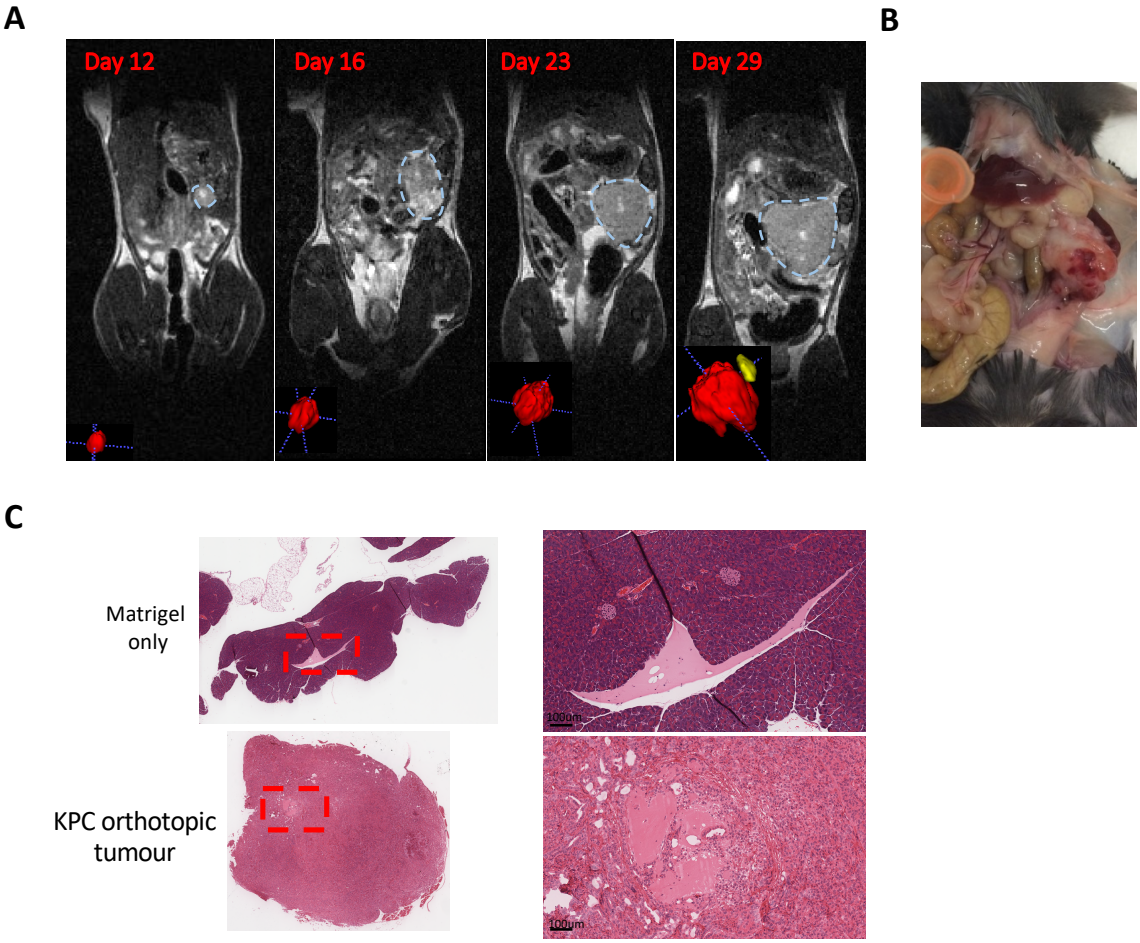


**Figure 7.10: Orthotopic injection of pancreatic cancer cells into mouse pancreas.** (A) *In vivo* MRI images of mouse abdomen orthotopically injected with KPC cell lines. Images acquired at different days show an increase in tumour volume over time. Tumour volume was manually segmented using ITK-Snap software. (B) An image of mouse pancreas harvested after cell injection displays tumour formation (arrow). (C) Histological analysis of pancreas from the orthotopic model demonstrated morphology of pancreatic tumour. H&E image of the pancreas injected with the Matrigel only displayed no tumour formation. Scale bar = 100µm. Orthotopic injection was done in collaboration with Simone Lanfredini along with the figures provided by Simone.

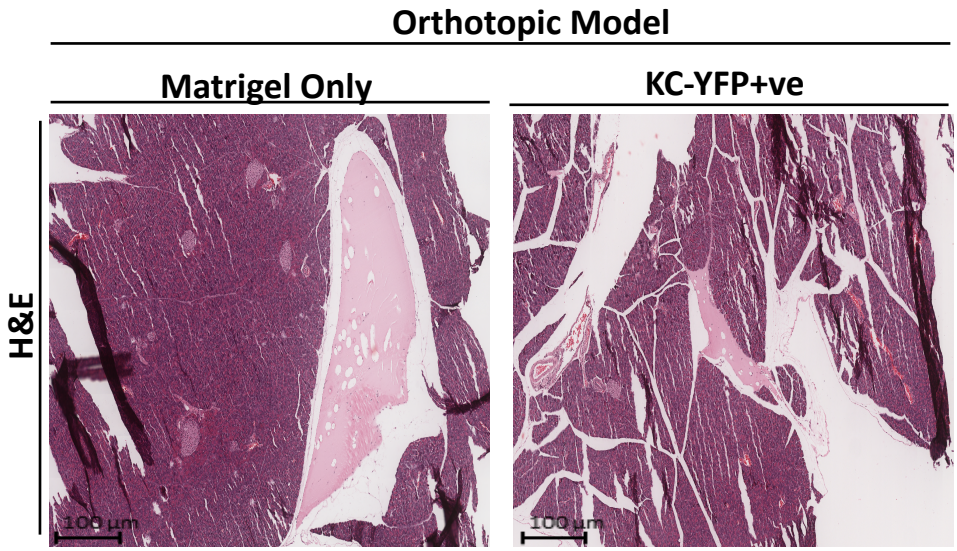


**Figure 7.11: Histological analysis of pancreas from the orthotopic model for site of injection.** Representative H&E images of pancreatic tissue from mice orthotopically injected either with organoids from *Kras*$^{LSL.G12D+/-}$*; Pdx-Cre; Rosa26 YFP* (KC-YFP+ve) mouse or with Matrigel only to demonstrate at the site of injection. Arrows indicate presence of the Matrigel injected with or without cells. Scale bar = 100µm.

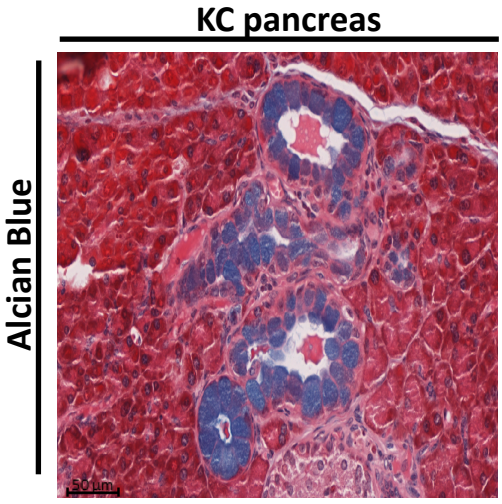


**Figure 7.12: Alcian blue staining in the PanIN lesions of KC pancreas as a reference for Alcian blue positivity.** Representative image of pancreatic tissue from *Kras*$^{LSL.G12D+/-}$*; Pdx-Cre* (KC) mouse stained with Alcian blue show positivity in the PanIN lesions. Scale bar = 50 µm.

# Appendix B Copyright Licences

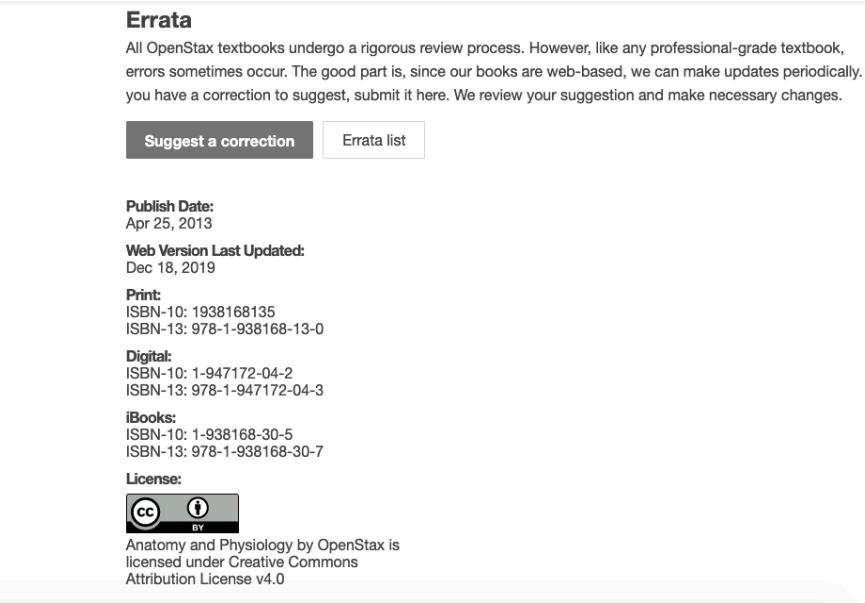

**Errata**

All OpenStax textbooks undergo a rigorous review process. However, like any professional-grade textbook, errors sometimes occur. The good part is, since our books are web-based, we can make updates periodically. If you have a correction to suggest, submit it here. We review your suggestion and make necessary changes.

Suggest a correction | Errata list

**Publish Date:**
Apr 25, 2013

**Web Version Last Updated:**
Dec 18, 2019

**Print:**
ISBN-10: 1938168135
ISBN-13: 978-1-938168-13-0

**Digital:**
ISBN-10: 1-947172-04-2
ISBN-13: 978-1-947172-04-3

**iBooks:**
ISBN-10: 1-938168-30-5
ISBN-13: 978-1-938168-30-7

**License:**

Anatomy and Physiology by OpenStax is licensed under Creative Commons Attribution License v4.0

Figure B.1: Copyright notice: Anatomy and Physiology by Open Stax.

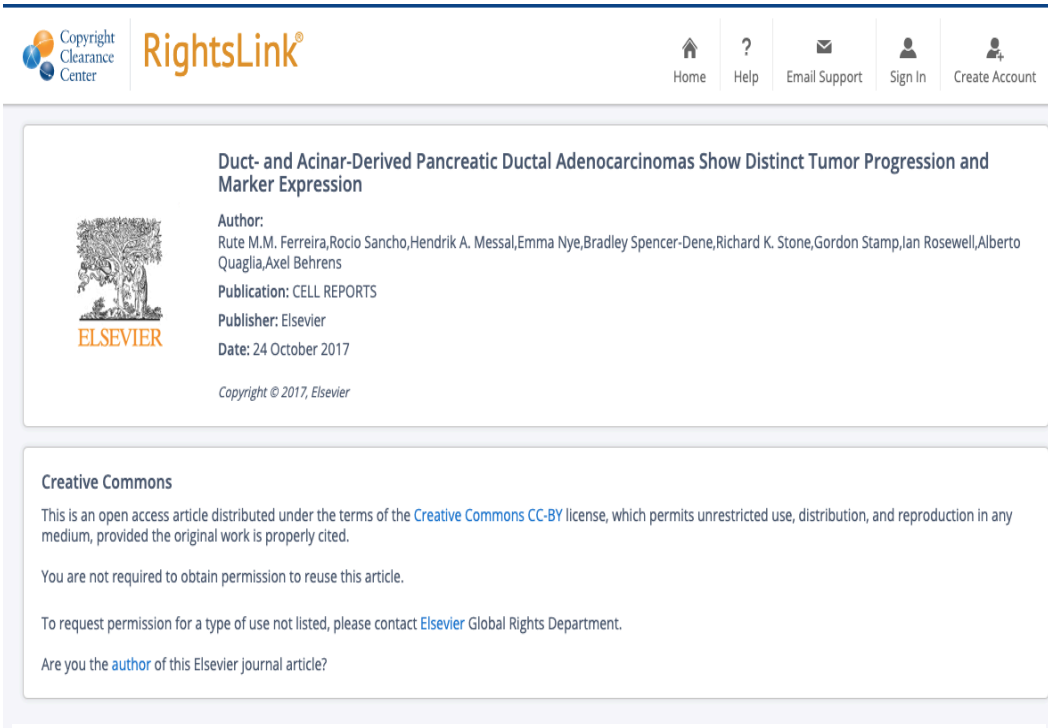

Copyright Clearance Center RightsLink®

Home | Help | Email Support | Sign In | Create Account

**Duct- and Acinar-Derived Pancreatic Ductal Adenocarcinomas Show Distinct Tumor Progression and Marker Expression**

**Author:**
Rute M.M. Ferreira,Rocio Sancho,Hendrik A. Messal,Emma Nye,Bradley Spencer-Dene,Richard K. Stone,Gordon Stamp,Ian Rosewell,Alberto Quaglia,Axel Behrens

**Publication:** CELL REPORTS

**Publisher:** Elsevier

**Date:** 24 October 2017

*Copyright © 2017, Elsevier*

**Creative Commons**

This is an open access article distributed under the terms of the Creative Commons CC-BY license, which permits unrestricted use, distribution, and reproduction in any medium, provided the original work is properly cited.

You are not required to obtain permission to reuse this article.

To request permission for a type of use not listed, please contact Elsevier Global Rights Department.

Are you the author of this Elsevier journal article?

Figure B.2: Copyright notice: Ferreira et al., 2017. Duct- and Acinar- Derived Pancreatic Ductal Adenocarcinomas Show Distinct Tumour Progression and Marker Expression.

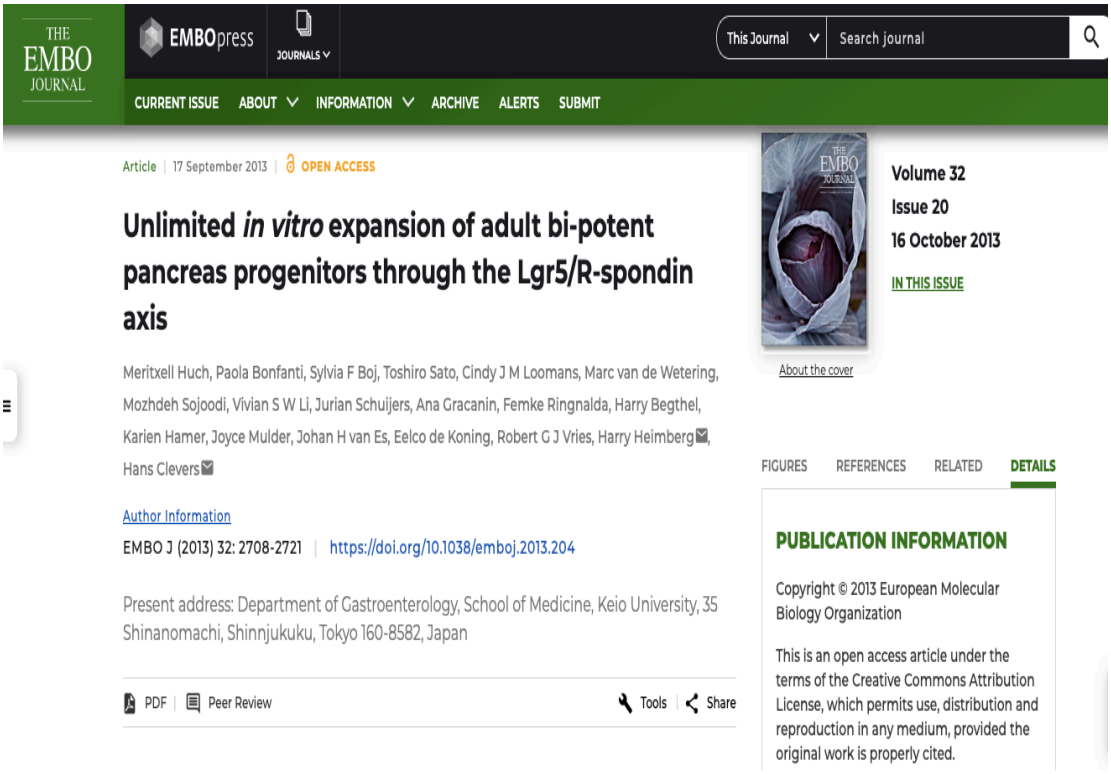


Figure B.3: Copyright notice: Huch et al., 2013. Unlimited *in vitro* expansion of adult bi-potent pancreas progenitors through the Lgr5/R-spondin axis.

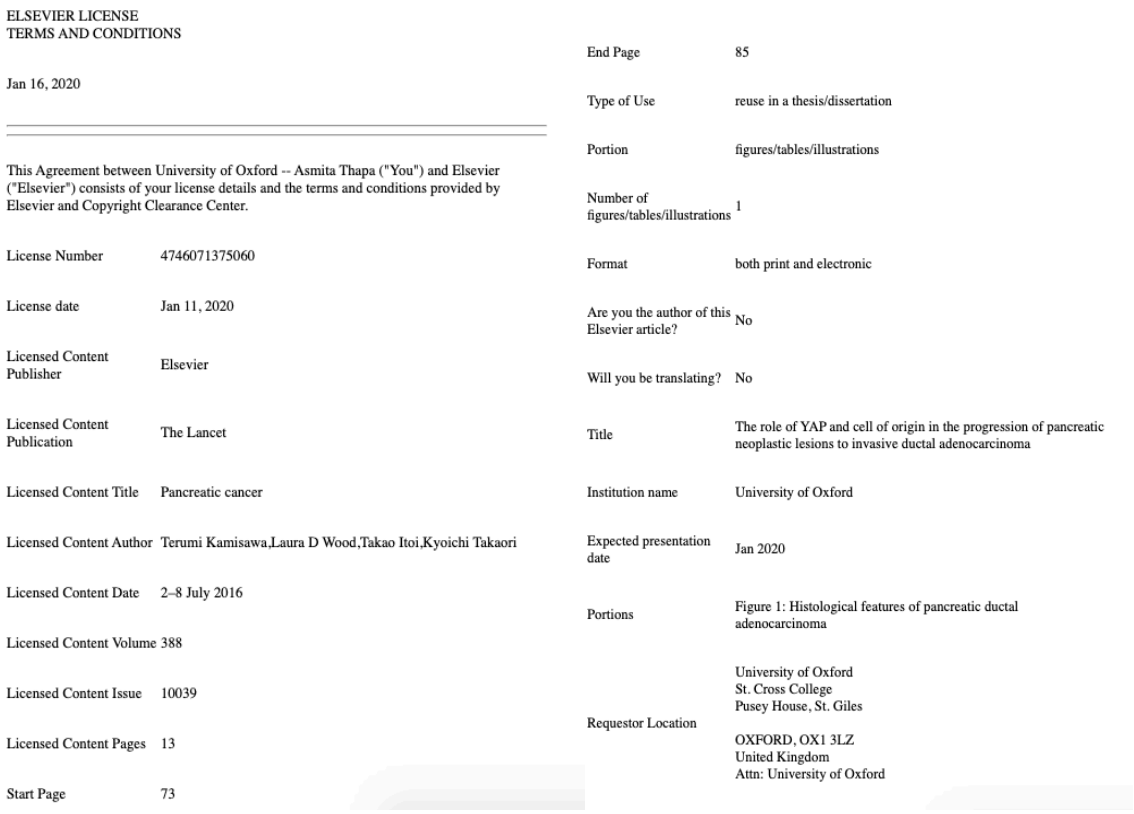

ELSEVIER LICENSE
TERMS AND CONDITIONS

Jan 16, 2020

This Agreement between University of Oxford -- Asmita Thapa ("You") and Elsevier ("Elsevier") consists of your license details and the terms and conditions provided by Elsevier and Copyright Clearance Center.

| | |
|---|---|
| License Number | 4746071375060 |
| License date | Jan 11, 2020 |
| Licensed Content Publisher | Elsevier |
| Licensed Content Publication | The Lancet |
| Licensed Content Title | Pancreatic cancer |
| Licensed Content Author | Terumi Kamisawa,Laura D Wood,Takao Itoi,Kyoichi Takaori |
| Licensed Content Date | 2–8 July 2016 |
| Licensed Content Volume | 388 |
| Licensed Content Issue | 10039 |
| Licensed Content Pages | 13 |
| Start Page | 73 |
| End Page | 85 |
| Type of Use | reuse in a thesis/dissertation |
| Portion | figures/tables/illustrations |
| Number of figures/tables/illustrations | 1 |
| Format | both print and electronic |
| Are you the author of this Elsevier article? | No |
| Will you be translating? | No |
| Title | The role of YAP and cell of origin in the progression of pancreatic neoplastic lesions to invasive ductal adenocarcinoma |
| Institution name | University of Oxford |
| Expected presentation date | Jan 2020 |
| Portions | Figure 1: Histological features of pancreatic ductal adenocarcinoma |
| Requestor Location | University of Oxford<br>St. Cross College<br>Pusey House, St. Giles<br><br>OXFORD, OX1 3LZ<br>United Kingdom<br>Attn: University of Oxford |

Figure B.4: Copyright notice: Kamisawa et al., 2016. Pancreatic Cancer

# Bibliography

Abbassi, R., and H. Algul. 2019. Palliative chemotherapy in pancreatic cancer-treatment sequences. *Transl Gastroenterol Hepatol*. 4:56.

Abkhezr, M., A.R. Keramati, S.N. Ostad, J. Davoodi, and M.H. Ghahremani. 2010. The time course of Akt and ERK activation on XIAP expression in HEK 293 cell line. *Mol Biol Rep*. 37:2037-2042.

Agalioti, T., A.D. Giannou, A.C. Krontira, N.I. Kanellakis, D. Kati, M. Vreka, M. Pepe, M. Spella, I. Lilis, D.E. Zazara, E. Nikolouli, N. Spiropoulou, A. Papadakis, K. Papadia, A. Voulgaridis, V. Harokopos, P. Stamou, S. Meiners, O. Eickelberg, L.A. Snyder, S.G. Antimisiaris, D. Kardamakis, I. Psallidas, A. Marazioti, and G.T. Stathopoulos. 2017. Mutant KRAS promotes malignant pleural effusion formation. *Nat Commun*. 8:15205.

Agathanggelou, A., S. Honorio, D.P. Macartney, A. Martinez, A. Dallol, J. Rader, P. Fullwood, A. Chauhan, R. Walker, J.A. Shaw, S. Hosoe, M.I. Lerman, J.D. Minna, E.R. Maher, and F. Latif. 2001. Methylation associated inactivation of RASSF1A from region 3p21.3 in lung, breast and ovarian tumours. *Oncogene*. 20:1509-1518.

Amato, E., S. Barbi, M. Fassan, C. Luchini, C. Vicentini, M. Brunelli, G. Malleo, A. Scarpa, and G. Malpeli. 2016. RASSF1 tumor suppressor gene in pancreatic ductal adenocarcinoma: correlation of expression, chromosomal status and epigenetic changes. *BMC Cancer*. 16:11.

American Cancer Society. 2020. Cancer Facts & Figures 2020. Atlanta: American Cancer Society.

Ansari, D., H. Ohlsson, C. Althini, M. Bauden, Q. Zhou, D. Hu, and R. Andersson. 2019. The Hippo Signaling Pathway in Pancreatic Cancer. *Anticancer Res*. 39:3317-3321.

Arias, A.E., and M. Bendayan. 1993. Differentiation of pancreatic acinar cells into duct-like cells in vitro. *Lab Invest*. 69:518-530.

Bailey, J.M., K.E. DelGiorno, and H.C. Crawford. 2014. The secret origins and surprising fates of pancreas tumors. *Carcinogenesis*. 35:1436-1440.

Bailey, J.M., B.J. Swanson, T. Hamada, J.P. Eggers, P.K. Singh, T. Caffery, M.M. Ouellette, and M.A. Hollingsworth. 2008. Sonic hedgehog promotes desmoplasia in pancreatic cancer. *Clin Cancer Res*. 14:5995-6004.

Baker, L.A., H. Tiriac, H. Clevers, and D.A. Tuveson. 2016. Modeling pancreatic cancer with organoids. *Trends Cancer*. 2:176-190.

Ballehaninna, U.K., and R.S. Chamberlain. 2011. The clinical utility of serum CA 19-9 in the diagnosis, prognosis and management of pancreatic adenocarcinoma: An evidence based appraisal. *Journal of Gastrointestinal Oncology*. 3:105-119.

Bansil, R., and B.S. Turner. 2006. Mucin structure, aggregation, physiological functions and biomedical applications. *Current Opinion in Colloid & Interface Science*. 11:164-170.

Bardeesy, N., K.H. Cheng, J.H. Berger, G.C. Chu, J. Pahler, P. Olson, A.F. Hezel, J. Horner, G.Y. Lauwers, D. Hanahan, and R.A. DePinho. 2006. Smad4 is dispensable for normal pancreas development yet critical in progression and tumor biology of pancreas cancer. *Genes Dev*. 20:3130-3146.

Bardeesy, N., and R.A. DePinho. 2002. Pancreatic cancer biology and genetics. *Nat Rev Cancer*. 2:897-909.

Bashyam, M.D., R. Bair, Y.H. Kim, P. Wang, T. Hernandez-Boussard, C.A. Karikari, R. Tibshirani, A. Maitra, and J.R. Pollack. 2005. Array-based comparative genomic hybridization identifies localized DNA amplifications and homozygous deletions in pancreatic cancer. *Neoplasia*. 7:556-562.

Basturk, O., S.M. Hong, L.D. Wood, N.V. Adsay, J. Albores-Saavedra, A.V. Biankin, L.A. Brosens, N. Fukushima, M. Goggins, R.H. Hruban, Y. Kato, D.S. Klimstra, G. Kloppel, A. Krasinskas, D.S. Longnecker, H. Matthaei, G.J. Offerhaus, M. Shimizu, K. Takaori, B. Terris, S. Yachida, I. Esposito, and T. Furukawa. 2015. A Revised Classification System and Recommendations From the Baltimore Consensus Meeting for Neoplastic Precursor Lesions in the Pancreas. *Am J Surg Pathol*. 39:1730-1741.

Bayram, S. 2012. RASSF1A Ala133Ser polymorphism is associated with increased susceptibility to hepatocellular carcinoma in a Turkish population. *Gene*. 498:264-269.

Biankin, A.V., N. Waddell, K.S. Kassahn, M.C. Gingras, L.B. Muthuswamy, A.L. Johns, D.K. Miller, P.J. Wilson, A.M. Patch, J. Wu, D.K. Chang, M.J. Cowley, B.B. Gardiner, S. Song, I. Harliwong, S. Idrisoglu, C. Nourse, E. Nourbakhsh, S. Manning, S. Wani, M. Gongora, M. Pajic, C.J. Scarlett, A.J. Gill, A.V. Pinho, I. Rooman, M. Anderson, O. Holmes, C. Leonard, D. Taylor, S. Wood, Q. Xu, K. Nones, J.L. Fink, A. Christ, T. Bruxner, N. Cloonan, G. Kolle, F. Newell, M. Pinese, R.S. Mead, J.L. Humphris, W. Kaplan, M.D. Jones, E.K. Colvin, A.M. Nagrial, E.S. Humphrey, A. Chou, V.T. Chin, L.A. Chantrill, A. Mawson, J.S. Samra, J.G. Kench, J.A. Lovell, R.J. Daly, N.D. Merrett, C. Toon, K. Epari, N.Q. Nguyen, A. Barbour, N. Zeps, N. Kakkar, F. Zhao, Y.Q. Wu, M. Wang, D.M. Muzny, W.E. Fisher, F.C. Brunicardi, S.E. Hodges, J.G. Reid, J. Drummond, K. Chang, Y. Han, L.R. Lewis, H. Dinh, C.J. Buhay, T. Beck, L. Timms, M. Sam, K. Begley, A. Brown, D. Pai, A. Panchal, N. Buchner, R. De Borja, R.E. Denroche, C.K. Yung, S. Serra, N. Onetto, D. Mukhopadhyay, M.S. Tsao, P.A. Shaw, G.M. Petersen, S. Gallinger, R.H. Hruban, A. Maitra, C.A. Iacobuzio-Donahue, R.D.

Schulick, C.L. Wolfgang, R.A. Morgan, et al. 2012. Pancreatic cancer genomes reveal aberrations in axon guidance pathway genes. *Nature*. 491:399-405.

Biga, L.M., S. Dawson, A. Harwell, R. Hopkins, J. Kaufmann, M. LeMaster, P. Matern, K. Morrison-Graham, D. Quick, and J. Runyeon. 2018. The Pancreas. *In* Anatomy and Physiology. Open Oregon State: Pressbooks.com, Oregon, USA.

Blair, A.B., V.P. Groot, G. Gemenetzis, J. Wei, J.L. Cameron, M.J. Weiss, M. Goggins, C.L. Wolfgang, J. Yu, and J. He. 2018. BRCA1/BRCA2 Germline Mutation Carriers and Sporadic Pancreatic Ductal Adenocarcinoma. *J Am Coll Surg*. 226:630-637.e631.

Boj, S., C. Hwang, L. Baker, I. Chio, D. Engle, V. Corbo, M. Jager, M. Ponz-Sarvise, H. Tiriac, M. Spector, A. Gracanin, T. Oni, K. Yu, R. van Boxtel, M. Huch, K. Rivera, J. Wilson, M. Feigin, D. Ohlund, A. Handly-Santana, C. Ardito-Abraham, M. Ludwig, E. Elyada, B. Alagesan, G. Biffi, G. Yordanov, B. Delcuze, B. Creighton, K. Wright, Y. Park, F. Morsink, I. Molenaar, I. Rinkes, E. Cuppen, Y. Hao, Y. Jin, I. Nijman, C. Iacobuzio-Donahue, S. Leach, D. Pappin, M. Hammell, D. Klimstra, O. Basturk, R. Hruban, G. Offerhaus, R. Vries, H. Clevers, and D. Tuveson. 2015a. Organoid Models of Human and Mouse Ductal Pancreatic Cancer. *Cell*. 160:324-338.

Boj, S.F., C.I. Hwang, L.A. Baker, D.D. Engle, D.A. Tuveson, and H. Clevers. 2016. Model organoids provide new research opportunities for ductal pancreatic cancer. *Mol Cell Oncol*. 3:e1014757.

Bonner-Weir, S., E. Toschi, A. Inada, P. Reitz, S.Y. Fonseca, T. Aye, and A. Sharma. 2004. The pancreatic ductal epithelium serves as a potential pool of progenitor cells. *Pediatr Diabetes*. 5 Suppl 2:16-22.

Bournet, B., C. Buscail, F. Muscari, P. Cordelier, and L. Buscail. 2016. Targeting KRAS for diagnosis, prognosis, and treatment of pancreatic cancer: Hopes and realities. *European Journal of Cancer*. 54:75-83.

Bowtell, D., P. Fu, M. Simon, and P. Senior. 1992. Identification of murine homologues of the Drosophila son of sevenless gene: potential activators of ras. *Proceedings of the National Academy of Sciences*. 89:6511-6515.

Brat, D.J., K.D. Lillemoe, C.J. Yeo, P.B. Warfield, and R.H. Hruban. 1998. Progression of pancreatic intraductal neoplasias to infiltrating adenocarcinoma of the pancreas. *Am J Surg Pathol*. 22:163-169.

Brembeck, F.H., F.S. Schreiber, T.B. Deramaudt, L. Craig, B. Rhoades, G. Swain, P. Grippo, D.A. Stoffers, D.G. Silberg, and A.K. Rustgi. 2003. The mutant K-ras oncogene causes pancreatic periductal lymphocytic infiltration and gastric mucous neck cell hyperplasia in transgenic mice. *Cancer Res*. 63:2005-2009.

Bretscher, A., K. Edwards, and R.G. Fehon. 2002. ERM proteins and merlin: integrators at the cell cortex. *Nature Reviews Molecular Cell Biology*. 3:586-599.

Brockie, E., A. Anand, and J. Albores-Saavedra. 1998. Progression of atypical ductal hyperplasia/carcinoma in situ of the pancreas to invasive adenocarcinoma. *Ann Diagn Pathol*. 2:286-292.

Burbee, D.G., E. Forgacs, S. Zochbauer-Muller, L. Shivakumar, K. Fong, B. Gao, D. Randle, M. Kondo, A. Virmani, S. Bader, Y. Sekido, F. Latif, S. Milchgrub, S. Toyooka, A.F. Gazdar, M.I. Lerman, E. Zabarovsky, M. White, and J.D. Minna. 2001. Epigenetic inactivation of RASSF1A in lung and breast cancers and malignant phenotype suppression. *J Natl Cancer Inst*. 93:691-699.

Burris, H.A., 3rd, M.J. Moore, J. Andersen, M.R. Green, M.L. Rothenberg, M.R. Modiano, M.C. Cripps, R.K. Portenoy, A.M. Storniolo, P. Tarassoff, R. Nelson, F.A. Dorr, C.D. Stephens, and D.D. Von Hoff. 1997. Improvements in survival and clinical benefit with gemcitabine as first-line therapy for patients with advanced pancreas cancer: a randomized trial. *J Clin Oncol*. 15:2403-2413.

Camargo, F.D., S. Gokhale, J.B. Johnnidis, D. Fu, G.W. Bell, R. Jaenisch, and T.R. Brummelkamp. 2007. YAP1 increases organ size and expands undifferentiated progenitor cells. *Curr Biol*. 17:2054-2060.

Capon, D.J., P.H. Seeburg, J.P. McGrath, J.S. Hayflick, U. Edman, A.D. Levinson, and D.V. Goeddel. 1983. Activation of Ki-ras2 gene in human colon and lung carcinomas by two different point mutations. *Nature*. 304:507-513.

Carpino, G., A. Renzi, V. Cardinale, A. Franchitto, P. Onori, D. Overi, M. Rossi, P.B. Berloco, D. Alvaro, L.M. Reid, and E. Gaudio. 2016. Progenitor cell niches in the human pancreatic duct system and associated pancreatic duct glands: an anatomical and immunophenotyping study. *J Anat*. 228:474-486.

Carrière, C., A.L. Young, J.R. Gunn, D.S. Longnecker, and M. Korc. 2009. Acute pancreatitis markedly accelerates pancreatic cancer progression in mice expressing oncogenic Kras. *Biochemical and biophysical research communications*. 382:561-565.

Catenacci, D.V.T., M.R. Junttila, T. Karrison, N. Bahary, M.N. Horiba, S.R. Nattam, R. Marsh, J. Wallace, M. Kozloff, L. Rajdev, D. Cohen, J. Wade, B. Sleckman, H.-J. Lenz, P. Stiff, P. Kumar, P. Xu, L. Henderson, N. Takebe, R. Salgia, X. Wang, W.M. Stadler, F.J. de Sauvage, and H.L. Kindler. 2015. Randomized Phase Ib/II Study of Gemcitabine Plus Placebo or Vismodegib, a Hedgehog Pathway Inhibitor, in Patients With Metastatic Pancreatic Cancer. *Journal of clinical oncology : official journal of the American Society of Clinical Oncology*. 33:4284-4292.

Cerami, E., J. Gao, U. Dogrusoz, B.E. Gross, S.O. Sumer, B.A. Aksoy, A. Jacobsen, C.J. Byrne, M.L. Heuer, E. Larsson, Y. Antipin, B. Reva, A.P. Goldberg, C. Sander, and N. Schultz. 2012. The cBio cancer genomics portal: an open platform for exploring multidimensional cancer genomics data. *Cancer Discov*. 2:401-404.

Chan, S.W., C.J. Lim, L.S. Loo, Y.F. Chong, C. Huang, and W. Hong. 2009. TEADs mediate nuclear retention of TAZ to promote oncogenic transformation. *J Biol Chem*. 284:14347-14358.

Chantrill, L.A., A.M. Nagrial, C. Watson, A.L. Johns, M. Martyn-Smith, S. Simpson, S. Mead, M.D. Jones, J.S. Samra, A.J. Gill, N. Watson, V.T. Chin, J.L. Humphris, A. Chou, B. Brown, A. Morey, M. Pajic, S.M. Grimmond, D.K. Chang, D. Thomas, L. Sebastian, K. Sjoquist, S. Yip, N. Pavlakis, R. Asghari, S. Harvey, P. Grimison, J. Simes, A.V. Biankin, I. Australian Pancreatic Cancer Genome, and G. Individualized Molecular Pancreatic Cancer Therapy Trial Management Committee of the Australasian Gastrointestinal Trials. 2015. Precision Medicine for Advanced Pancreas Cancer: The Individualized Molecular Pancreatic Cancer Therapy (IMPaCT) Trial. *Clin Cancer Res*. 21:2029-2037.

Chaudhary, P. 2015. Acinar Cell Carcinoma of the Pancreas: A Literature Review and Update. *Indian J Surg*. 77:226-231.

Chung, W.-J., A. Daemen, J.H. Cheng, J.E. Long, J.E. Cooper, B.-e. Wang, C. Tran, M. Singh, F. Gnad, Z. Modrusan, O. Foreman, and M.R. Junttila. 2017. Kras mutant genetically engineered mouse models of human cancers are genomically heterogeneous. *Proceedings of the National Academy of Sciences*. 114:E10947-E10955.

Collins, M.A., W. Yan, J.S. Sebolt-Leopold, and M. Pasca di Magliano. 2014. MAPK signaling is required for dedifferentiation of acinar cells and development of pancreatic intraepithelial neoplasia in mice. *Gastroenterology*. 146:822-834.e827.

Conroy, T., F. Desseigne, M. Ychou, O. Bouche, R. Guimbaud, Y. Becouarn, A. Adenis, J.L. Raoul, S. Gourgou-Bourgade, C. de la Fouchardiere, J. Bennouna, J.B. Bachet, F. Khemissa-Akouz, D. Pere-Verge, C. Delbaldo, E. Assenat, B. Chauffert, P. Michel, C. Montoto-Grillot, and M. Ducreux. 2011. FOLFIRINOX versus gemcitabine for metastatic pancreatic cancer. *N Engl J Med*. 364:1817-1825.

Corbett, T.H., B.J. Roberts, W.R. Leopold, J.C. Peckham, L.J. Wilkoff, D.P. Griswold, Jr., and F.M. Schabel, Jr. 1984. Induction and chemotherapeutic response of two transplantable ductal adenocarcinomas of the pancreas in C57BL/6 mice. *Cancer Res*. 44:717-726.

Cottini, F., T. Hideshima, C. Xu, M. Sattler, M. Dori, L. Agnelli, E. ten Hacken, M.T. Bertilaccio, E. Antonini, A. Neri, M. Ponzoni, M. Marcatti, P.G. Richardson, R.

Carrasco, A.C. Kimmelman, K.K. Wong, F. Caligaris-Cappio, G. Blandino, W.M. Kuehl, K.C. Anderson, and G. Tonon. 2014. Rescue of Hippo coactivator YAP1 triggers DNA damage-induced apoptosis in hematological cancers. *Nat Med*. 20:599-606.

Cox, A.D., S.W. Fesik, A.C. Kimmelman, J. Luo, and C.J. Der. 2014. Drugging the undruggable RAS: Mission Possible? *Nature Reviews Drug Discovery*. 13:828-851.

Cubilla, A.L., and P.J. Fitzgerald. 1976. Morphological lesions associated with human primary invasive nonendocrine pancreas cancer. *Cancer Res*. 36:2690-2698.

Dai, X., H. Liu, S. Shen, X. Guo, H. Yan, X. Ji, L. Li, J. Huang, X.-H. Feng, and B. Zhao. 2015. YAP activates the Hippo pathway in a negative feedback loop. *Cell Research*. 25:1175-1178.

Dammann, R., C. Li, J.H. Yoon, P.L. Chin, S. Bates, and G.P. Pfeifer. 2000. Epigenetic inactivation of a RAS association domain family protein from the lung tumour suppressor locus 3p21.3. *Nat Genet*. 25:315-319.

Dammann, R., U. Schagdarsurengin, L. Liu, N. Otto, O. Gimm, H. Dralle, B.O. Boehm, G.P. Pfeifer, and C. Hoang-Vu. 2003. Frequent RASSF1A promoter hypermethylation and K-ras mutations in pancreatic carcinoma. *Oncogene*. 22:3806-3812.

De Lisle, R.C., and C.D. Logsdon. 1990. Pancreatic acinar cells in culture: expression of acinar and ductal antigens in a growth-related manner. *Eur J Cell Biol*. 51:64-75.

Deer, E.L., J. Gonzalez-Hernandez, J.D. Coursen, J.E. Shea, J. Ngatia, C.L. Scaife, M.A. Firpo, and S.J. Mulvihill. 2010. Phenotype and genotype of pancreatic cancer cell lines. *Pancreas*. 39:425-435.

DeFeo, D., M.A. Gonda, H.A. Young, E.H. Chang, D.R. Lowy, E.M. Scolnick, and R.W. Ellis. 1981. Analysis of two divergent rat genomic clones homologous to the transforming gene of Harvey murine sarcoma virus. *Proc Natl Acad Sci U S A*. 78:3328-3332.

Delle Fave, G., E. Merola, G. Capurso, S. Festa, M. Piciucchi, and R. Valente. 2017. Molecular Pathology of Pancreatic Endocrine Tumors. *In* Pancreatic Cancer. J. Neoptolemos, R. Urrutia, J. Abbruzzese, and M.W. Büchler, editors. Springer New York, New York, NY. 1-32.

Der, C.J., T.G. Krontiris, and G.M. Cooper. 1982. Transforming genes of human bladder and lung carcinoma cell lines are homologous to the ras genes of Harvey and Kirsten sarcoma viruses. *Proc Natl Acad Sci U S A*. 79:3637-3640.

Diep, C.H., K.M. Zucker, G. Hostetter, A. Watanabe, C. Hu, R.M. Munoz, D.D. Von Hoff, and H. Han. 2012. Down-regulation of Yes Associated Protein 1 expression reduces cell proliferation and clonogenicity of pancreatic cancer cells. *PLoS One*. 7:e32783.

Distler, M., D. Aust, J. Weitz, C. Pilarsky, and R. Grutzmann. 2014. Precursor lesions for sporadic pancreatic cancer: PanIN, IPMN, and MCN. *Biomed Res Int*. 2014:474905.

Dong, J., G. Feldmann, J. Huang, S. Wu, N. Zhang, S.A. Comerford, M.F. Gayyed, R.A. Anders, A. Maitra, and D. Pan. 2007. Elucidation of a universal size-control mechanism in Drosophila and mammals. *Cell*. 130:1120-1133.

Dong, W., Y.K. Matsuno, and A. Kameyama. 2012. A procedure for Alcian blue staining of mucins on polyvinylidene difluoride membranes. *Anal Chem*. 84:8461-8466.

Donninger, H., T. Barnoud, N. Nelson, S. Kassler, J. Clark, T.D. Cummins, D.W. Powell, S. Nyante, R.C. Millikan, and G.J. Clark. 2011. RASSF1A and the rs2073498 Cancer Associated SNP. *Front Oncol*. 1:54.

Donninger, H., M.D. Vos, and G.J. Clark. 2007. The RASSF1A tumor suppressor. *J Cell Sci*. 120:3163-3172.

Eblen, S.T. 2018. Extracellular-Regulated Kinases: Signaling From Ras to ERK Substrates to Control Biological Outcomes. *Adv Cancer Res*. 138:99-142.

Ebrahimi, G., C.R.N. Rasch and G. van Tienhoven. 2017. Pain relief after a short course of palliative radiotherapy in pancreatic cancer, the Academic Medical Center (AMC) experience. *Acta Oncologica*. 57:697-700.

Edgar, B.A. 2006. From cell structure to transcription: Hippo forges a new path. *Cell*. 124:267-273.

Egan, S.E., B.W. Giddings, M.W. Brooks, L. Buday, A.M. Sizeland, and R.A. Weinberg. 1993. Association of Sos Ras exchange protein with Grb2 is implicated in tyrosine kinase signal transduction and transformation. *Nature*. 363:45-51.

Ellis, C.A., and G. Clark. 2000. The importance of being K-Ras. *Cellular Signalling*. 12:425-434.

Encyclopaedia Britannica. 2019. Pancreas. Vol. 2019. Encyclopaedia Britannica, Inc.

Engle, D.D., H. Tiriac, K.D. Rivera, A. Pommier, S. Whalen, T.E. Oni, B. Alagesan, E.J. Lee, M.A. Yao, M.S. Lucito, B. Spielman, B. Da Silva, C. Schoepfer, K. Wright, B. Creighton, L. Afinowicz, K.H. Yu, R. Grützmann, D. Aust, P.A. Gimotty, K.S. Pollard, R.H. Hruban, M.G. Goggins, C. Pilarsky, Y. Park, D.J. Pappin, M.A. Hollingsworth, D.A. Tuveson.

2019. The glycan CA19-9 promotes pancreatitis and pancreatic cancer in mice. *Science.* 364:1156-1162.

Everhart, J., and D. Wright. 1995. Diabetes Mellitus as a Risk Factor for Pancreatic Cancer: A Meta-analysis. *JAMA*. 273:1605-1609.

Fedchenko, N., and J. Reifenrath. 2014. Different approaches for interpretation and reporting of immunohistochemistry analysis results in the bone tissue - a review. *Diagn Pathol*. 9:221-221.

Feldmann, G., R. Beaty, R.H. Hruban, and A. Maitra. 2007. Molecular genetics of pancreatic intraepithelial neoplasia. *J Hepatobiliary Pancreat Surg*. 14:224-232.

Ferreira, R.M.M., R. Sancho, H.A. Messal, E. Nye, B. Spencer-Dene, R.K. Stone, G. Stamp, I. Rosewell, A. Quaglia, and A. Behrens. 2017. Duct- and Acinar-Derived Pancreatic Ductal Adenocarcinomas Show Distinct Tumor Progression and Marker Expression. *Cell Rep*. 21:966-978.

Fesinmeyer, M.D., M.A. Austin, C.I. Li, A.J. De Roos, and D.J. Bowen. 2005. Differences in Survival by Histologic Type of Pancreatic Cancer. *Cancer Epidemiology Biomarkers & Prevention*. 14:1766-1773.

Finch-Edmondson, M.L., R.P. Strauss, A.M. Passman, M. Sudol, G.C. Yeoh, and B.A. Callus. 2015. TAZ Protein Accumulation Is Negatively Regulated by YAP Abundance in Mammalian Cells. *J Biol Chem*. 290:27928-27938.

Furukawa, T., R. Chiba, M. Kobari, S. Matsuno, H. Nagura, and T. Takahashi. 1994. Varying grades of epithelial atypia in the pancreatic ducts of humans. Classification based on morphometry and multivariate analysis and correlated with positive reactions of carcinoembryonic antigen. *Archives of pathology & laboratory medicine*. 118:227-234.

Gale, N.W., S. Kaplan, E.J. Lowenstein, J. Schlessinger, and D. Bar-Sagi. 1993. Grb2 mediates the EGF-dependent activation of guanine nucleotide exchange on Ras. *Nature*. 363:88-92.

Gao, B., X.J. Xie, C. Huang, D.S. Shames, T.T. Chen, C.M. Lewis, A. Bian, B. Zhang, O.I. Olopade, J.E. Garber, D.M. Euhus, G.E. Tomlinson, and J.D. Minna. 2008. RASSF1A polymorphism A133S is associated with early onset breast cancer in BRCA1/2 mutation carriers. *Cancer Res*. 68:22-25.

Gao, J., B.A. Aksoy, U. Dogrusoz, G. Dresdner, B. Gross, S.O. Sumer, Y. Sun, A. Jacobsen, R. Sinha, E. Larsson, E. Cerami, C. Sander, and N. Schultz. 2013. Integrative analysis of complex cancer genomics and clinical profiles using the cBioPortal. *Sci Signal*. 6:pl1.

Garcia, P.L., L.N. Council, J.D. Christein, J.P. Arnoletti, M.J. Heslin, T.L. Gamblin, J.H. Richardson, M.-A. Bjornsti, and K.J. Yoon. 2013. Development and histopathological characterization of tumorgraft models of pancreatic ductal adenocarcinoma. *PloS one*. 8:e78183-e78183.

Garcia-Rendueles, M.E., J.C. Ricarte-Filho, B.R. Untch, I. Landa, J.A. Knauf, F. Voza, V.E. Smith, I. Ganly, B.S. Taylor, Y. Persaud, G. Oler, Y. Fang, S.C. Jhanwar, A. Viale, A. Heguy, K.H. Huberman, F. Giancotti, R. Ghossein, and J.A. Fagin. 2015. NF2 Loss Promotes Oncogenic RAS-Induced Thyroid Cancers via YAP-Dependent Transactivation of RAS Proteins and Sensitizes Them to MEK Inhibition. *Cancer Discov*. 5:1178-1193.

George, N.M., C.E. Day, B.P. Boerner, R.L. Johnson, and N.E. Sarvetnick. 2012. Hippo Signaling Regulates Pancreas Development through Inactivation of Yap. *Molecular and Cellular Biology*. 32:5116-5128.

Gillen, S., T. Schuster, C. Meyer Zum Buschenfelde, H. Friess, and J. Kleeff. 2010. Preoperative/neoadjuvant therapy in pancreatic cancer: a systematic review and meta-analysis of response and resection percentages. *PLoS Med*. 7:e1000267.

Golan, T., P. Hammel, M. Reni, E. Van Cutsem, T. Macarulla, M.J. Hall, J.O. Park, D. Hochhauser, D. Arnold, D.Y. Oh, A. Reinacher-Schick, G. Tortora, H. Algul, E.M. O'Reilly, D. McGuinness, K.Y. Cui, K. Schlienger, G.Y. Locker, and H.L. Kindler. 2019. Maintenance Olaparib for Germline BRCA-Mutated Metastatic Pancreatic Cancer. *N Engl J Med*. 381:317-327.

Gopinathan, A., J.P. Morton, D.I. Jodrell, and O.J. Sansom. 2015. GEMMs as preclinical models for testing pancreatic cancer therapies. *Dis Model Mech*. 8:1185-1200.

Grawenda, A.M., and E. O'Neill. 2015. Clinical utility of RASSF1A methylation in human malignancies. *Br J Cancer*. 113:372-381.

Gruber, R., R. Panayiotou, E. Nye, B. Spencer-Dene, G. Stamp, and A. Behrens. 2016. YAP1 and TAZ Control Pancreatic Cancer Initiation in Mice by Direct Up-regulation of JAK-STAT3 Signaling. *Gastroenterology*. 151:526-539.

Guerra, C., and M. Barbacid. 2013. Genetically engineered mouse models of pancreatic adenocarcinoma. *Molecular Oncology*. 7:232-247.

Guerra, C., A.J. Schuhmacher, M. Canamero, P.J. Grippo, L. Verdaguer, L. Perez-Gallego, P. Dubus, E.P. Sandgren, and M. Barbacid. 2007. Chronic pancreatitis is essential for

induction of pancreatic ductal adenocarcinoma by K-Ras oncogenes in adult mice. *Cancer Cell*. 11:291-302.

Guo, C., S. Tommasi, L. Liu, J.K. Yee, R. Dammann, and G.P. Pfeifer. 2007. RASSF1A is part of a complex similar to the Drosophila Hippo/Salvador/Lats tumor-suppressor network. *Curr Biol*. 17:700-705.

Guo, X., and B. Zhao. 2013. Integration of mechanical and chemical signals by YAP and TAZ transcription coactivators. *Cell Biosci*. 3:33.

Habbe, N., G. Shi, R.A. Meguid, V. Fendrich, F. Esni, H. Chen, G. Feldmann, D.A. Stoffers, S.F. Konieczny, S.D. Leach, and A. Maitra. 2008. Spontaneous induction of murine pancreatic intraepithelial neoplasia (mPanIN) by acinar cell targeting of oncogenic Kras in adult mice. *Proc Natl Acad Sci U S A*. 105:18913-18918.

Haeberle, L., and I. Esposito. 2019. Pathology of pancreatic cancer. *Translational gastroenterology and hepatology*. 4:50-50.

Halfdanarson, T.R., J. Rubin, M.B. Farnell, C.S. Grant, and G.M. Petersen. 2008. Pancreatic endocrine neoplasms: epidemiology and prognosis of pancreatic endocrine tumors. *Endocr Relat Cancer*. 15:409-427.

Hall, A., C.J. Marshall, N.K. Spurr, and R.A. Weiss. 1983. Identification of transforming gene in two human sarcoma cell lines as a new member of the ras gene family located on chromosome 1. *Nature*. 303:396-400.

Hall, P.A., and N.R. Lemoine. 1992. Rapid acinar to ductal transdifferentiation in cultured human exocrine pancreas. *J Pathol*. 166:97-103.

Hammel, P., F. Huguet, J. van Laethem, D. Goldstein, B. Glimelius, P. Artru, I. Borbath, O. Bouché, J. Shannon, T. André, L. Mineur, B. Chibaudel, F. Bonnetain and C. Louvet. 2016. **E**ffect of Chemoradiotherapy vs Chemotherapy on Survival in Patients With Locally Advanced Pancreatic Cancer Controlled After 4 Months of Gemcitabine With or Without Erlotinib: The LAP07 Randomized Clinical Trial. *The Journal of the American Medical Association.* 315:1844-53.

Han, X., Y. Li, Y. Xu, X. Zhao, Y. Zhang, X. Yang, Y. Wang, R. Zhao, G.J. Anderson, Y. Zhao, and G. Nie. 2018. Reversal of pancreatic desmoplasia by re-educating stellate cells with a tumour microenvironment-activated nanosystem. *Nat Commun*. 9:3390.

Hanahan, D., and R.A. Weinberg. 2000. The hallmarks of cancer. *Cell*. 100:57-70.

Hanahan, D., and Robert A. Weinberg. 2011. Hallmarks of Cancer: The Next Generation. *Cell*. 144:646-674.

Harvey, J.J. 1964. An Unidentified Virus which causes the Rapid Production of Tumours in Mice. *Nature*. 204:1104-1105.

Harvey, K.F., C.M. Pfleger, and I.K. Hariharan. 2003. The Drosophila Mst ortholog, hippo, restricts growth and cell proliferation and promotes apoptosis. *Cell*. 114:457-467.

Hayashi, H., T. Higashi, N. Yokoyama, T. Kaida, K. Sakamoto, Y. Fukushima, T. Ishimoto, H. Kuroki, H. Nitta, D. Hashimoto, A. Chikamoto, E. Oki, T. Beppu, and H. Baba. 2015. An Imbalance in TAZ and YAP Expression in Hepatocellular Carcinoma Confers Cancer Stem Cell-like Behaviors Contributing to Disease Progression. *Cancer Res*. 75:4985-4997.

He, P., J.W. Yang, V.W. Yang, and A.B. Bialkowska. 2018. Kruppel-like Factor 5, Increased in Pancreatic Ductal Adenocarcinoma, Promotes Proliferation, Acinar-to-Ductal Metaplasia, Pancreatic Intraepithelial Neoplasia, and Tumor Growth in Mice. *Gastroenterology*. 154:1494-1508.e1413.

Hezel, A.F., S. Gurumurthy, Z. Granot, A. Swisa, G.C. Chu, G. Bailey, Y. Dor, N. Bardeesy, and R.A. Depinho. 2008. Pancreatic LKB1 deletion leads to acinar polarity defects and cystic neoplasms. *Mol Cell Biol*. 28:2414-2425.

Hingorani, S., E. Petricoin, A. Maitra, V. Rajapakse, C. King, M. Jacobetz, S. Ross, T. Conrads, T. Veenstra, B. Hitt, Y. Kawaguchi, D. Johann, L. Liotta, H. Crawford, M. Putt, T. Jacks, C. Wright, R. Hruban, A. Lowy, and D. Tuveson. 2003. Preinvasive and invasive ductal pancreatic cancer and its early detection in the mouse. *Cancer Cell*. 4:437-450.

Hingorani, S.R., L. Wang, A.S. Multani, C. Combs, T.B. Deramaudt, R.H. Hruban, A.K. Rustgi, S. Chang, and D.A. Tuveson. 2005. Trp53R172H and KrasG12D cooperate to promote chromosomal instability and widely metastatic pancreatic ductal adenocarcinoma in mice. *Cancer Cell*. 7:469-483.

Hirsch, D., N. Barker, N. McNeil, Y. Hu, J. Camps, K. McKinnon, H. Clevers, T. Ried, and T. Gaiser. 2014. LGR5 positivity defines stem-like cells in colorectal cancer. *Carcinogenesis*. 35:849-858.

Hohwieler, M., #x00FC, M. ller, P.-O. Frappart, and S. Heller. 2019. Pancreatic Progenitors and Organoids as a Prerequisite to Model Pancreatic Diseases and Cancer. *Stem Cells International*. 2019:11.

Hruban, R.H., M. Goggins, J. Parsons, and S.E. Kern. 2000. Progression model for pancreatic cancer. *Clin Cancer Res*. 6:2969-2972.

Hruban, R.H., K. Takaori, D.S. Klimstra, N.V. Adsay, J. Albores-Saavedra, A.V. Biankin, S.A. Biankin, C. Compton, N. Fukushima, T. Furukawa, M. Goggins, Y. Kato, G. Kloppel,

D.S. Longnecker, J. Luttges, A. Maitra, G.J. Offerhaus, M. Shimizu, and S. Yonezawa. 2004. An illustrated consensus on the classification of pancreatic intraepithelial neoplasia and intraductal papillary mucinous neoplasms. *Am J Surg Pathol*. 28:977-987.

Huang, J., S. Wu, J. Barrera, K. Matthews, and D. Pan. 2005. The Hippo signaling pathway coordinately regulates cell proliferation and apoptosis by inactivating Yorkie, the Drosophila Homolog of YAP. *Cell*. 122:421-434.

Huch, M., P. Bonfanti, S.F. Boj, T. Sato, C.J. Loomans, M. van de Wetering, M. Sojoodi, V.S. Li, J. Schuijers, A. Gracanin, F. Ringnalda, H. Begthel, K. Hamer, J. Mulder, J.H. van Es, E. de Koning, R.G. Vries, H. Heimberg, and H. Clevers. 2013. Unlimited in vitro expansion of adult bi-potent pancreas progenitors through the Lgr5/R-spondin axis. *EMBO J*. 32:2708-2721.

Iodice, S., S. Gandini, P. Maisonneuve, and A.B. Lowenfels. 2008. Tobacco and the risk of pancreatic cancer: a review and meta-analysis. *Langenbeck's Archives of Surgery*. 393:535-545.

Ivanchuk, S.M., S. Mondal, P.B. Dirks and J.T. Rutka. 2001. The INK4A/ARF locus: Role in cell cycle control and apoptosis and implications for glioma growth. *Journal of Neuro-Oncology*. 51:219-229.

Izeradjene, K., C. Combs, M. Best, A. Gopinathan, A. Wagner, W.M. Grady, C.X. Deng, R.H. Hruban, N.V. Adsay, D.A. Tuveson, and S.R. Hingorani. 2007. Kras(G12D) and Smad4/Dpc4 haploinsufficiency cooperate to induce mucinous cystic neoplasms and invasive adenocarcinoma of the pancreas. *Cancer Cell*. 11:229-243.

Jackson, E., N. Willis, K. Mercer, R. Bronson, D. Crowley, R. Montoya, T. Jacks, and D. Tuveson. 2001. Analysis of lung tumor initiation and progression using conditional expression of oncogenic K-ras. *Genes & Development*. 15:3243-3248.

Jia, J., W. Zhang, B. Wang, R. Trinko, and J. Jiang. 2003. The Drosophila Ste20 family kinase dMST functions as a tumor suppressor by restricting cell proliferation and promoting apoptosis. *Genes Dev*. 17:2514-2519.

Jimenez, R.E., A.L. Warshaw, K. Z'Graggen, W. Hartwig, D.Z. Taylor, C.C. Compton, and C. Fernández-del Castillo. 1999. Sequential accumulation of K-ras mutations and p53 overexpression in the progression of pancreatic mucinous cystic neoplasms to malignancy. *Ann Surg*. 230:501-511.

Jonckheere, N., N. Skrypek, and I. Van Seuningen. 2010. Mucins and pancreatic cancer. *Cancers (Basel)*. 2:1794-1812.

Justice, R.W., O. Zilian, D.F. Woods, M. Noll, and P.J. Bryant. 1995. The Drosophila tumor suppressor gene warts encodes a homolog of human myotonic dystrophy kinase and is required for the control of cell shape and proliferation. *Genes Dev*. 9:534-546.

Kamisawa, T., L.D. Wood, T. Itoi, and K. Takaori. 2016. Pancreatic cancer. *Lancet*. 388:73-85.

Kanai, F., P.A. Marignani, D. Sarbassova, R. Yagi, R.A. Hall, M. Donowitz, A. Hisaminato, T. Fujiwara, Y. Ito, L.C. Cantley, and M.B. Yaffe. 2000. TAZ: a novel transcriptional co-activator regulated by interactions with 14-3-3 and PDZ domain proteins. *EMBO J*. 19:6778-6791.

Kanda, M., H. Matthaei, J. Wu, S.-M. Hong, J. Yu, M. Borges, R.H. Hruban, A. Maitra, K. Kinzler, B. Vogelstein, and M. Goggins. 2012. Presence of somatic mutations in most early-stage pancreatic intraepithelial neoplasia. *Gastroenterology*. 142:730-733.e739.

Kapoor, A., W. Yao, H. Ying, S. Hua, A. Liewen, Q. Wang, Y. Zhong, C.-J. Wu, A. Sadanandam, B. Hu, Q. Chang, Gerald C. Chu, R. Al-Khalil, S. Jiang, H. Xia, E. Fletcher-Sananikone, C. Lim, Gillian I. Horwitz, A. Viale, P. Pettazzoni, N. Sanchez, H. Wang, A. Protopopov, J. Zhang, T. Heffernan, Randy L. Johnson, L. Chin, Y.A. Wang, G. Draetta, and Ronald A. DePinho. 2014. Yap1 Activation Enables Bypass of Oncogenic Kras Addiction in Pancreatic Cancer. *Cell*. 158:185-197.

Karnoub, A.E., and R.A. Weinberg. 2008. Ras oncogenes: split personalities. *Nature Reviews Molecular Cell Biology*. 9:517-531.

Kastrinos, F., B. Mukherjee, N. Tayob, F. Wang, J. Sparr, V.M. Raymond, P. Bandipalliam, E.M. Stoffel, S.B. Gruber, and S. Syngal. 2009. Risk of pancreatic cancer in families with Lynch syndrome. *JAMA*. 302:1790-1795.

Kawada, N., H. Uehara, R. Takada, T. Yamai, N. Fukutake, K. Katayama, A. Takenaka, S. Nagata, and Y. Tomita. 2013. Microinvasion of high-grade pancreatic intraepithelial neoplasia. *Case Rep Gastroenterol*. 7:30-36.

Kent, O.A. 2018. Increased mutant KRAS gene dosage drives pancreatic cancer progression: evidence for wild-type KRAS as a tumor suppressor? *Hepatobiliary Surg Nutr*. 7:403-405.

Kern, S., R. Hruban, M.A. Hollingsworth, R. Brand, T.E. Adrian, E. Jaffee, and M.A. Tempero. 2001. A white paper: the product of a pancreas cancer think tank. *Cancer Res*. 61:4923-4932.

Keshet, R., J. Adler, I. Ricardo Lax, M. Shanzer, Z. Porat, N. Reuven, and Y. Shaul. 2015. c-Abl antagonizes the YAP oncogenic function. *Cell Death Differ*. 22:935-945.

Kiernan, J.A. 2006. Dyes and other colorants in microtechnique and biomedical research. *Coloration Technology*. 122:1-21.

Kim, M.K., J.W. Jang, and S.C. Bae. 2018. DNA binding partners of YAP/TAZ. *BMB Rep*. 51:126-133.

Kim, M.P., and G.E. Gallick. 2008. Gemcitabine resistance in pancreatic cancer: picking the key players. *Clin Cancer Res*. 14:1284-1285.

Kim, S., R. Lahmy, C. Riha, C. Yang, B.L. Jakubison, J. van Niekerk, C. Staub, Y. Wu, K. Gates, D.S. Dong, S.F. Konieczny, and P. Itkin-Ansari. 2015. The basic helix-loop-helix transcription factor E47 reprograms human pancreatic cancer cells to a quiescent acinar state with reduced tumorigenic potential. *Pancreas*. 44:718-727.

Kim, T.H., K.H. Choi, H.S. Song, J.W. Kim, and B.J. Jeon. 2013. Histology combined with cytology by endoscopic ultrasound-guided fine needle aspiration for the diagnosis of solid pancreatic mass and intra-abdominal lymphadenopathy. *Gut Liver*. 7:605-610.

Kimura, Y., A. Fukuda, S. Ogawa, T. Maruno, Y. Takada, M. Tsuda, Y. Hiramatsu, O. Araki, M. Nagao, T. Yoshikawa, K. Ikuta, T. Yoshioka, Z. Wang, H. Akiyama, C.V. Wright, K. Takaori, S. Uemoto, T. Chiba, and H. Seno. 2018. ARID1A Maintains Differentiation of Pancreatic Ductal Cells and Inhibits Development of Pancreatic Ductal Adenocarcinoma in Mice. *Gastroenterology*. 155:194-209.e192.

Kinchesh, P., P.D. Allen, S. Gilchrist, V. Kersemans, S. Lanfredini, A. Thapa, E. O'Neill, and S.C. Smart. 2019. Reduced respiratory motion artefact in constant TR multi-slice MRI of the mouse. *Magn Reson Imaging*. 60:1-6.

Kirsten, W.H., and L.A. Mayer. 1967. Morphologic Responses to a Murine Erythroblastosis Virus2. *JNCI: Journal of the National Cancer Institute*. 39:311-335.

Klimstra, D.S., and D.S. Longnecker. 1994. K-ras mutations in pancreatic ductal proliferative lesions. *Am J Pathol*. 145:1547-1550.

Kopp, J.L., C.L. Dubois, D.F. Schaeffer, A. Samani, F. Taghizadeh, R.W. Cowan, A.D. Rhim, B.L. Stiles, M. Valasek, and M. Sander. 2018. Loss of Pten and Activation of Kras Synergistically Induce Formation of Intraductal Papillary Mucinous Neoplasia From Pancreatic Ductal Cells in Mice. *Gastroenterology*. 154:1509-1523.e1505.

Kopp, J.L., G. von Figura, E. Mayes, F.F. Liu, C.L. Dubois, J.P.t. Morris, F.C. Pan, H. Akiyama, C.V. Wright, K. Jensen, M. Hebrok, and M. Sander. 2012. Identification of Sox9-

dependent acinar-to-ductal reprogramming as the principal mechanism for initiation of pancreatic ductal adenocarcinoma. *Cancer Cell*. 22:737-750.

Korsse, S.E., F. Harinck, M.G. van Lier, K. Biermann, G.J. Offerhaus, N. Krak, C.W. Looman, W. van Veelen, E.J. Kuipers, A. Wagner, E. Dekker, E.M. Mathus-Vliegen, P. Fockens, M.E. van Leerdam, and M.J. Bruno. 2013. Pancreatic cancer risk in Peutz-Jeghers syndrome patients: a large cohort study and implications for surveillance. *J Med Genet*. 50:59-64.

Kozuka, S., R. Sassa, T. Taki, K. Masamoto, S. Nagasawa, S. Saga, K. Hasegawa, and M. Takeuchi. 1979. Relation of pancreatic duct hyperplasia to carcinoma. *Cancer*. 43:1418-1428.

Lai, Z.C., X. Wei, T. Shimizu, E. Ramos, M. Rohrbaugh, N. Nikolaidis, L.L. Ho, and Y. Li. 2005. Control of cell proliferation and apoptosis by mob as tumor suppressor, mats. *Cell*. 120:675-685.

Lanfredini, S., A. Thapa, and E. O'Neill. 2019. RAS in pancreatic cancer. *Biochemical Society Transactions*. 47:961-972.

Lee, A.Y.L., C.L. Dubois, K. Sarai, S. Zarei, D.F. Schaeffer, M. Sander, and J.L. Kopp. 2018. Cell of origin affects tumour development and phenotype in pancreatic ductal adenocarcinoma. *Gut*.

Lee, J.J., R.M. Perera, H. Wang, D.C. Wu, X.S. Liu, S. Han, J. Fitamant, P.D. Jones, K.S. Ghanta, S. Kawano, J.M. Nagle, V. Deshpande, Y. Boucher, T. Kato, J.K. Chen, J.K. Willmann, N. Bardeesy, and P.A. Beachy. 2014. Stromal response to Hedgehog signaling restrains pancreatic cancer progression. *Proc Natl Acad Sci U S A*. 111:E3091-3100.

Lei, Q.-Y., H. Zhang, B. Zhao, Z.-Y. Zha, F. Bai, X.-H. Pei, S. Zhao, Y. Xiong, and K.-L. Guan. 2008. TAZ Promotes Cell Proliferation and Epithelial-Mesenchymal Transition and Is Inhibited by the Hippo Pathway. *Molecular and Cellular Biology*. 28:2426-2436.

Levy, D., Y. Adamovich, N. Reuven, and Y. Shaul. 2008. Yap1 phosphorylation by c-Abl is a critical step in selective activation of proapoptotic genes in response to DNA damage. *Mol Cell*. 29:350-361.

Li, D., E.J. Duell, K. Yu, H.A. Risch, S.H. Olson, C. Kooperberg, B.M. Wolpin, L. Jiao, X. Dong, B. Wheeler, A.A. Arslan, H.B. Bueno-de-Mesquita, C.S. Fuchs, S. Gallinger, M. Gross, P. Hartge, R.N. Hoover, E.A. Holly, E.J. Jacobs, A.P. Klein, A. LaCroix, M.T. Mandelson, G. Petersen, W. Zheng, I. Agalliu, D. Albanes, M.C. Boutron-Ruault, P.M. Bracci, J.E. Buring, F. Canzian, K. Chang, S.J. Chanock, M. Cotterchio, J.M. Gaziano, E.L. Giovannucci, M. Goggins, G. Hallmans, S.E. Hankinson, J.A. Hoffman Bolton, D.J. Hunter, A. Hutchinson, K.B. Jacobs, M. Jenab, K.T. Khaw, P. Kraft, V. Krogh, R.C. Kurtz, R.R. McWilliams, J.B. Mendelsohn, A.V. Patel, K.G. Rabe, E. Riboli, X.O. Shu,

A. Tjonneland, G.S. Tobias, D. Trichopoulos, J. Virtamo, K. Visvanathan, J. Watters, H. Yu, A. Zeleniuch-Jacquotte, L. Amundadottir, and R.Z. Stolzenberg-Solomon. 2012. Pathway analysis of genome-wide association study data highlights pancreatic development genes as susceptibility factors for pancreatic cancer. *Carcinogenesis*. 33:1384-1390.

Li, N., A. Batzer, R. Daly, V. Yajnik, E. Skolnik, P. Chardin, D. Bar-Sagi, B. Margolis, and J. Schlessinger. 1993. Guanine-nucleotide-releasing factor hSos1 binds to Grb2 and links receptor tyrosine kinases to Ras signalling. *Nature*. 363:85-88.

Lian, I., J. Kim, H. Okazawa, J. Zhao, B. Zhao, J. Yu, A. Chinnaiyan, M.A. Israel, L.S. Goldstein, R. Abujarour, S. Ding, and K.L. Guan. 2010. The role of YAP transcription coactivator in regulating stem cell self-renewal and differentiation. *Genes Dev*. 24:1106-1118.

Liou, G.Y., H. Doppler, K.E. DelGiorno, L. Zhang, M. Leitges, H.C. Crawford, M.P. Murphy, and P. Storz. 2016. Mutant KRas-Induced Mitochondrial Oxidative Stress in Acinar Cells Upregulates EGFR Signaling to Drive Formation of Pancreatic Precancerous Lesions. *Cell Rep*. 14:2325-2336.

Liou, G.Y., H. Doppler, B. Necela, M. Krishna, H.C. Crawford, M. Raimondo, and P. Storz. 2013. Macrophage-secreted cytokines drive pancreatic acinar-to-ductal metaplasia through NF-kappaB and MMPs. *J Cell Biol*. 202:563-577.

Liu, Q., Q. Liao, and Y. Zhao. 2017. Chemotherapy and tumor microenvironment of pancreatic cancer. *Cancer Cell Int*. 17:68-68.

Lowenfels, A.B., P. Maisonneuve, E.P. DiMagno, Y. Elitsur, L.K. Gates, Jr., J. Perrault, and D.C. Whitcomb. 1997. Hereditary pancreatitis and the risk of pancreatic cancer. International Hereditary Pancreatitis Study Group. *J Natl Cancer Inst*. 89:442-446.

Lynch, H.T., R.M. Fusaro, J.F. Lynch, and R. Brand. 2008. Pancreatic cancer and the FAMMM syndrome. *Familial Cancer*. 7:103-112.

Maddipati, R., and B.Z. Stanger. 2015. Pancreatic Cancer Metastases Harbor Evidence of Polyclonality. *Cancer Discov*. 5:1086-1097.

Maisonneuve, P., S. Amar, and A.B. Lowenfels. 2017. Periodontal disease, edentulism, and pancreatic cancer: a meta-analysis. *Ann Oncol*. 28:985-995.

Makohon-Moore, A.P., K. Matsukuma, M. Zhang, J.G. Reiter, J.M. Gerold, Y. Jiao, L. Sikkema, M.A. Attiyeh, S. Yachida, C. Sandone, R.H. Hruban, D.S. Klimstra, N. Papadopoulos, M.A. Nowak, K.W. Kinzler, B. Vogelstein, and C.A. Iacobuzio-Donahue. 2018. Precancerous neoplastic cells can move through the pancreatic ductal system. *Nature*. 561:201-205.

Manami, I., and T. Shoichiro. 2012. Insulin resistance and cancer: epidemiological evidence. *Endocr Relat Cancer*. 19:F1-F8.

Matallanas, D., D. Romano, K. Yee, K. Meissl, L. Kucerova, D. Piazzolla, M. Baccarini, J.K. Vass, W. Kolch, and E. O'Neill. 2007. RASSF1A elicits apoptosis through an MST2 pathway directing proapoptotic transcription by the p73 tumor suppressor protein. *Mol Cell*. 27:962-975.

McClatchey, A.I., and M. Giovannini. 2005. Membrane organization and tumorigenesis--the NF2 tumor suppressor, Merlin. *Genes Dev*. 19:2265-2277.

Mebratu, Y., and Y. Tesfaigzi. 2009. How ERK1/2 activation controls cell proliferation and cell death: Is subcellular localization the answer? *Cell Cycle*. 8:1168-1175.

Meloche, S., and J. Pouyssegur. 2007. The ERK1/2 mitogen-activated protein kinase pathway as a master regulator of the G1- to S-phase transition. *Oncogene*. 26:3227-3239.

Miesfeld, J.B., G. Gestri, B.S. Clark, M.A. Flinn, R.J. Poole, J.R. Bader, J.C. Besharse, S.W. Wilson, and B.A. Link. 2015. Yap and Taz regulate retinal pigment epithelial cell fate. *Development*. 142:3021-3032.

Mocci, E., R.L. Milne, E.Y. Mendez-Villamil, J.L. Hopper, E.M. John, I.L. Andrulis, W.K. Chung, M. Daly, S.S. Buys, N. Malats, and D.E. Goldgar. 2013. Risk of pancreatic cancer in breast cancer families from the breast cancer family registry. *Cancer Epidemiol Biomarkers Prev*. 22:803-811.

Mohammad, R.M., A. Al-Katib, G.R. Pettit, V.K. Vaitkevicius, U. Joshi, V. Adsay, A. Majumdar and F.H. Sarkar. 1998. An Orthotopic Model of Human Pancreatic Cancer in Severe Combined Immunodeficient Mice: Potential Application for Preclinical Studies. *Clinical Cancer Research*. 4:887-894.

Moodie, S., B. Willumsen, M. Weber, and A. Wolfman. 1993. Complexes of Ras.GTP with Raf-1 and mitogen-activated protein kinase kinase. *Science*. 260:1658-1661.

Moreira, L., B. Bakir, P. Chatterji, Z. Dantes, M. Reichert, and A.K. Rustgi. 2017. Pancreas 3D Organoids: Current and Future Aspects as a Research Platform for Personalized Medicine in Pancreatic Cancer. *Cell Mol Gastroenterol Hepatol*. 5:289-298.

Morgan, R.G., A.C. Chambers, D.N. Legge, S.J. Coles, A. Greenhough, and A.C. Williams. 2018. Optimized delivery of siRNA into 3D tumor spheroid cultures in situ. *Sci Rep*. 8:7952.

Morin-Kensicki, E.M., B.N. Boone, M. Howell, J.R. Stonebraker, J. Teed, J.G. Alb, T.R. Magnuson, W. O'Neal, and S.L. Milgram. 2006. Defects in yolk sac vasculogenesis,

chorioallantoic fusion, and embryonic axis elongation in mice with targeted disruption of Yap65. *Mol Cell Biol*. 26:77-87.

Moroishi, T., H.W. Park, B. Qin, Q. Chen, Z. Meng, S.W. Plouffe, K. Taniguchi, F.X. Yu, M. Karin, D. Pan, and K.L. Guan. 2015. A YAP/TAZ-induced feedback mechanism regulates Hippo pathway homeostasis. *Genes Dev*. 29:1271-1284.

Morris, J.P.t., S.C. Wang, and M. Hebrok. 2010. KRAS, Hedgehog, Wnt and the twisted developmental biology of pancreatic ductal adenocarcinoma. *Nature reviews. Cancer*. 10:683-695.

Morton, J.P., M.E. Mongeau, D.S. Klimstra, J.P. Morris, Y.C. Lee, Y. Kawaguchi, C.V.E. Wright, M. Hebrok and B.C. Lewis. 2007. Sonic hedgehog acts at multiple stages during pancreatic tumorigenesis. *PNAS.* 104:5103-5108.

Morvaridi, S., D. Dhall, M.I. Greene, S.J. Pandol, and Q. Wang. 2015a. Role of YAP and TAZ in pancreatic ductal adenocarcinoma and in stellate cells associated with cancer and chronic pancreatitis. *Scientific reports*. 5:16759-16759.

Morvaridi, S., D. Dhall, M.I. Greene, S.J. Pandol, and Q. Wang. 2015b. Role of YAP and TAZ in pancreatic ductal adenocarcinoma and in stellate cells associated with cancer and chronic pancreatitis. *Sci Rep*. 5:16759.

Mueller, S., T. Engleitner, R. Maresch, M. Zukowska, S. Lange, T. Kaltenbacher, B. Konukiewitz, R. Öllinger, M. Zwiebel, A. Strong, H.-Y. Yen, R. Banerjee, S. Louzada, B. Fu, B. Seidler, J. Götzfried, K. Schuck, Z. Hassan, A. Arbeiter, N. Schönhuber, S. Klein, C. Veltkamp, M. Friedrich, L. Rad, M. Barenboim, C. Ziegenhain, J. Hess, O.M. Dovey, S. Eser, S. Parekh, F. Constantino-Casas, J. de la Rosa, M.I. Sierra, M. Fraga, J. Mayerle, G. Klöppel, J. Cadiñanos, P. Liu, G. Vassiliou, W. Weichert, K. Steiger, W. Enard, R.M. Schmid, F. Yang, K. Unger, G. Schneider, I. Varela, A. Bradley, D. Saur, and R. Rad. 2018. Evolutionary routes and KRAS dosage define pancreatic cancer phenotypes. *Nature*. 554:62-68.

Mullan, M.H., P.G. Gauger, and N.W. Thompson. 2001. Endocrine tumours of the pancreas: Review and recent advances. *ANZ Journal of Surgery*. 71:475-482.

Murtaugh, L.C., and S.D. Leach. 2007. A case of mistaken identity? Nonductal origins of pancreatic "ductal" cancers. *Cancer Cell*. 11:211-213.

Muzumdar, M.D., P.-Y. Chen, K.J. Dorans, K.M. Chung, A. Bhutkar, E. Hong, E.M. Noll, M.R. Sprick, A. Trumpp, and T. Jacks. 2017. Survival of pancreatic cancer cells lacking KRAS function. *Nature Communications*. 8:1090.

Neesse, A., H. Algul, D.A. Tuveson, and T.M. Gress. 2015. Stromal biology and therapy in pancreatic cancer: a changing paradigm. *Gut*. 64:1476-1484.

Neto-Silva, R.M., S. de Beco, and L.A. Johnston. 2010. Evidence for a growth-stabilizing regulatory feedback mechanism between Myc and Yorkie, the Drosophila homolog of Yap. *Dev Cell*. 19:507-520.

O'Brien, D.P., N.S. Sandanayake, C. Jenkinson, A. Gentry-Maharaj, S. Apostolidou, E.O. Fourkala, S. Camuzeaux, O. Blyuss, R. Gunu, A. Dawnay, A. Zaikin, R.C. Smith, I.J. Jacobs, U. Menon, E. Costello, S.P. Pereira, and J.F. Timms. 2015. Serum CA19-9 is significantly upregulated up to 2 years before diagnosis with pancreatic cancer: implications for early disease detection. *Clin Cancer Res*. 21:622-631.

Oh, H., and K.D. Irvine. 2008. In vivo regulation of Yorkie phosphorylation and localization. *Development*. 135:1081-1088.

Oh, H.J., K.K. Lee, S.J. Song, M.S. Jin, M.S. Song, J.H. Lee, C.R. Im, J.O. Lee, S. Yonehara, and D.S. Lim. 2006. Role of the tumor suppressor RASSF1A in Mst1-mediated apoptosis. *Cancer Res*. 66:2562-2569.

Ouelle D.E., F. Zindy, R.A. Ashmun and C.J. Sherr. 1995. Alternative reading frames of the *INK4a* tumor suppressor gene encode two unrelated proteins capable of inducing cell cycle arrest. *Cell*. 83:993-1000.

Overholtzer, M., J. Zhang, G.A. Smolen, B. Muir, W. Li, D.C. Sgroi, C.-X. Deng, J.S. Brugge, and D.A. Haber. 2006. Transforming properties of YAP, a candidate oncogene on the chromosome 11q22 amplicon. *Proceedings of the National Academy of Sciences of the United States of America*. 103:12405-12410.

Pandol, S.J. 2010. Colloquium Series on Integrated Systems Physiology: From Molecule to Function to Disease. *In* The Exocrine Pancreas. Morgan & Claypool Life Sciences
Copyright (c) 2011 by Morgan & Claypool Life Sciences., San Rafael (CA).

Pantalacci, S., N. Tapon, and P. Leopold. 2003. The Salvador partner Hippo promotes apoptosis and cell-cycle exit in Drosophila. *Nat Cell Biol*. 5:921-927.

Papaspyropoulos, A., L. Bradley, A. Thapa, C.Y. Leung, K. Toskas, D. Koennig, D.E. Pefani, C. Raso, C. Grou, G. Hamilton, N. Vlahov, A. Grawenda, S. Haider, J. Chauhan, L. Buti, A. Kanapin, X. Lu, F. Buffa, G. Dianov, A. von Kriegsheim, D. Matallanas, A. Samsonova, M. Zernicka-Goetz, and E. O'Neill. 2018. RASSF1A uncouples Wnt from Hippo signalling and promotes YAP mediated differentiation via p73. *Nat Commun*. 9:424.

Parada, L.F., C.J. Tabin, C. Shih, and R.A. Weinberg. 1982. Human EJ bladder carcinoma oncogene is homologue of Harvey sarcoma virus ras gene. *Nature*. 297:474-478.

Park, G.S., H. Oh, M. Kim, T. Kim, R.L. Johnson, K.D. Irvine, and D.S. Lim. 2016. An evolutionarily conserved negative feedback mechanism in the Hippo pathway

reflects functional difference between LATS1 and LATS2. *Oncotarget*. 7:24063-24075.

Park, H.S., J.M. Lee, H.K. Choi, S.H. Hong, J.K. Han, and B.I. Choi. 2009. Preoperative evaluation of pancreatic cancer: comparison of gadolinium-enhanced dynamic MRI with MR cholangiopancreatography versus MDCT. *J Magn Reson Imaging*. 30:586-595.

Pefani, D.E., D. Pankova, A.G. Abraham, A.M. Grawenda, N. Vlahov, S. Scrace, and O.N. E. 2016. TGF-beta Targets the Hippo Pathway Scaffold RASSF1A to Facilitate YAP/SMAD2 Nuclear Translocation. *Mol Cell*. 63:156-166.

Peters, M.L.B., A. Eckel, P.P. Mueller, A.C. Tramontano, D.T. Weaver, A. Lietz, C. Hur, C.Y. Kong, and P.V. Pandharipande. 2018. Progression to pancreatic ductal adenocarcinoma from pancreatic intraepithelial neoplasia: Results of a simulation model. *Pancreatology*. 18:928-934.

Prior, I.A., P.D. Lewis, and C. Mattos. 2012. A comprehensive survey of Ras mutations in cancer. *Cancer research*. 72:2457-2467.

Quan, M., J. Cui, T. Xia, Z. Jia, D. Xie, D. Wei, S. Huang, Q. Huang, S. Zheng, and K. Xie. 2015. Merlin/NF2 Suppresses Pancreatic Tumor Growth and Metastasis by Attenuating the FOXM1-Mediated Wnt/beta-Catenin Signaling. *Cancer Res*. 75:4778-4789.

Quante, A.S., C. Ming, M. Rottmann, J. Engel, S. Boeck, V. Heinemann, C.B. Westphalen, and K. Strauch. 2016. Projections of cancer incidence and cancer-related deaths in Germany by 2020 and 2030. *Cancer Med*. 5:2649-2656.

Rahib, L., B.D. Smith, R. Aizenberg, A.B. Rosenzweig, J.M. Fleshman, and L.M. Matrisian. 2014. Projecting cancer incidence and deaths to 2030: the unexpected burden of thyroid, liver, and pancreas cancers in the United States. *Cancer Res*. 74:2913-2921.

Raimondi, S., A.B. Lowenfels, A.M. Morselli-Labate, P. Maisonneuve, and R. Pezzilli. 2010. Pancreatic cancer in chronic pancreatitis; aetiology, incidence, and early detection. *Best Pract Res Clin Gastroenterol*. 24:349-358.

Rajalingam, K., R. Schreck, U.R. Rapp, and Š. Albert. 2007. Ras oncogenes and their downstream targets. *Biochimica et Biophysica Acta (BBA) - Molecular Cell Research*. 1773:1177-1195.

Rao, C.V., and A. Mohammed. 2015. New insights into pancreatic cancer stem cells. *World J Stem Cells*. 7:547-555.

Rawla, P., K.C. Thandra, and T. Sunkara. 2019. Pancreatic cancer and obesity: epidemiology, mechanism, and preventive strategies. *Clin J Gastroenterol*. 12:285-291.

Ray, K.C., K.M. Bell, J. Yan, G. Gu, C.H. Chung, M.K. Washington, and A.L. Means. 2011. Epithelial tissues have varying degrees of susceptibility to Kras(G12D)-initiated tumorigenesis in a mouse model. *PloS one*. 6:e16786-e16786.

Rebours, V., M.C. Boutron-Ruault, M. Schnee, C. Ferec, F. Maire, P. Hammel, P. Ruszniewski, and P. Levy. 2008. Risk of pancreatic adenocarcinoma in patients with hereditary pancreatitis: a national exhaustive series. *Am J Gastroenterol*. 103:111-119.

Redston, M.S., C. Caldas, A.B. Seymour, R.H. Hruban, L. da Costa, C.J. Yeo, and S.E. Kern. 1994. p53 mutations in pancreatic carcinoma and evidence of common involvement of homocopolymer tracts in DNA microdeletions. *Cancer Res*. 54:3025-3033.

Ren, B., X. Liu, and A.A. Suriawinata. 2019. Pancreatic Ductal Adenocarcinoma and Its Precursor Lesions: Histopathology, Cytopathology, and Molecular Pathology. *Am J Pathol*. 189:9-21.

Rhim, A.D., P.E. Oberstein, D.H. Thomas, E.T. Mirek, C.F. Palermo, S.A. Sastra, E.N. Dekleva, T. Saunders, C.P. Becerra, I.W. Tattersall, C.B. Westphalen, J. Kitajewski, M.G. Fernandez-Barrena, M.E. Fernandez-Zapico, C. Iacobuzio-Donahue, K.P. Olive, and B.Z. Stanger. 2014. Stromal elements act to restrain, rather than support, pancreatic ductal adenocarcinoma. *Cancer Cell*. 25:735-747.

Ricard Masia, Mari Mino-Kenudson, Andrew L. Warshaw, Martha B. Pitman, and Joseph Misdraji. 2011. Pancreatic Mucinous Cystic Neoplasm of the Main Pancreatic Duct. *Archives of Pathology & Laboratory Medicine*. 135:264-267.

Rouleau, G.A., P. Merel, M. Lutchman, M. Sanson, J. Zucman, C. Marineau, K. Hoang-Xuan, S. Demczuk, C. Desmaze, B. Plougastel, and et al. 1993. Alteration in a new gene encoding a putative membrane-organizing protein causes neuro-fibromatosis type 2. *Nature*. 363:515-521.

Rozengurt, E., J. Sinnett-Smith, and G. Eibl. 2018. Yes-associated protein (YAP) in pancreatic cancer: at the epicenter of a targetable signaling network associated with patient survival. *Signal Transduct Target Ther*. 3:11.

Scarpa, A., D.K. Chang, K. Nones, V. Corbo, A.M. Patch, P. Bailey, R.T. Lawlor, A.L. Johns, D.K. Miller, A. Mafficini, B. Rusev, M. Scardoni, D. Antonello, S. Barbi, K.O. Sikora, S. Cingarlini, C. Vicentini, S. McKay, M.C. Quinn, T.J. Bruxner, A.N. Christ, I. Harliwong, S. Idrisoglu, S. McLean, C. Nourse, E. Nourbakhsh, P.J. Wilson, M.J. Anderson, J.L. Fink, F. Newell, N. Waddell, O. Holmes, S.H. Kazakoff, C. Leonard, S. Wood, Q. Xu, S.H. Nagaraj, E. Amato, I. Dalai, S. Bersani, I. Cataldo, A.P. Dei Tos, P. Capelli, M.V. Davi, L. Landoni, A. Malpaga, M. Miotto, V.L. Whitehall, B.A. Leggett, J.L. Harris, J. Harris, M.D. Jones, J. Humphris, L.A. Chantrill, V. Chin, A.M. Nagrial, M. Pajic, C.J.

Scarlett, A. Pinho, I. Rooman, C. Toon, J. Wu, M. Pinese, M. Cowley, A. Barbour, A. Mawson, E.S. Humphrey, E.K. Colvin, A. Chou, J.A. Lovell, N.B. Jamieson, F. Duthie, M.C. Gingras, W.E. Fisher, R.A. Dagg, L.M. Lau, M. Lee, H.A. Pickett, R.R. Reddel, J.S. Samra, J.G. Kench, N.D. Merrett, K. Epari, N.Q. Nguyen, N. Zeps, M. Falconi, M. Simbolo, G. Butturini, G. Van Buren, S. Partelli, M. Fassan, K.K. Khanna, A.J. Gill, D.A. Wheeler, R.A. Gibbs, E.A. Musgrove, C. Bassi, G. Tortora, P. Pederzoli, J.V. Pearson, et al. 2017. Whole-genome landscape of pancreatic neuroendocrine tumours. *Nature*. 543:65-71.

Schutte, M., R.H. Hruban, J. Geradts, R. Maynard, W. Hilgers, S.K. Rabindran, C.A. Moskaluk, S.A. Hahn, I. Schwarte-Waldhoff, W. Schmiegel, S.B. Baylin, S.E. Kern, and J.G. Herman. 1997. Abrogation of the Rb/p16 tumor-suppressive pathway in virtually all pancreatic carcinomas. *Cancer Res*. 57:3126-3130.

Scott, J.E. 1996. Alcian blue. Now you see it, now you don't. *European Journal of Oral Sciences*. 104:2-9.

Serrano M., G.J. Hannon and D. Beach. 1993. A new regulatory motif in cell-cycle control causing specific inhibition of cyclin D/CDK4. *Nature*. 366:704-707.

Shao, Diane D., W. Xue, Elsa B. Krall, A. Bhutkar, F. Piccioni, X. Wang, Anna C. Schinzel, S. Sood, J. Rosenbluh, Jong W. Kim, Y. Zwang, Thomas M. Roberts, David E. Root, T. Jacks, and William C. Hahn. 2014. KRAS and YAP1 Converge to Regulate EMT and Tumor Survival. *Cell*. 158:171-184.

Shen, X., L. Zhang, J. Li, Y. Li, Y. Wang, and Z.-X. Xu. 2019. Recent Findings in the Regulation of Programmed Death Ligand 1 Expression. *Front Immunol*. 10:1337-1337.

Shi, C., S.M. Hong, P. Lim, H. Kamiyama, M. Khan, R.A. Anders, M. Goggins, R.H. Hruban, and J.R. Eshleman. 2009. KRAS2 mutations in human pancreatic acinar-ductal metaplastic lesions are limited to those with PanIN: implications for the human pancreatic cancer cell of origin. *Mol Cancer Res*. 7:230-236.

Shih, H.P., J.L. Kopp, M. Sandhu, C.L. Dubois, P.A. Seymour, A. Grapin-Botton, and M. Sander. 2012. A Notch-dependent molecular circuitry initiates pancreatic endocrine and ductal cell differentiation. *Development*. 139:2488-2499.

Shivakumar, L., J. Minna, T. Sakamaki, R. Pestell, and M.A. White. 2002. The RASSF1A tumor suppressor blocks cell cycle progression and inhibits cyclin D1 accumulation. *Mol Cell Biol*. 22:4309-4318.

Skoulidis, F., L.D. Cassidy, V. Pisupati, J.G. Jonasson, H. Bjarnason, J.E. Eyfjord, F.A. Karreth, M. Lim, L.M. Barber, S.A. Clatworthy, S.E. Davies, K.P. Olive, D.A. Tuveson, and A.R. Venkitaraman. 2010. Germline Brca2 heterozygosity promotes Kras(G12D) -driven

carcinogenesis in a murine model of familial pancreatic cancer. *Cancer Cell*. 18:499-509.

Slack, J.M. 1995. Developmental biology of the pancreas. *Development*. 121:1569-1580.

Sommers, S.C., S.A. Murphy, and S. Warren. 1954. Pancreatic duct hyperplasia and cancer. *Gastroenterology*. 27:629-640.

Steedman, H.F. 1950. Alcian blue 8GS: a new stain for mucin. *Q J Microsc Sci*. 91:477-479.

Storz, P. 2017. Acinar cell plasticity and development of pancreatic ductal adenocarcinoma. *Nat Rev Gastroenterol Hepatol*. 14:296-304.

Strauss, V.Y., R. Shaw, P.S. Virdee, C.N. Hurt, E. Ward, B. Tranter, N. Patel, J. Bridgewater, P. Parsons, G. RAdhakrishna, E. O'Neill, D. Sebag-Montefiore, M. Hawkins, P.G. Corrie, T. Maughan and S. Mukherjee. 2019. Study protocol: a multi-centre randomised study of induction chemotherapy followed by capecitabine ± nelfinavir with high- or standard-dose radiotherapy for locally advanced pancreatic cancer (SCALOP-2). *BMC Cancer*. 19:121.

Strobel, O., Y. Dor, J. Alsina, A. Stirman, G. Lauwers, A. Trainor, C.F. Castillo, A.L. Warshaw, and S.P. Thayer. 2007. In vivo lineage tracing defines the role of acinar-to-ductal transdifferentiation in inflammatory ductal metaplasia. *Gastroenterology*. 133:1999-2009.

Strobel, O., D.E. Rosow, E.Y. Rakhlin, G.Y. Lauwers, A.G. Trainor, J. Alsina, C. Fernandez-Del Castillo, A.L. Warshaw, and S.P. Thayer. 2010. Pancreatic duct glands are distinct ductal compartments that react to chronic injury and mediate Shh-induced metaplasia. *Gastroenterology*. 138:1166-1177.

Sudol, M. 1994. Yes-associated protein (YAP65) is a proline-rich phosphoprotein that binds to the SH3 domain of the Yes proto-oncogene product. *Oncogene*. 9:2145-2152.

Sultana, A., P. Ghaneh, D. Cunningham, N. Starling, J.P. Neoptolemos, and C.T. Smith. 2008. Gemcitabine based combination chemotherapy in advanced pancreatic cancer-indirect comparison. *BMC cancer*. 8:192-192.

Taha, Z., H.J. Janse van Rensburg, and X. Yang. 2018. The Hippo Pathway: Immunity and Cancer. *Cancers (Basel)*. 10:94.

Tapon, N., K.F. Harvey, D.W. Bell, D.C. Wahrer, T.A. Schiripo, D. Haber, and I.K. Hariharan. 2002. salvador Promotes both cell cycle exit and apoptosis in Drosophila and is mutated in human cancer cell lines. *Cell*. 110:467-478.

Tiriac, H., P. Belleau, D.D. Engle, D. Plenker, A. Deschenes, T.D.D. Somerville, F.E.M. Froeling, R.A. Burkhart, R.E. Denroche, G.H. Jang, K. Miyabayashi, C.M. Young, H. Patel, M. Ma, J.F. LaComb, R.L.D. Palmaira, A.A. Javed, J.C. Huynh, M. Johnson, K. Arora, N. Robine, M. Shah, R. Sanghvi, A.B. Goetz, C.Y. Lowder, L. Martello, E. Driehuis, N. LeComte, G. Askan, C.A. Iacobuzio-Donahue, H. Clevers, L.D. Wood, R.H. Hruban, E. Thompson, A.J. Aguirre, B.M. Wolpin, A. Sasson, J. Kim, M. Wu, J.C. Bucobo, P. Allen, D.V. Sejpal, W. Nealon, J.D. Sullivan, J.M. Winter, P.A. Gimotty, J.L. Grem, D.J. DiMaio, J.M. Buscaglia, P.M. Grandgenett, J.R. Brody, M.A. Hollingsworth, G.M. O'Kane, F. Notta, E. Kim, J.M. Crawford, C. Devoe, A. Ocean, C.L. Wolfgang, K.H. Yu, E. Li, C.R. Vakoc, B. Hubert, S.E. Fischer, J.M. Wilson, R. Moffitt, J. Knox, A. Krasnitz, S. Gallinger, and D.A. Tuveson. 2018. Organoid Profiling Identifies Common Responders to Chemotherapy in Pancreatic Cancer. *Cancer Discov*. 8:1112-1129.

Tommasi, S., R. Dammann, Z. Zhang, Y. Wang, L. Liu, W.M. Tsark, S.P. Wilczynski, J. Li, M. You, and G.P. Pfeifer. 2005. Tumor susceptibility of Rassf1a knockout mice. *Cancer Res*. 65:92-98.

Torphy, R.J., Y. Zhu, and R.D. Schulick. 2018. Immunotherapy for pancreatic cancer: Barriers and breakthroughs. *Ann Gastroenterol Surg*. 2:274-281.

Torres, M.P., S. Rachagani, J.J. Souchek, K. Mallya, S.L. Johansson, and S.K. Batra. 2013. Novel pancreatic cancer cell lines derived from genetically engineered mouse models of spontaneous pancreatic adenocarcinoma: applications in diagnosis and therapy. *PLoS One*. 8:e80580.

Trikudanathan, G., A. Philip, C.A. Dasanu, and W.L. Baker. 2011. Association between Helicobacter pylori infection and pancreatic cancer. A cumulative meta-analysis. *Jop*. 12:26-31.

Trofatter, J.A., M.M. MacCollin, J.L. Rutter, J.R. Murrell, M.P. Duyao, D.M. Parry, R. Eldridge, N. Kley, A.G. Menon, K. Pulaski, and et al. 1993. A novel moesin-, ezrin-, radixin-like gene is a candidate for the neurofibromatosis 2 tumor suppressor. *Cell*. 72:791-800.

Tsai, F.D., M.S. Lopes, M. Zhou, H. Court, O. Ponce, J.J. Fiordalisi, J.J. Gierut, A.D. Cox, K.M. Haigis, and M.R. Philips. 2015. K-Ras4A splice variant is widely expressed in cancer and uses a hybrid membrane-targeting motif. *Proc Natl Acad Sci U S A*. 112:779-784.

Tsai, S., L. McOlash, K. Palen, B. Johnson, C. Duris, Q. Yang, M.B. Dwinell, B. Hunt, D.B. Evans, J. Gershan, and M.A. James. 2018. Development of primary human pancreatic cancer organoids, matched stromal and immune cells and 3D tumor microenvironment models. *BMC Cancer*. 18:335.

Tseng, W.W., D. Winer, J.A. Kenkel, O. Choi, A.H. Shain, J.R. Pollack, R. French, A.M. Lowy, and E.G. Engleman. 2010. Development of an orthotopic model of invasive pancreatic cancer in an immunocompetent murine host. *Clin Cancer Res*. 16:3684-3695.

Tsuda, M., A. Fukuda, N. Roy, Y. Hiramatsu, L. Leonhardt, N. Kakiuchi, K. Hoyer, S. Ogawa, N. Goto, K. Ikuta, Y. Kimura, Y. Matsumoto, Y. Takada, T. Yoshioka, T. Maruno, Y. Yamaga, G.E. Kim, H. Akiyama, S. Ogawa, C.V. Wright, D. Saur, K. Takaori, S. Uemoto, M. Hebrok, T. Chiba, and H. Seno. 2018. The BRG1/SOX9 axis is critical for acinar cell-derived pancreatic tumorigenesis. *J Clin Invest*. 128:3475-3489.

Tu, B., J. Yao, S. Ferri-Borgogno, J. Zhao, S. Chen, Q. Wang, L. Yan, X. Zhou, C. Zhu, S. Bang, Q. Chang, C.A. Bristow, Y. Kang, H. Zheng, H. Wang, J.B. Fleming, M. Kim, T.P. Heffernan, G.F. Draetta, D. Pan, A. Maitra, W. Yao, S. Gupta, and H. Ying. 2019. YAP1 oncogene is a context-specific driver for pancreatic ductal adenocarcinoma. *JCI Insight*. 4.

Tummala, P., O. Junaidi, and B. Agarwal. 2011. Imaging of pancreatic cancer: An overview. *Journal of gastrointestinal oncology*. 2:168-174.

Udan, R.S., M. Kango-Singh, R. Nolo, C. Tao, and G. Halder. 2003. Hippo promotes proliferation arrest and apoptosis in the Salvador/Warts pathway. *Nat Cell Biol*. 5:914-920.

Ueki, T., M. Toyota, T. Sohn, C.J. Yeo, J.P. Issa, R.H. Hruban, and M. Goggins. 2000. Hypermethylation of multiple genes in pancreatic adenocarcinoma. *Cancer Res*. 60:1835-1839.

Uzunparmak, B., and I.H. Sahin. 2019. Pancreatic cancer microenvironment: a current dilemma. *Clinical and Translational Medicine*. 8:2.

van der Weyden, L., K.K. Tachibana, M.A. Gonzalez, D.J. Adams, B.L. Ng, R. Petty, A.R. Venkitaraman, M.J. Arends, and A. Bradley. 2005. The RASSF1A isoform of RASSF1 promotes microtubule stability and suppresses tumorigenesis. *Mol Cell Biol*. 25:8356-8367.

Varelas, X. 2014. The Hippo pathway effectors TAZ and YAP in development, homeostasis and disease. *Development*. 141:1614-1626.

Vassilev, A., K.J. Kaneko, H. Shu, Y. Zhao, and M.L. DePamphilis. 2001. TEAD/TEF transcription factors utilize the activation domain of YAP65, a Src/Yes-associated protein localized in the cytoplasm. *Genes Dev*. 15:1229-1241.

Versteijne, E., M. Suker, K. Groothuis, JM. Akkermans-Vogelaar, M.G. Besselink, B.A. Bonsing, J. Buijsen, O.R. Busch, G.M. Creemers, R.M. van Dam, F. Eskens, S.

Festen, J.W.B. de Groot, B.G. Koerkamp, I.H. de Hingh, M.Y.V. Homs, J.E. van Hooft, E.D. Kerver, S.A.C. Luelmo, K.J. Neelis, J. Nuyttens, G. Paardekooper, G.A. Patijn, M.J.C. van der Sangen, J. de Vos-Geelen, J.W. Wilmink, A.H. Zwinderman, C.J. Punt, C.H. van Eijck, and G. van Tienhoven. 2020. Preoperative Chemoradiotherapy Versus Immediate Surgery for Resectable and Borderline Resectable Pancreatic Cancer: Results of the Dutch Randomized Phase III PREOPANC Trial [published online ahead of print February 27 2020]. Journal of Clinical Oncology. JCO1902274.

Vezeridis, M., C.M. Doremus, L.M. Tibbetts, G. Tzanakakis and B.T. Jackson. 1989. Invasion and Metastasis Following Orthotopic Transplantation of Human Pancreatic Cancer in the Nude Mouse. *Journal of Surgical Oncology.* 40:261-265.

Vogelstein, B., N. Papadopoulos, V.E. Velculescu, S. Zhou, L.A. Diaz, and K.W. Kinzler. 2013. Cancer Genome Landscapes. *Science*. 339:1546.

Vojtek, A.B., S.M. Hollenberg, and J.A. Cooper. 1993. Mammalian Ras interacts directly with the serine/threonine kinase raf. *Cell*. 74:205-214.

Voltes, A., C.F. Hevia, C. Engel-Pizcueta, C. Dingare, S. Calzolari, J. Terriente, C. Norden, V. Lecaudey, and C. Pujades. 2019. Yap/Taz-TEAD activity links mechanical cues to progenitor cell behavior during zebrafish hindbrain segmentation. *Development*. 146:dev176735.

von Figura, G., A. Fukuda, N. Roy, M.E. Liku, J.P. Morris Iv, G.E. Kim, H.A. Russ, M.A. Firpo, S.J. Mulvihill, D.W. Dawson, J. Ferrer, W.F. Mueller, A. Busch, K.J. Hertel, and M. Hebrok. 2014. The chromatin regulator Brg1 suppresses formation of intraductal papillary mucinous neoplasm and pancreatic ductal adenocarcinoma. *Nat Cell Biol*. 16:255-267.

Von Hoff, D.D., T. Ervin, F.P. Arena, E.G. Chiorean, J. Infante, M. Moore, T. Seay, S.A. Tjulandin, W.W. Ma, M.N. Saleh, M. Harris, M. Reni, S. Dowden, D. Laheru, N. Bahary, R.K. Ramanathan, J. Tabernero, M. Hidalgo, D. Goldstein, E. Van Cutsem, X. Wei, J. Iglesias, and M.F. Renschler. 2013. Increased Survival in Pancreatic Cancer with nab-Paclitaxel plus Gemcitabine. *New England Journal of Medicine*. 369:1691-1703.

Vos, M.D., C.A. Ellis, A. Bell, M.J. Birrer, and G.J. Clark. 2000. Ras uses the novel tumor suppressor RASSF1 as an effector to mediate apoptosis. *J Biol Chem*. 275:35669-35672.

Vos, M.D., A. Martinez, C. Elam, A. Dallol, B.J. Taylor, F. Latif, and G.J. Clark. 2004. A role for the RASSF1A tumor suppressor in the regulation of tubulin polymerization and genomic stability. *Cancer Res*. 64:4244-4250.

Vousden, K.H., and C.J. Marshall. 1984. Three different activated ras genes in mouse tumours; evidence for oncogene activation during progression of a mouse lymphoma. *EMBO J*. 3:913-917.

Wang, L., H. Wu, L. Wang, J. Lu, H. Duan, X. Liu, and Z. Liang. 2016. Expression of amphiregulin predicts poor outcome in patients with pancreatic ductal adenocarcinoma. *Diagn Pathol*. 11:60-60.

Waters, A.M., and C.J. Der. 2018. KRAS: The Critical Driver and Therapeutic Target for Pancreatic Cancer. *Cold Spring Harb Perspect Med*. 8:a031435.

Weden, S., M. Klemp, I.P. Gladhaug, M. Moller, J.A. Eriksen, G. Gaudernack, and T. Buanes. 2011. Long-term follow-up of patients with resected pancreatic cancer following vaccination against mutant K-ras. *Int J Cancer*. 128:1120-1128.

Westphalen, C., and K. Olive. 2012. Genetically Engineered Mouse Models of Pancreatic Cancer. *Cancer Journal*. 18:502-510.

Williams, K.A., M. Lee, Y. Hu, J. Andreas, S.J. Patel, S. Zhang, P. Chines, A. Elkahloun, S. Chandrasekharappa, J.S. Gutkind, A.A. Molinolo, and N.P. Crawford. 2014. A systems genetics approach identifies CXCL14, ITGAX, and LPCAT2 as novel aggressive prostate cancer susceptibility genes. *PLoS Genet*. 10:e1004809.

Witkiewicz, A.K., E.A. McMillan, U. Balaji, G. Baek, W.-C. Lin, J. Mansour, M. Mollaee, K.-U. Wagner, P. Koduru, A. Yopp, M.A. Choti, C.J. Yeo, P. McCue, M.A. White, and E.S. Knudsen. 2015. Whole-exome sequencing of pancreatic cancer defines genetic diversity and therapeutic targets. *Nature Communications*. 6:6744.

Wolpin, B.M., P. Kraft, M. Gross, K. Helzlsouer, H.B. Bueno-de-Mesquita, E. Steplowski, R.Z. Stolzenberg-Solomon, A.A. Arslan, E.J. Jacobs, A. Lacroix, G. Petersen, W. Zheng, D. Albanes, N.E. Allen, L. Amundadottir, G. Anderson, M.-C. Boutron-Ruault, J.E. Buring, F. Canzian, S.J. Chanock, S. Clipp, J.M. Gaziano, E.L. Giovannucci, G. Hallmans, S.E. Hankinson, R.N. Hoover, D.J. Hunter, A. Hutchinson, K. Jacobs, C. Kooperberg, S.M. Lynch, J.B. Mendelsohn, D.S. Michaud, K. Overvad, A.V. Patel, A. Rajkovic, M.-J. Sanchéz, X.-O. Shu, N. Slimani, G. Thomas, G.S. Tobias, D. Trichopoulos, P. Vineis, J. Virtamo, J. Wactawski-Wende, K. Yu, A. Zeleniuch-Jacquotte, P. Hartge, and C.S. Fuchs. 2010. Pancreatic cancer risk and ABO blood group alleles: results from the pancreatic cancer cohort consortium. *Cancer research*. 70:1015-1023.

Wolny-Rokicka, E., K. Sutkowski, A. Grzadziel, Z. Dorsz, A. Tukiendorf, J. Lipinski and J. Wydmanski. 2016. Tolerance and efficacy of palliative radiotherapy for advanced pancreatic cancer: A retrospective analysis of single-institutional experiences. *Molecular and Clinical Oncology.* 4:1088-1092.

Wong, C.H., Y.J. Li, and Y.C. Chen. 2016. Therapeutic potential of targeting acinar cell reprogramming in pancreatic cancer. *World J Gastroenterol*. 22:7046-7057.

Wu, S., J. Huang, J. Dong, and D. Pan. 2003. hippo encodes a Ste-20 family protein kinase that restricts cell proliferation and promotes apoptosis in conjunction with salvador and warts. *Cell*. 114:445-456.

Xing-mao, Z., Z. Hong-juan, L. Qing, and H. Qiang. 2018. Pancreatic acinar cell carcinoma—case report and literature review. *BMC Cancer*. 18:1083.

Xu, M.Z., S.W. Chan, A.M. Liu, K.F. Wong, S.T. Fan, J. Chen, R.T. Poon, L. Zender, S.W. Lowe, W. Hong, and J.M. Luk. 2011. AXL receptor kinase is a mediator of YAP-dependent oncogenic functions in hepatocellular carcinoma. *Oncogene*. 30:1229-1240.

Xu, T., W. Wang, S. Zhang, R.A. Stewart, and W. Yu. 1995. Identifying tumor suppressors in genetic mosaics: the Drosophila lats gene encodes a putative protein kinase. *Development*. 121:1053-1063.

Xu, Y., J. Liu, M. Nipper, and P. Wang. 2019. Ductal vs. acinar? Recent insights into identifying cell lineage of pancreatic ductal adenocarcinoma. *Ann Pancreat Cancer*. 2.

Yadav, D., and A.B. Lowenfels. 2013. The epidemiology of pancreatitis and pancreatic cancer. *Gastroenterology*. 144:1252-1261.

Yagi, R., L.F. Chen, K. Shigesada, Y. Murakami, and Y. Ito. 1999. A WW domain-containing yes-associated protein (YAP) is a novel transcriptional co-activator. *EMBO J*. 18:2551-2562.

Yamada, H., T. Yoshida, H. Sakamoto, M. Terada, and T. Sugimura. 1986. Establishment of a human pancreatic adenocarcinoma cell line (PSN-1) with amplifications of both c-myc and activated c-Ki-ras by a point mutation. *Biochem Biophys Res Commun*. 140:167-173.

Yamaguchi, J., A.S. Liss, A. Sontheimer, M. Mino-Kenudson, C.F.-d. Castillo, A.L. Warshaw, and S.P. Thayer. 2015. Pancreatic duct glands (PDGs) are a progenitor compartment responsible for pancreatic ductal epithelial repair. *Stem Cell Research*. 15:190-202.

Yamaguchi, T., Y. Shirai, N. Nakamura, K. Sudo, K. Nakamura, S. Hironaka, T. Hara, and T. Denda. 2012. Usefulness of brush cytology combined with pancreatic juice cytology in the diagnosis of pancreatic cancer: significance of pancreatic juice cytology after brushing. *Pancreas*. 41:1225-1229.

Yee, K.S., L. Grochola, G. Hamilton, A. Grawenda, E.E. Bond, H. Taubert, P. Würl, G.L. Bond, and E. Neill. 2012. A RASSF1A polymorphism restricts p53/p73 activation and

associates with poor survival and accelerated age of onset of soft tissue sarcoma. *Cancer Research*:canres.2906.2011.

Ying, H., P. Dey, W. Yao, A.C. Kimmelman, G.F. Draetta, A. Maitra, and R.A. DePinho. 2016. Genetics and biology of pancreatic ductal adenocarcinoma. *Genes Dev*. 30:355-385.

Yotsumoto, F., T. Fukami, H. Yagi, A. Funakoshi, T. Yoshizato, M. Kuroki, and S. Miyamoto. 2010. Amphiregulin regulates the activation of ERK and Akt through epidermal growth factor receptor and HER3 signals involved in the progression of pancreatic cancer. *Cancer Science*. 101:2351-2360.

Yu, F.-X., and K.-L. Guan. 2013. The Hippo pathway: regulators and regulations. *Genes & development*. 27:355-371.

Yui, S., T. Nakamura, T. Sato, Y. Nemoto, T. Mizutani, X. Zheng, S. Ichinose, T. Nagaishi, R. Okamoto, K. Tsuchiya, H. Clevers, and M. Watanabe. 2012. Functional engraftment of colon epithelium expanded in vitro from a single adult Lgr5(+) stem cell. *Nat Med*. 18:618-623.

Zanconato, F., M. Cordenonsi, and S. Piccolo. 2016. YAP/TAZ at the Roots of Cancer. *Cancer Cell*. 29:783-803.

Zenzmaier, C., M. Hermann, P. Hengster, and P. Berger. 2012. Dickkopf-3 maintains the PANC-1 human pancreatic tumor cells in a dedifferentiated state. *Int J Oncol*. 40:40-46.

Zhang, J., J.Y. Ji, M. Yu, M. Overholtzer, G.A. Smolen, R. Wang, J.S. Brugge, N.J. Dyson, and D.A. Haber. 2009. YAP-dependent induction of amphiregulin identifies a non-cell-autonomous component of the Hippo pathway. *Nat Cell Biol*. 11:1444-1450.

Zhang, N., H. Bai, K.K. David, J. Dong, Y. Zheng, J. Cai, M. Giovannini, P. Liu, R.A. Anders, and D. Pan. 2010. The Merlin/NF2 tumor suppressor functions through the YAP oncoprotein to regulate tissue homeostasis in mammals. *Dev Cell*. 19:27-38.

Zhang, W., N. Nandakumar, Y. Shi, M. Manzano, A. Smith, G. Graham, S. Gupta, E.E. Vietsch, S.Z. Laughlin, M. Wadhwa, M. Chetram, M. Joshi, F. Wang, B. Kallakury, J. Toretsky, A. Wellstein, and C. Yi. 2014. Downstream of mutant KRAS, the transcription regulator YAP is essential for neoplastic progression to pancreatic ductal adenocarcinoma. *Sci Signal*. 7:ra42.

Zhang, X., C. Guo, X. Wu, A.X. Li, L. Liu, W. Tsark, R. Dammann, H. Shen, S.L. Vonderfecht, and G.P. Pfeifer. 2016. Analysis of Liver Tumor-Prone Mouse Models of the Hippo Kinase Scaffold Proteins RASSF1A and SAV1. *Cancer Res*. 76:2824-2835.

Zhang, Y., J.P.t. Morris, W. Yan, H.K. Schofield, A. Gurney, D.M. Simeone, S.E. Millar, T. Hoey, M. Hebrok, and M. Pasca di Magliano. 2013. Canonical wnt signaling is required for pancreatic carcinogenesis. *Cancer research*. 73:4909-4922.

Zhao, B., X. Wei, W. Li, R.S. Udan, Q. Yang, J. Kim, J. Xie, T. Ikenoue, J. Yu, L. Li, P. Zheng, K. Ye, A. Chinnaiyan, G. Halder, Z.C. Lai, and K.L. Guan. 2007. Inactivation of YAP oncoprotein by the Hippo pathway is involved in cell contact inhibition and tissue growth control. *Genes Dev*. 21:2747-2761.

Zhao, B., X. Ye, J. Yu, L. Li, W. Li, S. Li, J. Yu, J.D. Lin, C.Y. Wang, A.M. Chinnaiyan, Z.C. Lai, and K.L. Guan. 2008. TEAD mediates YAP-dependent gene induction and growth control. *Genes Dev*. 22:1962-1971.

Zhou, Q., A.C. Law, J. Rajagopal, W.J. Anderson, P.A. Gray, and D.A. Melton. 2007. A multipotent progenitor domain guides pancreatic organogenesis. *Dev Cell*. 13:103-114.

Zhou, S.L., J. Cui, Z.M. Fan, X.M. Li, J.L. Li, B.C. Liu, D.Y. Zhang, H.Y. Liu, X.K. Zhao, X. Song, R. Wang, Z.C. Yan, H.X. Yi, and L.D. Wang. 2013. Polymorphism of A133S and promoter hypermethylation in Ras association domain family 1A gene (RASSF1A) is associated with risk of esophageal and gastric cardia cancers in Chinese population from high incidence area in northern China. *BMC Cancer*. 13:259.

Zhou, Z., Y. Hao, N. Liu, L. Raptis, M.S. Tsao, and X. Yang. 2011. TAZ is a novel oncogene in non-small cell lung cancer. *Oncogene*. 30:2181-2186.

Ziv, O., B. Glaser, and Y. Dor. 2013. The plastic pancreas. *Dev Cell*. 26:3-7.